AD-A066 160 AERONAUTICAL RESEARCH ASSOCIATES OF PRINCETON INC N J F/G 4/1
SEASONAL VARIATIONS IN ULTRAVIOLET SINGLE SCATTERING PHASE FUNC--ETC(U)
FEB 79 J M SCHLUPF, C R DICKSON, M E NEER N00014-76-C-1094
UNCLASSIFIED ARAP-383 NL

1 OF 3
ADA
066160

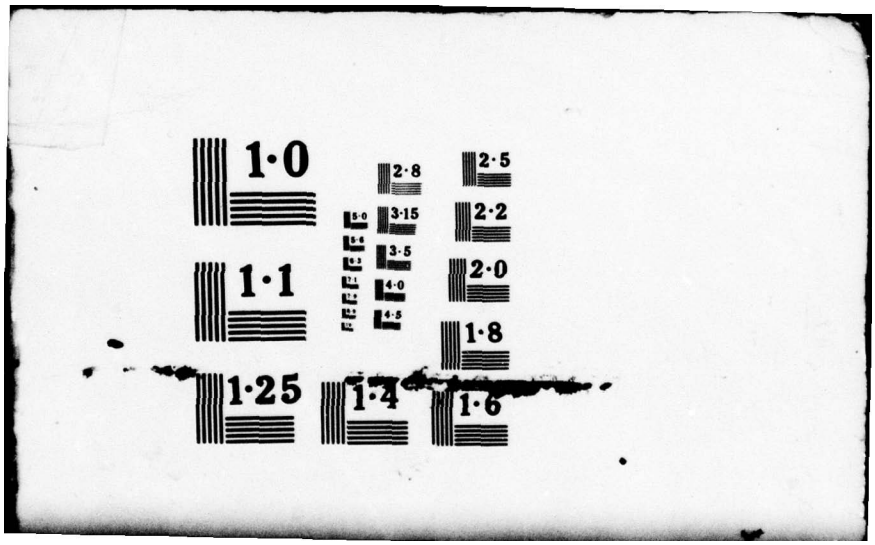
1·0
1·1
1·25
2·8
3·15
3·5
4·0
4·5
1·4
2·5
2·2
2·0
1·8
1·6

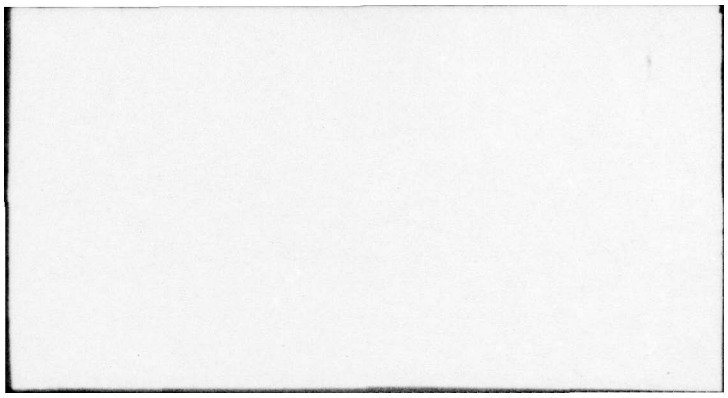

A.R.A.P. Report No. 383

(12)

SEASONAL VARIATIONS IN ULTRAVIOLET SINGLE SCATTERING PHASE FUNCTIONS

Final Report

Contract No. N00014-76-C-1094

by

Joseph M. Schlupf
C. Robert Dickson
Michael E. Neer

Submitted to

Department of the Navy
Office of Naval Research
Arlington, Virginia 22217

AERONAUTICAL RESEARCH ASSOCIATES OF PRINCETON, INC.
50 Washington Road, P.O. Box 2229
Princeton, New Jersey 08540
(609) 452-2950

February 1979

UNCLASSIFIED

SECURITY CLASSIFICATION OF THIS PAGE (When Data Entered)

REPORT DOCUMENTATION PAGE

READ INSTRUCTIONS BEFORE COMPLETING FORM

1. REPORT NUMBER (4)

2. GOVT ACCESSION NO.

3. RECIPIENT'S CATALOG NUMBER

4. TITLE (and Subtitle)
SEASONAL VARIATIONS IN ULTRAVIOLET SINGLE SCATTERING PHASE FUNCTIONS.

5. TYPE OF REPORT & PERIOD COVERED (9)
Final Report.

6. PERFORMING ORG. REPORT NUMBER
A.R.A.P. Report No. 383

7. AUTHOR(s) (10)
Joseph M. Schlupf
C. Robert Dickson
Michael E. Neer

8. CONTRACT OR GRANT NUMBER(s) (15)
N0014-76-C-1094

9. PERFORMING ORGANIZATION NAME AND ADDRESS
Aeronautical Research Associates of Princeton, Inc.
50 Washington Road, P.O. Box 2229
Princeton, New Jersey 08540

10. PROGRAM ELEMENT, PROJECT, TASK AREA & WORK UNIT NUMBERS

11. CONTROLLING OFFICE NAME AND ADDRESS
Department of the Navy
Office of Naval Research
Arlington, Virginia 22217

12. REPORT DATE (11)
Feb[redacted]79

13. NUMBER OF PAGES (12)
265 pages 266p.

14. MONITORING AGENCY NAME & ADDRESS (if different from Controlling Office) (14)
ARAP-383

15. SECURITY CLASS. (of this report)
Unclassified

15a. DECLASSIFICATION/DOWNGRADING SCHEDULE

16. DISTRIBUTION STATEMENT (of this Report)
"Approved for public release; distribution unlimited."

17. DISTRIBUTION STATEMENT (of the abstract entered in Block 20, if different from Report)

18. SUPPLEMENTARY NOTES

19. KEY WORDS (Continue on reverse side if necessary and identify by block number)
Single scattering phase function
Ultraviolet scattering
Rayleigh scattering
Aerosol scattering
Ozone absorption
Solar blind
Polar Nephelometer

20. ABSTRACT (Continue on reverse side if necessary and identify by block number)
Ultraviolet single scattering phase functions have been measured with a scanning polar nephelometer in a wide variety of weather conditions for rural, industrial, maritime, and desert atmospheres. Good correlation between measured phase functions and those predicted from Mie and Rayleigh theory using measured aerosol particle size distributions was generally observed in the fall and winter months and in fogs. Measured phase functions generally exceeded predicted values in the spring and summer months because of inadequacies in either the particle size measurement technique or the representation of → next page

DD FORM 1 JAN 73 1473 EDITION OF 1 NOV 65 IS OBSOLETE

UNCLASSIFIED

SECURITY CLASSIFICATION OF THIS PAGE (When Data Entered)

008 400

JOB

aerosol particles as spherical dielectrics. Attempts to verify the phase functions measured at scattering angles below ten degrees with variable field of view attenuation and scattering techniques were generally unsuccessful due to rapidly changing aerosol and ozone concentrations. An algorithm has been found for correlating the ultraviolet aerosol scattering coefficient with visibility.

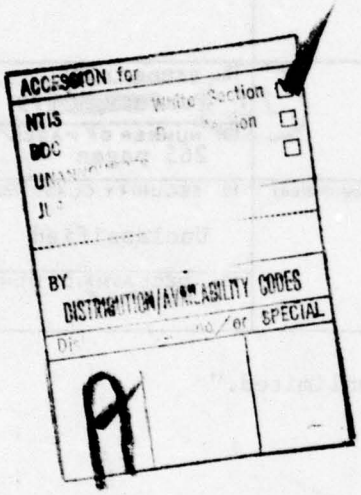

ABSTRACT

Ultraviolet single scattering phase functions have been measured with a scanning polar nephelometer in a wide variety of weather conditions for rural, industrial, maritime, and desert atmospheres. Good correlation between measured phase functions and those predicted from Mie and Rayleigh theory using measured aerosol particle size distributions was generally observed in the fall and winter months and in fogs. Measured phase functions generally exceeded predicted values in the spring and summer months because of inadequacies in either the particle size measurement technique or the representation of aerosol particles as spherical dielectrics. Attempts to verify the phase functions measured at scattering angles below ten degrees with variable field of view attenuation and scattering techniques were generally unsuccessful due to rapidly changing aerosol and ozone concentrations. An algorithm has been found for correlating the ultraviolet aerosol scattering coefficient with visibility.

TABLE OF CONTENTS

LIST OF FIGURES

1. INTRODUCTION

The ultraviolet, single scattering phase functions of naturally occurring atmospheric aerosols are important for two basic reasons. First, the propagation of ultraviolet radiation through the atmosphere depends strongly on the shape and magnitude of the phase function. Second, the manner in which the shape and magnitude of the phase functions vary with aerosol size distribution and composition could be a basis for developing remote sensing techniques.

Of particular interest is the solar blind portion of the ultraviolet spectrum (220 to 280 nm) where ozone in the upper atmosphere prevents solar radiation from reaching the earth's surface. Within this solar blind region, ultraviolet voice communications systems, missile launch detectors, tail warning receivers and remote sensing devices can operate day or night without interference from the sun. The high scattering cross sections of both aerosols and molecular species in the solar blind add an attractive, nonline of sight potential to many of these applications.

The potential for remote sensing of atmospheric aerosols such as those related to smoke stack effluents, particle size distributions and rising thermals, pollutant concentrations, and changing weather conditions is quite promising. Even more promising is the potential for laboratory diagnostics of processes involving aerosols such as the vaporization of

fuel sprays, condensation phenomena, soot formation and erosion or ablation phenomena.

The single scattering phase function is a key factor in characterizing the scattering, absorption and propagation of ultraviolet radiation through the atmosphere. The single scattering phase function $F(\theta,\lambda)$ is of fundamental importance for the following reasons. $F(\theta,\lambda)$ is a primary input parameter to all atmospheric propagation models. $F(\theta,\lambda)$ is necessary to separate the scattering coefficient $k_{SCAT}(\lambda)$ from the absorption coefficient $k_{ABS}(\lambda)$ which sum to the extinction coefficient $k_{EXT}(\lambda)$ as shown in Equation 1.

$$k_{EXT}(\lambda) = 2\pi \int_0^{\pi} F(\theta,\lambda)\ \sin\theta d\theta + k_{ABS}(\lambda)$$
$$= k_{SCAT}(\lambda) + k_{ABS}(\lambda) \qquad (1)$$

$F(\theta,\lambda)$ is necessary to back out aerosol absorption coefficient as indicated in Equation 2. $F(\theta,\lambda)$ and $k_{ABS,A}(\lambda)$ can be

$$k_{ABS,A}(\lambda) = k_{EXT}(\lambda) - k_{SCAT}(\lambda) - k_{ABS,M}(\lambda) \qquad (2)$$

used to infer effective refractive indices of aerosols from Mie scattering calculations. Finally, $F(\theta,\lambda)$ at near forward angles $\theta \leq 10^{o}$ has great significance with respect to atmospheric propagation for both threat warning and UV communications.

While Mie theory calculations of the scattering properties can be used in lieu of measurements, they are often inadequate

for predicting phase functions. The input parameters required for the Mie calculations such as the aerosol particle size distributions and refractive indices are unknown and are generally more difficult to measure than the phase functions themselves. Furthermore, the results of the present investigation indicate that even if particle size distributions are measured using state-of-the-art techniques and the assumed refractive indices are varied greatly, agreement between measured and predicted phase functions cannot always be obtained.

This report presents the results of the continuing investigation of the scattering of ultraviolet radiation by naturally occurring atmospheric aerosols. The primary purpose of this work is to provide a broad data base of ultraviolet single scattering phase functions for correlation with weather conditions and aerosol type. Since the measurements were carried out in conjunction with related experimental programs supported by the Naval Weapons Center,[1] Naval Electronics System Command,[2] the Naval Ocean Systems Center, and the Air Force Avionics Laboratory,[2] considerable supporting data is available.

Single scattering phase functions between 220 and 280 nm of naturally occurring atmospheric aerosols have been measured in a variety of weather conditions over a one year period. These measurements were carried out in industrial, rural, maritime and desert atmospheres. Simultaneously, the aerosol

particle size distribution, temperature, humidity, ozone concentration, visibility and other relevant weather conditions were measured. On many occasions, the atmospheric extinction coefficients and the atmospheric scattered radiance fields were measured.

Mie scattering theory, as well as field measurements, indicate that the single scattering phase functions in the ultraviolet portion of the spectrum are highly peaked in the forward direction. It is not uncommon for 50% of all radiation scattered to be scattered at angles less than 10^{o} from the original, or forward, direction. While the phase functions tend to flatten out at low scattering angles in the visible and infrared portions of the spectrum, the phase function in the ultraviolet portion of the spectrum can increase by orders of magnitude as the scattering angle is decreased from 10^{o} to 0^{o}. Consequently, it is very important that suitable techniques be developed for measuring low angle scattering in the ultraviolet.

Three different techniques for measuring the single scattering phase function at angles below 10^{o} have been attempted in the present investigation. The first technique involves the use of the A.R.A.P. scanning polar nephelometer described below in Section 3.1 and in Reference 3. The scanning polar nephelometer is believed to be accurate down to an angle of 2^{o} from the forward direction. Since the phase functions measured below 10^{o} with this device often

do not agree with Mie theory calculations, it has been necessary to develop alternate techniques of measuring low angle scattering in order to verify the results obtained with the nephelometer.

A variable field of view attenuation coefficient measurement technique has been developed to determine the values of phase functions at scattering angles less than 10°. A radiometer with a half angle field of view of approximately 10° is pointed directly at an ultraviolet radiation source from a distance exceeding one kilometer. A portion of the radiation received by this radiometer can be attributed to scattered light while the remaining portion is due to directly transmitted radiation, from which the attenuation or extinction coefficient can be determined. As the radiometer angular field of view is decreased, the scattered portion of the radiation decreases while the directly transmitted radiation remains the same. As the angular field of view of the radiometer approaches zero, the received radiation can be associated entirely with directly transmitted radiation.

Since most of the scattered radiation observed with these narrow fields of view can be associated with atmospheric scattering at very low angles, it was hoped that the rate of change of received radiation with field of view angle could be used to back out the nature of the forward scattering phase functions at low angles. Unfortunately, the variable field of view attenuation technique proved unsuccessful due to

rapidly changing ozone and aerosol concentrations over the long source to detector pathlength.

A scattering technique using a variable field of view was therefore developed which required much shorter pathlengths. In this case, the radiometer was pointed directly at the radiation source with a fixed field of view and a billboard was placed between the radiation source and the radiometer. Openings were placed in the billboard permitting scattered radiation to enter the radiometer from predetermined angles while the directly transmitted radiation was blocked entirely. The success of the scattering technique was also limited, however, by rapidly changing weather conditions.

For those cases in which measured values of the single scattering phase functions did not agree with Mie theory predictions, attempts were made to achieve agreement through parametric variation of the real and imaginary portions of the refractive index. An attempt was also made to obtain independent information regarding the imaginary portion of the refractive index by measuring the absorption coefficient of the aerosol particles. The absorption coefficient of the aerosol particles was measured by subtracting the measured aerosol scattering coefficient (obtained by integrating the measured single scattering phase function) and the ozone absorption coefficient (obtained from ozone concentration measurements) from the measured extinction, or attenuation coefficient.

All of the measured single scattering phase functions measured over a one year period in a wide variety of weather conditions and geographic locations are presented in this report. The results of the various investigations to infer the characteristics of the single scattering phase functions at low scattering angles and the refractive indices of the ambient aerosols are also presented.

2. MEASUREMENT SITES

Ultraviolet single scattering phase functions were measured at four different geographic locations over the year-long measurement period. Thus, the measurements were made for a wide variation in both geographic location and weather conditions. Measurements were made at A.R.A.P.'s Princeton location from November of 1977 through the fall of 1978. A brief series of measurements were made at the Wayside laser test range at Ft. Monmouth, New Jersey on July 26 and July 28 of 1978. Measurements were made during the week of October 10-13, 1978 on San Nicolas Island in the Pacific Ocean. Measurements were also made in the desert at the Naval Weapons Center, China Lake, California during the week of October 17-20, 1978.

2.1 Princeton Site

A detailed topological map of the Princeton area is shown in Figure 1. The single scattering phase functions were measured at A.R.A.P. (the 3.6 km site) typically between 10:00 a.m. and 2:00 p.m. Total attenuation measurements were made from the .55 km, 1.2 km, and 2.3 km sites with the mercury-xenon lamp (source) placed at the top of Princeton University's Jadwin Physics Building.

2.2 Fort Monmouth Site

Infrared laser scattering measurements were made on July 24, 26 and 28, 1978 at the Wayside laser test range at

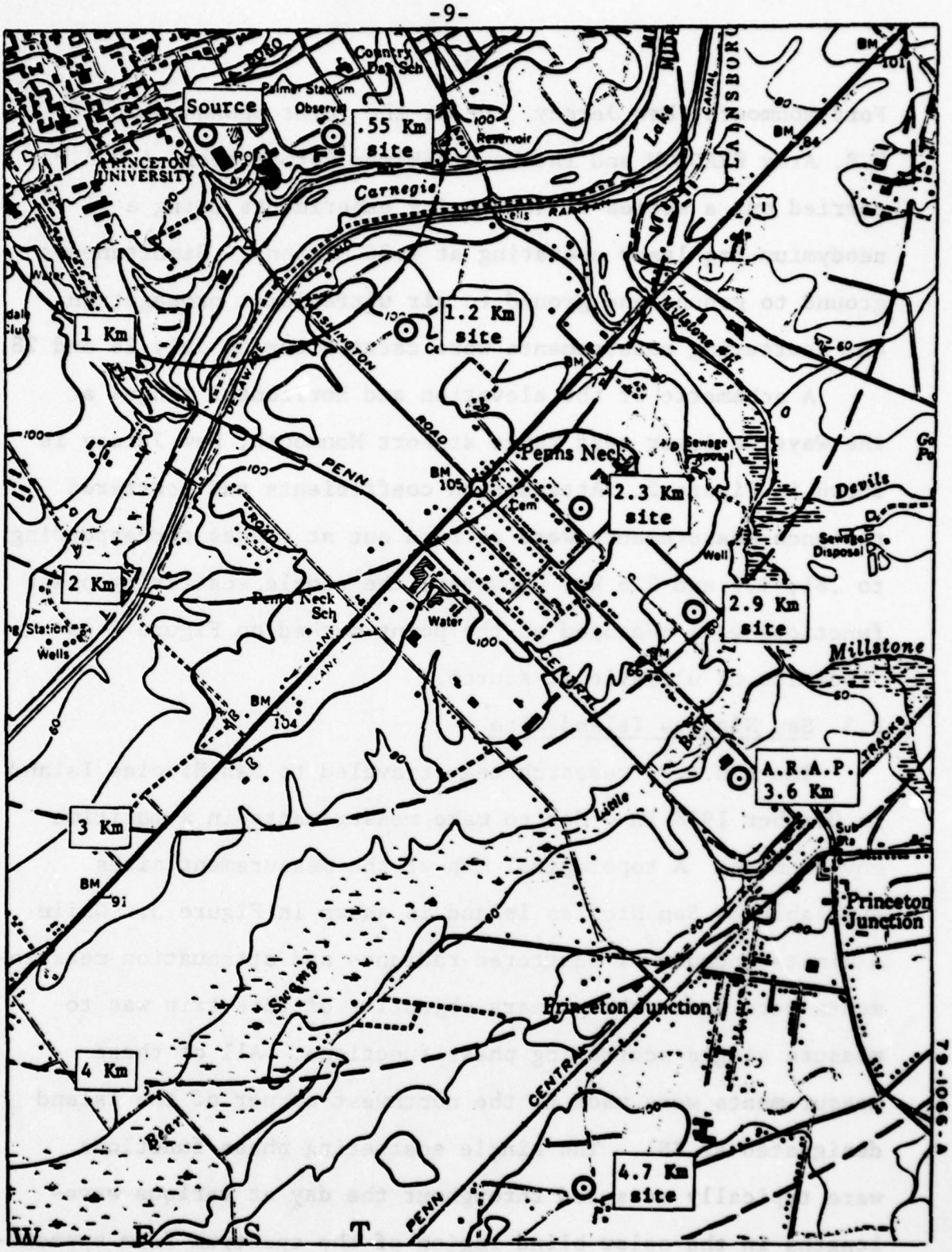

Figure 1. Topological Map of the Measurement Sites at Princeton, N.J.

Fort Monmouth, New Jersey. Under the joint sponsorship of U.S. Army ERADCOM and the Perkin-Elmer Corporation, A.R.A.P. carried out a series of scattering experiments using a neodymium-Yag laser operating at 1.06 microns. Simultaneous ground to ground and ground to air ultraviolet propagation and scattering measurements were carried out on July 26 and 28.

A schematic of the elevation and horizontal ranges at the Wayside laser test range at Fort Monmouth, New Jersey is shown in Figure 2. Attenuation coefficients and scattered radiance measurements were carried out at ranges corresponding to .81, 1.9 and 2.6 km. However, the single scattering phase functions were measured at the point marked on Figure 2 as "location of ultraviolet source."

2.3 San Nicolas Island Site

The A.R.A.P. research team traveled to San Nicolas Island in October 1978 in order to make measurements in a maritime environment. A topological map of the measurement sites available at San Nicolas Island is shown in Figure 3. While a limited number of scattered radiance and attenuation measurements were made, the primary objective of this trip was to measure single scattering phase functions. All of these measurements were made at the northwest corner of the island designated as SN1. The single scattering phase functions were typically measured throughout the day at various wavelengths in the solar blind region of the spectrum from approximately 8:00 a.m. to 11:00 p.m.

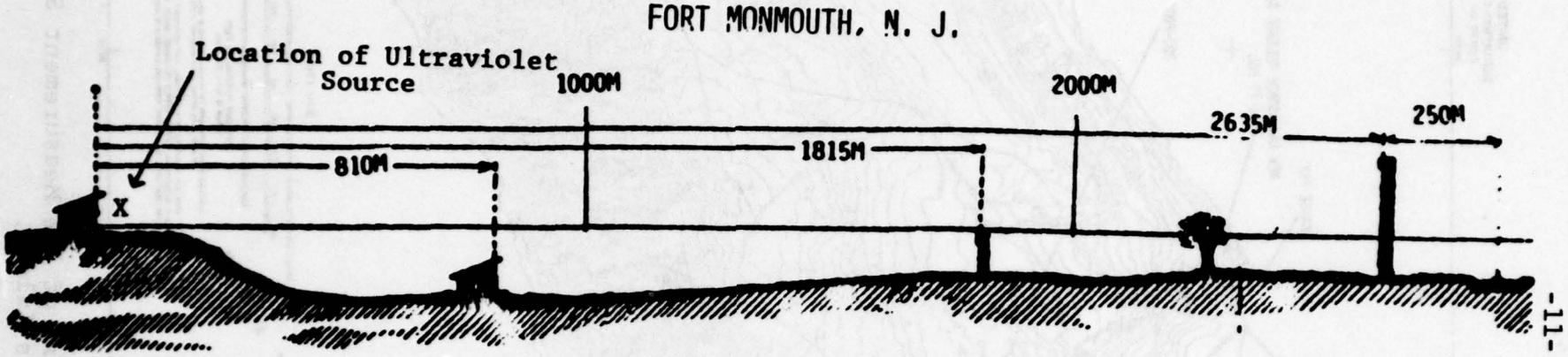

Figure 2. Elevation Map of Wayside Measurement Range at Fort Monmouth, New Jersey.

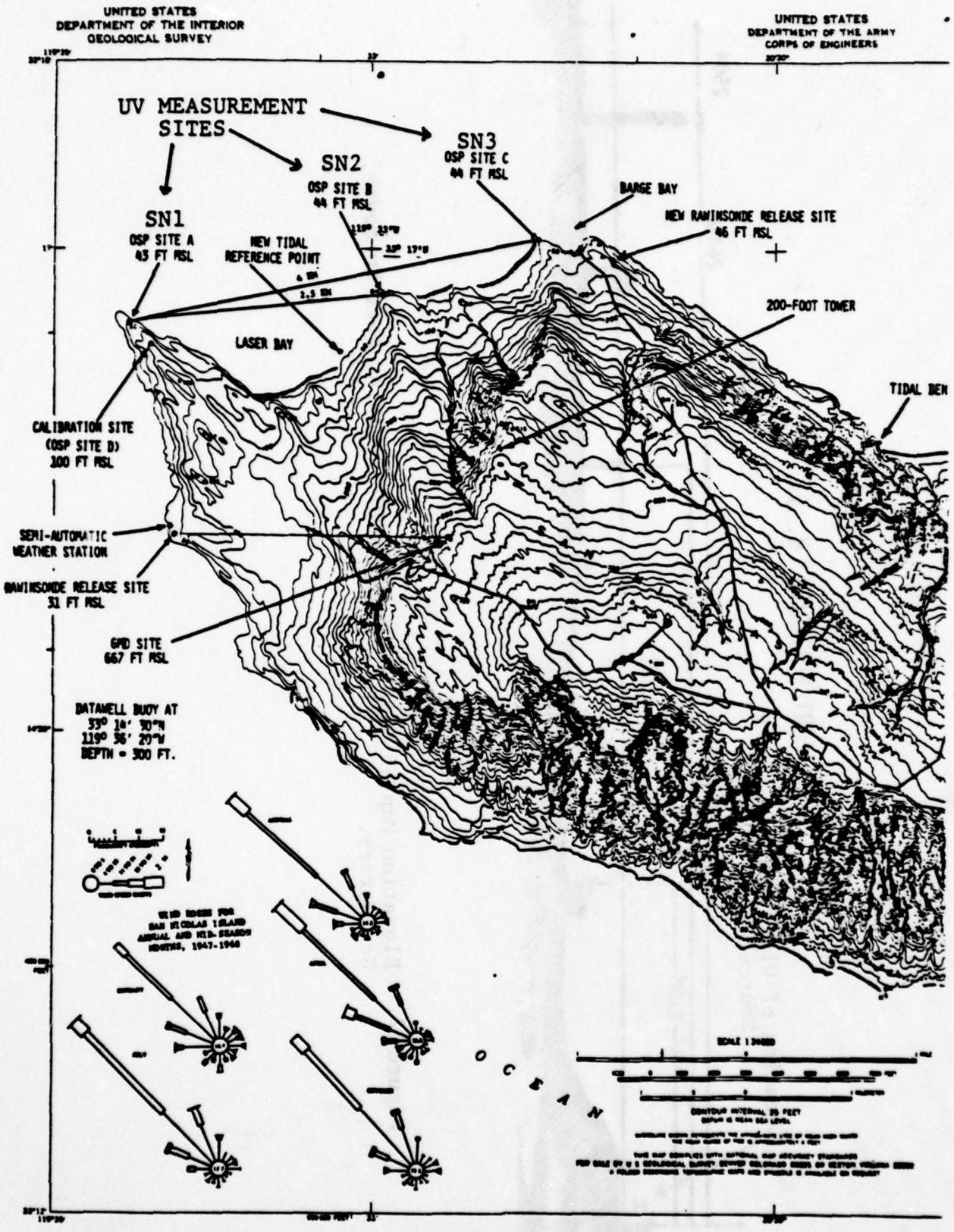

Figure 3. Topological Map of the Measurement Sites at San Nicolas Island.

2.4 China Lake Site

Following the trip to San Nicolas Island, the A.R.A.P. research team traveled to the Naval Weapons Center located at China Lake, California to make scattered radiance measurements using a KrF excimer laser under contract N60530-78-C-0227. Single scattering phase functions and the prevailing atmospheric conditions were measured in conjunction with the laser scattering measurements. A topological map showing the Naval Weapons Center and the location over which laser scattering measurements were made is shown in Figure 4. The single scattering phase functions were measured on the roof of the Lauristen Laboratory which is located at the center of the circle in the lower righthand corner of the map.

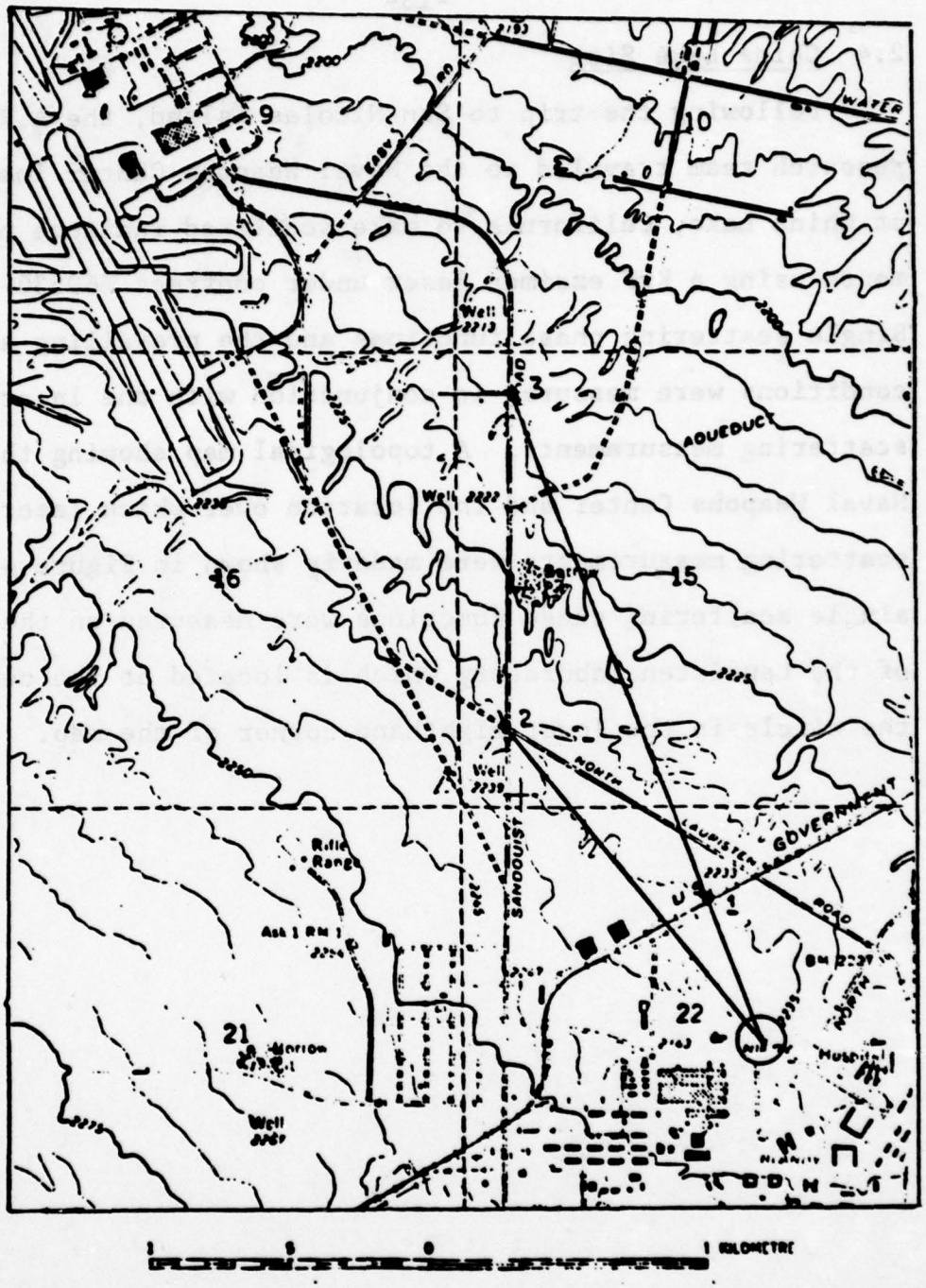

Figure 4. Topological map of the NWC at China Lake, CA.

3. EXPERIMENTAL APPARATUS AND TECHNIQUES

A detailed description of the experimental apparatus and techniques used to measure the single scattering phase functions is given in Reference 3. Therefore, only a brief overview of the procedure will be presented here.

3.1 Equipment for Measuring Single Scattering Phase Functions

A schematic of the apparatus used to measure the single scattering phase functions is shown in Figure 5. The source of the ultraviolet radiation is a Model 6111 Oriel Universal Arc Lamp which incorporates a 200 watt HgXe arc lamp. An Oriel Model 6207 Ultracollimator which was specifically modified by the Oriel Corporation to operate in the ultraviolet, has been added to the lamp to provide a clean, incident beam. The lamp is mounted on the end of a rotating 4 ft aluminum channel that allows for any scattering angle from 0 to 170°.

The detector assembly consists of a collecting lens, a Jarrell-Ash Model 82-410 quarter meter monochrometer, a spectral filter and a phototube. The collecting lens is mounted in front of the entrance slit of the monochrometer at a distance equal to its focal length. The phototube is an EMR photoelectric 542P with rubidium telluride photocathode. The quantum efficiency of this tube is 10% in the range of 200 to 250 nm and drops to about 1% at 300 nm. A series of filters is used together with the photomultiplier tube to

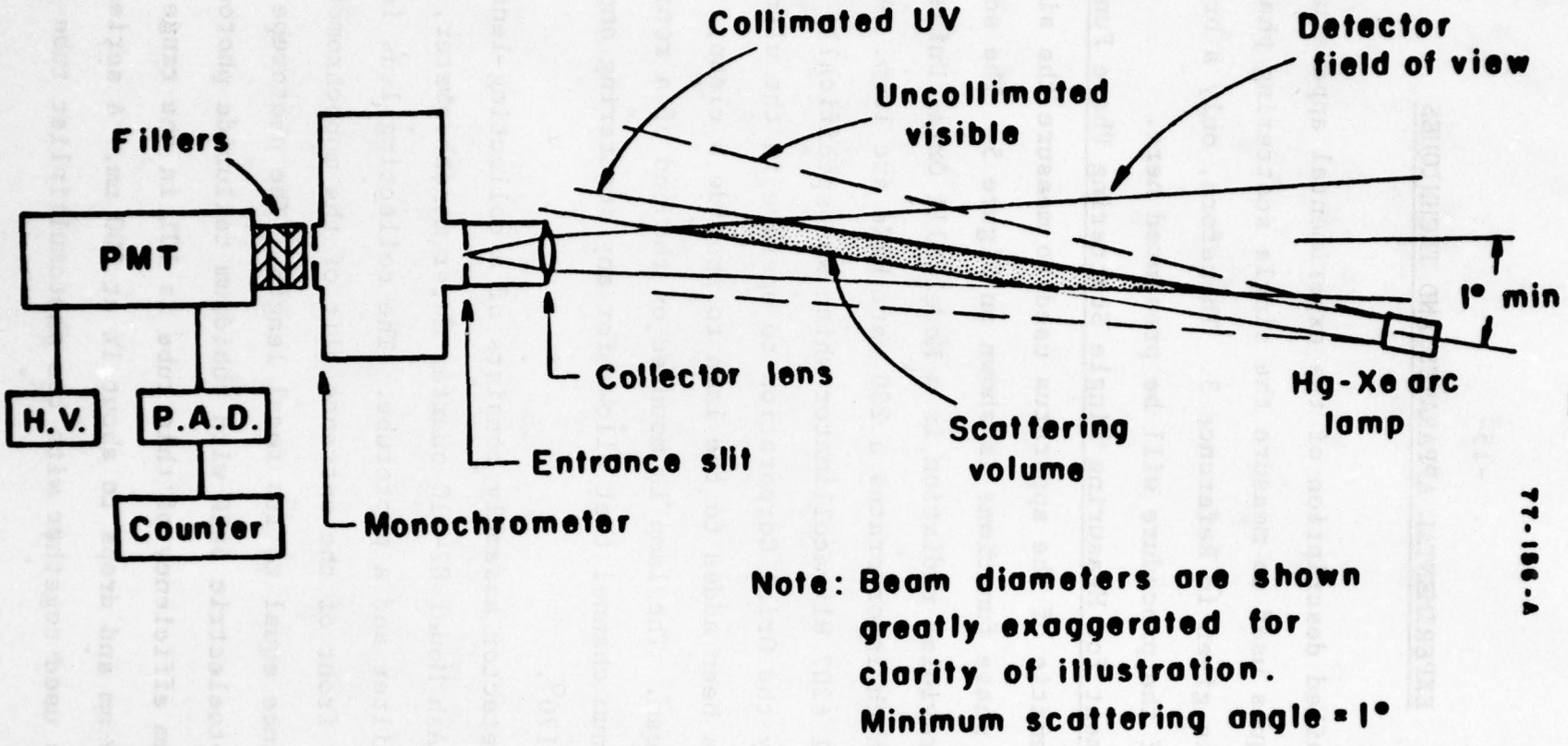

Figure 5. A.R.A.P. scanning UV nephelometer.

improve the stray light rejection provided by the monochrometer. These filters are especially necessary at low scattering angles (2^{o}-5^{o}) where the visible and near ultraviolet light from the source lamp (which is out of focus) actually falls directly on the collector lens.

In order to measure the single scattering phase function at low angles (less than 5^{o}) it is essential that the stray light rejection of the detection system be maximized and that any stray light that does get through be subtracted. The detector field of view is restricted in the scattering plane to 0.1^{o} for scattering angles of 2^{o} to 5^{o}. The use of filters and the monochrometer together effectively removes all stray light at wavelengths other than that being measured. However, the filter and monochrometer are unable to remove stray light at the wavelength being measured.

While the optical system has been designed so that no light at the wavelength being measured could enter the detector unless it was scattered by the aerosols and molecules in the scattering volume, a series of tests were performed to prove that stray light had been rejected. A large plastic bag was used to completely surround the phase function device and the bag was first filled with room air and then with dry nitrogen. For the case that the bag was filled with room air, the scattering signal was equal to that which was observed without the bag. For the case that the bag was filled with dry aerosol-free nitrogen, it was determined that the measured

phase function was only 11% above that due to Rayleigh scattering alone at an angle of 2^{o}, and 3% above the Rayleigh scattering value at an angle of 3^{o}. The small errors which can be attributed to stray light are insignificant compared to the total aerosol and molecular scattering at these low angles. At angles above 4^{o} no stray light was observed and the measured phase functions corresponded to those predicted theoretically from Rayleigh scattering theory.

In order to determine the distribution of radiation within the beam coming from the HgXe lamp and ultracollimator, it was necessary to make detailed measurements of the beam intensity at several axial locations. The results of the measurements are shown in Figure 6 for positions along the beam corresponding to the center of the scattering volume and the collecting lens position at which the absolute intensity of the beam is measured. The measurements shown in Figure 6 have been carried out for a wavelength of 250 nm.

3.2 Equipment Used for Atmospheric Documentation Measurements

Aerosol concentrations and size distributions have been measured with a Thermo Systems Model 3030 Particle Size Analyzer and a Particle Measuring Systems, Inc., Knollenberg, analyzer. The Knollenberg particle size analyzer (PDS Model 200 with ASASP-300 and CSASP-100HV heads) measures particle sizes between .075 and 16 microns radius, while the Thermo Systems analyzer measures particle sizes between 0.015 and .5 microns. Humidity measurements were made using an aspirated

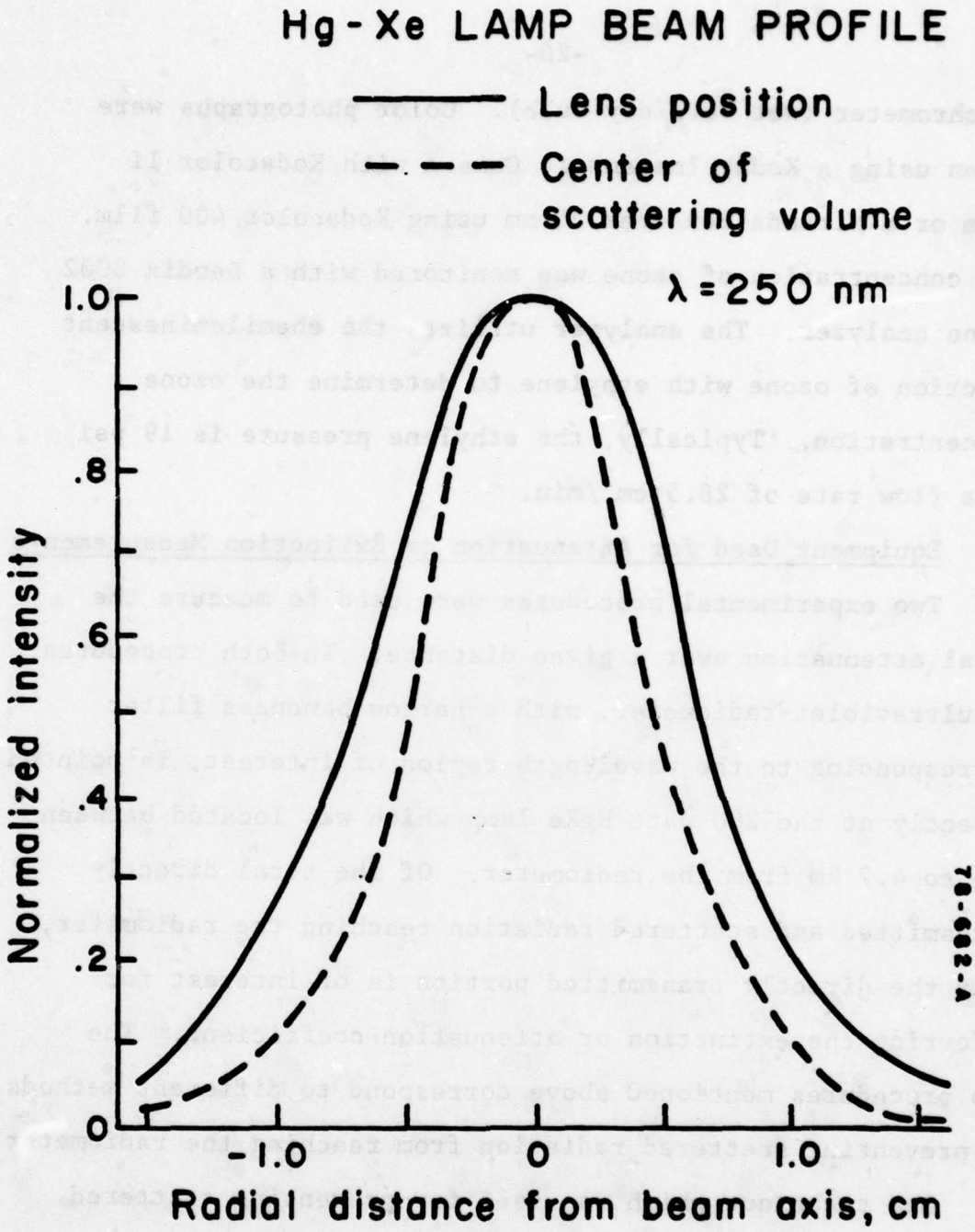

Figure 6. Hg-Xe lamp beam profile.

psychrometer (wet bulb/dry bulb). Color photographs were taken using a Kodak Instamatic Camera with Kodacolor II film or a Miranda Sensorex 35 mm using Kodacolor 400 film. The concentration of ozone was monitored with a Bendix 8002 ozone analyzer. The analyzer utilizes the chemiluminescent reaction of ozone with ethylene to determine the ozone concentration. Typically, the ethylene pressure is 19 psi at a flow rate of 28.5 cm^3/min.

3.3 Equipment Used for Attenuation or Extinction Measurements

Two experimental procedures were used to measure the total attenuation over a given distance. In both procedures, an ultraviolet radiometer, with a narrow bandpass filter corresponding to the wavelength region of interest, is pointed directly at the 200 watt HgXe lamp which was located between .55 to 4.7 km from the radiometer. Of the total directly transmitted and scattered radiation reaching the radiometer, only the directly transmitted portion is of interest for inferring the extinction or attenuation coefficient. The two procedures mentioned above correspond to different methods of preventing scattered radiation from reaching the radiometer.

One technique which was used for preventing scattered radiation from being measured was to place an iris at the focal point of the collecting lens in front of the photo-multiplier tube. As the iris was closed down, the angular field of view of the radiometer became smaller and smaller thus preventing off-axis scattered radiation from reaching

the photomultiplier tube. The field of view of the radiometer could be varied from 1.5 to 15° half angle as the iris was opened or closed.

The second technique for preventing scattered radiation from being measured was to place a long tube on the front of the radiometer with a very narrow field of view. A two foot long aluminum tube with either 1/8" diameter apertures of 1/4" diameter apertures at each end is used to provide a half angle field of view of either 0.3° or 0.6°, respectively. To eliminate scattering within the tube, a number of light baffles with holes concentric to the tube axis were placed inside the tube.

3.4 Billboard Technique for Low Angle Scattering Measurements

Both the billboarding technique described in this section and the variable field of view attenuation procedure described above can be used to directly measure the angular distribution of scattered light incident on the receiver for angles of less than 10° from the source to receiver line of sight. This scattering data can be used together with the A.R.A.P. atmospheric propagation and scattering model to back out or infer values of the single scattering phase function at low scattering angles. It should be remembered that the scattered radiation received at a given detector angle is the summation of radiation scattered at a large number of angles corresponding to many different scattering volume elements within the detector field of view at the angle in question. The convolution

of the single scattering phase function into the angular distribution of scattered radiance measured at the detector is quite complex.

A schematic diagram of the apparatus used in the billboarding technique is shown in Figure 7. A billboard was placed 10.3 ft in front of the UV radiometer and 745 ft from the 200 watt HgXe lamp. The billboard contained a semicircular cutout for which both the inner and outer radius could be varied to change the detector's field of view. Directly transmitted radiation was blocked by placing a small semicircular stop on the billboard along the detector to source axis. Semicircular cutouts were used as opposed to full circular cutouts to prevent the observation of ground reflections. In order to obtain better angular definition between the finite sized detector aperture and the billboard cutouts, the collecting aperture of the radiometer was limited to a 1/2" diameter. The 1/2" diameter aperture located 10.3 ft from the billboard cutouts resulted in a .23^{o} angular resolution.

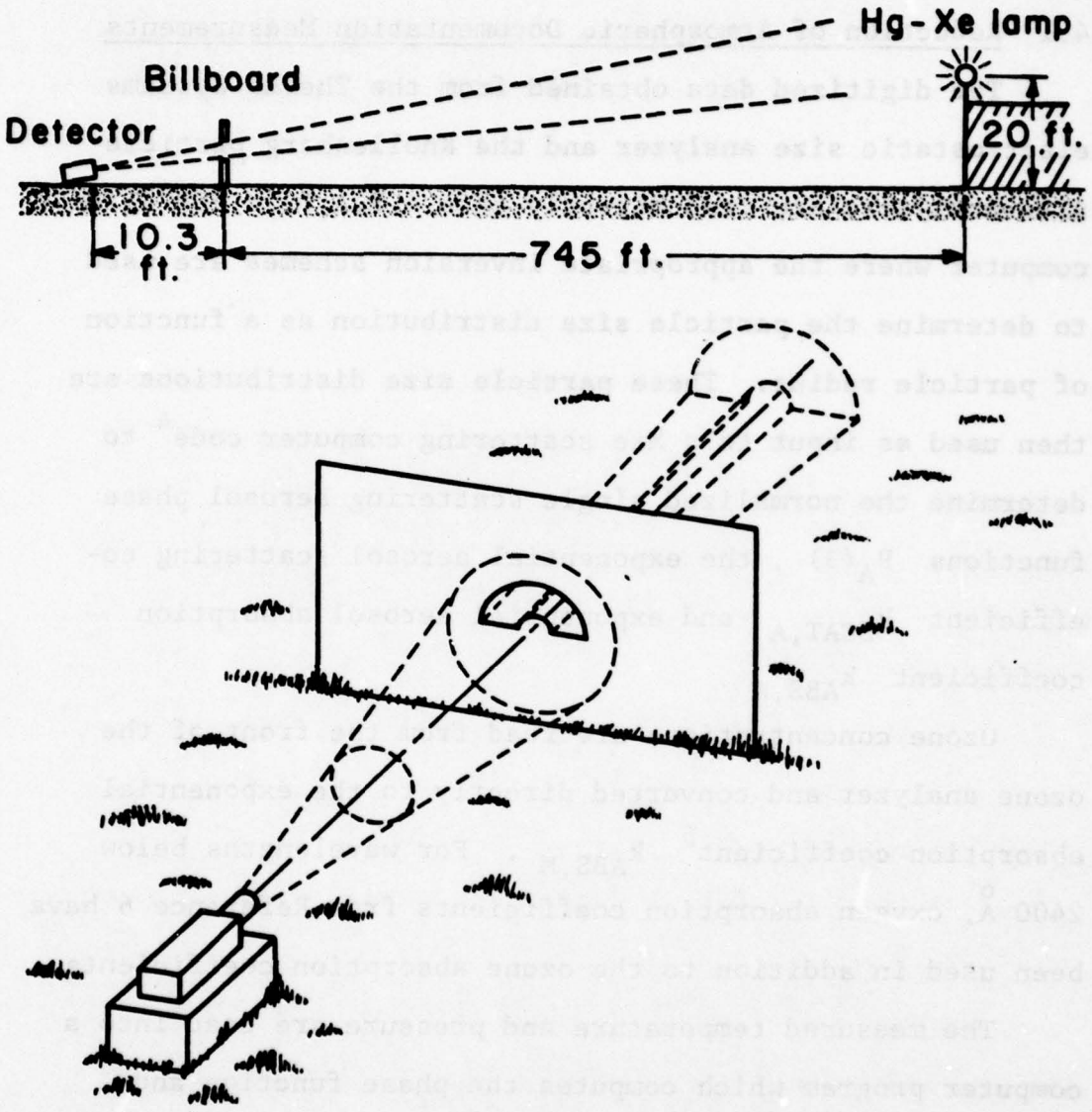

Figure 7. The Billboard experiment used to measure scattered UV radiance at angles less than seven degrees.

4. DATA REDUCTION PROCEDURES

4.1 Reduction of Atmospheric Documentation Measurements

The digitized data obtained from the Thermo Systems electrostatic size analyzer and the Knollenberg particle size analyzers are read directly into A.R.A.P.'s PDP 1170 computer where the appropriate inversion schemes are used to determine the particle size distribution as a function of particle radius. These particle size distributions are then used as input to a Mie scattering computer code[4] to determine the normalized single scattering aerosol phase functions $P_A(\theta)$, the exponential aerosol scattering coefficient $k_{SCAT,A}$ and exponential aerosol absorption coefficient $k_{ABS,A}$.

Ozone concentrations are read from the front of the ozone analyzer and converted directly to the exponential absorption coefficient[5] $k_{ABS,M}$. For wavelengths below 2400 $\mathring{A}$, oxygen absorption coefficients from Reference 6 have been used in addition to the ozone absorption coefficients.

The measured temperature and pressure are read into a computer program which computes the phase function and exponential scattering coefficient due to molecular scattering. The relative humidity is used to predict a refractive index which is used as an input to the Mie scattering code discussed above.

A predicted extinction coefficient is determined by

summing the exponential scattering and absorption coefficients due to aerosols and molecular species. Likewise, the theoretical single scattering phase function is determined by summing the phase functions due to aerosol and molecular scattering. These theoretical extinction coefficients and phase functions are compared to those measured in the field.

The ground level photographs taken at the Princeton site are examined to determine a visibility for each day that measurements are carried out. A series of water towers appearing along the horizon at known distances are used as an indication of the visibility. It is recognized that this technique does not yield true visibility as it is affected strongly by the total light level and by contrast problems. However, this form of visibility is closely related to that which would be observed with the naked eye on a given day and therefore may be quite relevant to some applications.

4.2 Reduction of Single Scattering Phase Function Data

A ray tracing computer program is used to reduce the single scattering phase function data. A schematic of the technique used in the ray tracing program is shown in Figures 8 and 9. Each small volume element within the scattering volume such as dV_1 and dV_2 are followed through the collecting lens and into the monochrometer entrance slit. As can be seen from Figure 9, not all of the radiation from the volume element dV_2 would pass through the collecting lens and therefore, radiation from this position would be

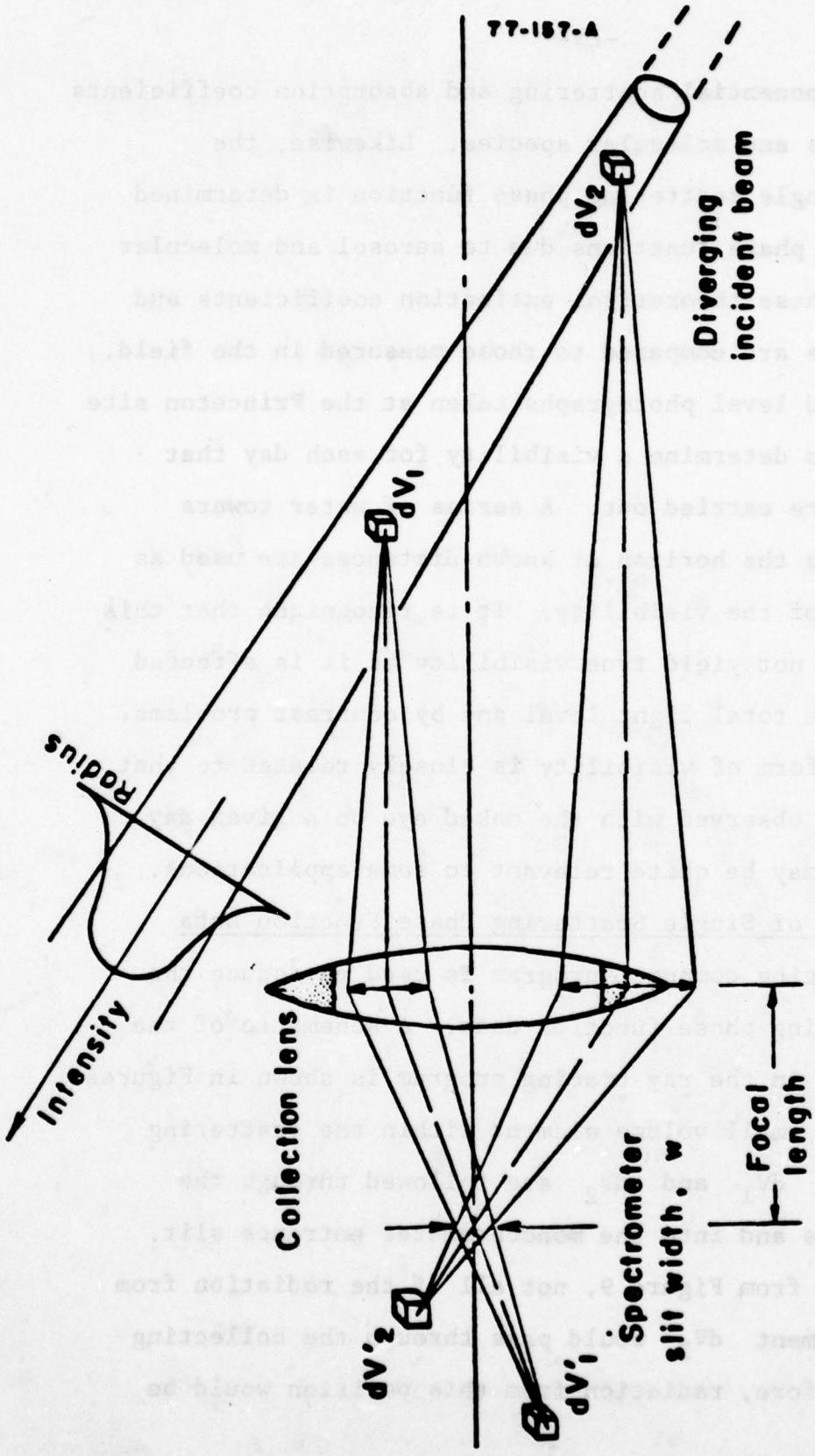

Figure 8. Schematic of Ray Tracing Program.

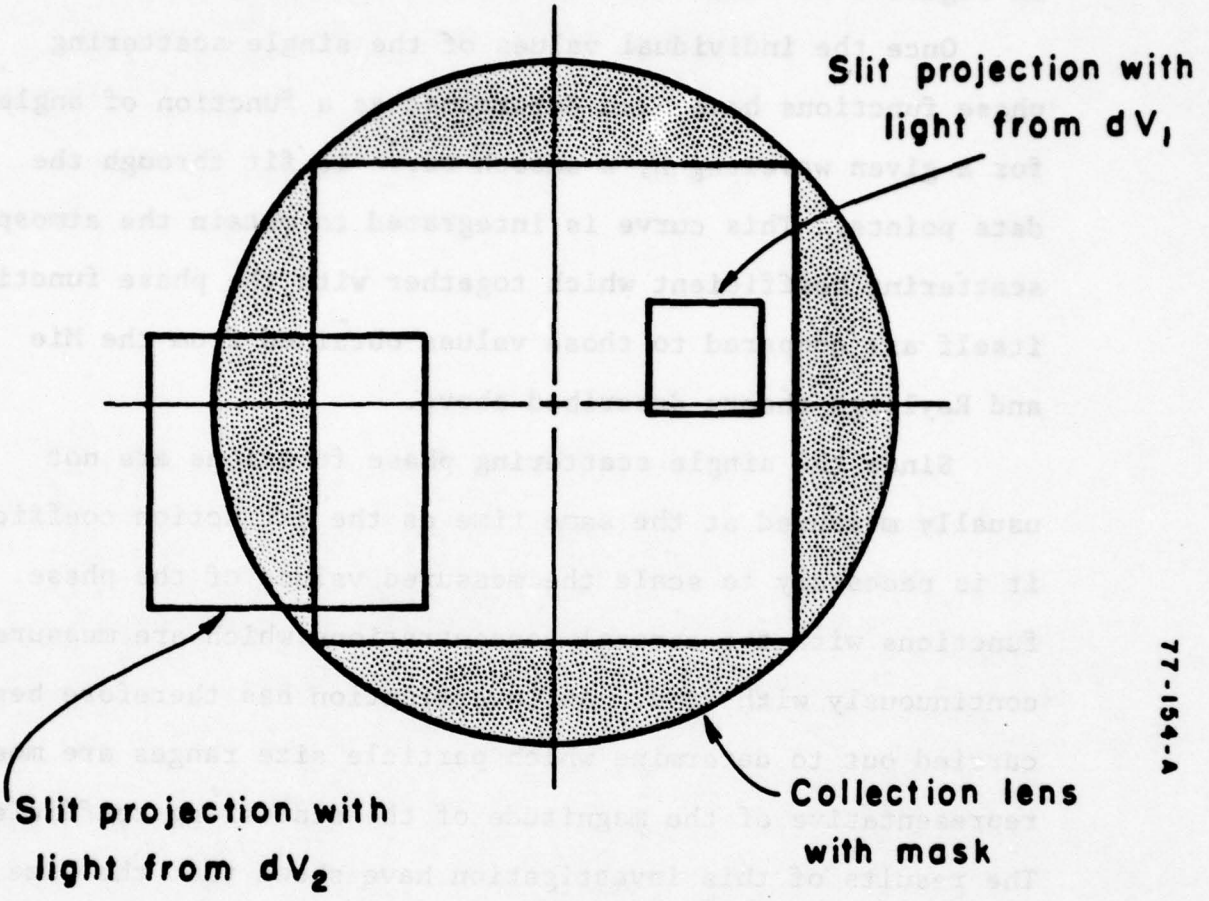

Figure 9. Slit Projections on Collecting Aperture.

reduced accordingly. The intensity profile of the beam shown in Figure 6 is taken into account in this program.

Once the individual values of the single scattering phase functions have been determined as a function of angle for a given wavelength, a smooth curve is fit through the data points. This curve is integrated to obtain the atmospheric scattering coefficient which together with the phase function itself are compared to those values obtained from the Mie and Rayleigh theory described above.

Since the single scattering phase functions are not usually measured at the same time as the extinction coefficients, it is necessary to scale the measured values of the phase functions with the aerosol concentrations which are measured continuously with time. An investigation has therefore been carried out to determine which particle size ranges are most representative of the magnitude of the scattering coefficient. The results of this investigation have shown that the size range about .25 microns is the most representative of the relative contribution to the scattering coefficient from the various particle sizes. Therefore, the time varying scattering coefficient is assumed to be proportional to the aerosol number density within this size range while the normalized phase function is assumed to be constant. In a similar fashion, the ozone absorption coefficient is varied according to the time dependent ozone concentration measurements.

The scattering coefficient k_{SCAT} is obtained by

integrating the single scattering phase function over three dimensional space according to Equation 3. The scattering

$$k_{SCAT}(\lambda) = 2\Pi \int_{o}^{\Pi} F(\theta)\sin(\theta)d\theta \qquad (3)$$

coefficients obtained for the measured phase functions are recorded on the same figures on which the measured phase functions are presented (see Appendix A). When Mie scattering calculations are carried out for the measured aerosol particle size distributions, theoretical values of the single scattering phase functions are obtained. A comparison of the measured and theoretical phase functions are also given in the figures presented in Appendix A.

4.3 Attenuation Measurements

The total attenuation or extinction coefficient k_{EXT} along a given pathlength R is determined by Equation 4

$$k_{EXT} = \frac{1}{R} \ln \frac{I}{I_o} \qquad (4)$$

where I is the directly transmitted radiant intensity measured at a distance R from the radiation source and I_o is the radiant intensity which would be measured in a vacuum at a distance R from the radiation source. In order to use Equation 4 to solve for the extinction coefficient, it is necessary to have an absolute intensity calibration of the source-radiometer combination. As an alternative, the attenuation coefficient can be obtained by ratioing the directly transmitted radiation measured at two different

locations. In this case, the vacuum intensity need not be known and the extinction coefficient is given by Equation 5

$$k_{EXT} = \frac{1}{R_2 - R_1} \ln \left[\frac{R_1^2}{R_2^2} \frac{I_1}{I_2} \right] \tag{5}$$

where I_1 and I_2 are the directly transmitted intensities measured at distances R_1 and R_2 from the radiation source respectively. Both of these methods have been used to analyze the attenuation data.

For the case that the radiometer with the variable field of view was used to measure the directly transmitted radiation, the following procedure was generally followed. For each field of view angle, the received signal was substituted into Equation 4 as the directly transmitted radiant intensity. The "extinction coefficient" obtained in this manner was then plotted as a function of the steradiancy associated with that field of view angle. As the field of view angle, or steradiancy decreased, the effective or apparent extinction coefficient would be expected to increase as the scattered light is reduced and the ratio of I/I_o decreases. The "apparent" extinction coefficients versus detector steradiancy or field of view angle have been plotted in this fashion in order that the results could be extrapolated to the zero field of view case. Since a real detector must always have a finite field of view and therefore would always admit some scattered light, this technique would supposedly allow one to determine what

the directly transmitted radiation alone would have been if a zero degree field of view detector had actually been used. Unfortunately, as will be discussed in Section 5.5, the "apparent" attenuation coefficient did not always increase as the field of view angle was decreased. Evidently, rapid changes in the concentrations of ozone and aerosol species along the transmission path occasionally cause the apparent attenuation coefficient to decrease as the field of view angle is decreased. This effect will be discussed further in Section 5.5.

5. DATA AND ANALYSIS

The ultraviolet single scattering phase functions measured over an entire one year period in a wide variety of weather conditions and geographic locations are presented in Appendix A. Most of the measurements were carried out at A.R.A.P.'s Princeton location which is a rural area subject to intermittent industrial pollution from Trenton and Philadelphia. A relatively large number of measurements were carried out during the month of October at San Nicolas Island, which is assumed to represent a typical maritime atmosphere. Measurements were also carried out during the month of October at the Naval Weapons Center at China Lake, California which should represent a typical desert type atmosphere. Finally, a limited number of measurements were carried out in July at the Fort Monmouth Wayside laser test range which is basically a rural, wooded area.

The data in Appendix A are presented on a day-by-day basis in chronological order. The first page of each day's data contains a ground level photograph showing prevailing weather conditions, a general description of the weather conditions, the visibility, temperature, humidity, ozone concentration, ozone absorption coefficient, and the wavelength dependent total scattering coefficients. The particle size distributions and measured phase functions are then presented according to the time sequence in which they were measured.

For most of the measured phase functions a theoretical phase function is also presented. The theoretical phase function is the summation of the theoretical aerosol scattering phase function computed for the measured particle size distribution and the Rayleigh phase function computed from the measured temperature and pressure.

Appendix A represents a broad data base of single scattering phase functions and particle size distributions measured in the solar blind portion of the spectrum between 230 and 280 nm. Table 1 gives a summary of the data presented in Appendix A. The entries for the scattering coefficient are in some cases "representative" values out of several that may have been measured on that day.

5.1 Seasonal Variations

For the year round measurements made at A.R.A.P.'s Princeton location, large variations in both the shape and magnitude of the single scattering phase function have been observed at all wavelengths. Phase functions measured in fogs are typically the highest in magnitude and exhibit very strong forward peaking. With the exception of the fogs, the phase functions measured in the spring and summer are generally higher in magnitude than the phase functions measured in the fall and the winter. For a wavelength of 265 nm, typical single scattering phase functions measured in December of 1977, January 1978 and April of 1978 are presented in Figure 10. In keeping with the general trend, the phase function

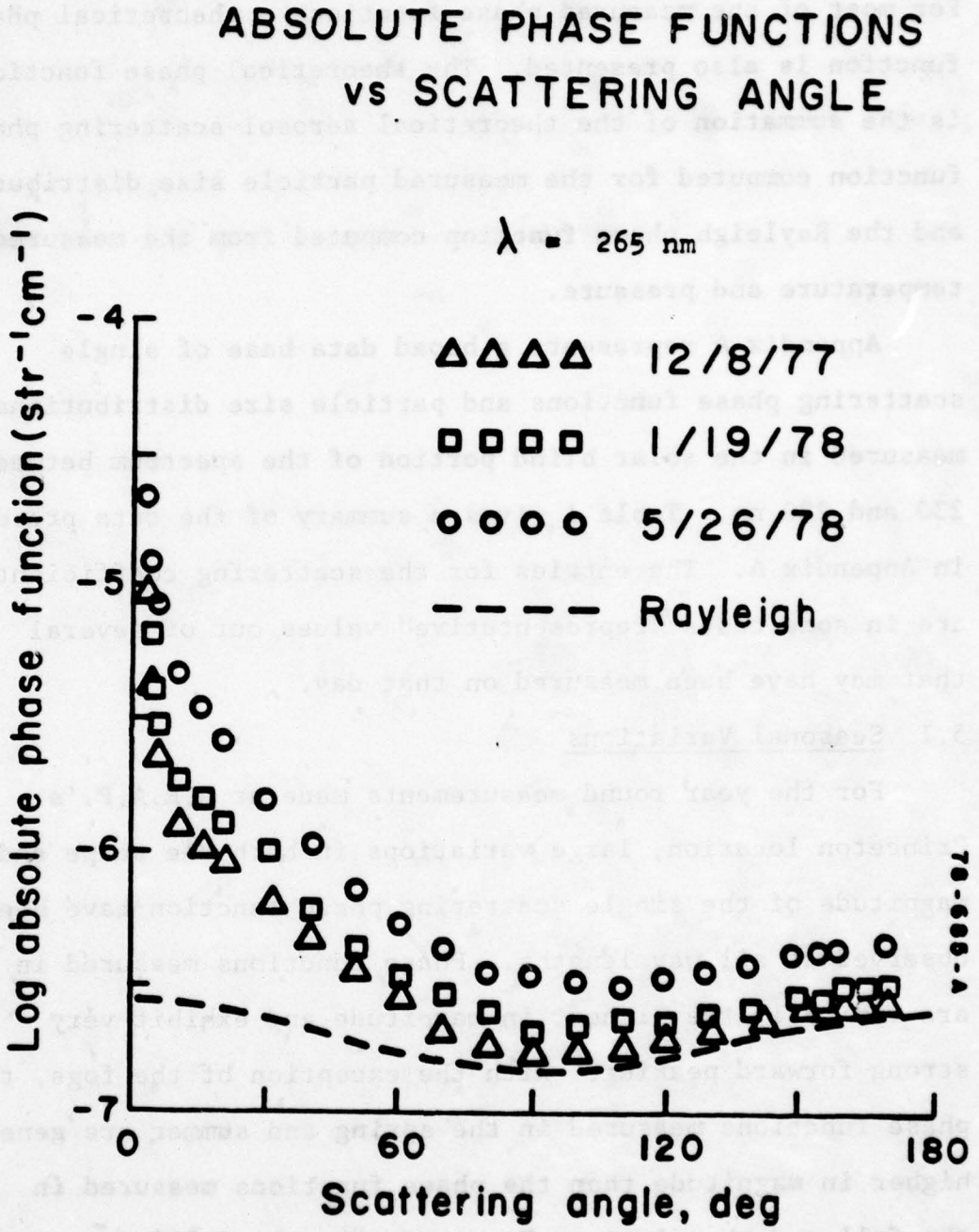

Figure 10. Seasonal variations of the single scattering phase function measured at 265 nm.

SUMMARY OF DATA

DATE	WEATHER	VIS (km)	TEMP (°F)	HUM (%)	OZONE		TOTAL $k_{SCAT}(km^{-1})$			
					PPM	$k_{ABS}(km^{-1})$	230NM	250NM	265NM	280NM
11/9/77	overcast, low ceiling, moderate haze	10	64	65	0.002	0.05	-	0.86	1.07	-
11/16/77	partly cloudy, low haze	25	61	40	0.0005	0.01	-	0.66	0.62	-
11/21/77	overcast, intermittant rain	15	53	75	0.001	0.025	-	0.42	-	-
11/22/77	overcast, intermittant rain, icing at 4700 ft	30	45	70	0.0004	0.01	-	0.37	-	-
11/23/77	overcast, foggy, 200 ft ceiling	2	41	100	0.0	0.0	-	1.58	-	1.95
11/29/77	overcast, snow, sleet	1.5	33	100	0.0	0.0	1.58	1.40	-	1.93
12/1/77	heavy ground fog	0.2	47	100	0.0	0.0	5.43	3.49	-	7.36

TABLE 1.

SUMMARY OF DATA

DATE	WEATHER	VIS (km)	TEMP (°F)	HUM (%)	OZONE		TOTAL $k_{SCAT}(km^{-1})$			
					PPM	$k_{ABS}(km^{-1})$ λ=265NM	230NM	250NM	265NM	280NM
12/8/77	clear, sunny	25	31	-	0.025	0.63	0.56	0.50	0.38	0.33
12/9/77	overcast → clear	20	39	90	0.012	0.30	.81	1.04	0.56	0.58
1/19/78	overcast, thermal inversion, snow on ground	10	27	-	0.002	0.05	.61	.46	0.48	0.32
4/7/78	partly cloudy, low haze	20	65	48	0.03	0.076	-	1.24	0.92	0.87
5/26/78 AM	overcast, moderate haze	15	71	70	0.028	0.71	0.87	0.96	0.82	0.66
5/31/78 AM	overcast, high haze	10	76	70	-.10	2.53	-	1.05	-	-

TABLE 1.
(continued)

TABLE 1

SUMMARY OF DATA

DATE	WEATHER	VIS (km)	TEMP (°F)	HUM (%)	OZONE		TOTAL $k_{SCAT}(km^{-1})$			
					PPM	$k_{ABS}(km^{-1})$ λ=265NM	230NM	250NM	265NM	280NM
7/26/78	clear	25	75	71	0.007	.18	-	.62	.60	-
7/28/78	rain, haze	8	79	73	0.02	.50	-	-	1.34	-
8/31/78	rainy day; high mist	8	78	83	0.04	1.00	-	-	1.41	-
9/22/78	cloudy-hazy	12	74	84	0.005	.13	-	-	1.35	-
10/10/78	sunny, variable fog	5	65	90	-	-	1.03	-	0.80	1.33
10/11/78	variable fog	1.5	63	89	-	-	1.19	1.42	1.49	1.15
10/12/78	clear, sunny a.m. - heavy fog p.m.	15 to 1.5	65	86	0.082	2.06	1.19	1.09	.81	.87
10/13/78	layered fog	1.5	62	94	0.075	1.88	2.31	3.4	-	1.5
10/17/78	clear, hazy	25	85	12	0.075	1.88	-	.49	.31	-
10/18/78	clear, hazy	25	80	15	0.09	2.26	-	.58	.57	-
10/19/78	clear, hazy	25	75	21	0.06	1.51	-	.45	.31	-
10/20/78	rain, cloudy	10	65	65	0.06	1.51	-	.81	-	-
1/31/79	cloudy, over-cast	10	34	50	-	-	-	-	1.08	-

measured in the spring is higher than that measured in the winter. It should be pointed out, however, that large variations in the single scattering phase function at a given wavelength can occur over a period of one week or even one day. Phase functions measured the week of July 13 through July 20, 1977 (Reference 3) for a wavelength of 248.5 nm is shown in Figure 11. As can be seen from Figure 11, nearly an order of magnitude difference in the absolute phase function can be observed at low scattering angles during this one week period. Also shown in Figure 11 is a single scattering phase function measured in a fog on September 2, 1977. Comparisons of the magnitude of the phase functions measured in the fog with those measured on the 14th of July indicate that nearly a two order of magnitude difference in the single scattering phase function can be observed in the same season of the year.

Comparisons between measured phase functions and those predicted from Mie and Rayleigh scattering theory are generally more successful in the fall and winter months than during the spring and summer. It can be seen from Appendix A that measured phase functions in the spring and summer months are typically larger than those predicted. The magnitudes of phase functions not only vary strongly from day to day, but typically vary by two to four orders of magnitude as the scattering angle increases from 0^{o} to 180^{o}. If, on an absolute scale, the measured and predicted values of the phase functions agree to within a factor of 1.5 at all scattering

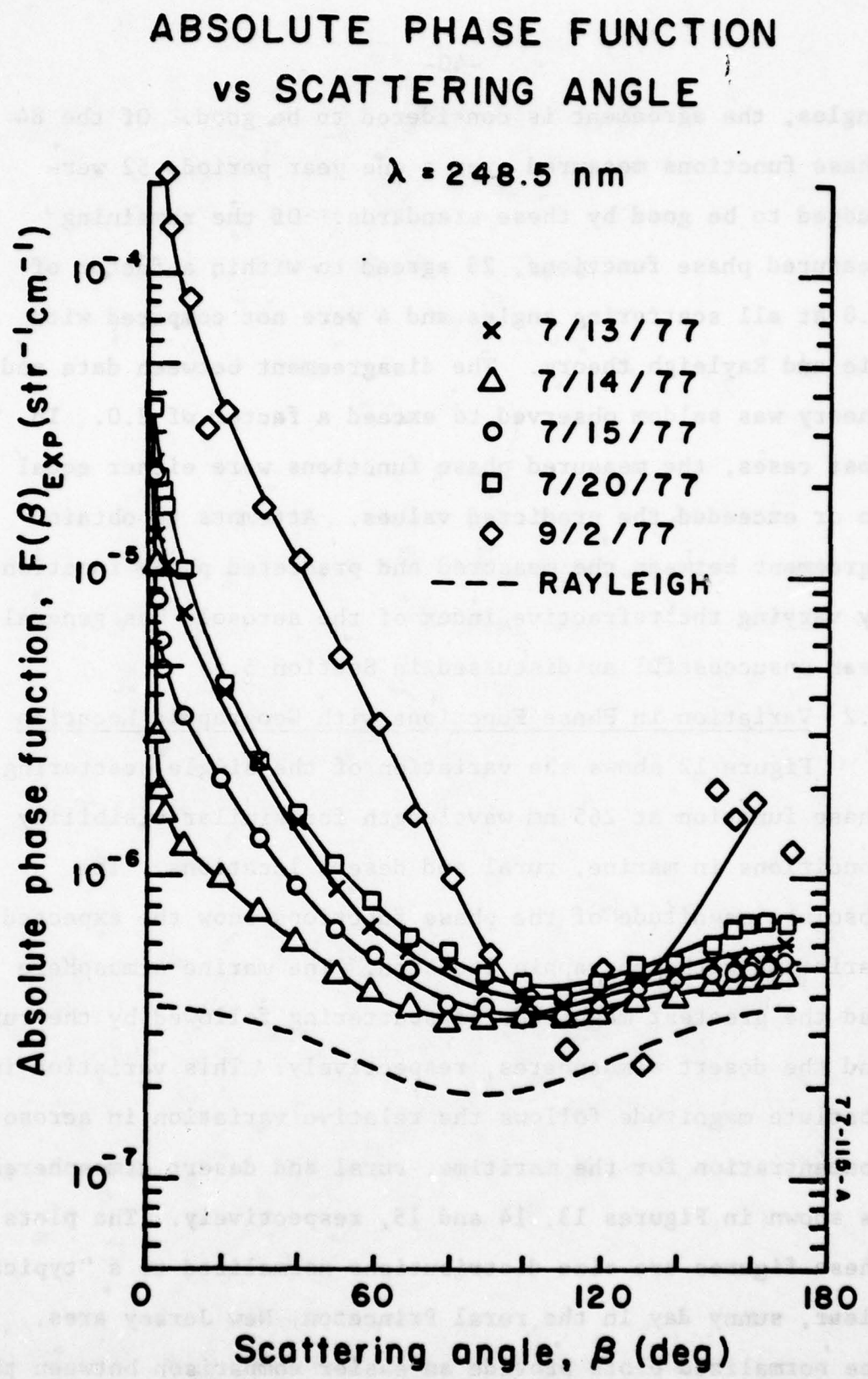

Figure 11. Seasonal variations of the single scattering phase function measured at 248.5 nm.

angles, the agreement is considered to be good. Of the 84 phase functions measured over a one year period, 52 were judged to be good by these standards. Of the remaining measured phase functions, 28 agreed to within a factor of 2.0 at all scattering angles and 4 were not compared with Mie and Rayleigh theory. The disagreement between data and theory was seldom observed to exceed a factor of 2.0. In most cases, the measured phase functions were either equal to or exceeded the predicted values. Attempts to obtain agreement between the measured and predicted phase functions by varying the refractive index of the aerosols has generally been unsuccessful as discussed in Section 5.4

5.2 Variation in Phase Functions with Geographic Location

Figure 12 shows the variation of the single scattering phase function at 265 nm wavelength for similar visibility conditions in marine, rural and desert locations. The absolute magnitude of the phase functions show the expected variation with geographic location. The marine atmosphere had the greatest magnitude of scattering followed by the rural and the desert atmospheres, respectively. This variation in absolute magnitude follows the relative variation in aerosol concentration for the maritime, rural and desert atmospheres as shown in Figures 13, 14 and 15, respectively. The plots in these figures are size distributions normalized to a "typical" clear, sunny day in the rural Princeton, New Jersey area. The normalized plots provide an easier comparison between the

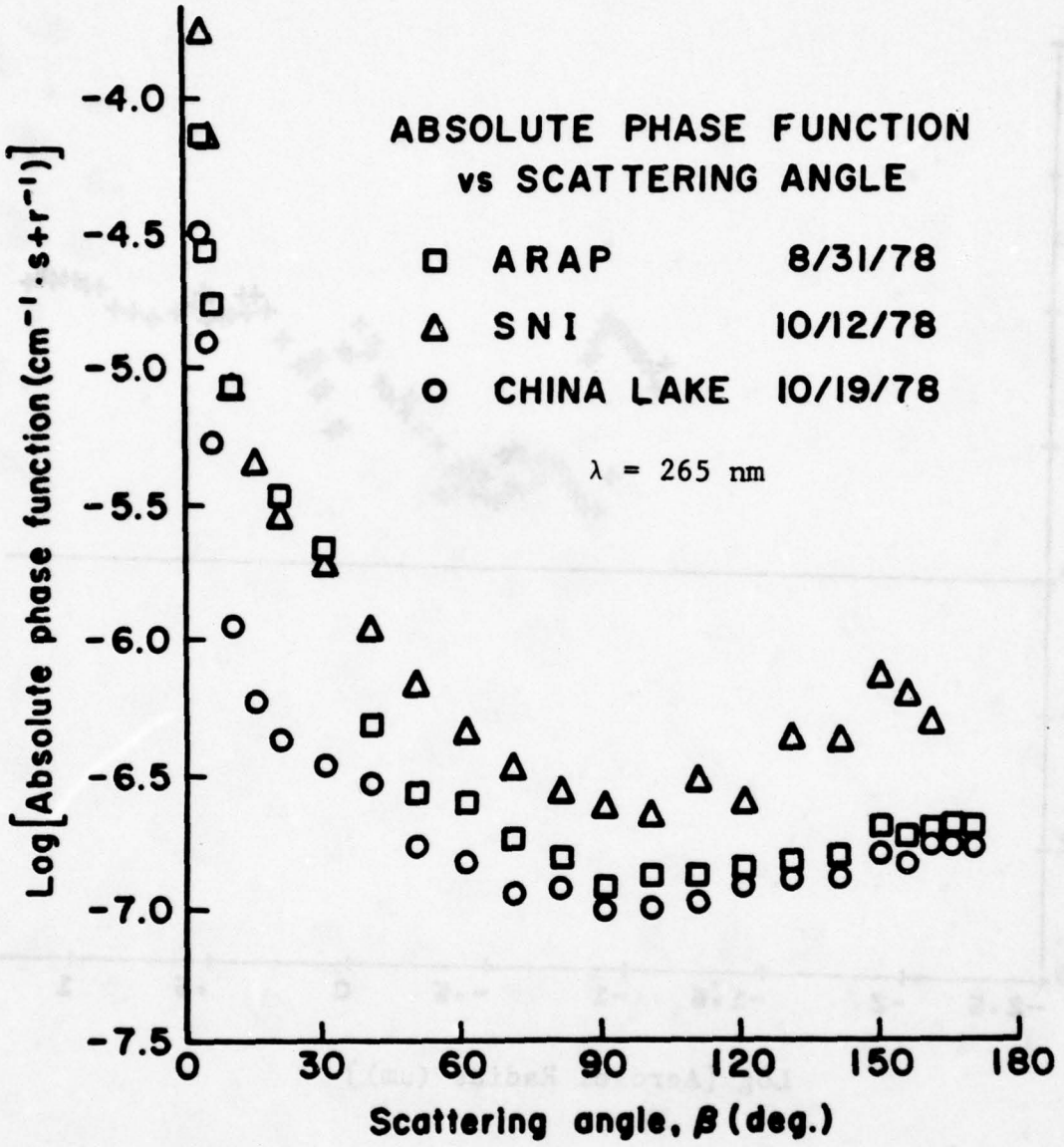

Figure 12. Variation of the single scattering phase function with environment at 265 nm.

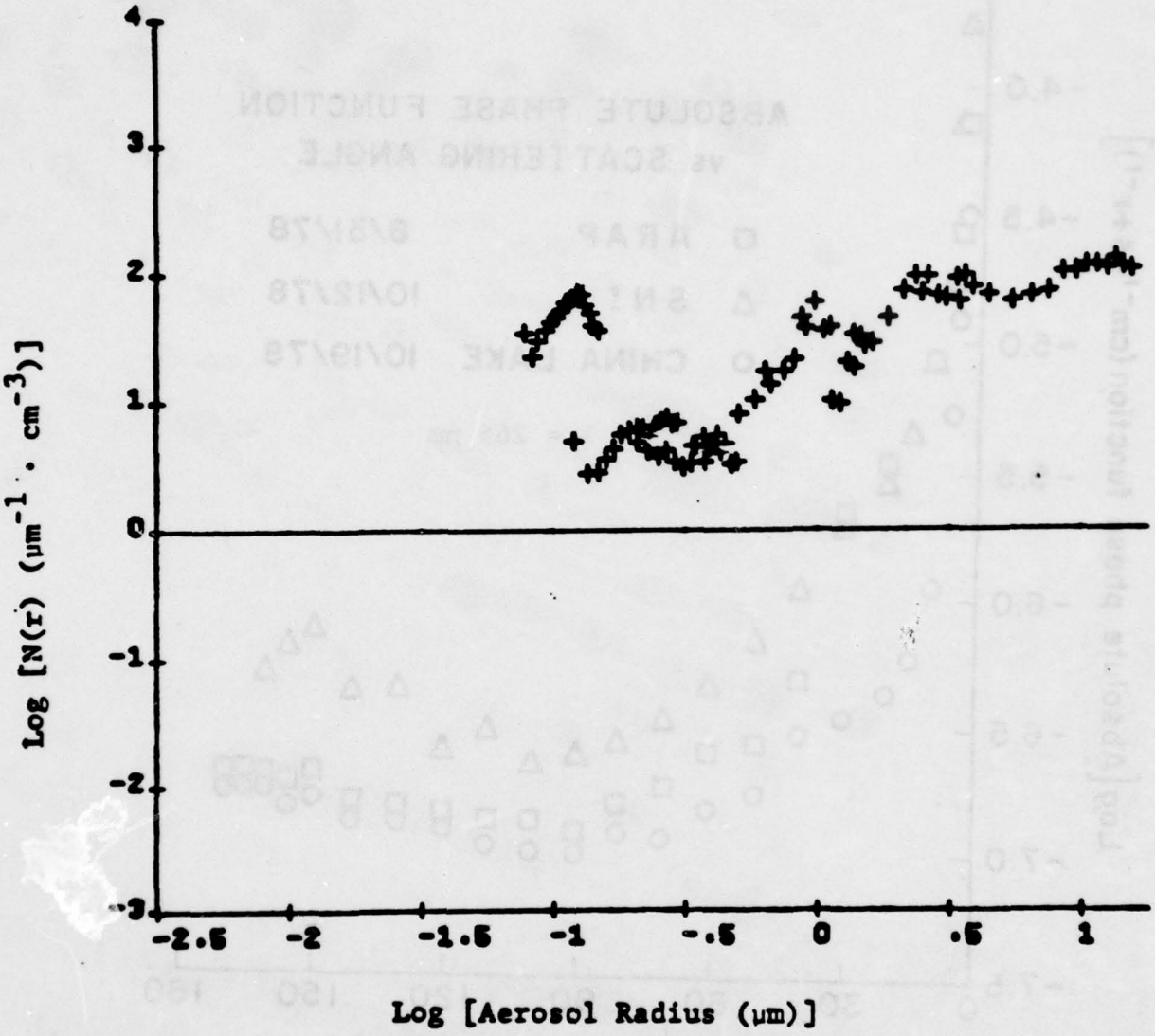

Figure 13. Typical normalized particle size distribution measured on October 13, 1978 at San Nicolas Island.

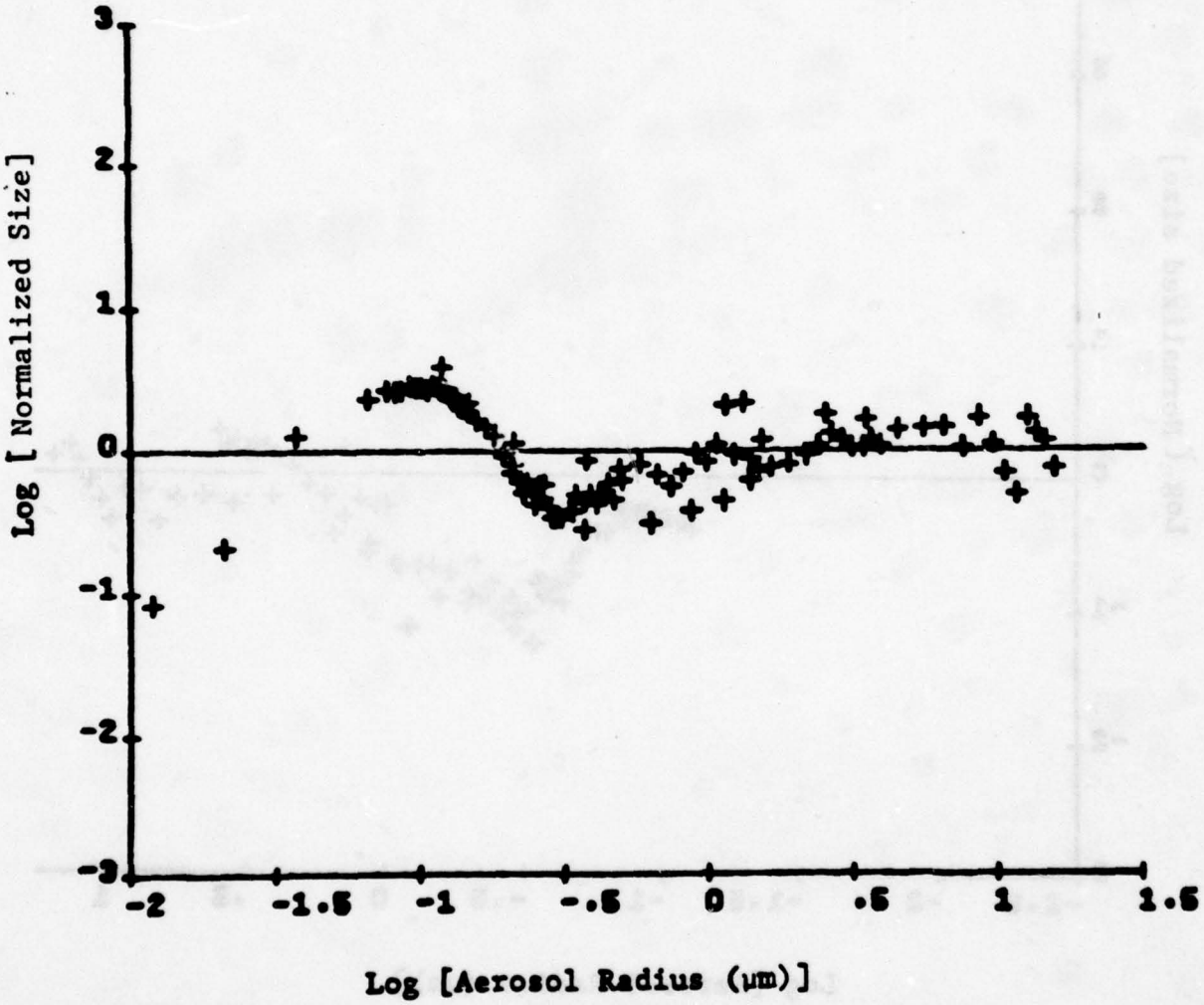

Figure 14. Normalized size distribution measured on November 16, 1977 at Princeton, N.J.

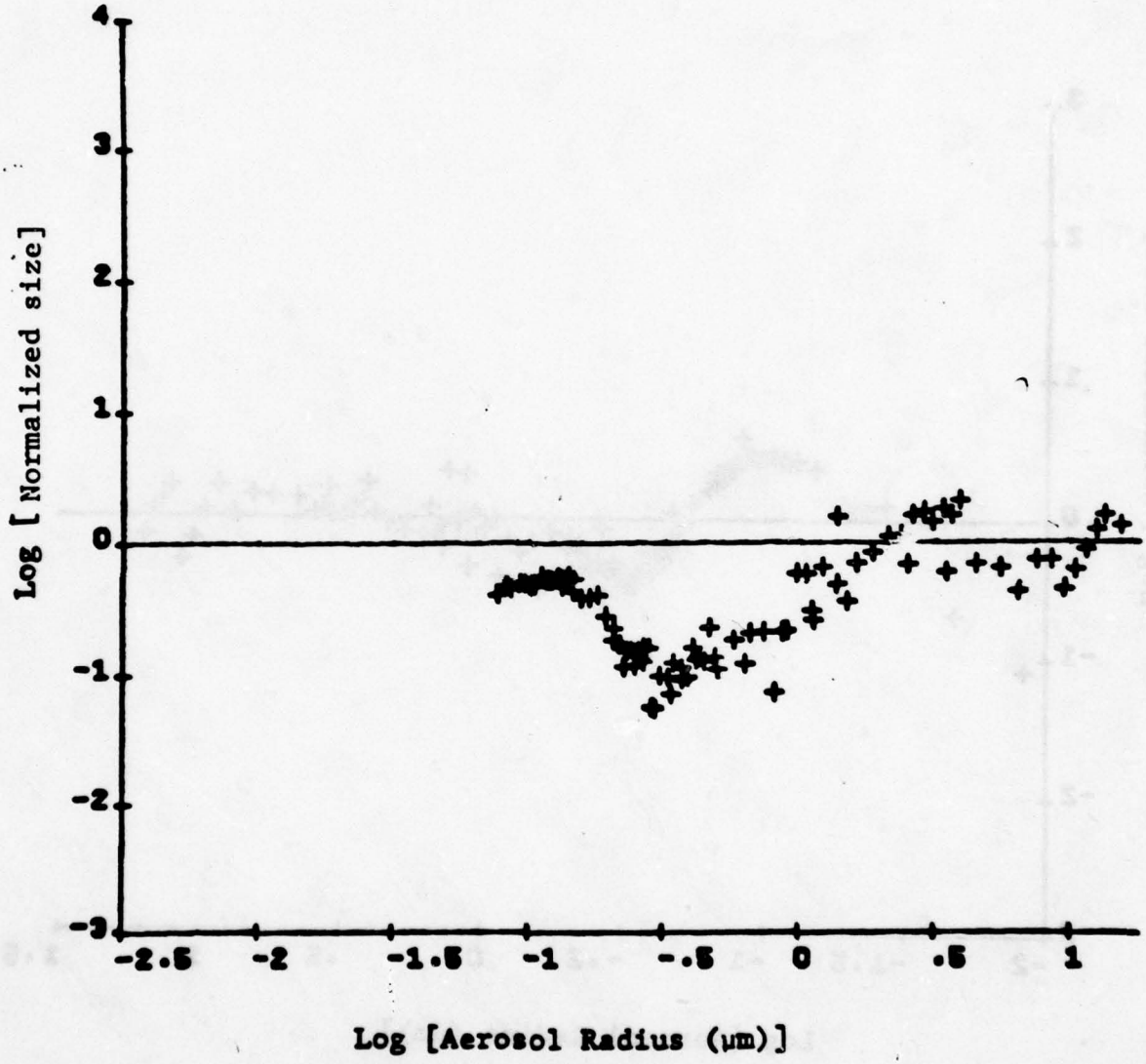

Figure 15. Typical particle size distribution measured on October 18, 1978 at China Lake, CA.

size distributions on two different days than the regular size distribution plots. It can be seen by comparing Figures 13 and 14 that the maritime atmosphere at San Nicolas Island had more particles at all size ranges than the rural New Jersey atmosphere. The desert atmosphere, on the other hand, shown in Figure 15, had fewer small particles than the New Jersey atmosphere.

Since the magnitudes of the ultraviolet phase functions at most scattering angles are proportional to the concentrations of small particles, the relative magnitudes of the phase functions shown in Figure 12 for the three geographic locations are consistent with the aerosol concentrations shown in Figures 13 through 15. The magnitudes of the phase functions at very small scattering angles, however, are more sensitive to the larger particle size ranges. It is interesting to note that the phase functions measured in the desert exhibit high forward peaking consistent with the relatively large numbers of larger particles in the larger size ranges shown in Figure 15.

5.3 Wavelength Variations at Each Geographic Location

In order to determine the wavelength dependence of the ultraviolet single scattering phase functions, the phase functions were measured at a variety of wavelengths over a very short period of time at each geographic location. Typical results obtained at San Nicolas Island, A.R.A.P. and China Lake are shown in Figures 16 through 18, respectively. Since

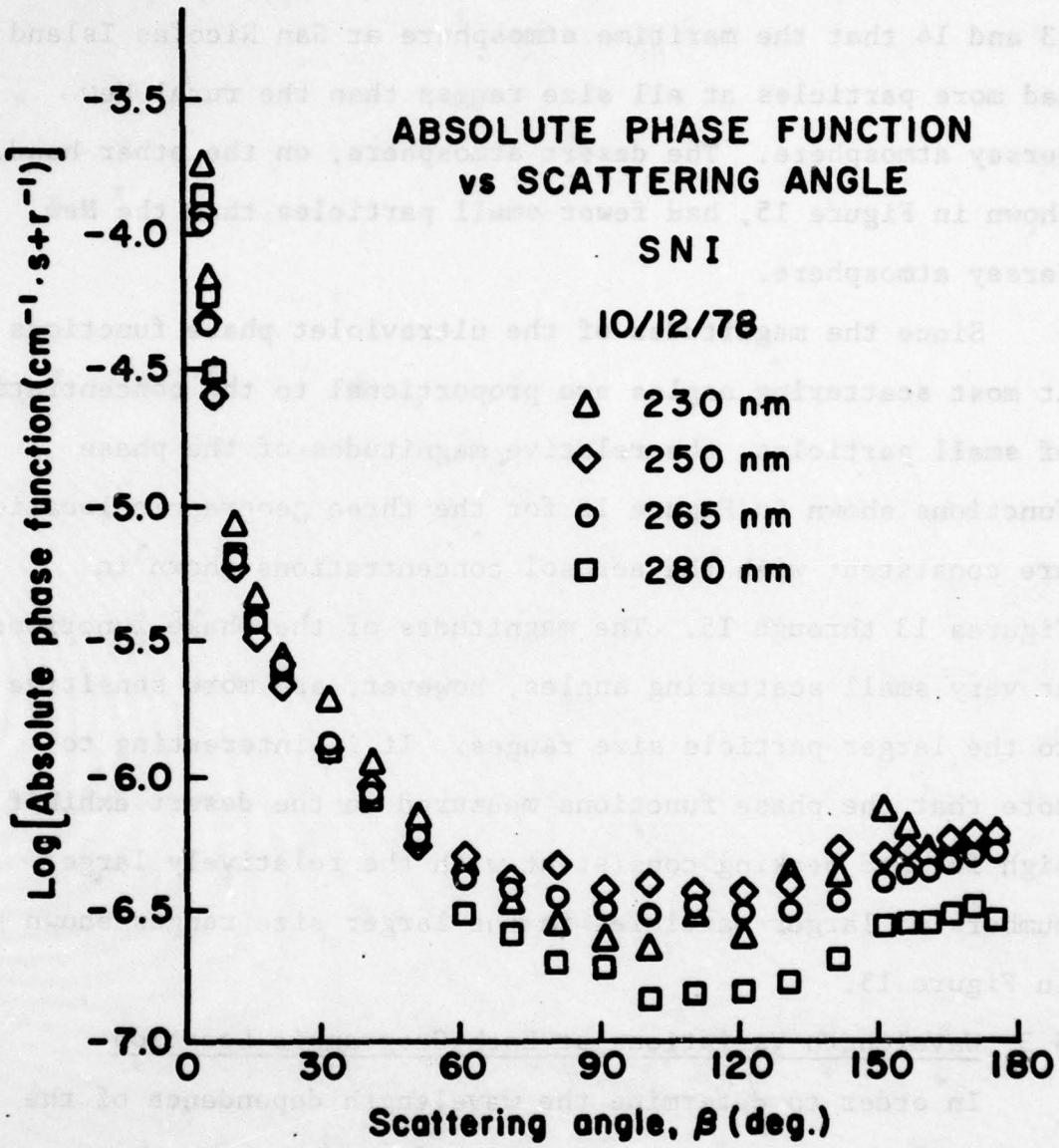

Figure 16. Wavelength variation of the single scattering phase function measured at San Nicolas Island.

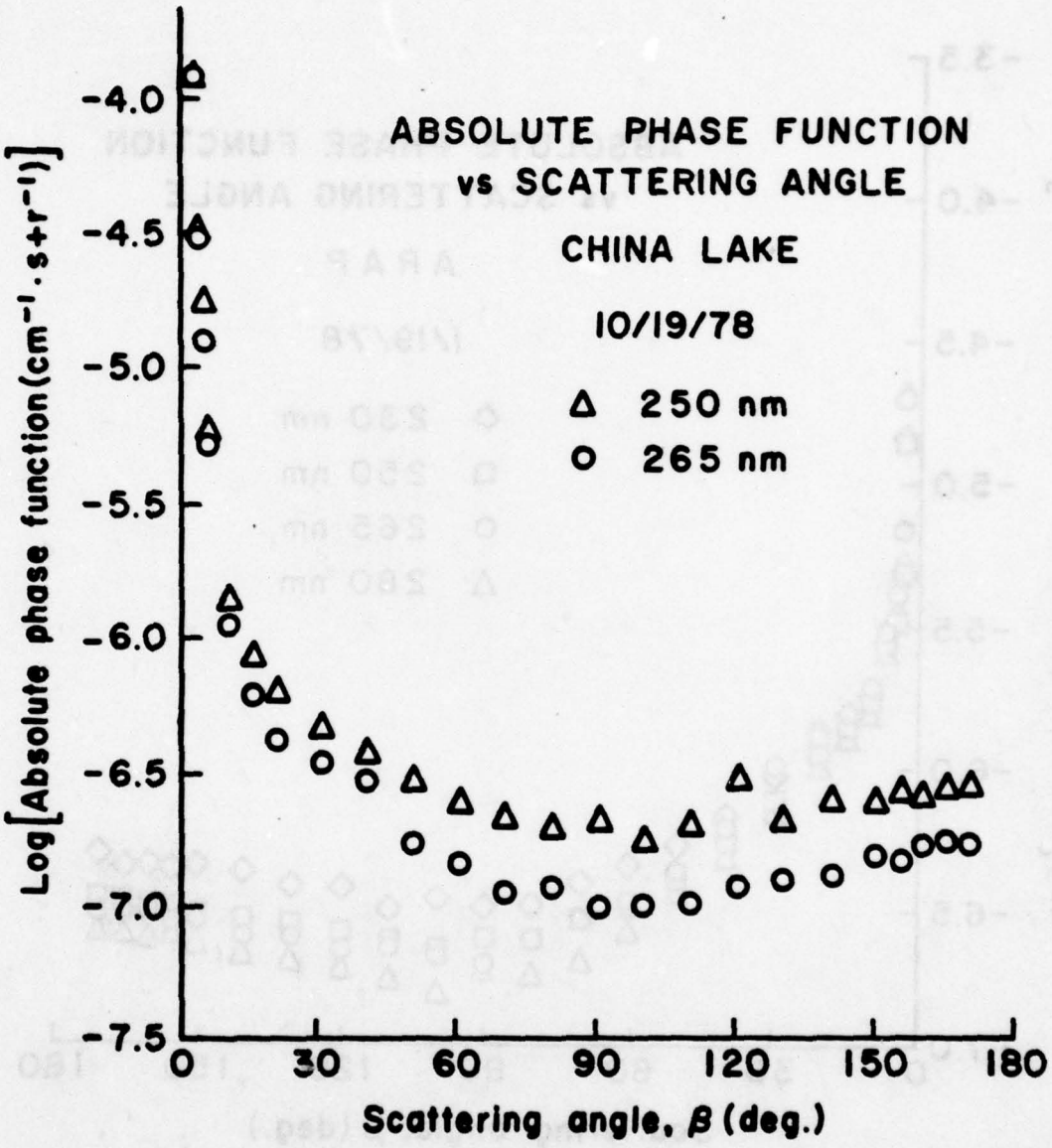

Figure 17. Wavelength variation of single scattering phase function measured at China Lake, CA.

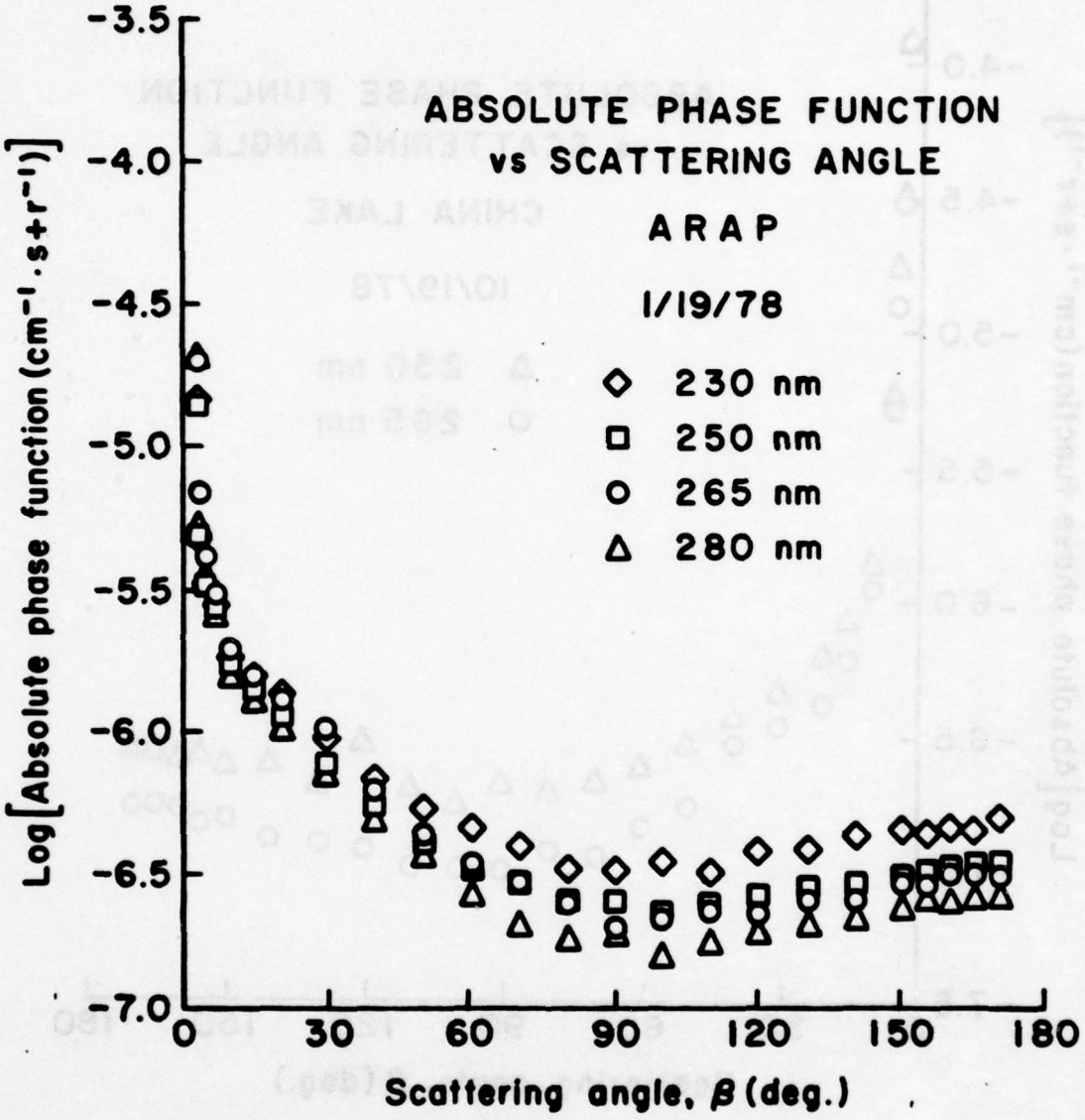

Figure 18. Wavelength variation of single scattering phase function measured at A.R.A.P. in Princeton, N.J.

aerosol scattering does not vary as strongly with wavelength as Rayleigh scattering, it is not surprising that the greatest differences between phase functions measured at various wavelengths occurred at the higher scattering angles where Rayleigh scattering dominates. While the magnitudes of the phase functions may vary significantly during the time required to make measurements at several wavelengths, due to time variations in the aerosol concentrations, it can generally be stated that the magnitudes of the phase functions are higher at lower wavelengths.

5.4 Refractive Index Variation

An attempt was made to determine effective refractive indices which when used as input to the Mie scattering calculations would give the best agreement to both the shape and magnitude of the measured phase functions. The maritime atmosphere at San Nicolas Island and the desert atmosphere at China Lake were chosen as extreme examples. At a wavelength of 265 nm, typical experimental phase functions were chosen for the maritime and desert atmospheres. In each case, the real and imaginary portion of the refractive index were varied as shown in Figures 19 and 20. The real part of the refractive index was varied from 1.3 to 2.0 while the imaginary part was varied from -0.01 to -0.09. As can be seen from Figures 19 and 20 the choice of refractive index made very little difference in the relative agreement between theory and experiment. While it is well known that the single scattering

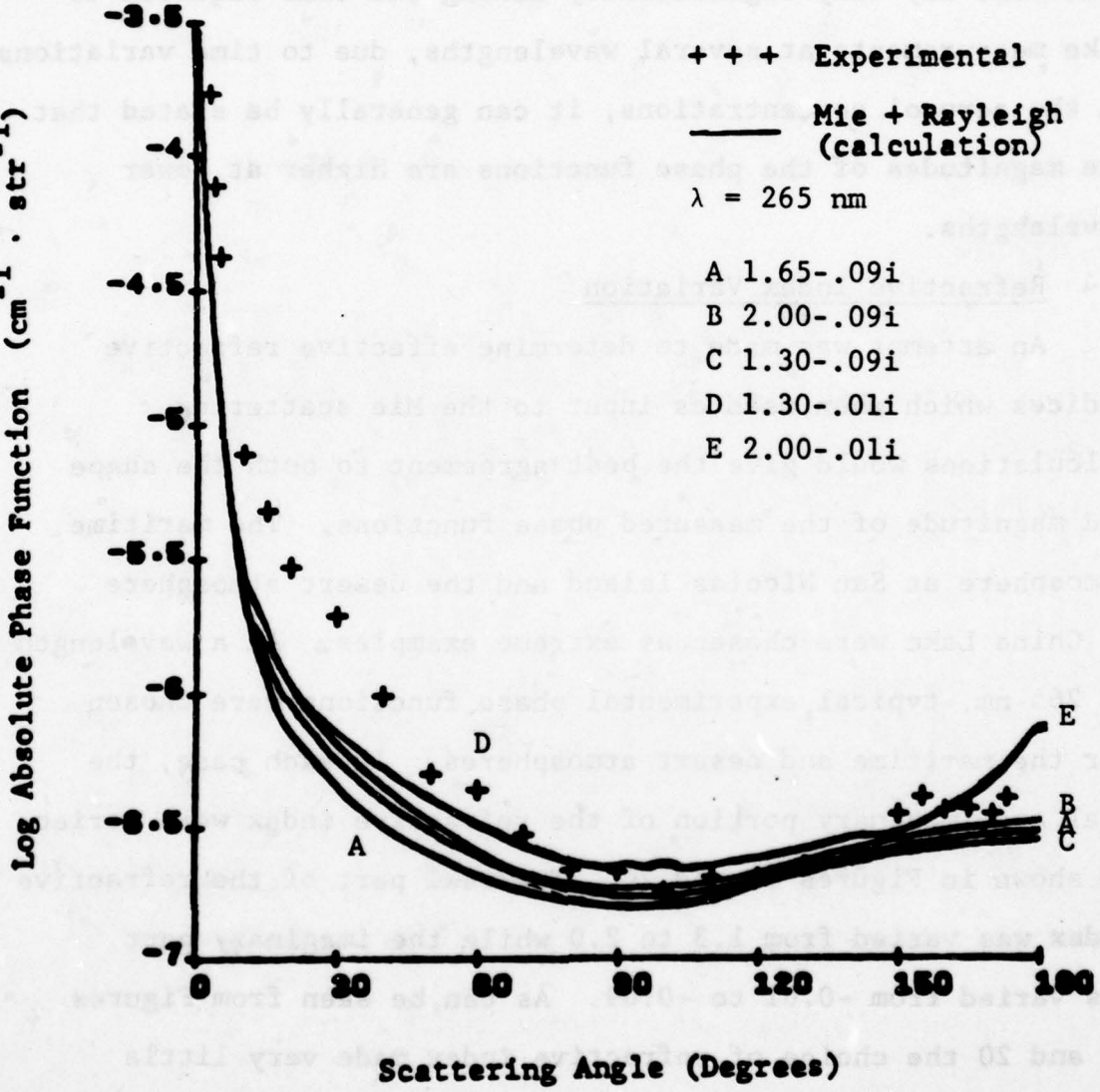

Figure 19. Variation of the refractive index on the phase function calculated from Mie theory. The experimental data is from San Nicolas Island.

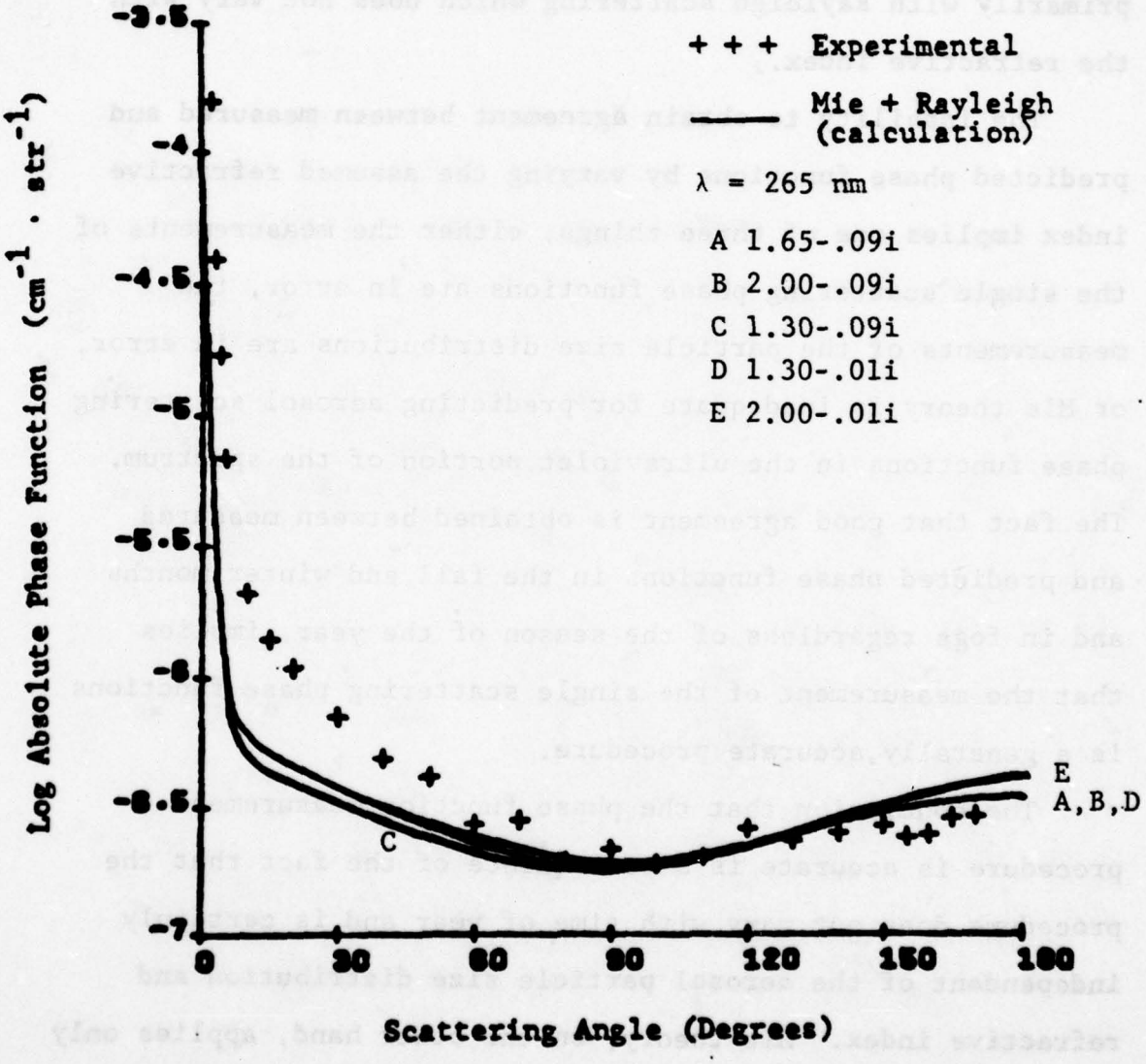

Figure 20. Variation of the refractive index on the phase function calculated from Mie theory. The experimental data is from China Lake, CA.

phase function is insensitive to refractive index in the forward direction[3] it may seem surprising that the phase function at higher scattering angles is so insensitive. It must be remembered, however, that the major portion of the phase function beyond a scattering angle of 90^{o} is associated primarily with Rayleigh scattering which does not vary with the refractive index.

The inability to obtain agreement between measured and predicted phase functions by varying the assumed refractive index implies one of three things; either the measurements of the single scattering phase functions are in error, the measurements of the particle size distributions are in error, or Mie theory is inadequate for predicting aerosol scattering phase functions in the ultraviolet portion of the spectrum. The fact that good agreement is obtained between measured and predicted phase functions in the fall and winter months and in fogs regardless of the season of the year, implies that the measurement of the single scattering phase functions is a generally accurate procedure.

The conclusion that the phase function measurement procedure is accurate is a consequence of the fact that the procedure does not vary with time of year and is certainly independent of the aerosol particle size distribution and refractive index. Mie theory, on the other hand, applies only to spherical dielectrics of known refractive index. Thus, since fogs are composed of spherical water droplets with a

well known refractive index, one would expect that Mie theory would accurately predict the single scattering phase functions of fogs. Conversely, if the aerosol particulates on a given occasion are nonspherical in nature, then it is possible that Mie theory would not be accurate in predicting the phase functions.

The Knollenberg particle size analyzers measure the size of aerosol particles on the basis of the intensity of radiation scattered in the forward direction. The necessary assumption that the intensity of light scattered in the forward direction is independent of refractive index is actually obtained from Mie theory. The Knollenberg devices[7] are calibrated using latex spheres with refractive indices nearly equal to that of water. Thus, it is not surprising that Mie scattering calculations using measured particle size distributions from the Knollenberg particle size analyzers would give agreement with the measured phase functions in fog-type aerosols.

It therefore seems reasonable to conclude that the measured ultraviolet phase functions are more accurate than those predicted from particle size distributions and Mie theory. Furthermore, in the opinion of the authors, it is easier to measure the single scattering phase functions directly at a given wavelength than to attempt to measure the aerosol particle size distribution and calculate the single scattering phase function using Mie theory.

5.5 Attenuation Coefficient Measurements

Attenuation, or extinction, coefficients k_{EXT} were measured over several pathlengths on numerous days when the single scattering phase functions were measured. When the variable field of view technique described in Section 4.3 was used, the expected trend of an increasing effective attenuation coefficient with decreasing field of view or steradiancy, was not always observed. Figure 21 shows a steady decrease in the apparent attenuation coefficient with decreasing steradiancy for the case that a solar blind filter (denoted as S) was used to define the detector bandpass. When a narrow bandpass filter centered at 275 nm (denoted as R in Figure 21) was used, the expected steady increase in the apparent attenuation coefficient was observed. When a narrow bandpass filter centered at 255 nm (denoted B) was used, an increase followed by a decrease was observed as the steradiancy was decreased.

Increases in the apparent attenuation coefficient as the steradiancy was decreased was observed on several other occasions as shown in Figures 22 and 23. A series of experiments was initiated to determine the cause of these apparent anomalies. For these experiments, the radiometer was pointed directly at the distant radiation source with a constant field of view angle and data was recorded over periods of time equal to the amount of time usually required to make a series of measurements using the decreasing field

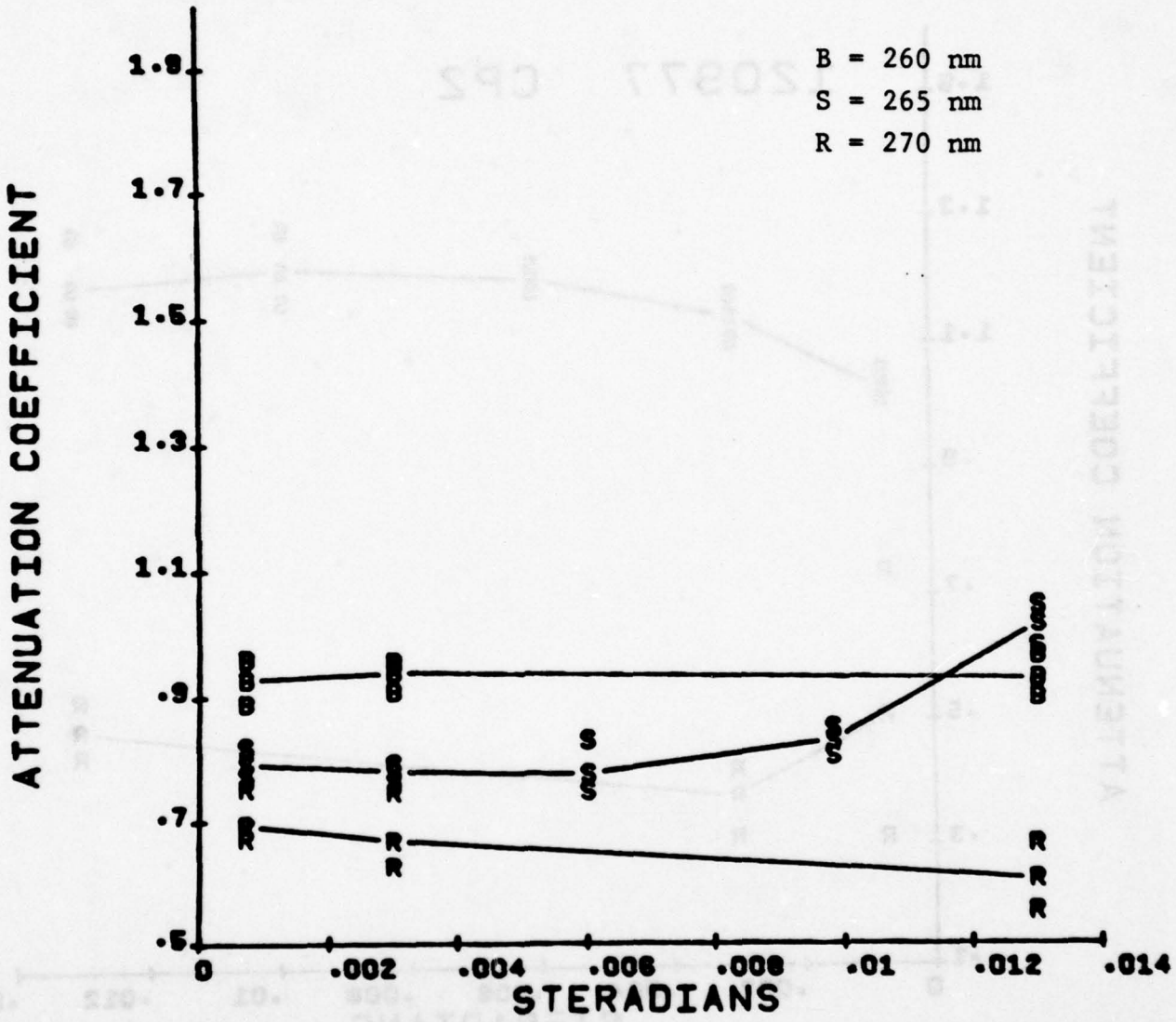

Figure 21. Wavelength Dependence of Attenuation Coefficients Measured in the Air on Nov. 21, 1977.
This plot also shows the variation of the attenuation coefficient with detector steradiancy.

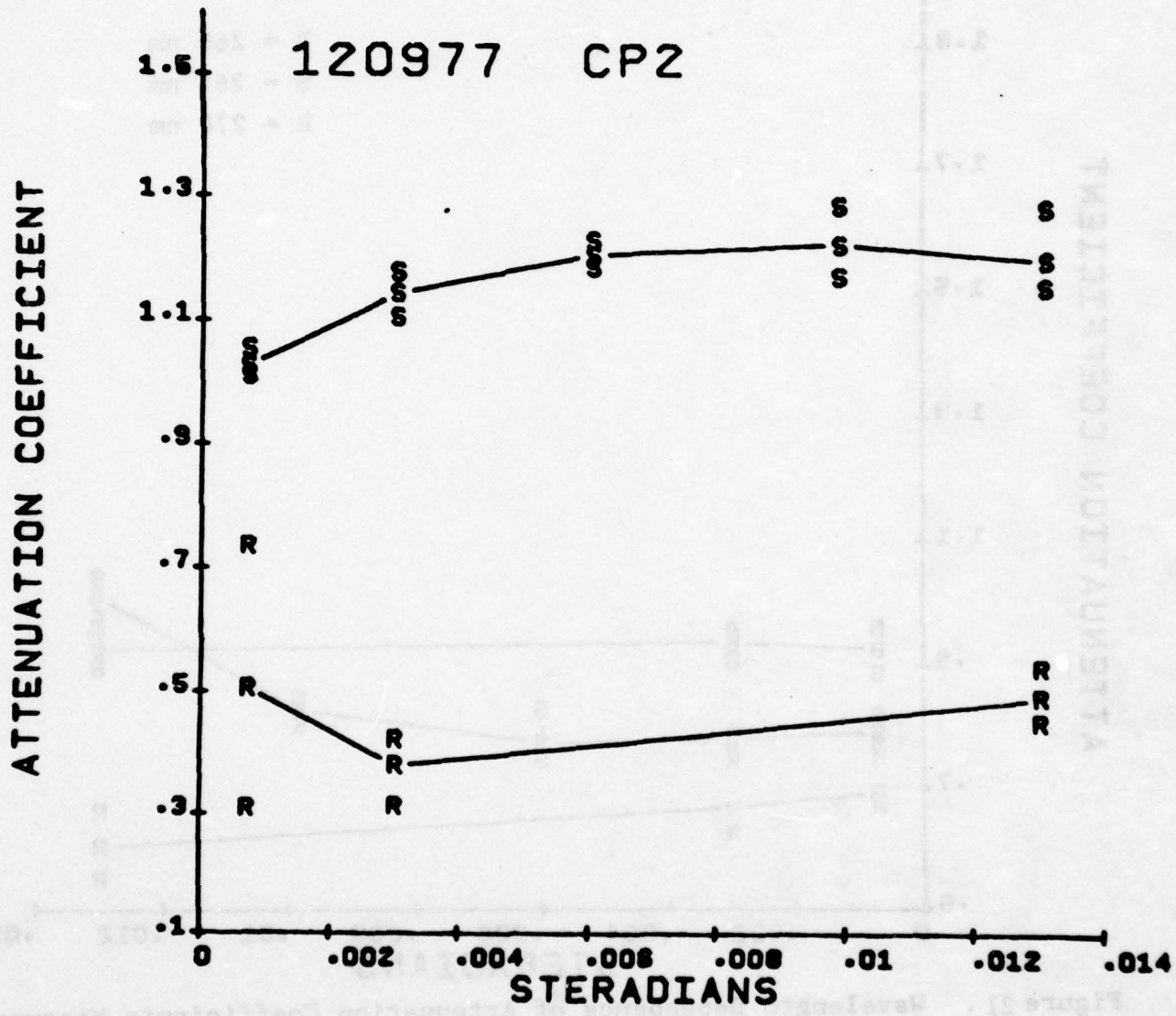

Figure 22. Wavelength dependence of attenuation coefficients measured on the ground on Dec. 9, 1977. This plot also shows the variation of the attenuation coefficient with detector steradiancy.

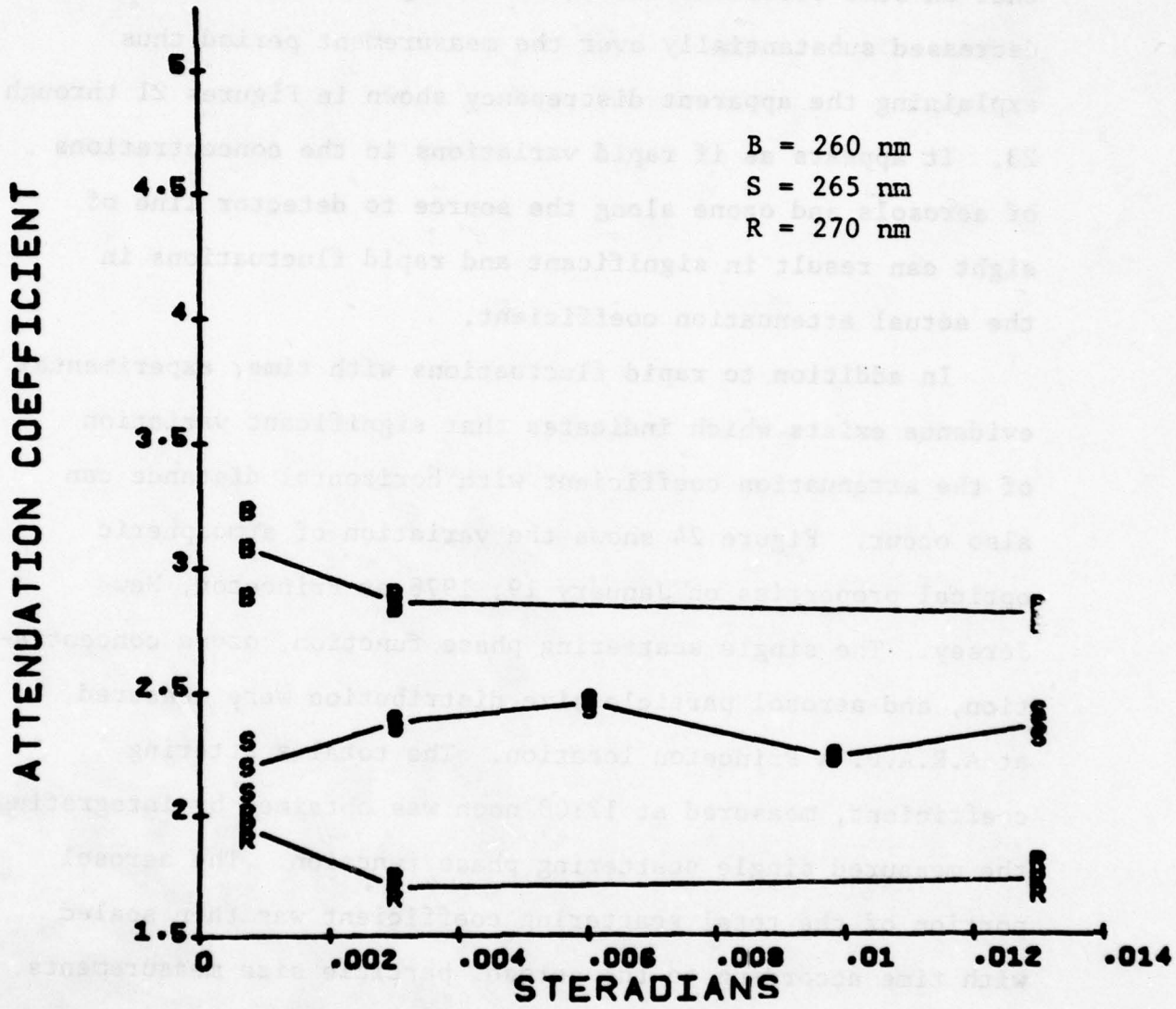

Figure 23. Wavelength dependence of attenuation coefficients measured in the air on May 31, 1978. This plot also shows the variation of attenuation coefficient with detector steradiancy.

of view technique. The results of these experiments indicated that on some occasions the measured signals increased and decreased substantially over the measurement period thus explaining the apparent discrepancy shown in Figures 21 through 23. It appears as if rapid variations in the concentrations of aerosols and ozone along the source to detector line of sight can result in significant and rapid fluctuations in the actual attenuation coefficient.

In addition to rapid fluctuations with time, experimental evidence exists which indicates that significant variation of the attenuation coefficient with horizontal distance can also occur. Figure 24 shows the variation of atmospheric optical properties on January 19, 1978 at Princeton, New Jersey. The single scattering phase function, ozone concentration, and aerosol particle size distribution were measured at A.R.A.P.'s Princeton location. The total scattering coefficient, measured at 12:00 noon was obtained by integrating the measured single scattering phase function. The aerosol portion of the total scattering coefficient was then scaled with time according to the aerosol particle size measurements. The molecular portion of the total scattering coefficient was determined using Rayleigh theory and the aerosol absorption coefficient was determined using the measured particle size distribution and Mie theory. The summation of these various coefficients, which were measured, inferred or calculated based on measurements made at A.R.A.P., yields the extinction

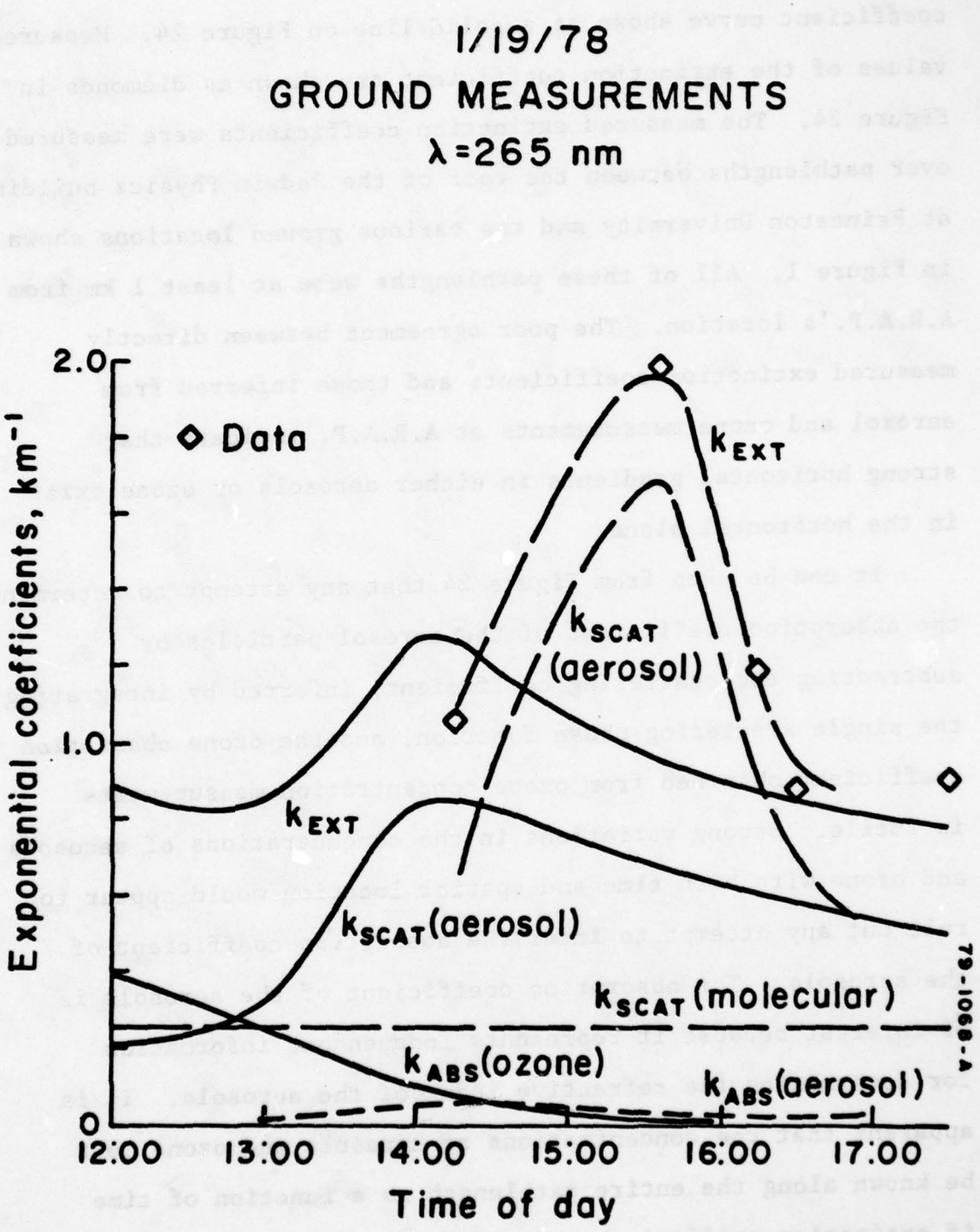

Figure 24. Time Variation of Atmospheric Optical Properties on Jan. 19, 1978.

coefficient curve shown as a solid line on Figure 24. Measured values of the extinction coefficient are shown as diamonds in Figure 24. The measured extinction coefficients were measured over pathlengths between the roof of the Jadwin Physics building at Princeton University and the various ground locations shown in Figure 1. All of these pathlengths were at least 1 km from A.R.A.P.'s location. The poor agreement between directly measured extinction coefficients and those inferred from aerosol and ozone measurements at A.R.A.P. indicate that strong horizontal gradients in either aerosols or ozone exist in the horizontal plane.

It can be seen from Figure 24 that any attempt to determine the absorption coefficient of the aerosol particles by subtracting the scattering coefficient, inferred by integrating the single scattering phase function, and the ozone absorption coefficient obtained from ozone concentration measurements is futile. Strong variations in the concentrations of aerosols and ozone with both time and spatial location would appear to rule out any attempt to infer the absorption coefficient of the aerosols. The absorption coefficient of the aerosols is of interest because it represents independent information for determining the refractive index of the aerosols. It is apparent that the concentrations of aerosols and ozone must be known along the entire pathlength as a function of time if extinction coefficients are to be predicted accurately.

5.6 Correlation of Scattering Coefficient with Visibility

It would be useful to those who must operate ultraviolet systems on a day to day basis if an estimate of the system performance could be inferred from the prevailing visibility. Unfortunately, atmospheric ozone, which is responsible for a major portion of the extinction coefficient in the ultraviolet, is not visible to the naked eye and therefore must be measured independently. However, the results of the present investigation indicate that the aerosol scattering coefficient portion of the extinction coefficient can be inferred from the prevailing visibility. Figure 25 shows the correlation of the measured aerosol scattering coefficient at 250 nm wavelength with measured values of the visibility.

It should be pointed out that the measurement of visibility in the present investigation was accomplished by photographing the horizon and searching the photographs for water towers at known distances from the camera. The visibility estimates are therefore quantized according to the most distant water tower which is visible in the photograph. Thus, all of the measured aerosol scattering coefficients will be associated with a relatively small number of discrete visibilities as shown in Figure 25. Nevertheless, it can be seen from Figure 25 that a straight line can be used to represent the aerosol scattering coefficient as a function of the logarithm of the visibility.

Thus, within the experimental errors of the visibility

CORRELATION OF THE 250 NM ULTRAVIOLET AEROSOL SCATTERING COEFFICIENT WITH VISIBILITY

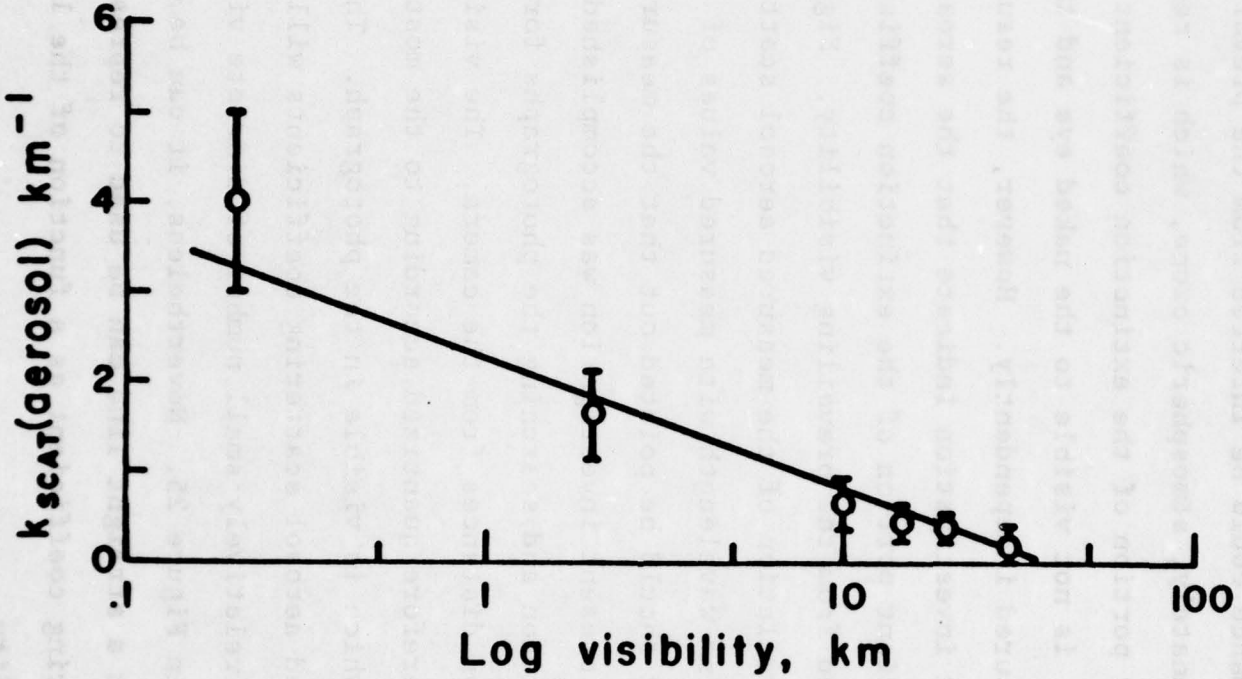

Figure 25. Correlation Between Visibility and Aerosol Scattering Coefficient at 250 nm.

measurements, it appears as if visibility can be used to give a reasonable estimate of the aerosol scattering coefficient. Since the Rayleigh scattering coefficient is relatively constant at ground level, depending only weakly on the prevailing temperature and pressure, the total scattering coefficient due to both molecular and aerosol species can easily be determined. If an independent measurement of the ozone is available, the total extinction coefficient can therefore be inferred.

5.7 Small Angle Scattering

The results of using the billboard technique to measure the small angle scattering is shown in Figure 26. The solid data points represent two different series of measurements where the inner radius of the cutout was varied while the outer radius was held fixed. The open data points represent two different measurement series where the outer radius was varied while the inner radius was held fixed. The directly transmitted radiation was on the order of 650,000 counts when the lamp was in full view of the detector. Since the measured scattering using the semi-circular fields of view were on the order of a few thousand counts the necessity of blocking the direct radiation is apparent.

The solid line in Figure 26 is the calculated scattered radiance as given by the A.R.A.P. UV propagation model. The input to this model is the result of the Mie theory calculations using the measured particle size distribution shown in Figure 27. The A.R.A.P. UV propagation

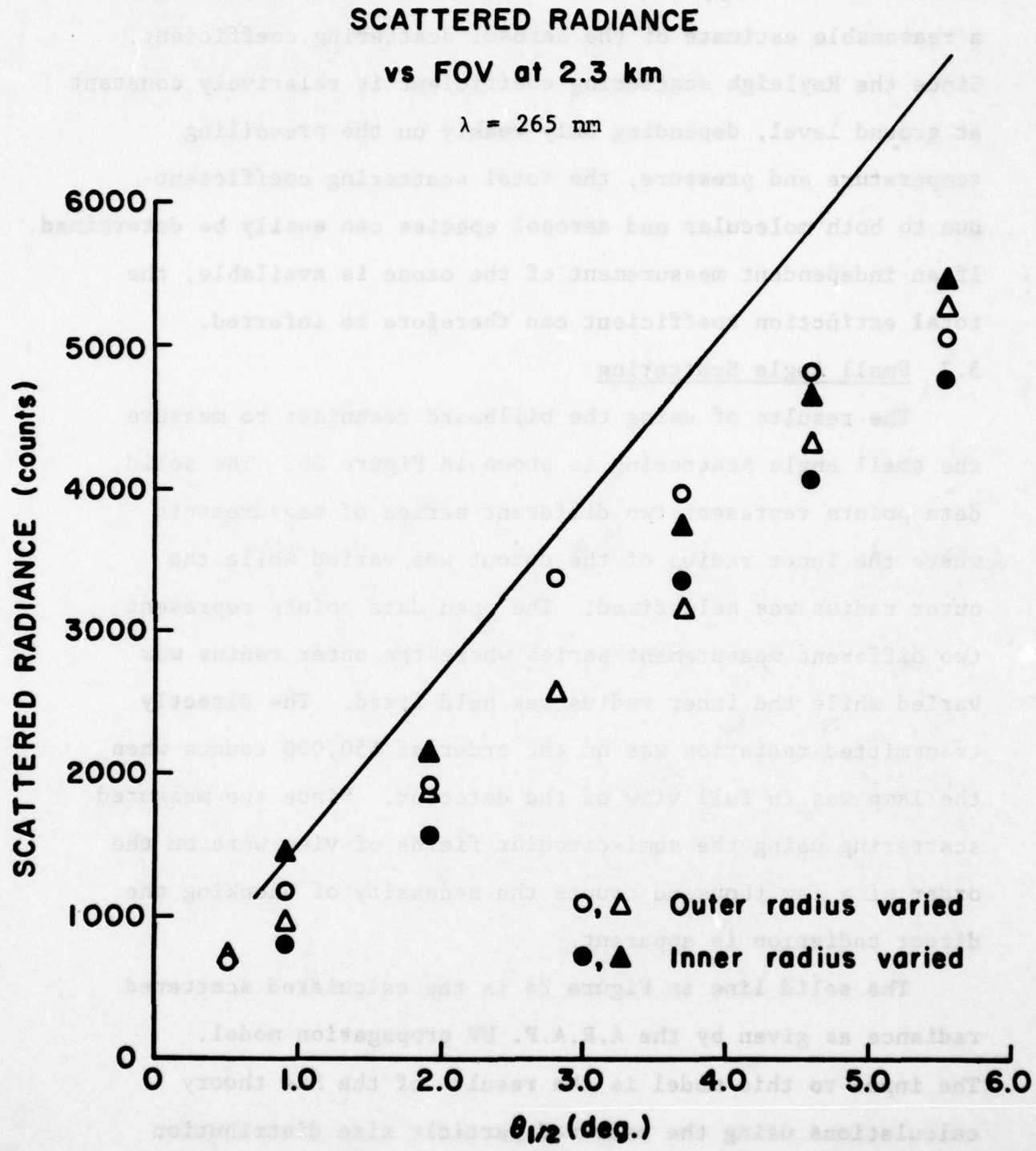

Figure 26. Scattered radiance at 265 nm measured as a function of detector field of view. Direct radiation is eliminated.

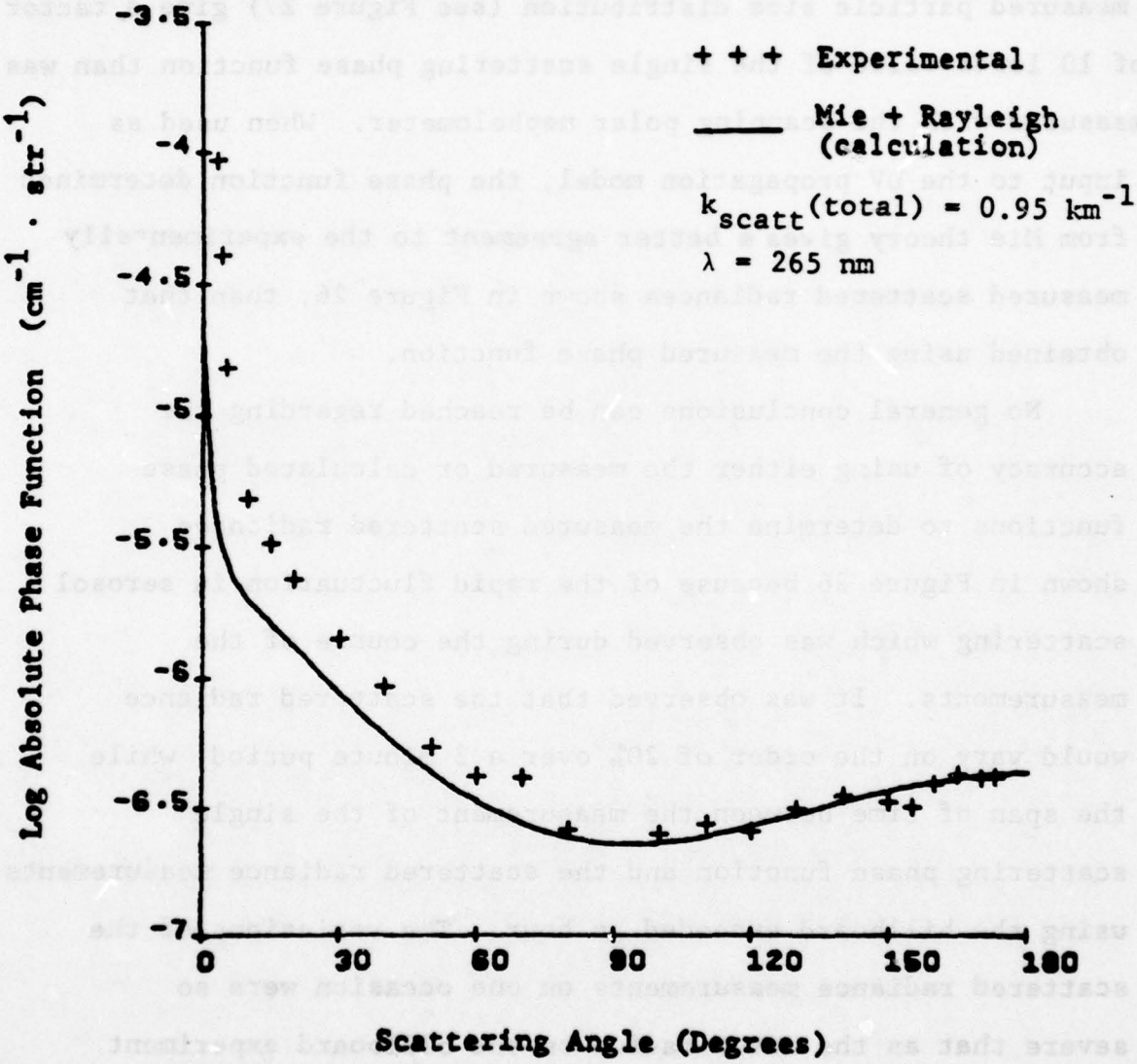

Figure 27. Phase function measured on January 31, 1979.

model has generally been shown to accurately predict the scattered radiance.[2] It can be seen from Figure 26 that the A.R.A.P. UV propagation model predicts higher levels of scattered radiance than those which were measured. It is interesting to note that the Mie theory calculations using the measured particle size distribution (see Figure 27) give a factor of 10 lower value of the single scattering phase function than was measured with the scanning polar nephelometer. When used as input to the UV propagation model, the phase function determined from Mie theory gives a better agreement to the experimentally measured scattered radiances shown in Figure 26, than that obtained using the measured phase function.

No general conclusions can be reached regarding the accuracy of using either the measured or calculated phase functions to determine the measured scattered radiances shown in Figure 26 because of the rapid fluctuation in aerosol scattering which was observed during the course of the measurements. It was observed that the scattered radiance would vary on the order of 20% over a 3 minute period, while the span of time between the measurement of the single scattering phase function and the scattered radiance measurements using the billboard exceeded an hour. The variations of the scattered radiance measurements on one occasion were so severe that as the outer radius on the billboard experiment was decreased with the inner radius held constant, the scattered radiance measurement actually increased instead of

decreased. The phase function which would be inferred from this obviously extreme case would be negative and would obviously have no validity.

Thus, just as in the case of the collapsing field of view attenuation technique, the measurement of the single scattering phase functions at low angles using the small angle scattering billboard technique is inhibited by the rapid fluctuations of atmospheric aerosols. Perhaps the only accurate way to measure low angle phase functions would be to use an ultraviolet laser which would have a beam divergence on the order of milliradians and would permit the accurate measurement of the single scattering phase function down to tenths of a degree.

6. CONCLUSIONS AND RECOMMENDATIONS

An extensive series of ultraviolet single scattering phase functions have been measured at several wavelengths within the solar blind portion of the spectrum. These phase functions have been measured in a wide variety of weather conditions and geographic locations over a one year period. Measurements have been made at A.R.A.P.'s Princeton location, the Wayside laser test range at Fort Monmouth, New Jersey, on San Nicolas Island in the Pacific Ocean and at the Naval Weapons Center at China Lake, California. Thus, ultraviolet single scattering phase functions have been measured in rural, industrial, maritime and desert atmospheres.

The phase functions measured in the maritime atmosphere on San Nicolas Island were generally greater in magnitude than those measured in New Jersey, while phase functions measured in the desert at China Lake were generally lower. While the highest magnitudes of the phase functions were measured in fogs, the phase functions measured in the spring and summer months were generally higher than those measured in the fall and winter months. However, as much as a two order of magnitude variation in the magnitude of the single scattering phase functions at low scattering angles were observed over as little as a six week period of time.

Correlation between measured single scattering phase functions and those predicted from Mie and Rayleigh theories

using measured particle size distributions was generally good in the fall and winter months and in fogs. The magnitudes of phase functions measured in the spring and summer months including those made on San Nicolas Island and at China Lake generally exceeded the theoretical values. Attempts to vary the refractive index of the aerosols so as to obtain agreement between experiment and theory was generally unsuccessful. The aerosol phase functions are generally insensitive to refractive index in the forward direction while the measured phase functions are dominated by Rayleigh scattering which does not depend on refractive index in the backward direction.

It has been concluded that in those instances for which measured and predicted phase functions are in disagreement, the measured phase functions are more accurate than those which are predicted. This conclusion is based on the observation that agreement between theory and experiment is obtained when the atmospheric aerosols are known to be spherical dielectrics with refractive indices equal to the latex spheres used to calibrate the particle size analyzers. Since the technique used to measure the single scattering phase functions does not depend on aerosol type nor refractive index it has been hypothesized that in those cases where measured and predicted phase functions do not agree, the prevailing atmospheric aerosols cannot be represented by spherical dielectrics and therefore neither the Mie theory nor the particle size measuring device are accurate.

Attempts to correlate the measured atmospheric extinction coefficients with those predicted from measured phase functions and ozone concentrations have been marginally successful but not nearly accurate enough to infer the absorption coefficients of ambient aerosols. The disagreement between the measured extinction coefficients and those inferred from measured scattering coefficients and ozone concentration measurements have been attributed to rapid variation in ozone and aerosol concentration with both time and horizontal distance. It is recommended that a differential absorption lidar technique be used to measure spatially resolved ozone concentration and extinction coefficient along the entire pathlength of interest at a given instant in time.

Attempts to develop alternate techniques for measuring ultraviolet single scattering phase functions at scattering angles below 10^{o} have generally been unsuccessful due to the rapid variations in aerosol concentrations with time. Two techniques were attempted, one involving a collapsing field of view attenuation measurement and the other a billboarding technique to measure the scattered radiance at low angles to the source to receiver line of sight. Both techniques would involve using the A.R.A.P. atmospheric propagation and scattering code to determine the shape and magnitude of the single scattering phase function which would yield the measured results. It has been recommended that an ultraviolet laser be used to measure the single scattering phase function at

angles below 7^{o}. Such a laser with a divergence on the order of milliradians would permit the accurate measurement of the single scattering phase function down to angles of tenths of degrees.

One of the goals of the present investigation was to determine whether a simple technique could be developed by which the operator of an ultraviolet system could estimate system performance on a day to day basis. It has been observed that the ultraviolet aerosol scattering coefficient can be correlated with the prevailing visibility. Thus, if an independent measurement of the ozone concentration or ozone absorption coefficient were available, the UV extinction coefficient could be determined by summing the ozone absorption coefficient, the aerosol absorption coefficient, and the Rayleigh scattering coefficient which is relatively constant from day to day.

One of the major conclusions of the present investigation is that it is perhaps easier to directly measure the single scattering phase function at a given wavelength and obtain the total scattering coefficient by integrating that phase function than it is to measure the particle size distribution and calculate a phase function using Mie and Rayleigh theory. Since the results of the present investigation have implied that measured particle size distributions and Mie theory do not always give accurate determinations of the phase function or the scattering coefficient, it would seem that the direct

measurement of the single scattering phase function is preferable to the measurement of particle size distribution for those applications in which the optical properties of the atmosphere are of prime concern.

REFERENCES

1. Hughes, R.S., Dickson, C.R., Schlupf, J.M. and Neer, M.E., "Measurements of the Atmospheric Scattering from a Pulsed Krypton-Fluoride Laser Operating at .249 Microns," Interim Technical Report for Contract No. N60530-78-C-0227, January 1979.

2. Neer, M.E., Schlupf, J.M., Petersen, P.C., and Dickson, C.R., "Atmospheric Propagation of Ultraviolet Radiation Through the Lower Atmosphere," A.R.A.P. Report No. 374b, November 1978.

3. Neer, M.E., Schlupf, J.M., and Petersen, P.C., "Ultraviolet Single Scattering Phase Functions of Naturally Occurring Atmospheric Aerosols," A.R.A.P. Report No. 314, September 1977.

4. Blattner, W.G. and Livesay, R.B., "Utilization Instructions for Operation of the TPART-I Monte Carlo Procedure and the SCRIB1 Analysis Program," Research Note RRA-N7704, 18th August 1977, Radiation Research Associates Inc., 3550 Hulen Street, Fort Worth, Texas.

5. Inn, E.C.Y. and Tanaka, Y., "Ozone Chemistry and Technology," Advances in Chemistry, No. 21, American Chemical Society, Applied Replicative, 1959, p. 263.

6. McNesby, J.R. and Okabe, H., "Vacuum Ultraviolet Photochemistry," Advances in Photochemistry, Vol. III, ed. by W.A. Noyes, Jr., G.S. Hammond, and J.N. Pitts, Jr., Interscience Publishers, a division of John Wiley & Sons, New York, 1964, p. 157.

7. Pinnick, R.G. and Stenmark, E.B., "Response Calculations for a Commercial Light Scattering Aerosol Counter," Atmospheric Sciences Laboratory, White Sands Missile Range, New Mexico, July 1976.

APPENDIX A

INTRODUCTION

Appendix A presents a chronological documentation of the single scattering phase functions and the relevant atmospheric data accumulated over the past year. These include measurements at Princeton, New Jersey, Fort Monmouth, New Jersey, San Nicolas Island, and China Lake, California. The first page of each day's data contains a ground level photograph showing prevailing weather conditions with the date and location of the measurements. Also given on this page is a summary of the weather conditions, visibility, humidity, temperature, ozone concentration, ozone absorption coefficient, and the total scattering coefficients. The page is followed by a normalized size distribution (see page 40 text), a size distribution, and the measured single scattering phase functions including theoretical phase functions obtained from Mie and Rayleigh scattering theory using measured aerosol particle size distributions. For the San Nicolas Island data, a size distribution is presented for each phase function measured.

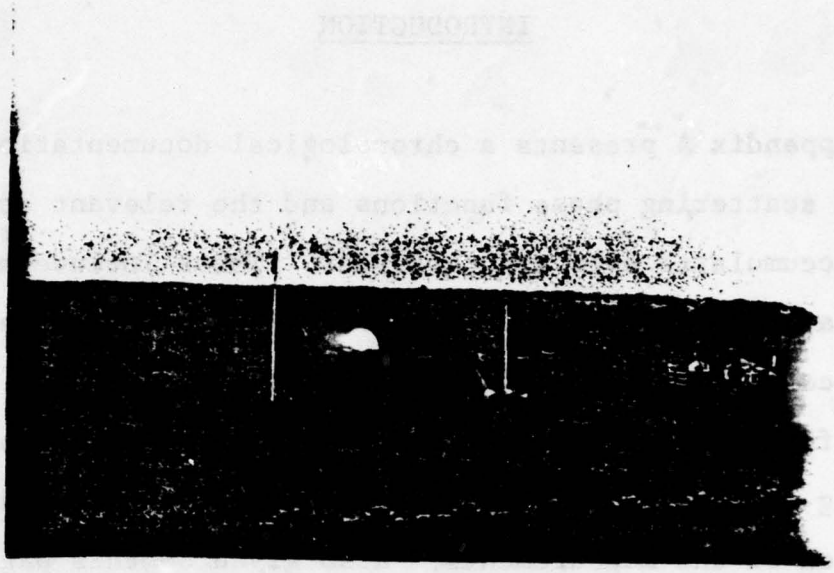

Ground level photograph

November 9,1977-- Princeton

Weather.....	overcast, low ceiling, low haze
Visibility.....	10 km
Temperature.....	64°F
Humidity.....	65%
Ozone concentration...	0.002 ppm
$k_{abs}(O_3)$.....	0.05 km^{-1}
k_{scat}(total).....	0.861 at 250 nm
.....	1.07 at 265 nm

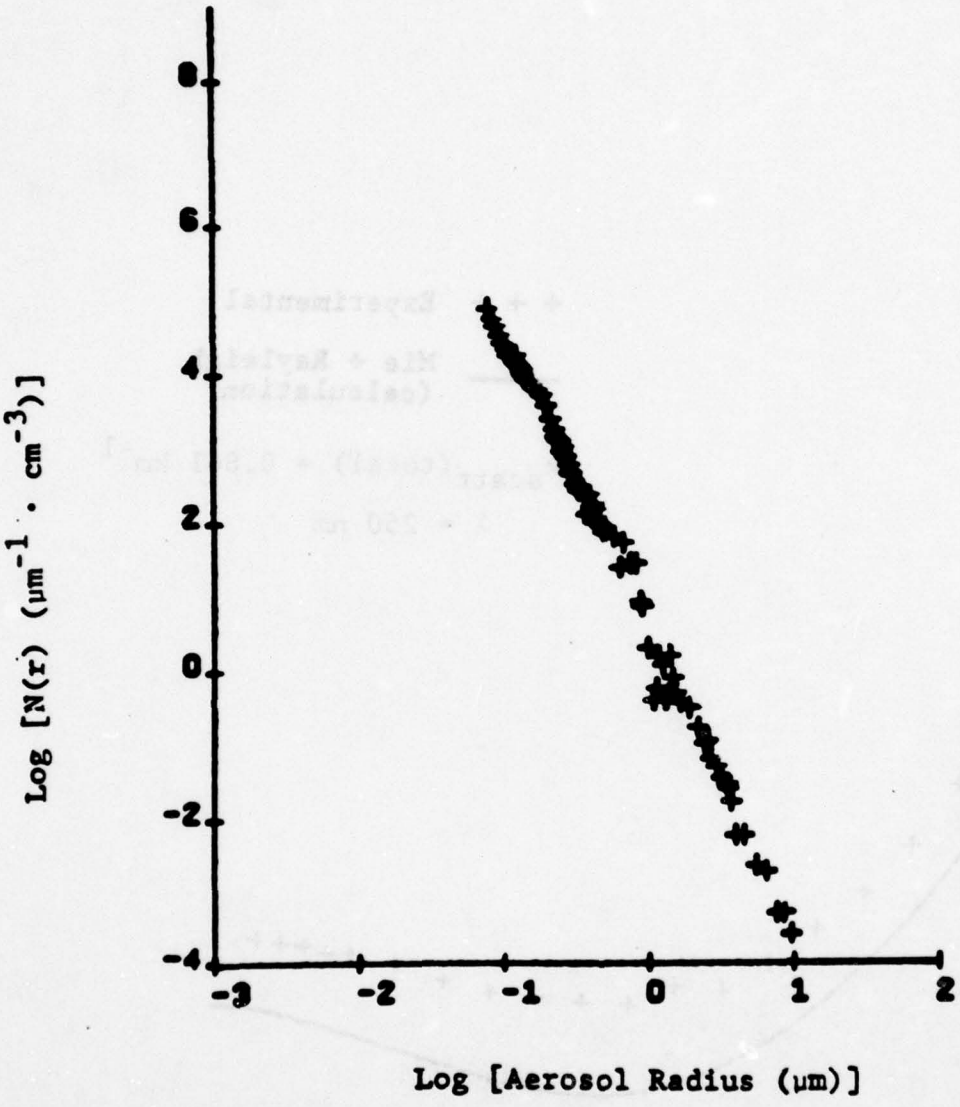

Size distribution measured on November 9, 1977.

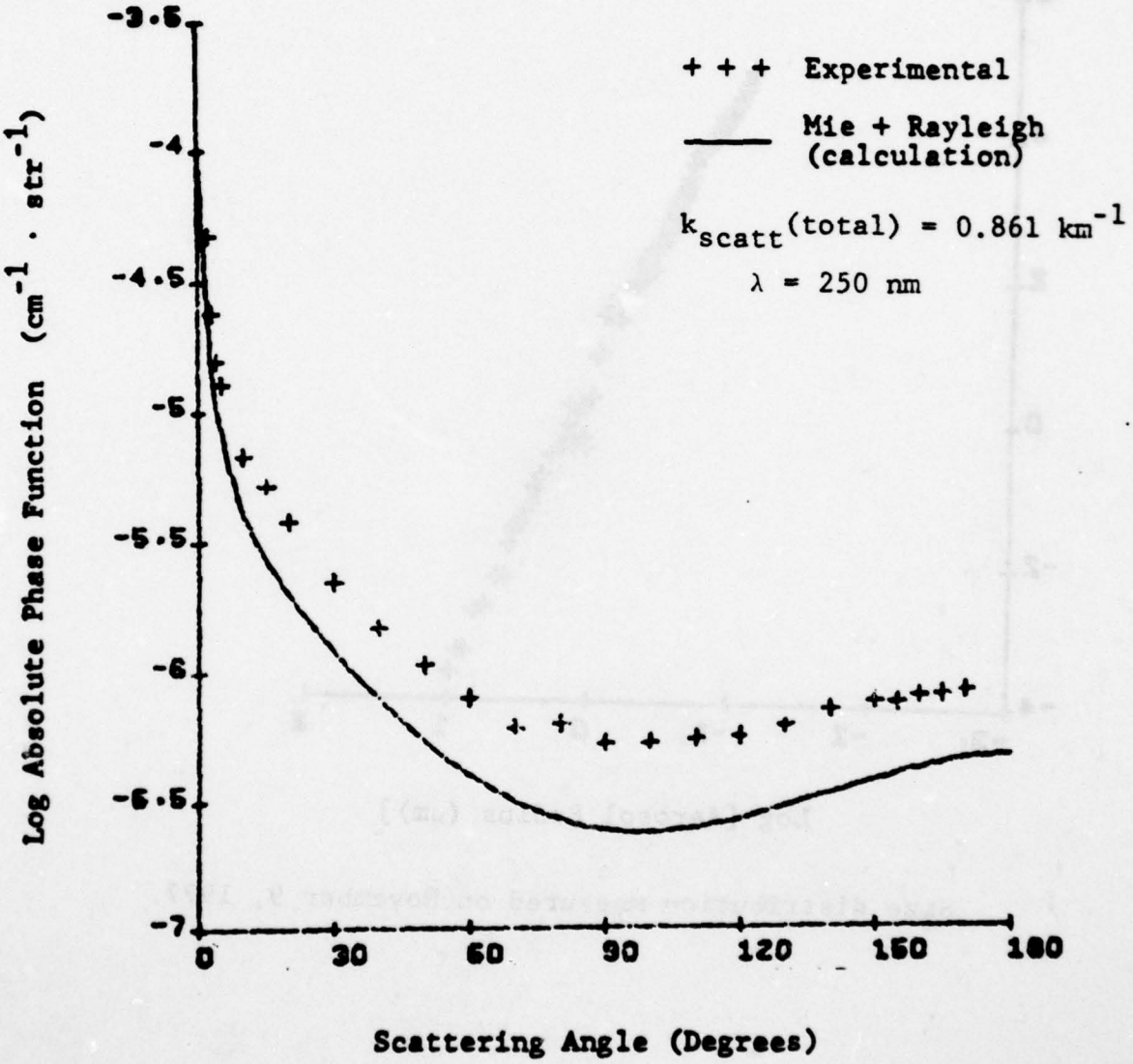

Phase function measured on November 9, 1977.

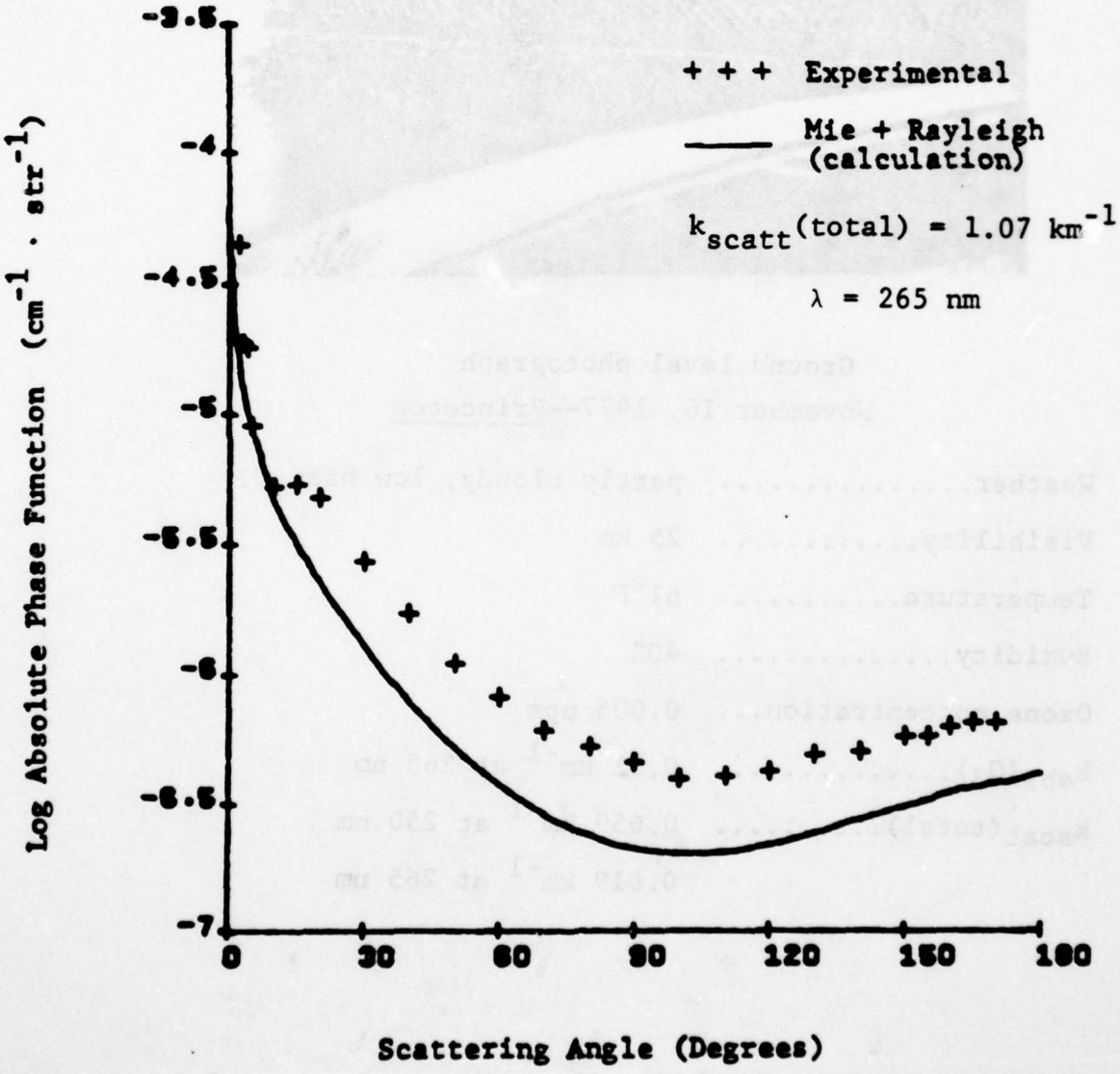

Phase function measured on November 9, 1977.

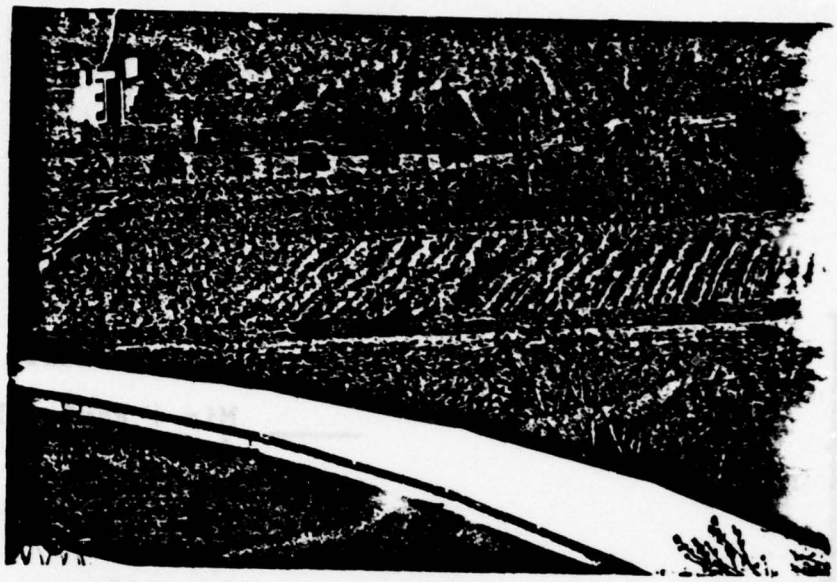

Ground level photograph
November 16, 1977--Princeton

Weather.....	partly cloudy, low haze
Visibility.....	25 km
Temperature.....	61°F
Humidity.....	40%
Ozone concentration...	0.005 ppm
$k_{abs}(O_3)$.....	0.01 km^{-1} at 265 nm
k_{scat}(total).....	0.659 km^{-1} at 250 nm
	0.619 km^{-1} at 265 nm

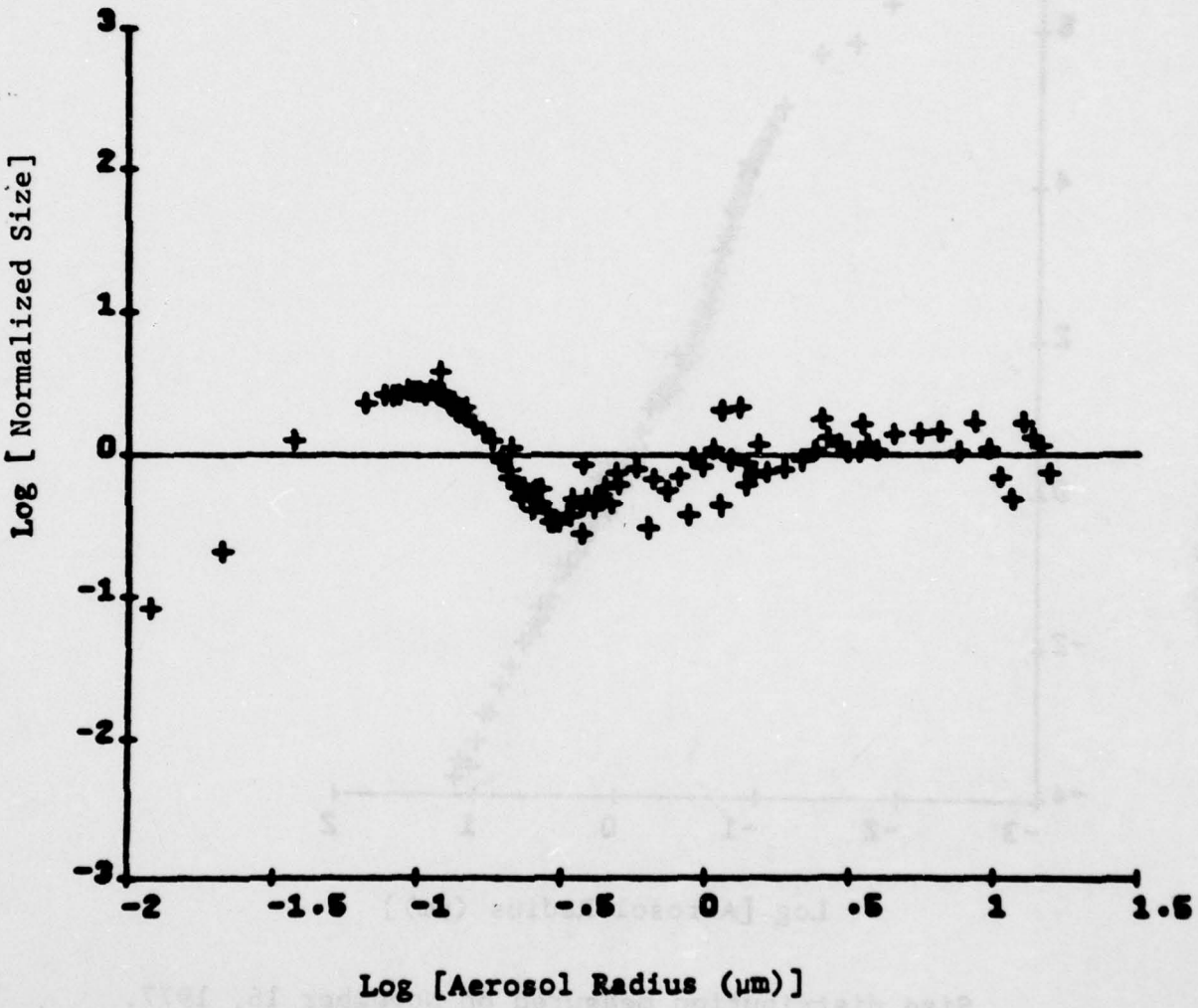

Normalized size distribution measured on
November 16, 1977.

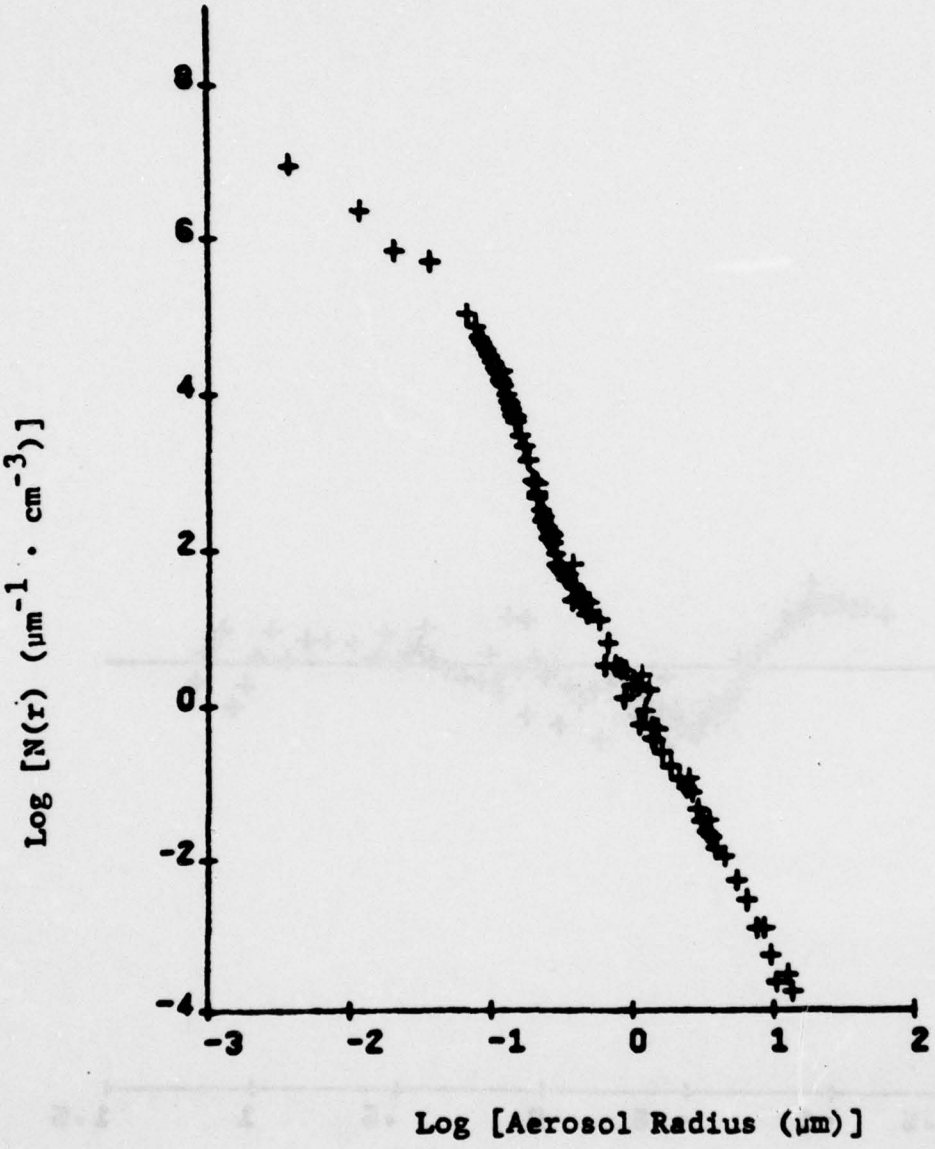

Size distribution measured on November 16, 1977.

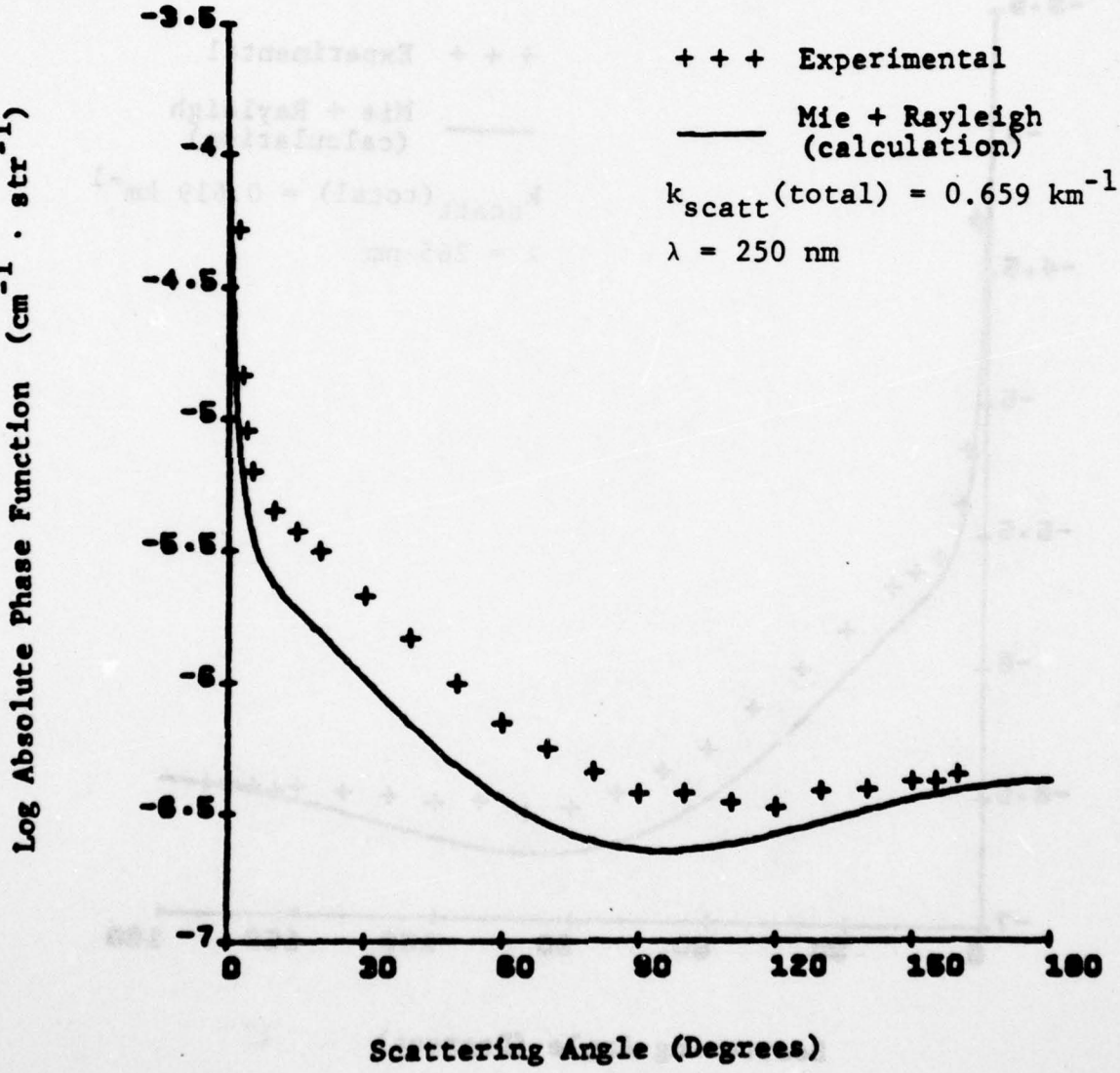

Phase function measured on November 16, 1977.

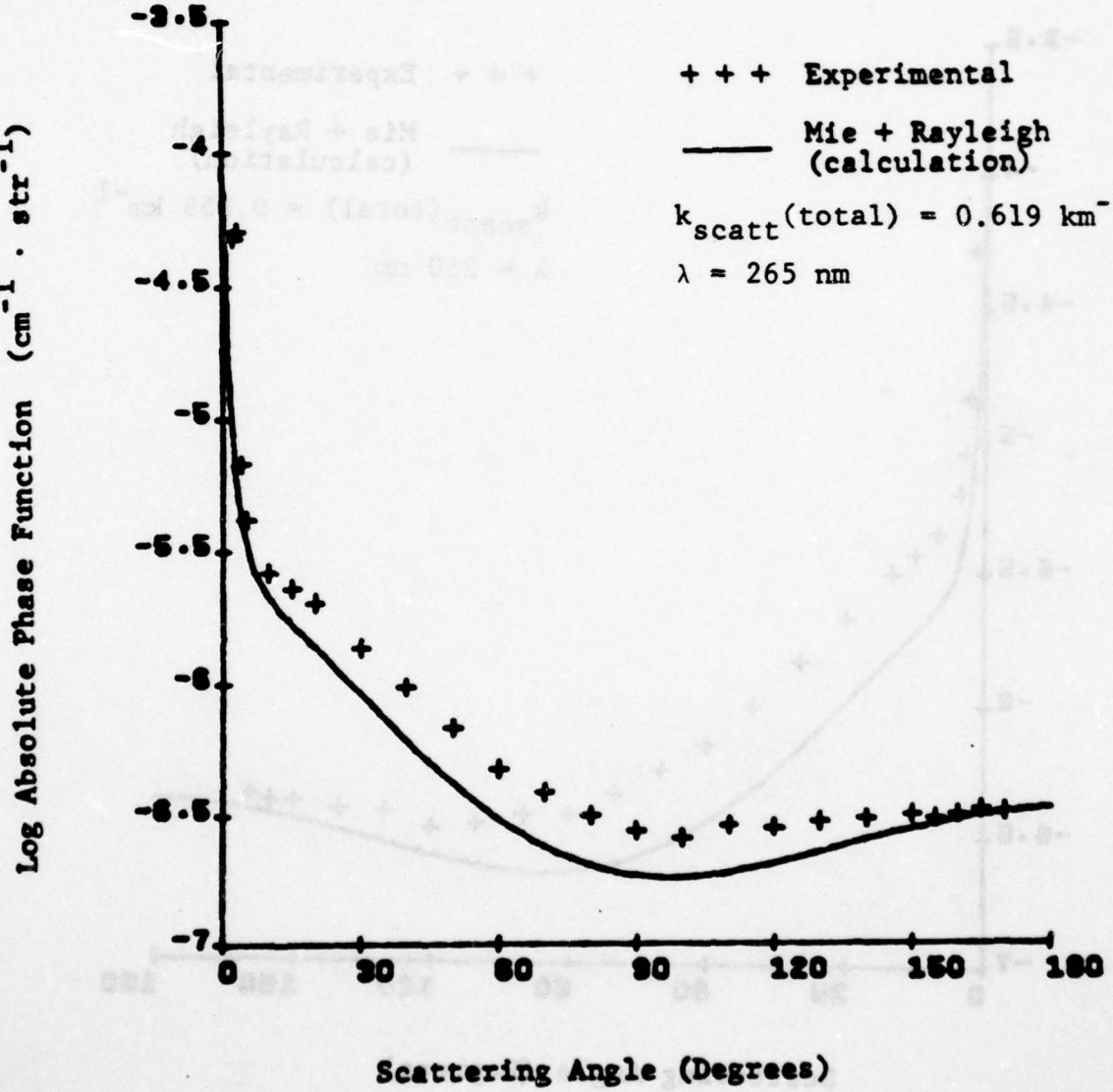

Phase function measured on November 16, 1977.

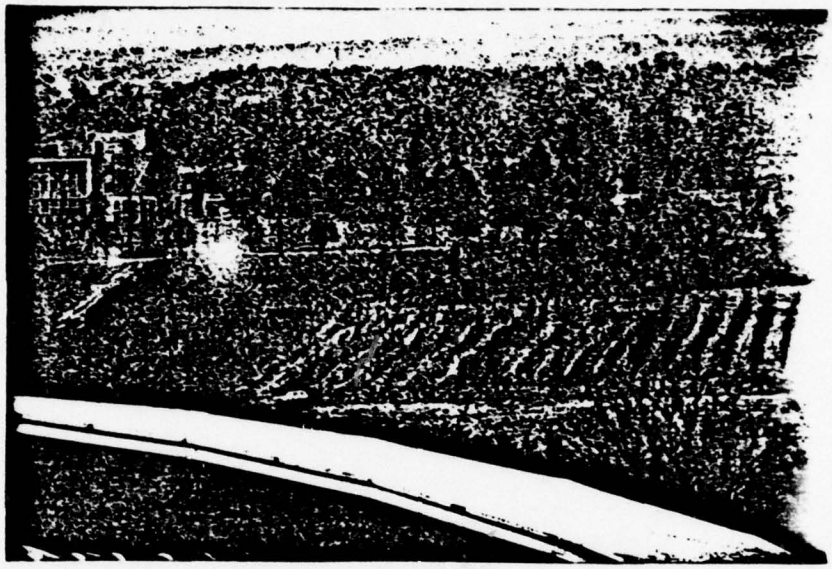

Ground level photograph
November 21, 1977--Princeton

Weather.....	overcast, intermittant rain
Visibility.....	15 km
Temperature.....	53°F
Humidity.....	75%
Ozone concentration...	0.001 ppm
$k_{abs}(O_3)$.....	0.025 km^{-1} at 265 nm
k_{scat}(total).....	0.418 km^{-1} at 250 nm

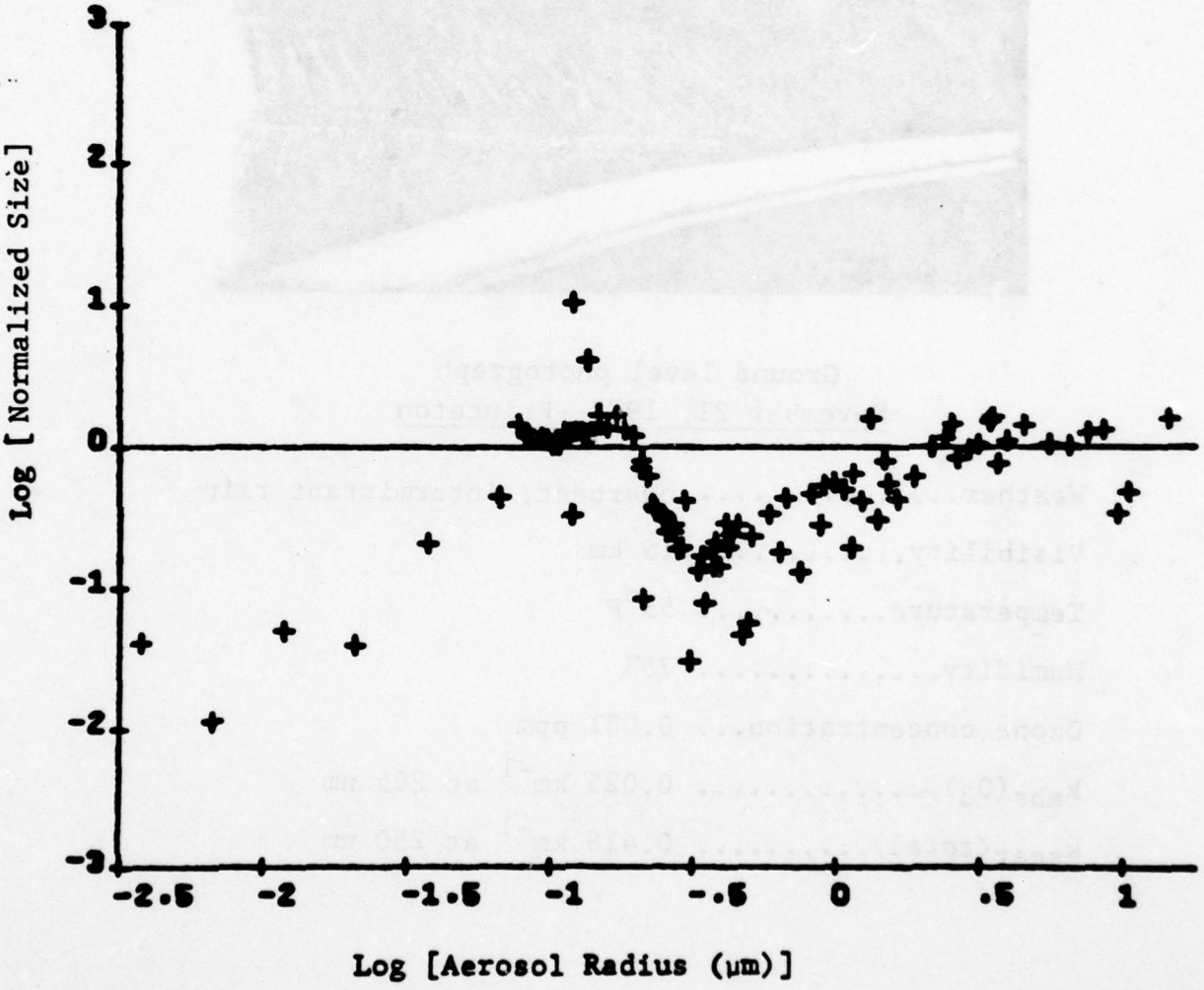

Normalized size distribution measured on November 21, 1977.

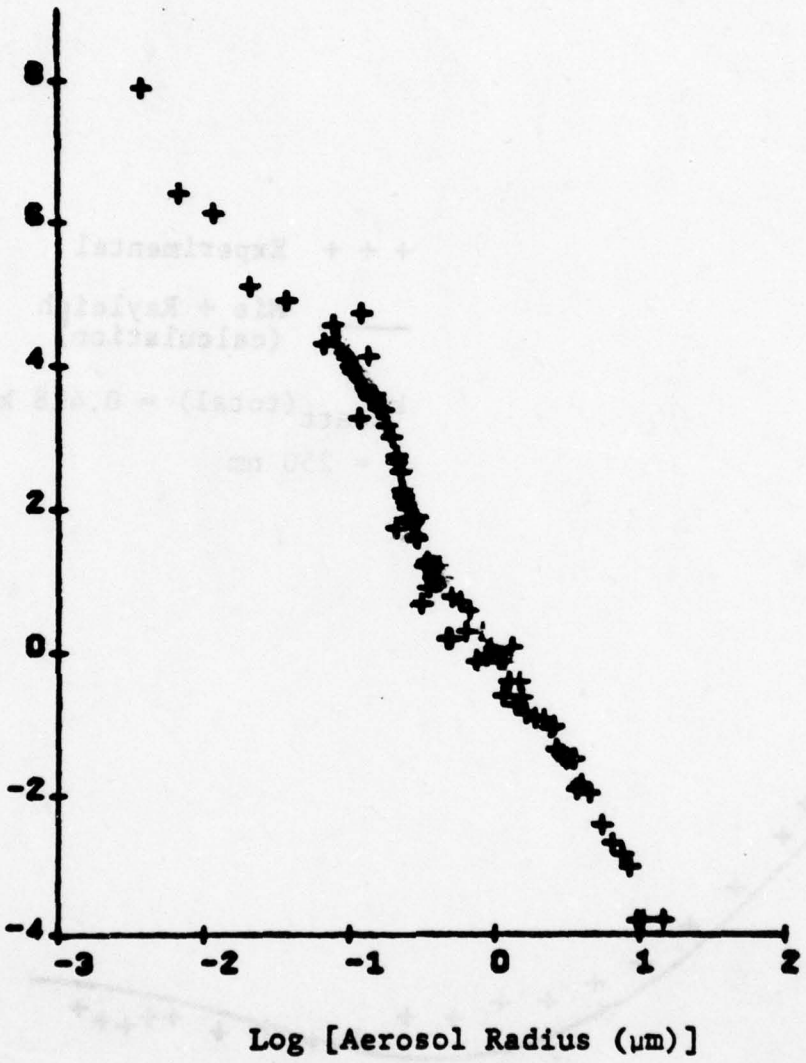

Size distribution measured on November 21, 1977.

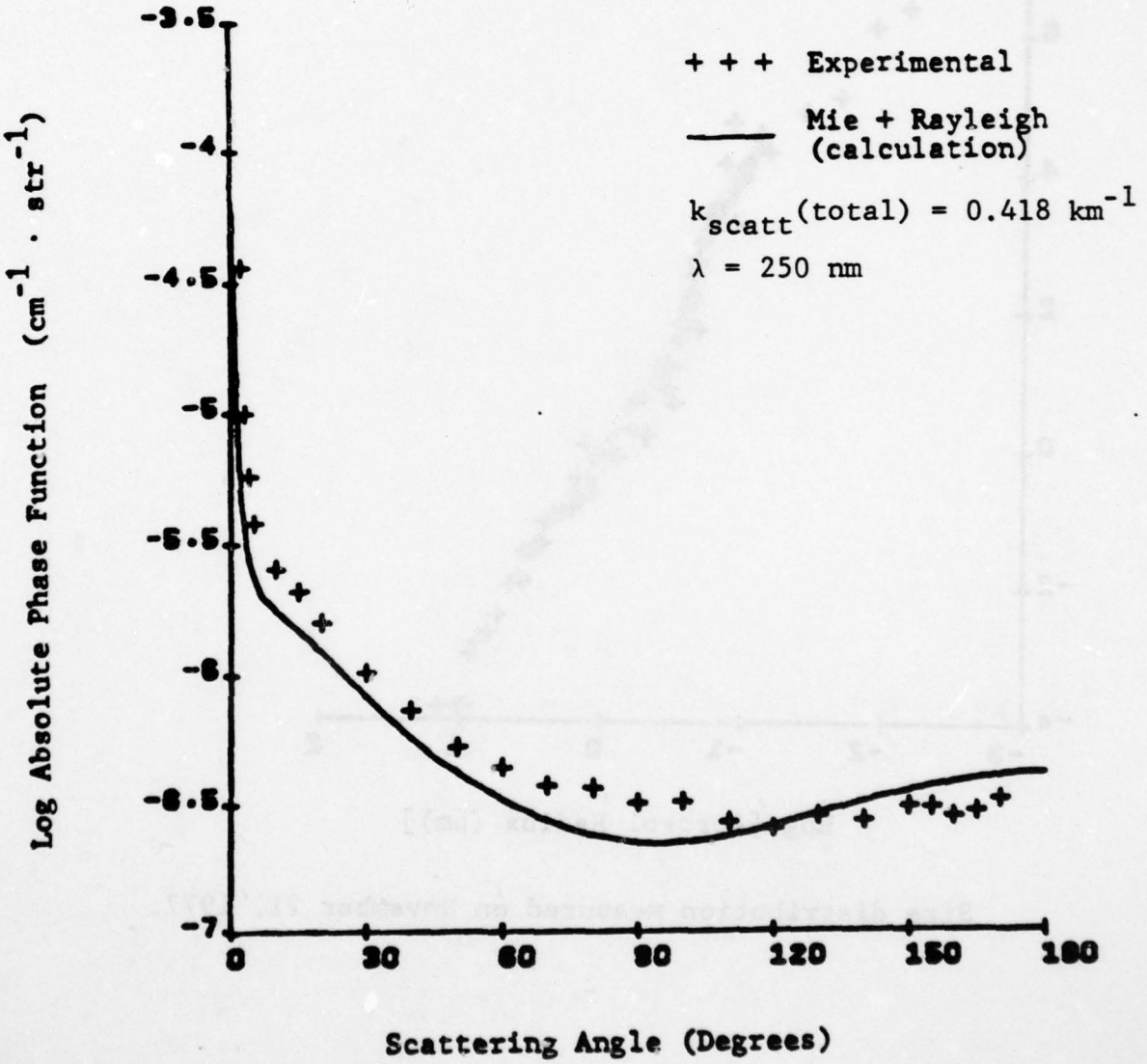

Phase function measured on November 21, 1977.

AD-A066 160 AERONAUTICAL RESEARCH ASSOCIATES OF PRINCETON INC N J F/G 4/1
SEASONAL VARIATIONS IN ULTRAVIOLET SINGLE SCATTERING PHASE FUNC--ETC(U)
FEB 79 J M SCHLUPF, C R DICKSON, M E NEER N00014-76-C-1094
UNCLASSIFIED ARAP-383 NL

2 OF 3
ADA
066160

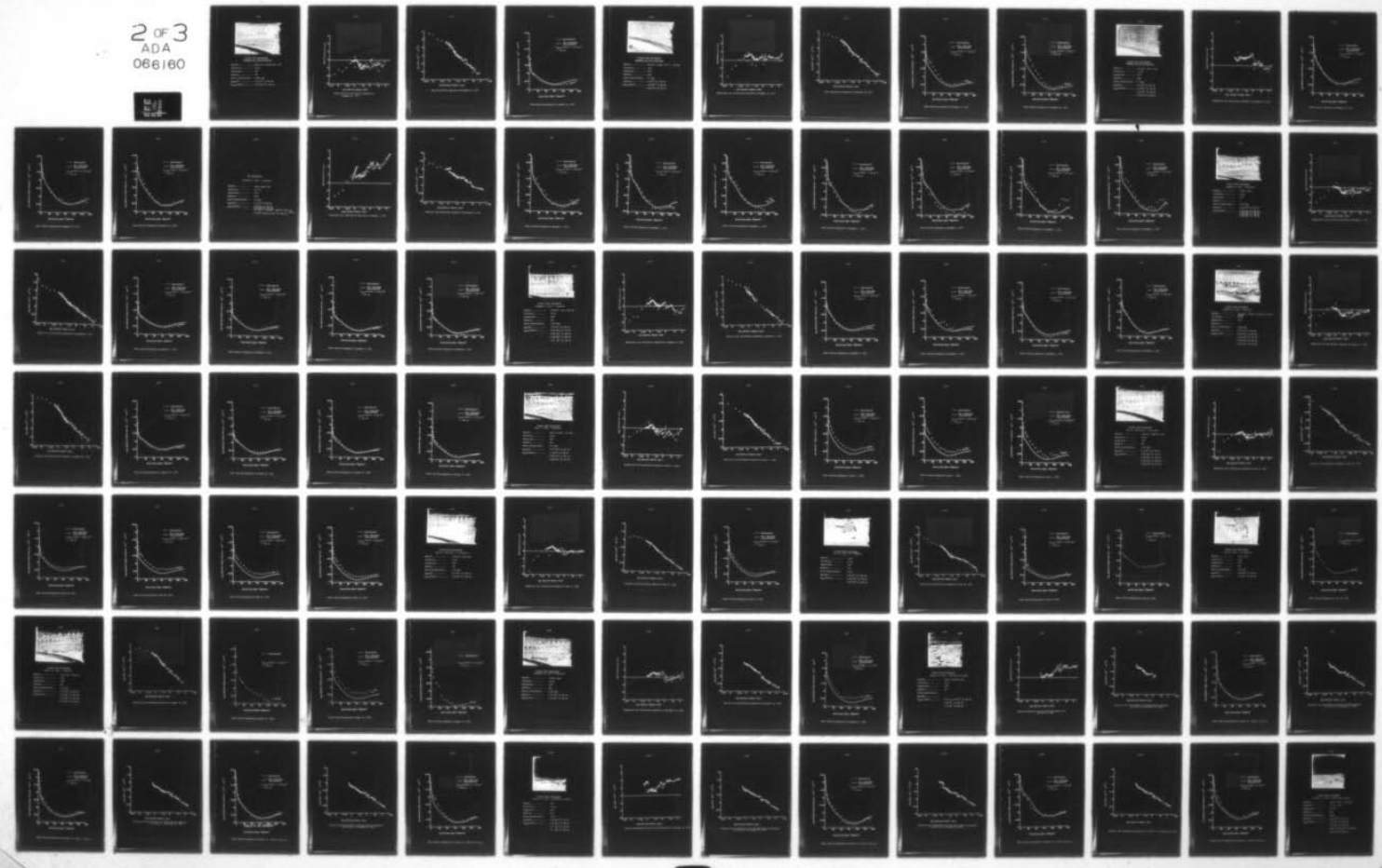

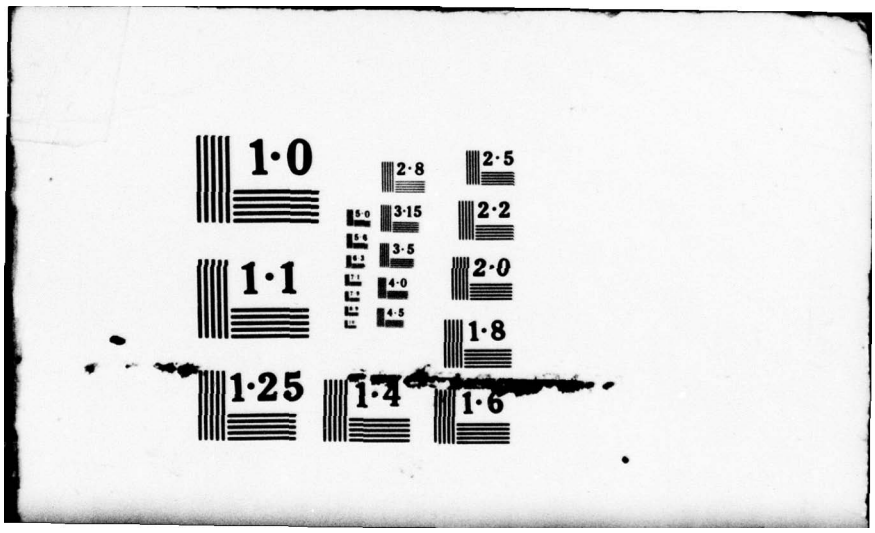
1·0
1·1
1·25
1·4
1·6
1·8
2·0
2·2
2·5
2·8
3·15
3·5
4·0
4·5
5·0

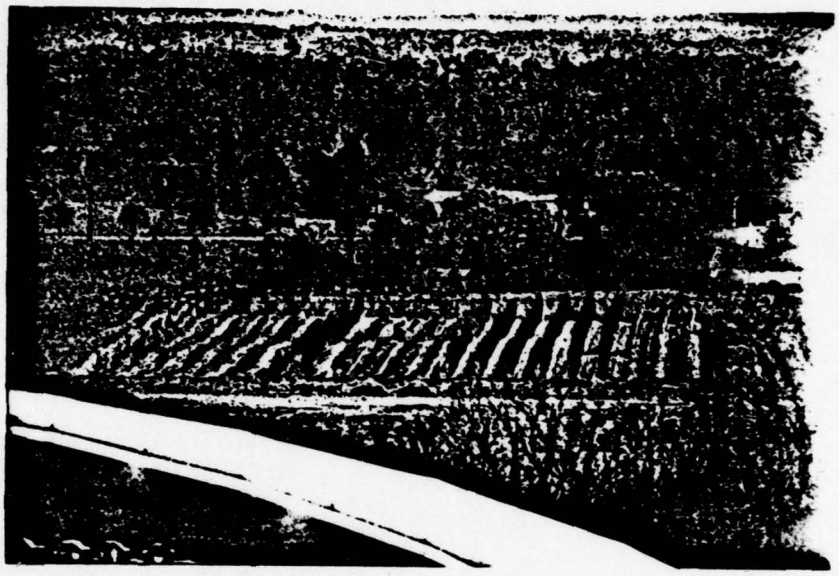

Ground level photograph
November 22, 1977--Princeton

Weather.....	overcast, intermittant rain
Visibility.....	30 km
Temperature.....	45°F
Humidity.....	70%
Ozone concentration...	0.0004 ppm
$k_{abs}(O_3)$.....	0.01 km^{-1} at 265 nm
k_{scat}(total).....	0.371 km^{-1} at 250 nm

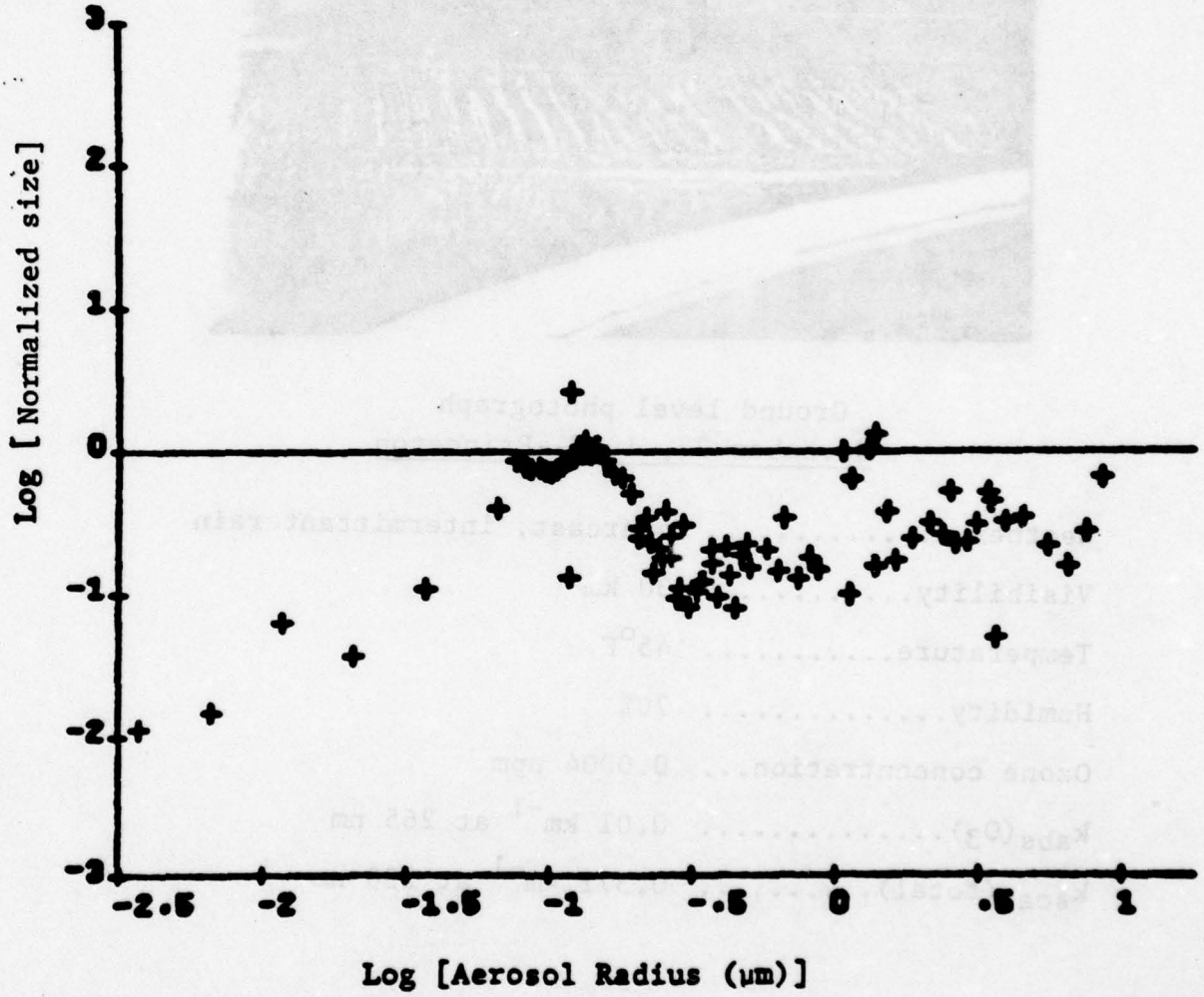

Normalized size distribution measured on November 22, 1977.

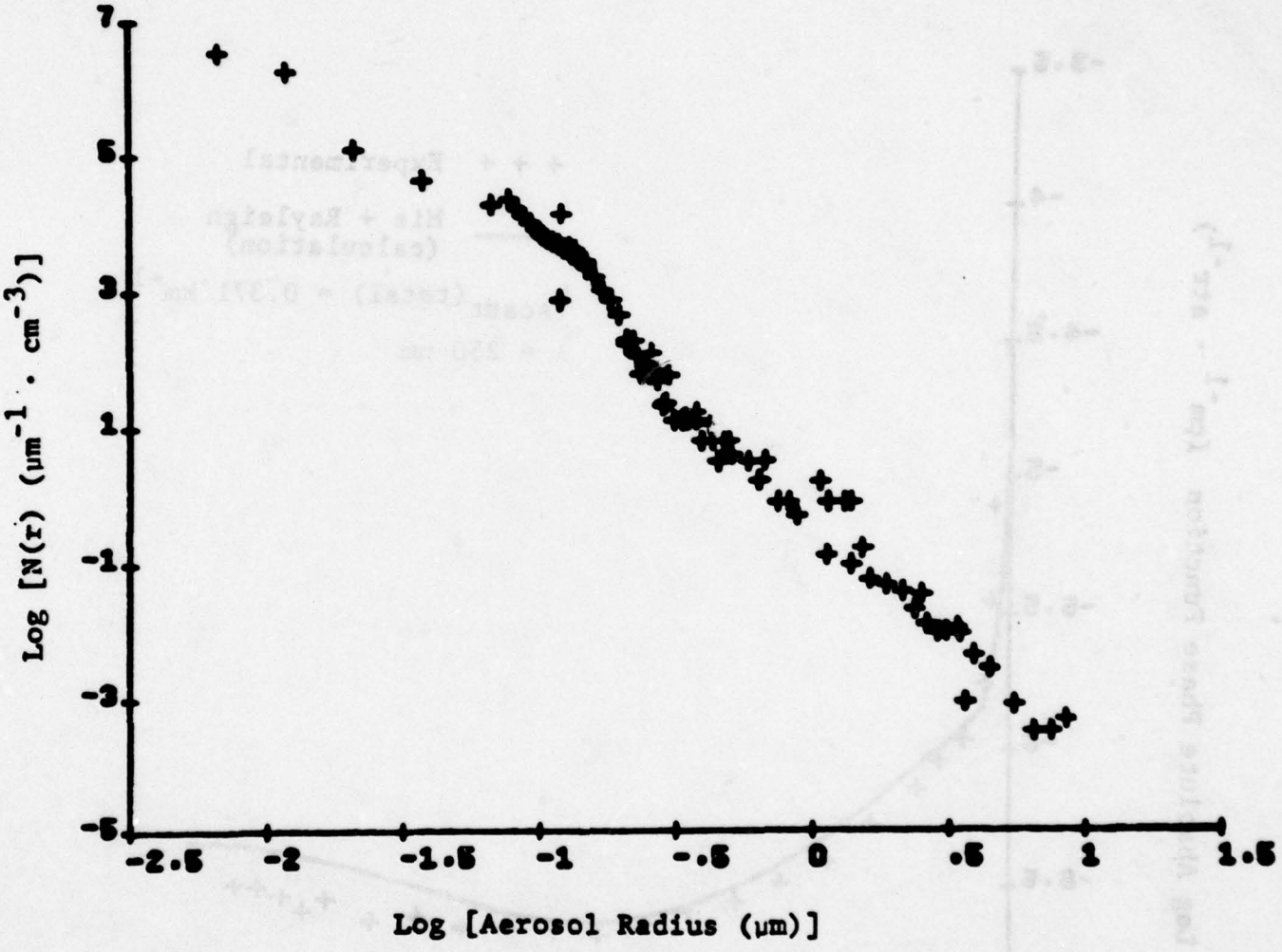

Size distribution measured on November 22, 1977.

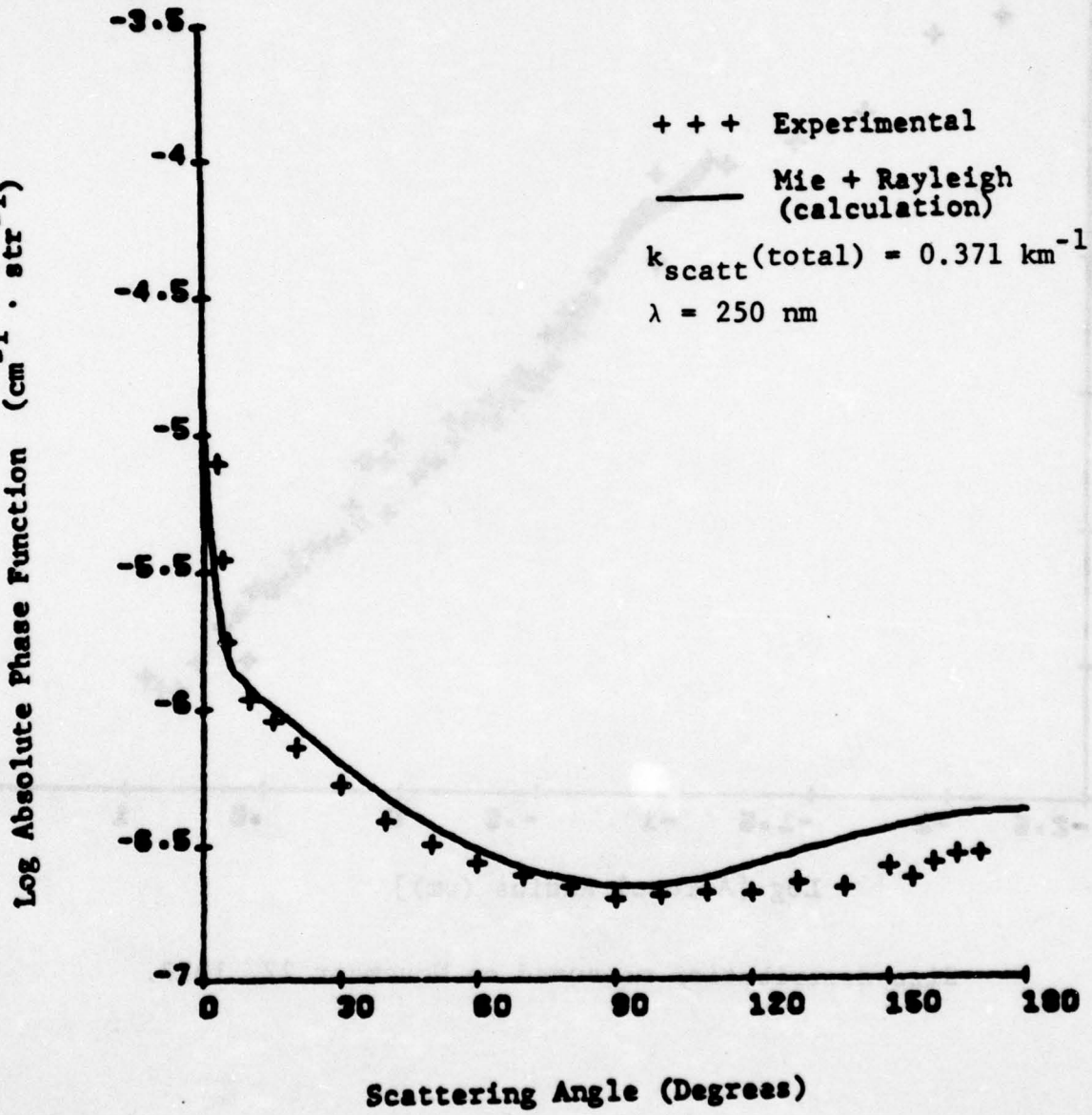

Phase function measured on November 22, 1977.

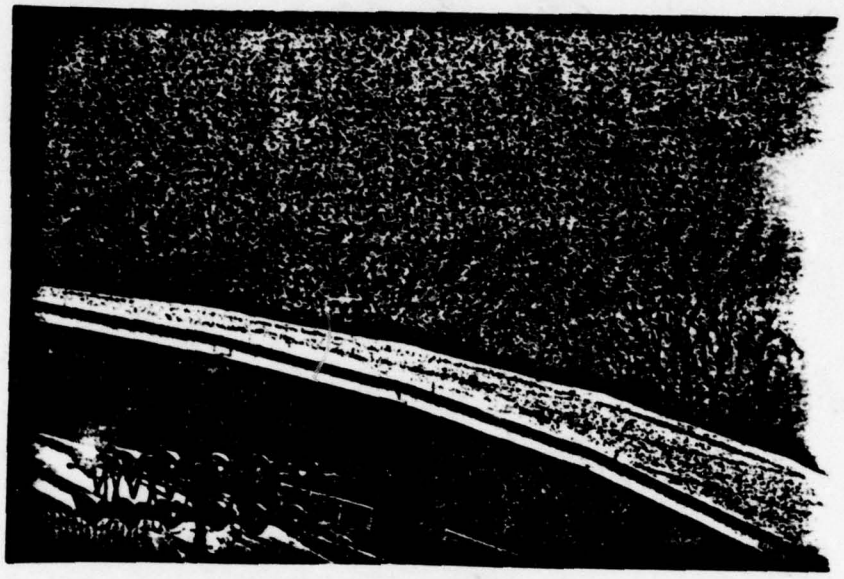

Ground level photograph
November 23, 1977--Princeton

Weather.....	overcast, foggy, 200 ft. ceiling
Visibility.....	2 km
Temperature.....	45°F
Humidity.....	100%
Ozone concentration...	0.0 ppm
$k_{abs}(O_3)$.....	0.0 km^{-1} at 265 nm
k_{scat}(total).....	1.58 km^{-1} at 250 nm
	1.96 km^{-1} at 275 nm

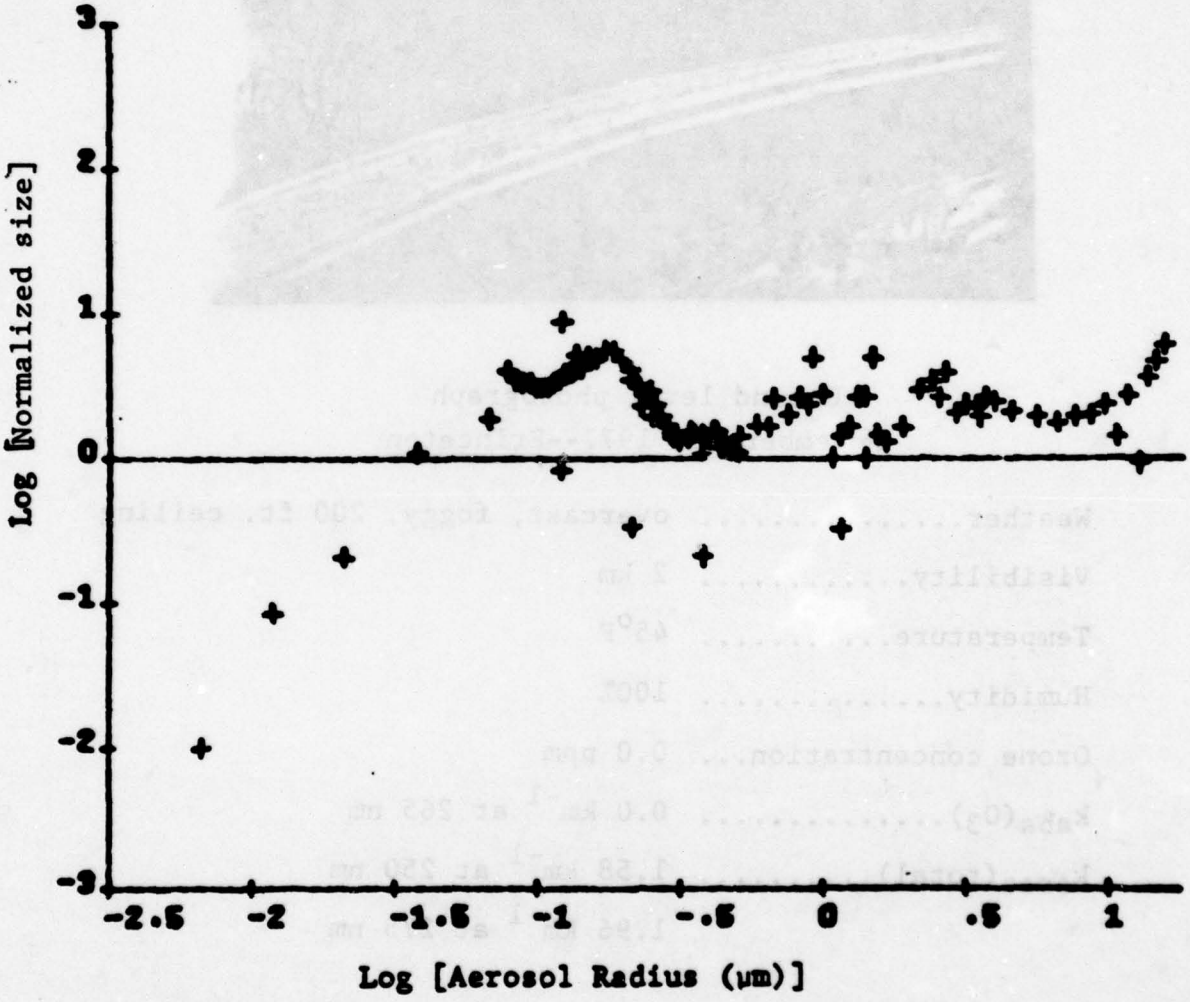

Normalized size distribution measured on November 23, 1977

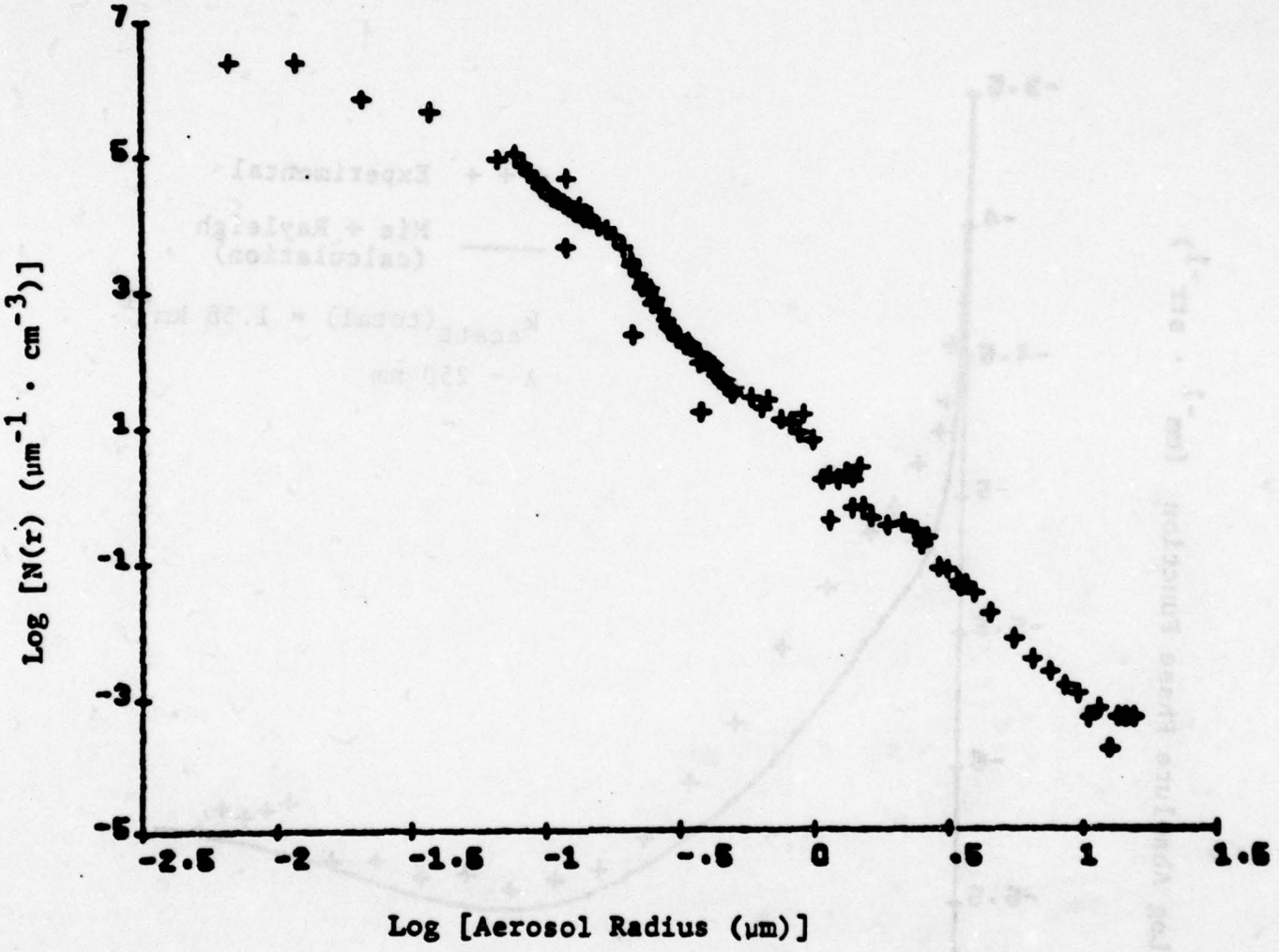

Size distribution measured on November 23, 1977.

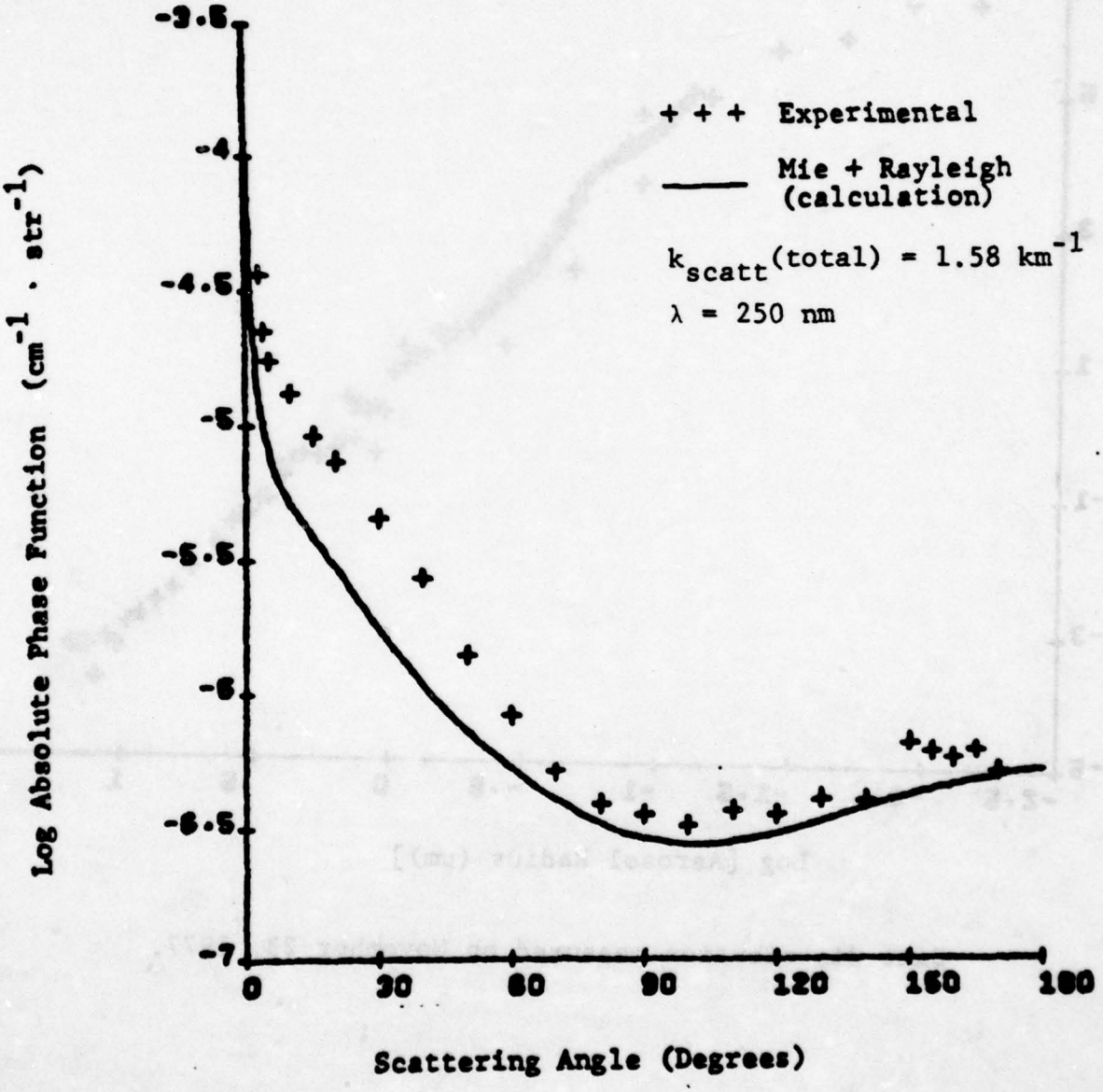

Phase function measured on November 23, 1977.

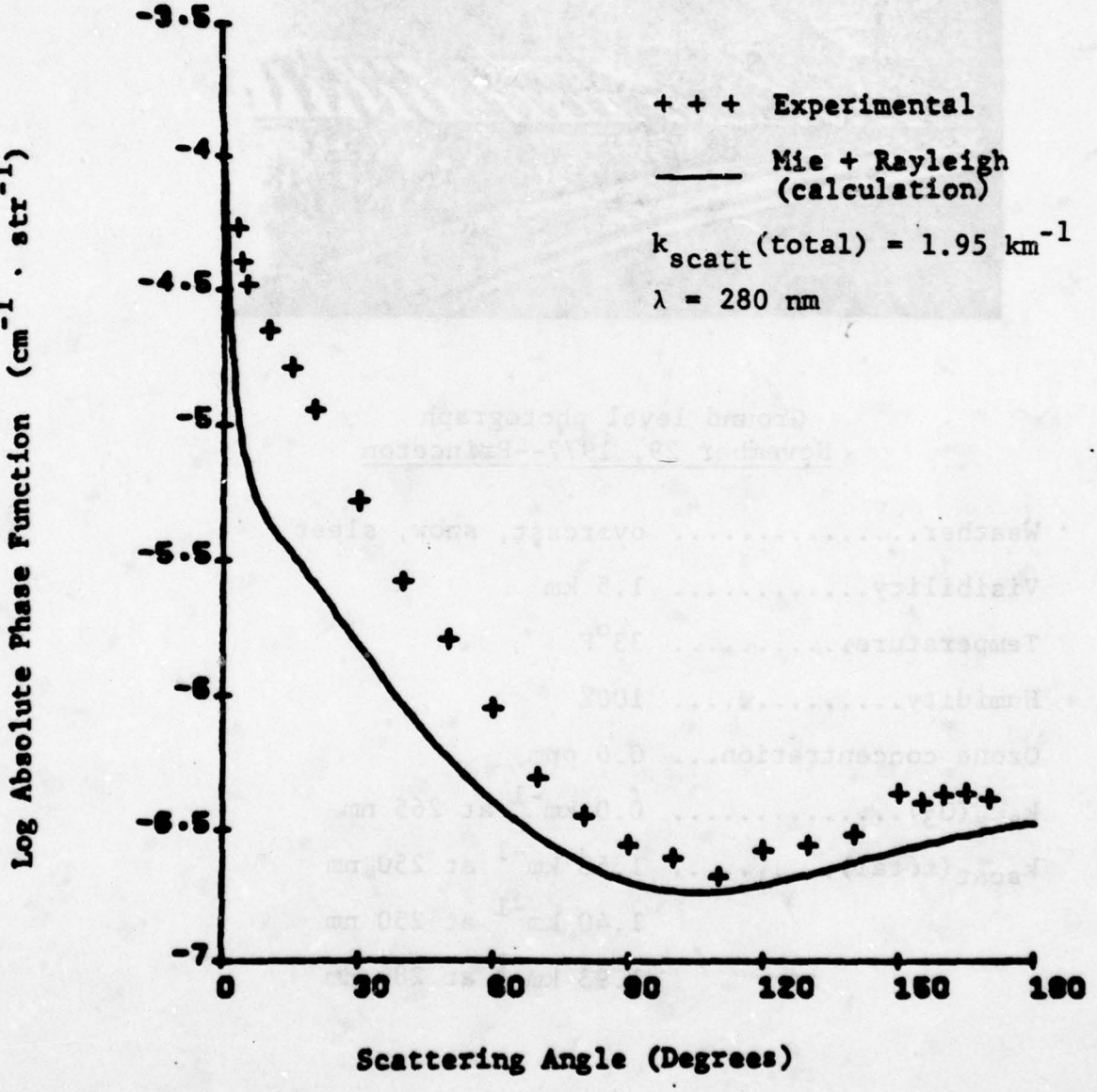

Phase function measured on November 23, 1977.

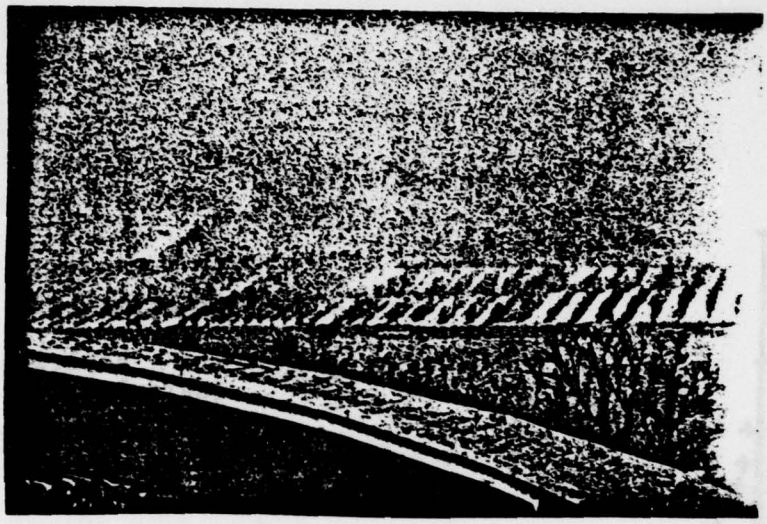

Ground level photograph
November 29, 1977--Princeton

Weather.....	overcast, snow, sleet
Visibility.....	1.5 km
Temperature.....	33°F
Humidity.....	100%
Ozone concentration...	0.0 ppm
$k_{abs}(O_3)$.....	0.0 km^{-1} at 265 nm
k_{scat}(total).....	1.58 km^{-1} at 250 nm
	1.40 km^{-1} at 250 nm
	1.93 km^{-1} at 280 nm

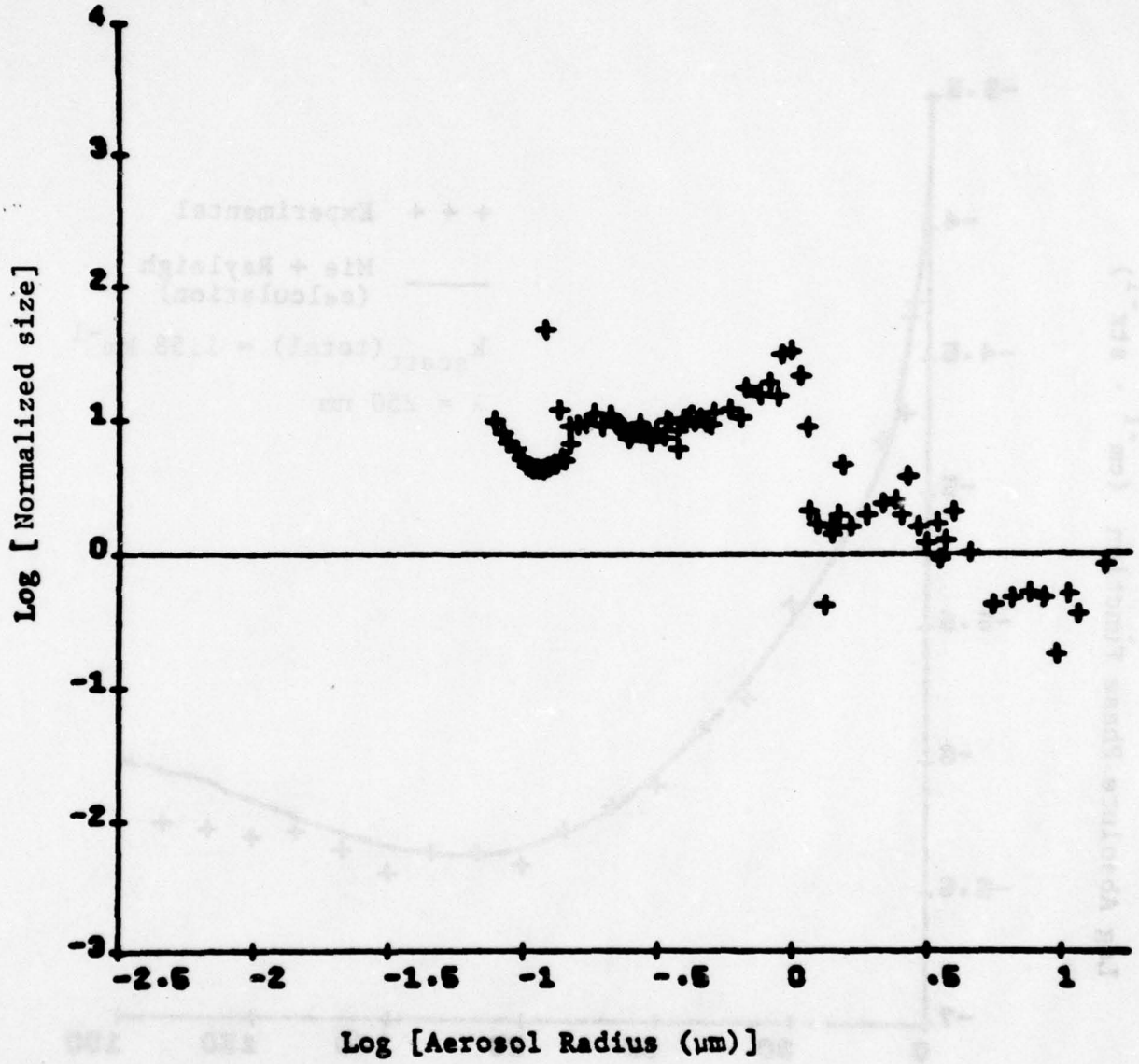

Normalized size distribution measured on November 29, 1977.

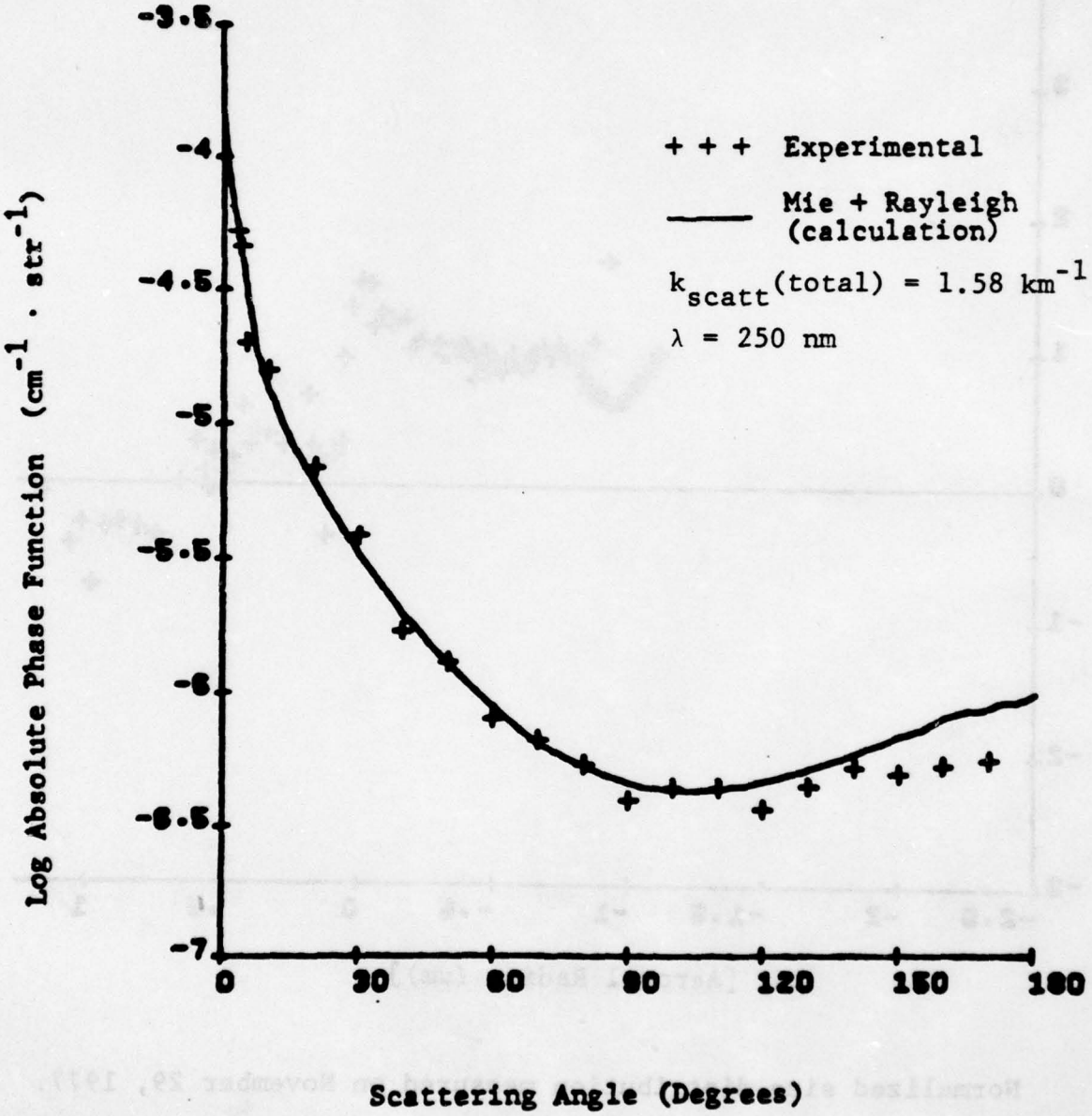

Phase function measured on November 29, 1977.

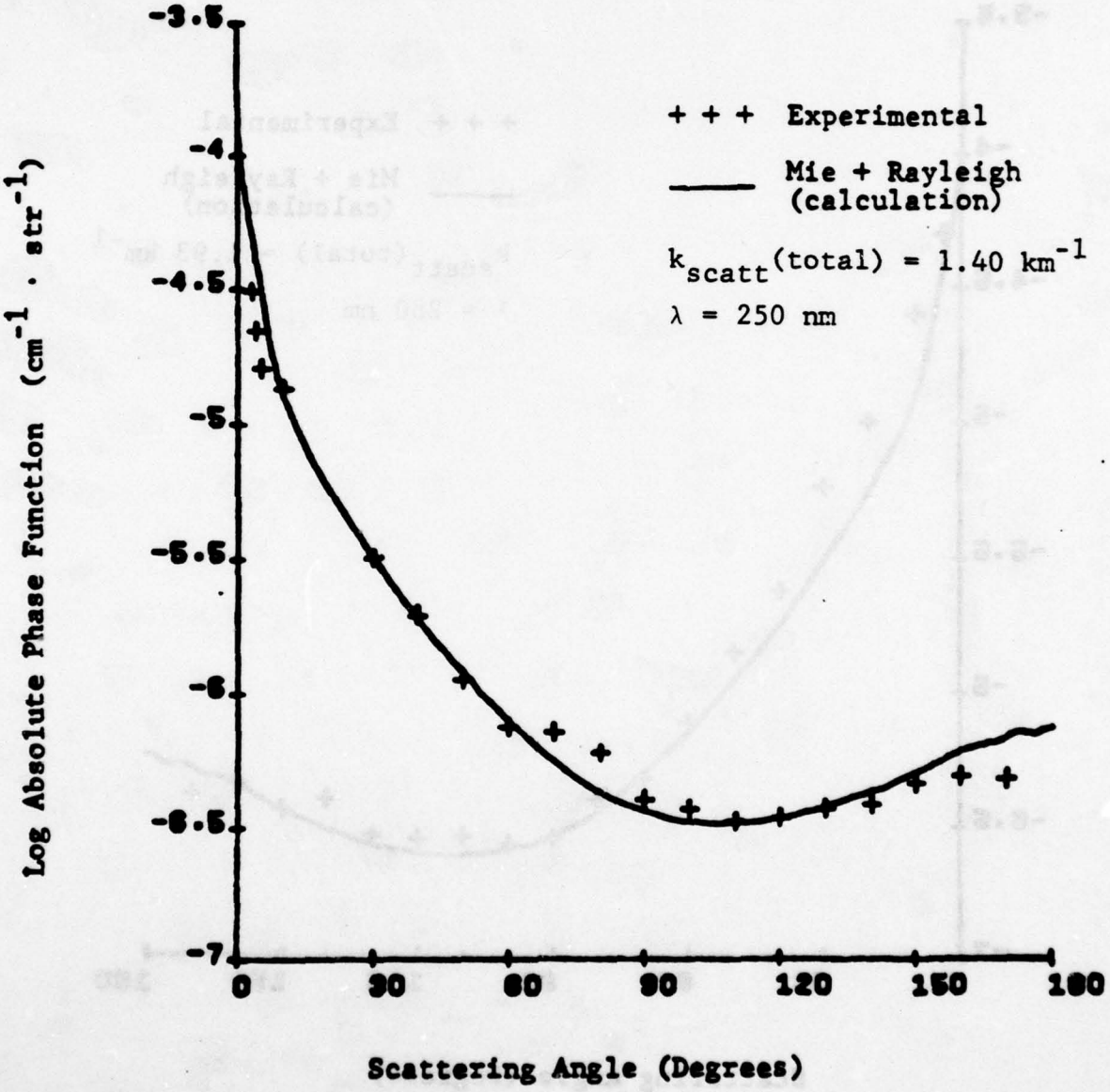

Phase function measured on November 29, 1977.

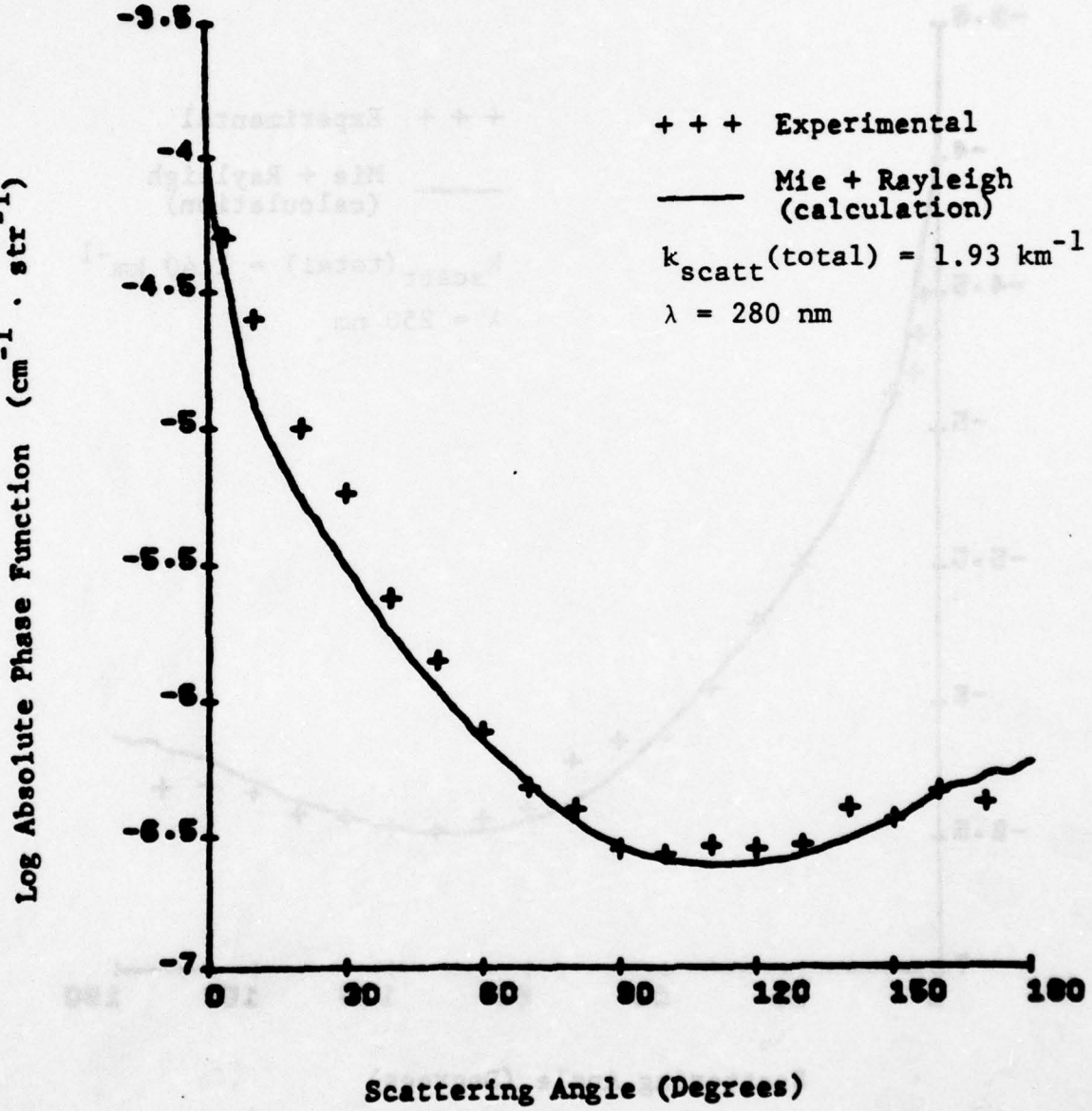

Phase function measured on November 29, 1977.

(No Photograph)

December 1, 1977 -- Princeton

Weather.....	heavy ground fog
Visibility.....	0.2 km
Temperature.....	47°F
Humidity.....	100%
Ozone concentration...	0.0 ppm
$k_{abs}(O_3)$.....	0.0 km^{-1} at 265 nm
k_{scat}(total).....	6.58 km^{-1} at 220 nm 5.43 km^{-1} at 230 nm 3.43 km^{-1}, 3.49 km^{-1}, and 8.75 km^{-1} at 250 nm 7.36 km^{-1} and 10.4 km^{-1} at 280 nm

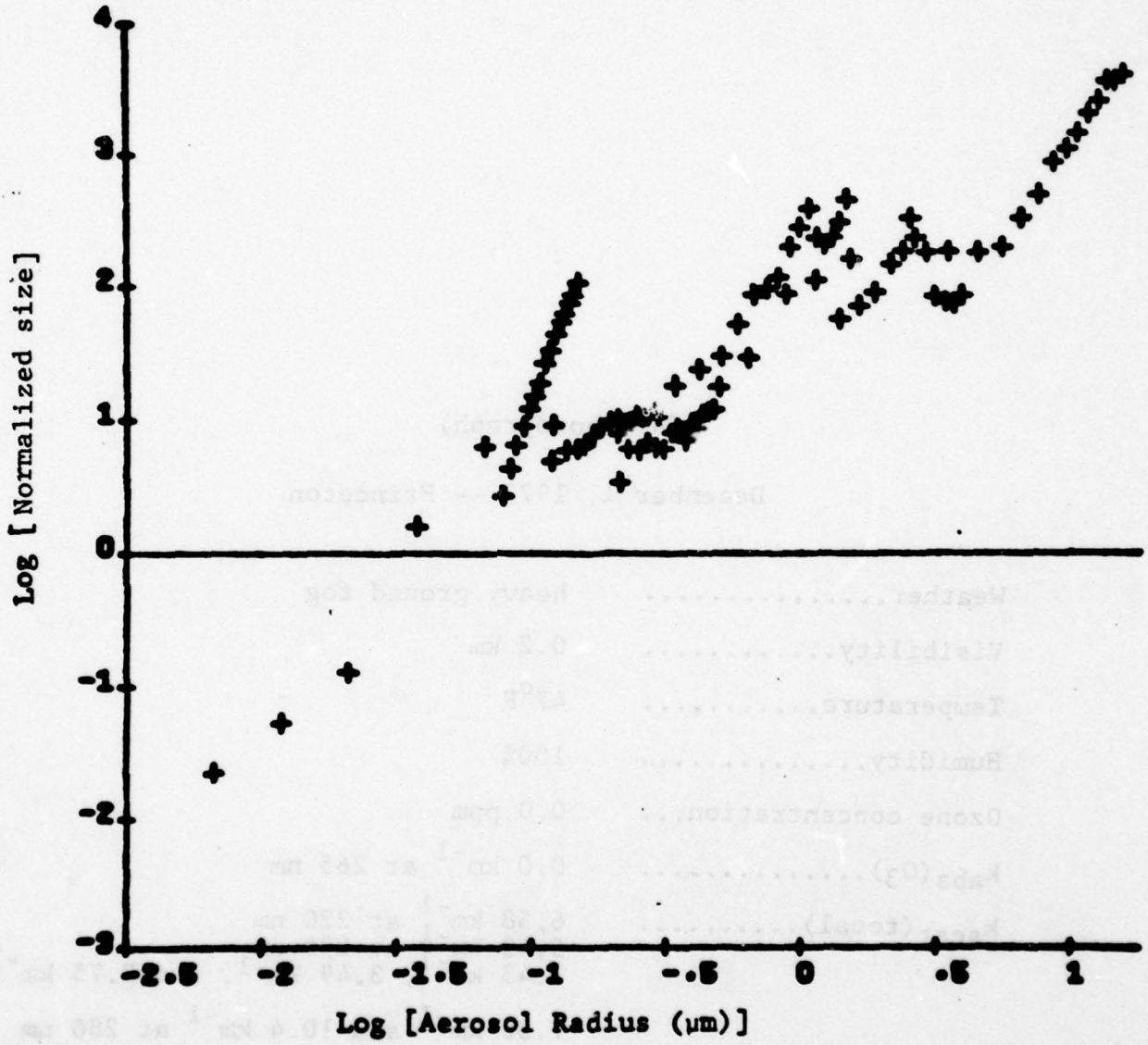

Normalized size distribution measured on December 1, 1977

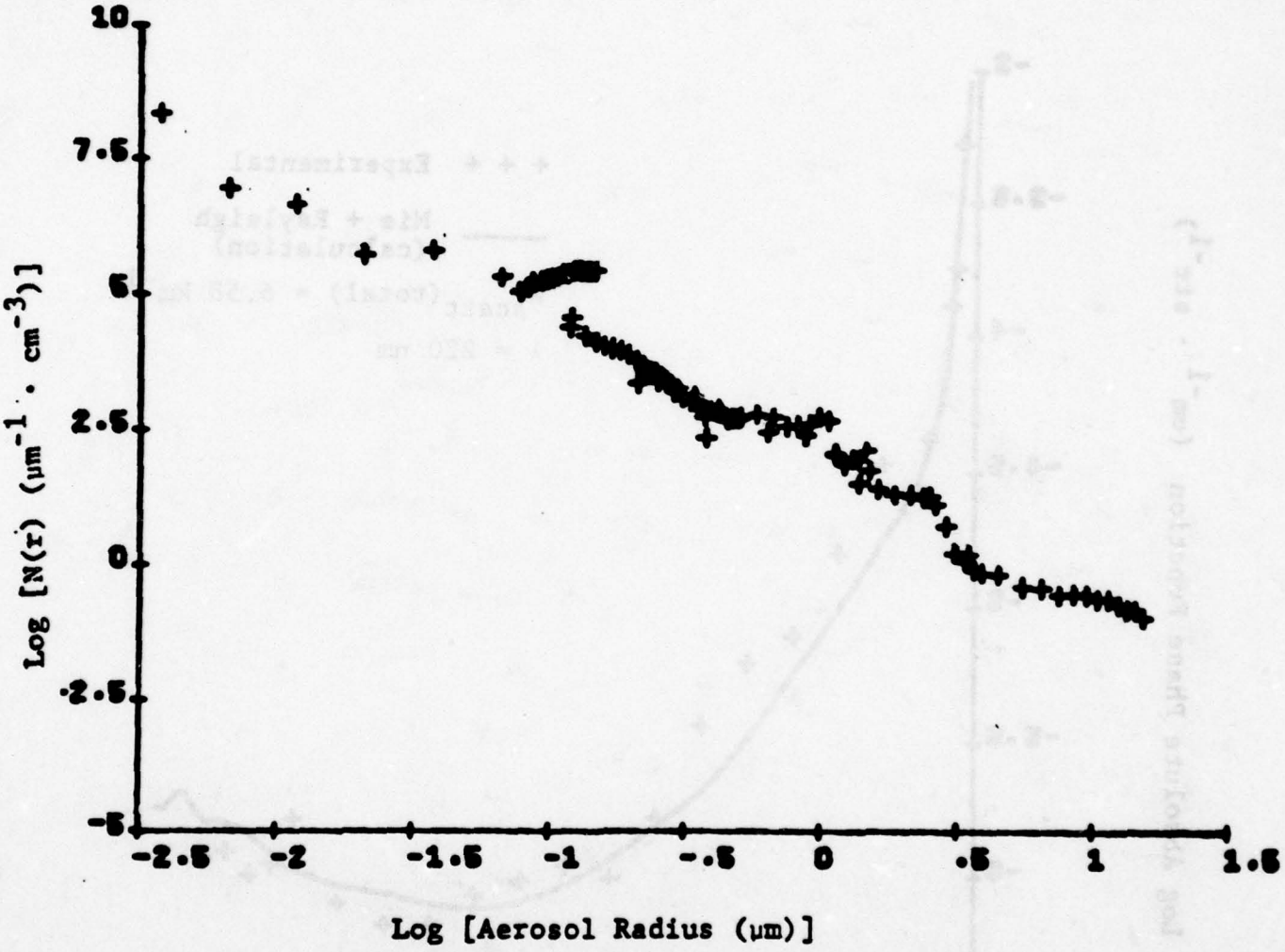

Particle size distribution measured on December 1, 1977.

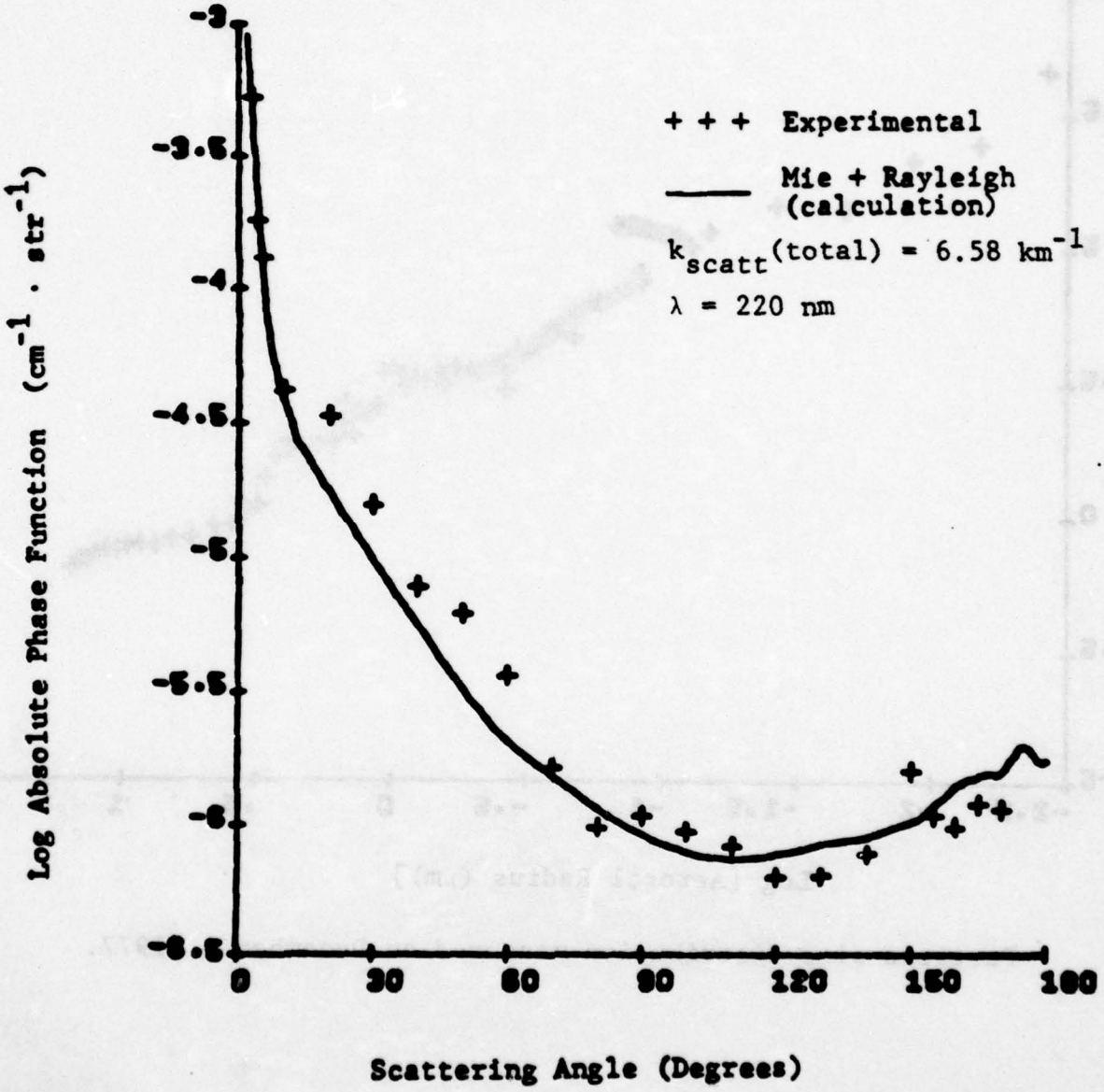

Phase function measured on December 1, 1977.

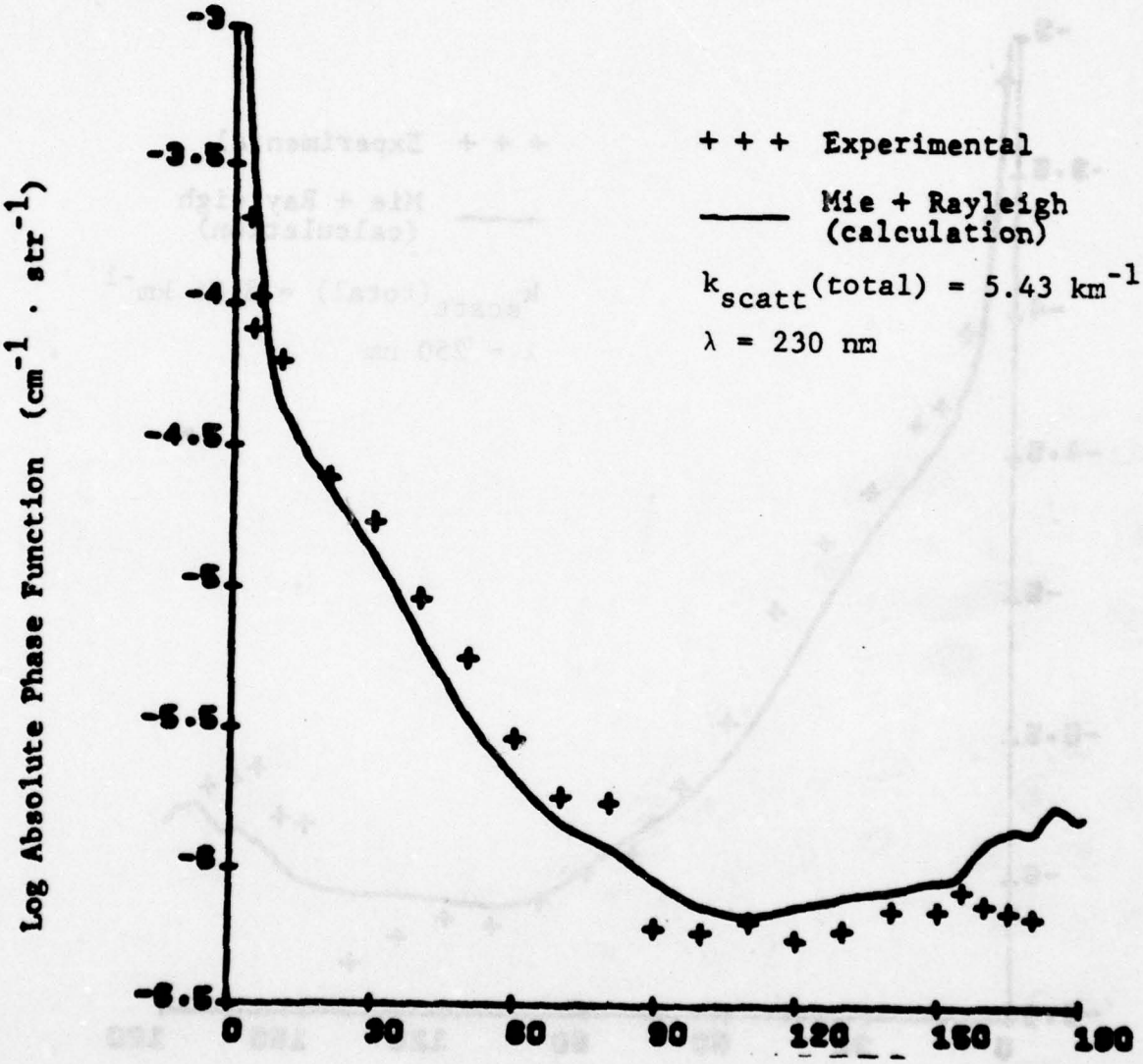

Phase function measured on December 1, 1977.

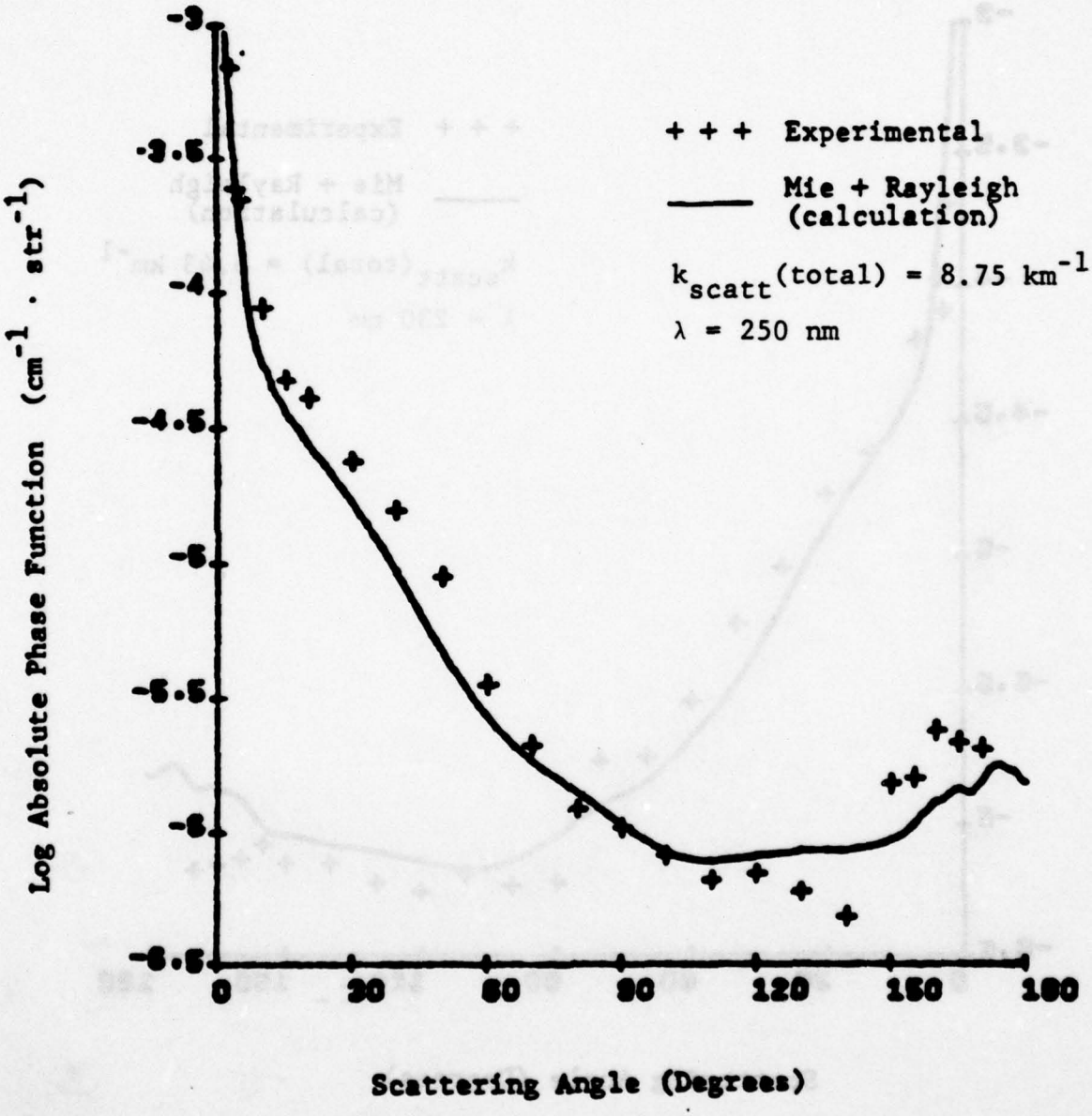

Phase function measured on December 1, 1977.

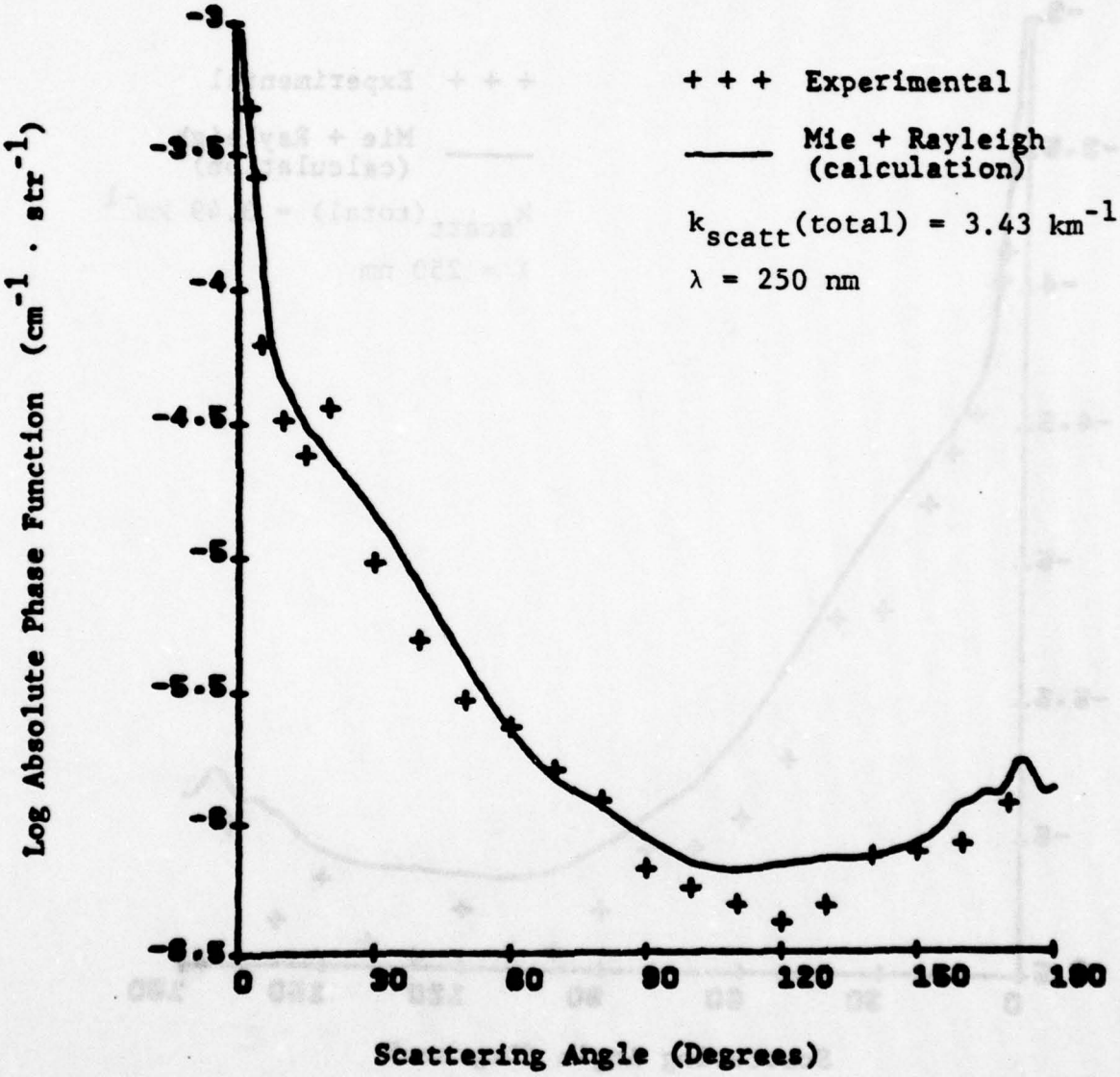

Phase function measured on December 1, 1977.

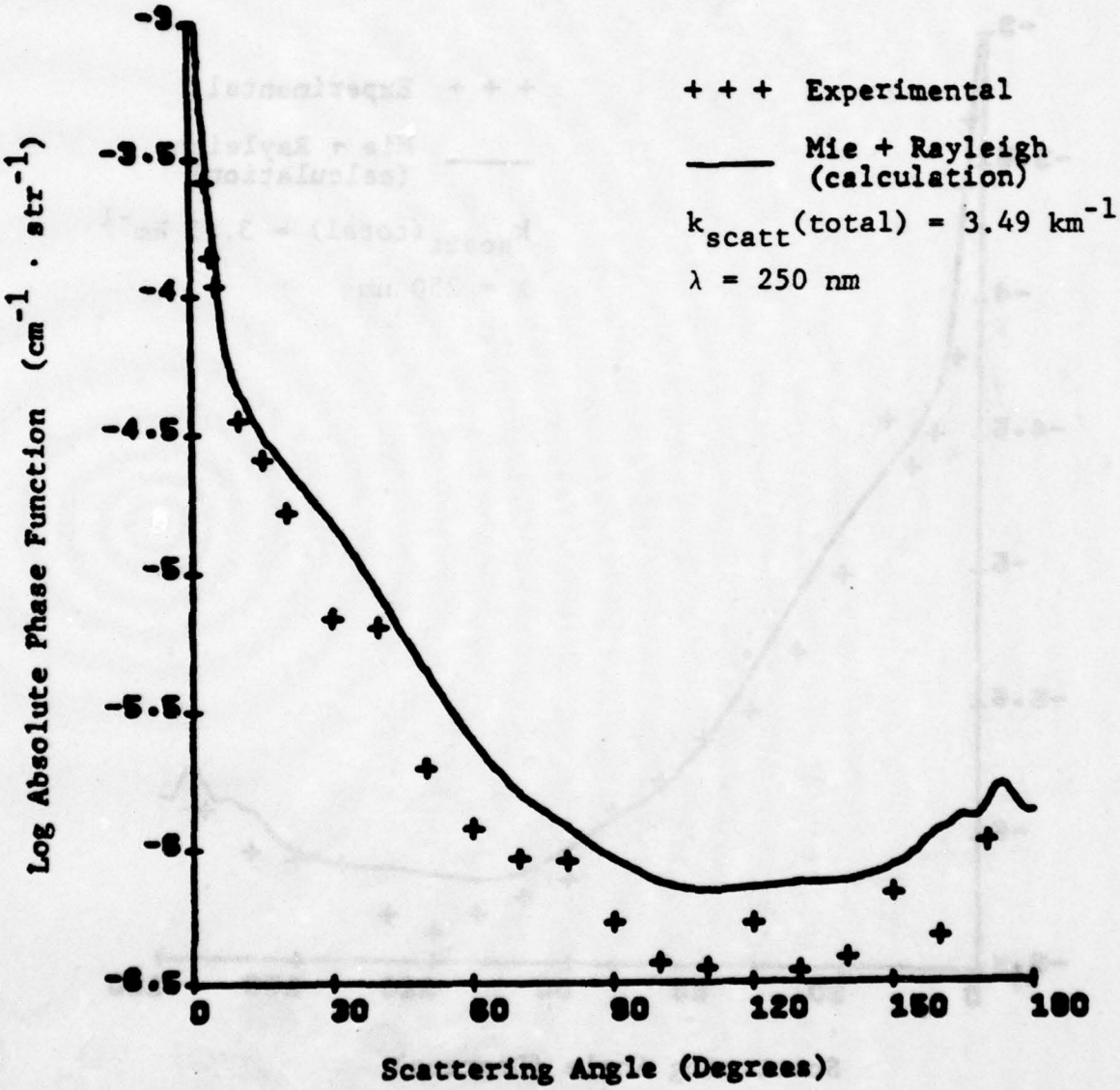

Phase function measured on December 1, 1977.

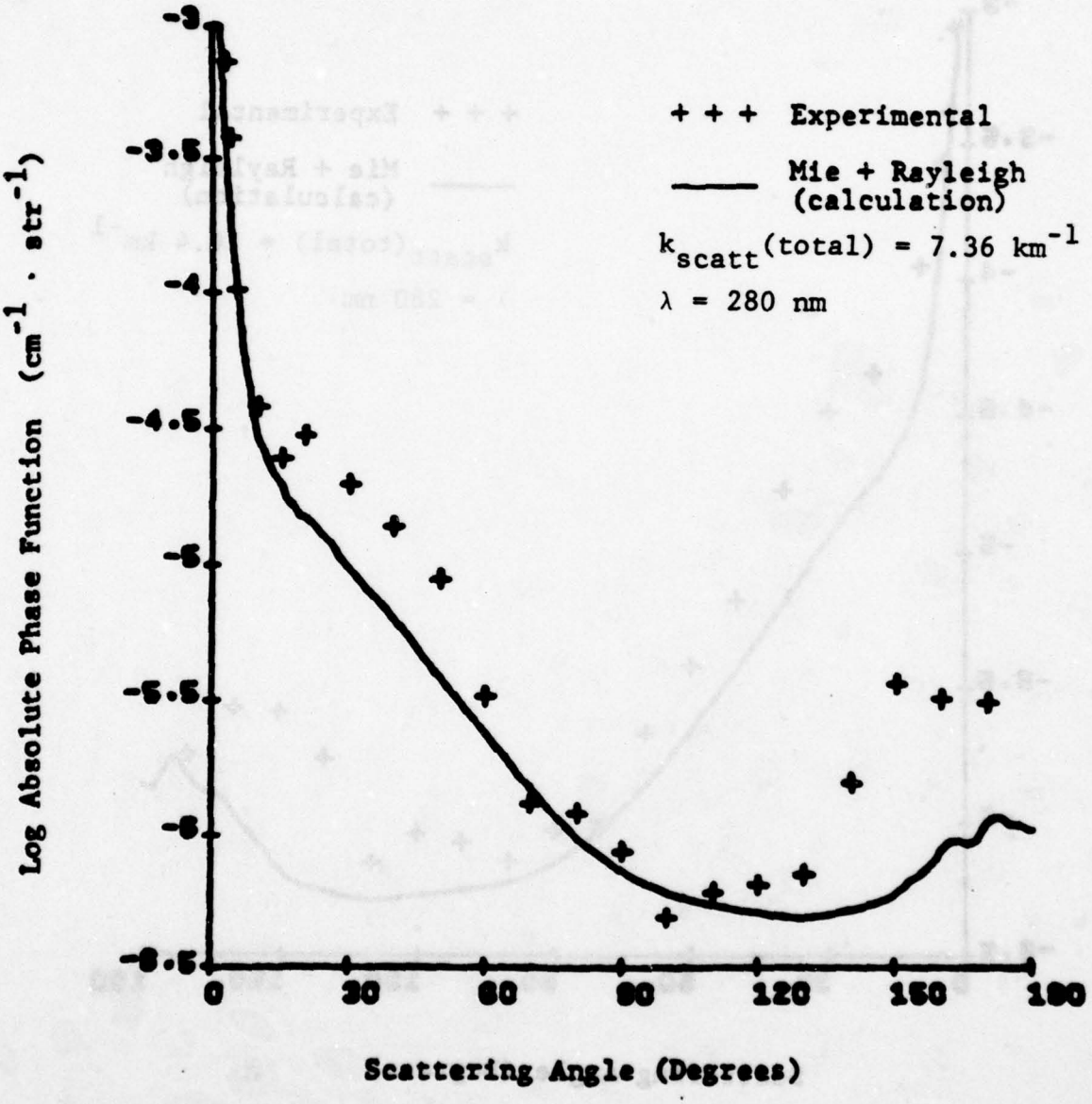

Phase function measured on December 1, 1977.

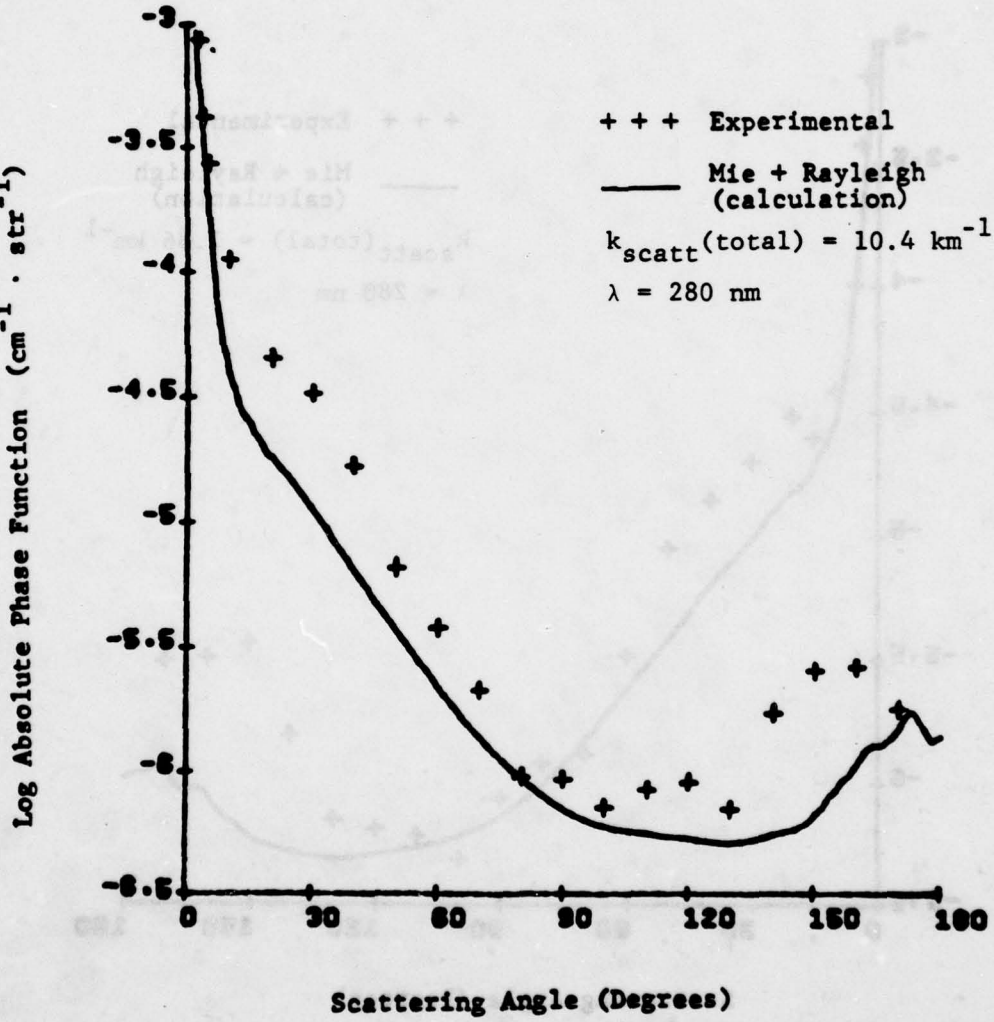

Phase function measured on December 1, 1977.

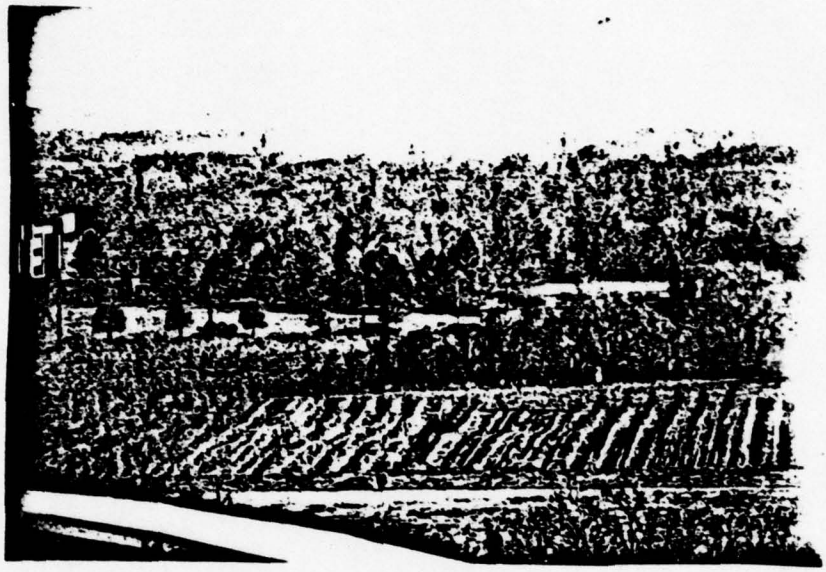

Ground level photograph

December 8, 1977 -- Princeton

Weather.....	clear, sunny
Visibility.....	25 km
Temperature.....	$31^{o}F$
Humidity.....	-
Ozone concentration...	0.025 ppm
$k_{abs}(O_3)$.....	0.63 km^{-1} at 265 nm
k_{scat}(total).....	0.563 km^{-1} at 230 nm 0.497 km^{-1} at 250 nm 0.376 km^{-1} at 265 nm 0.332 km^{-1} at 280 nm

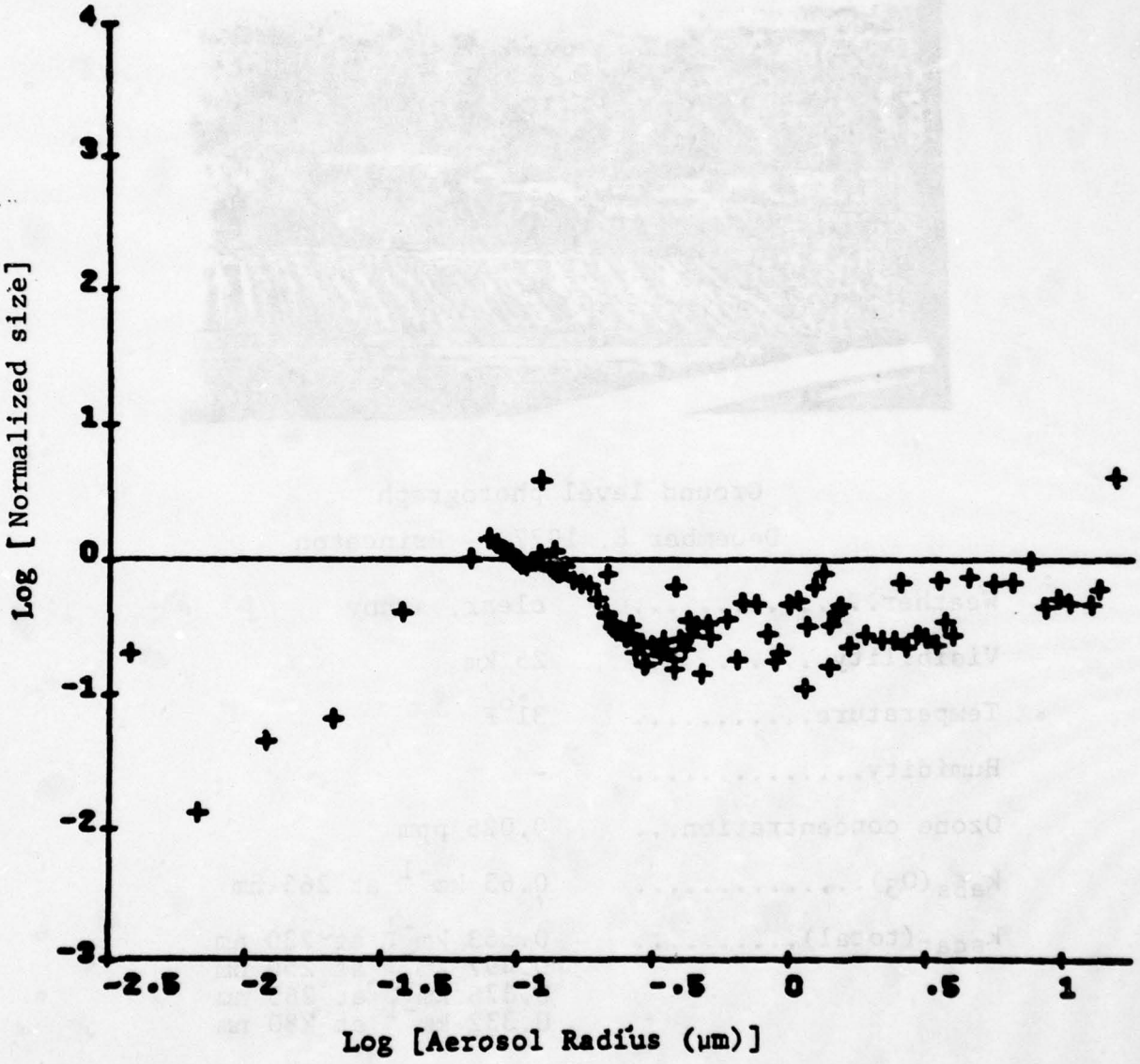

Normalized size distribution measured on December 8, 1977.

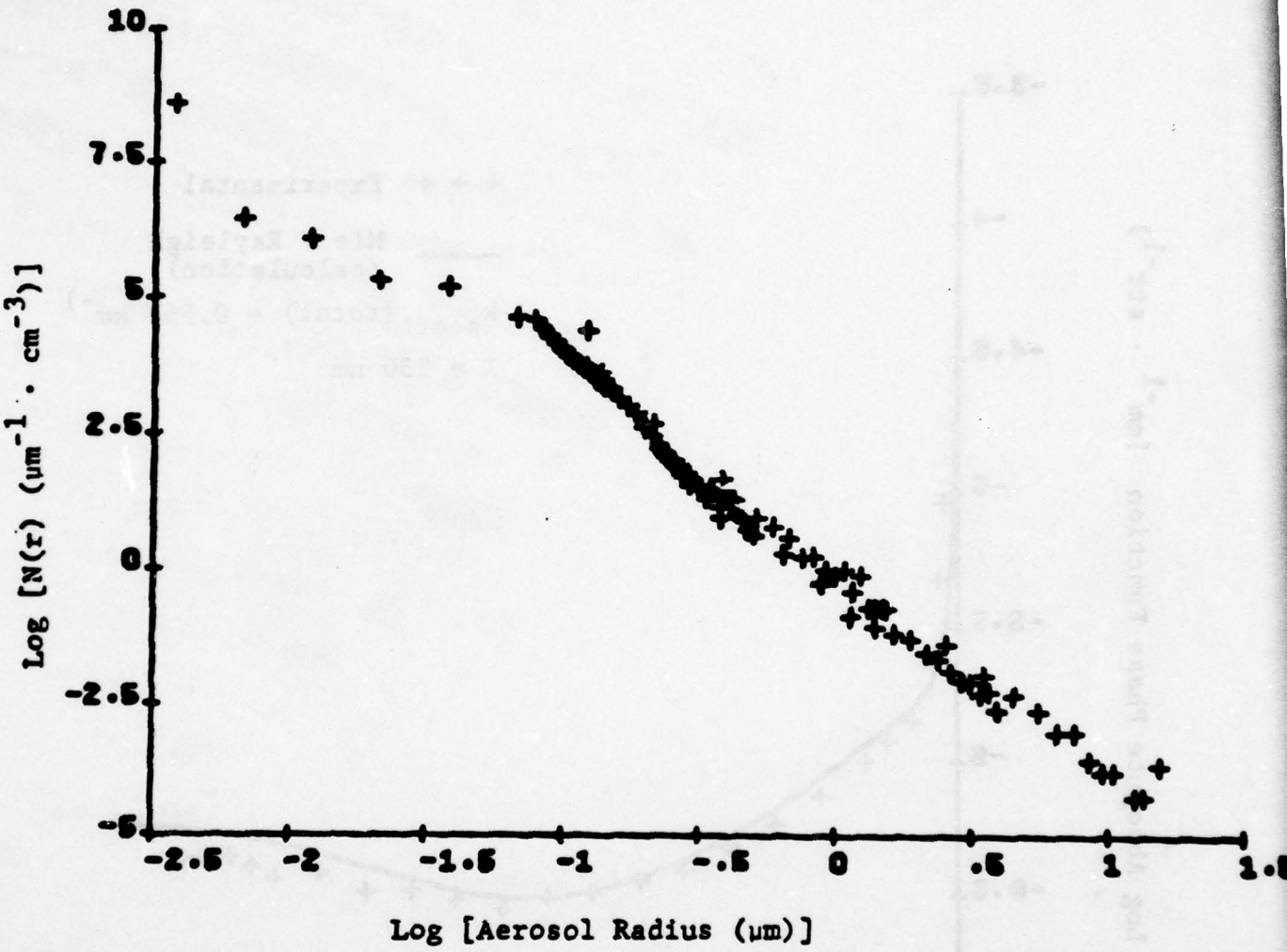

Particle size distribution measured on December 8, 1977.

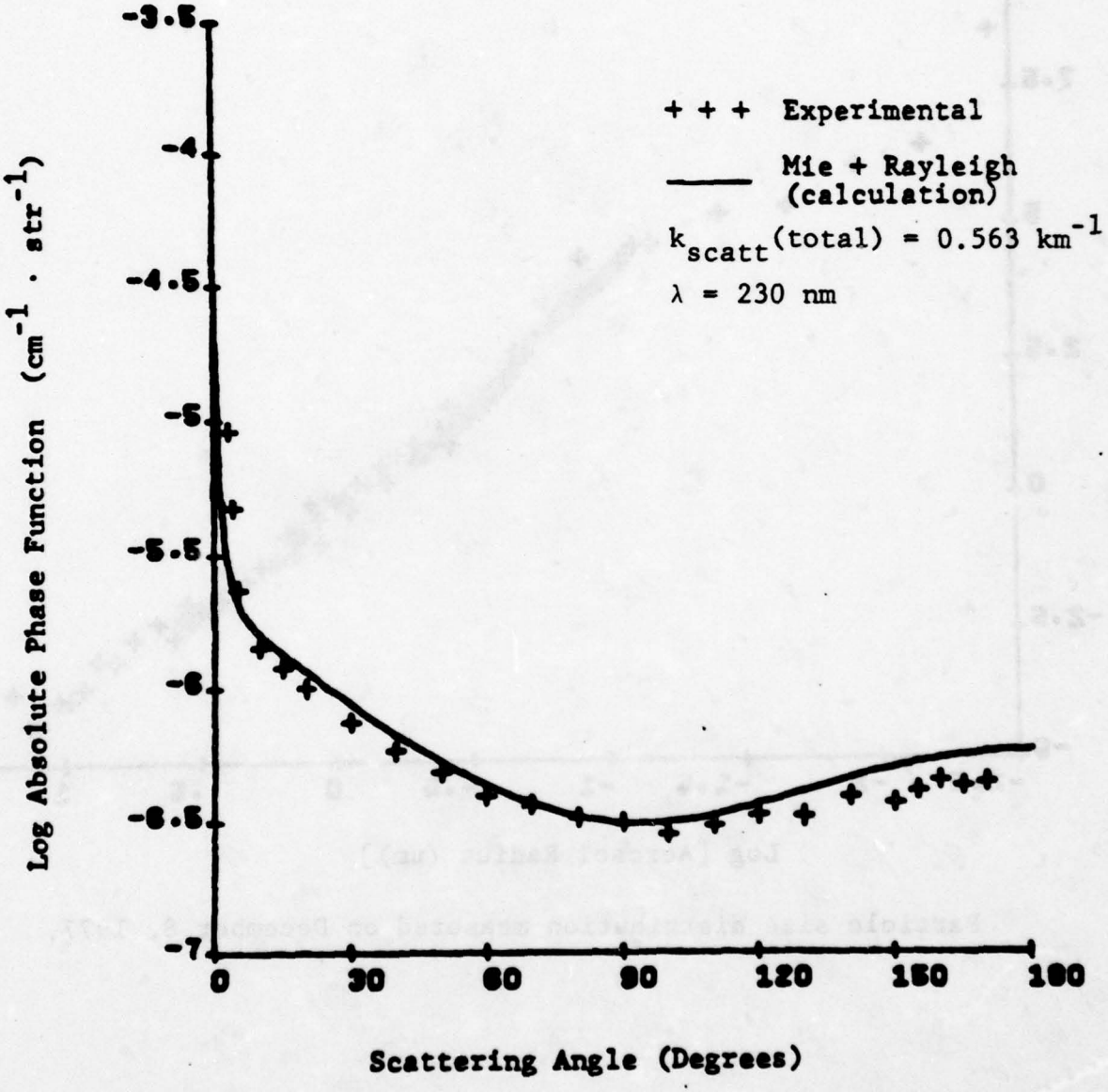

Phase function measured on December 8, 1977.

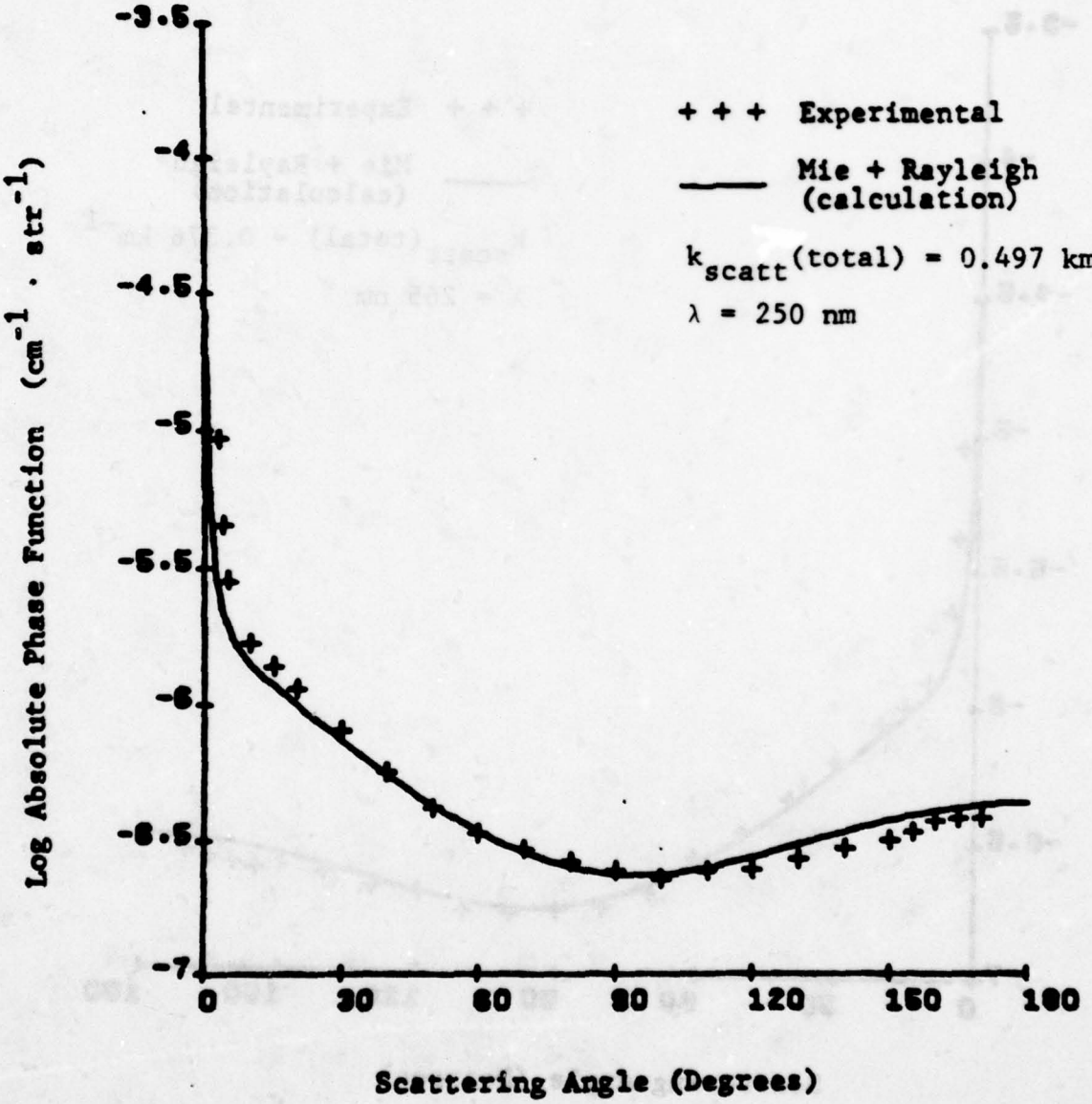

Phase function measured on December 8, 1977.

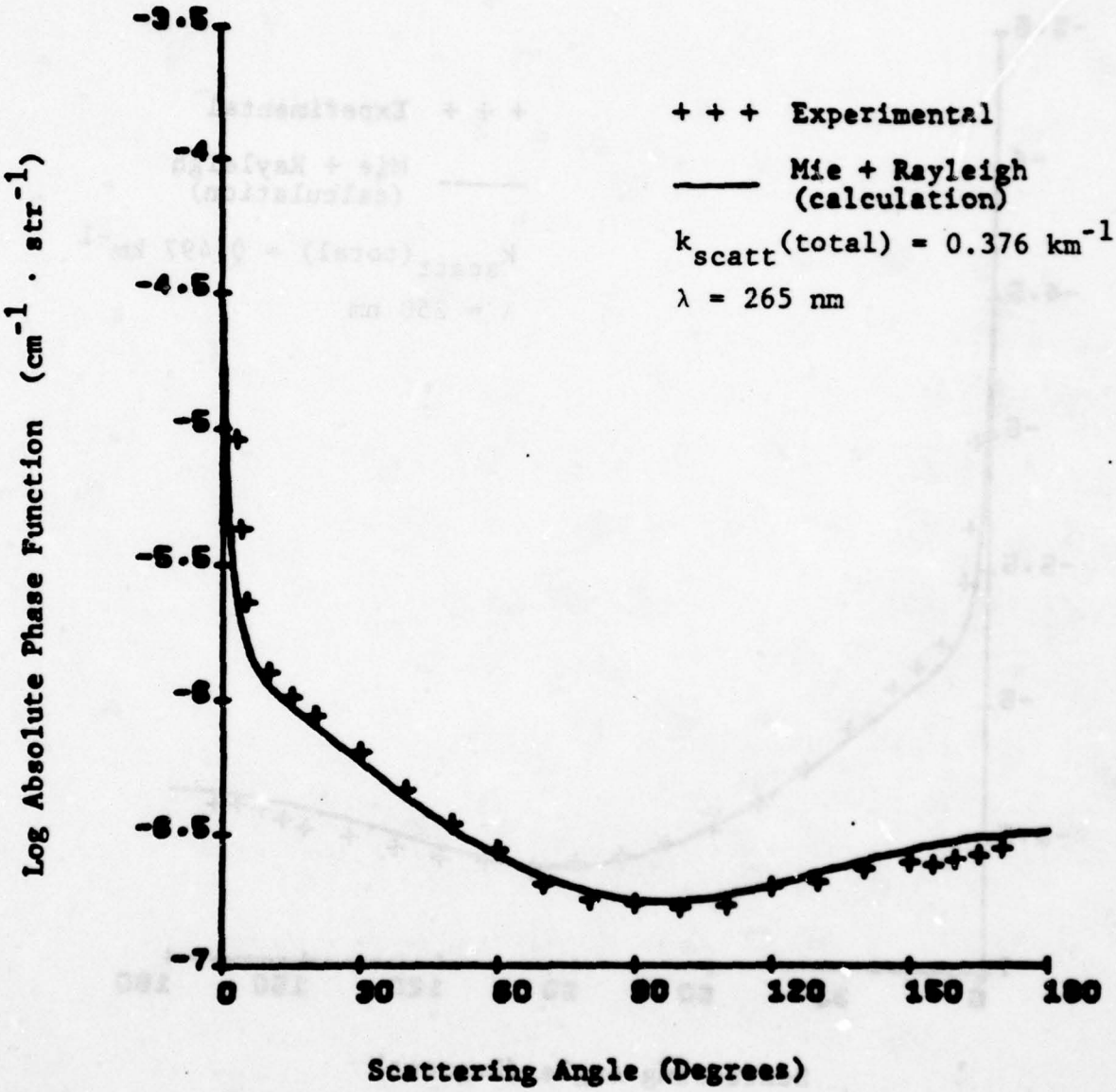

Phase function measured on December 8, 1977.

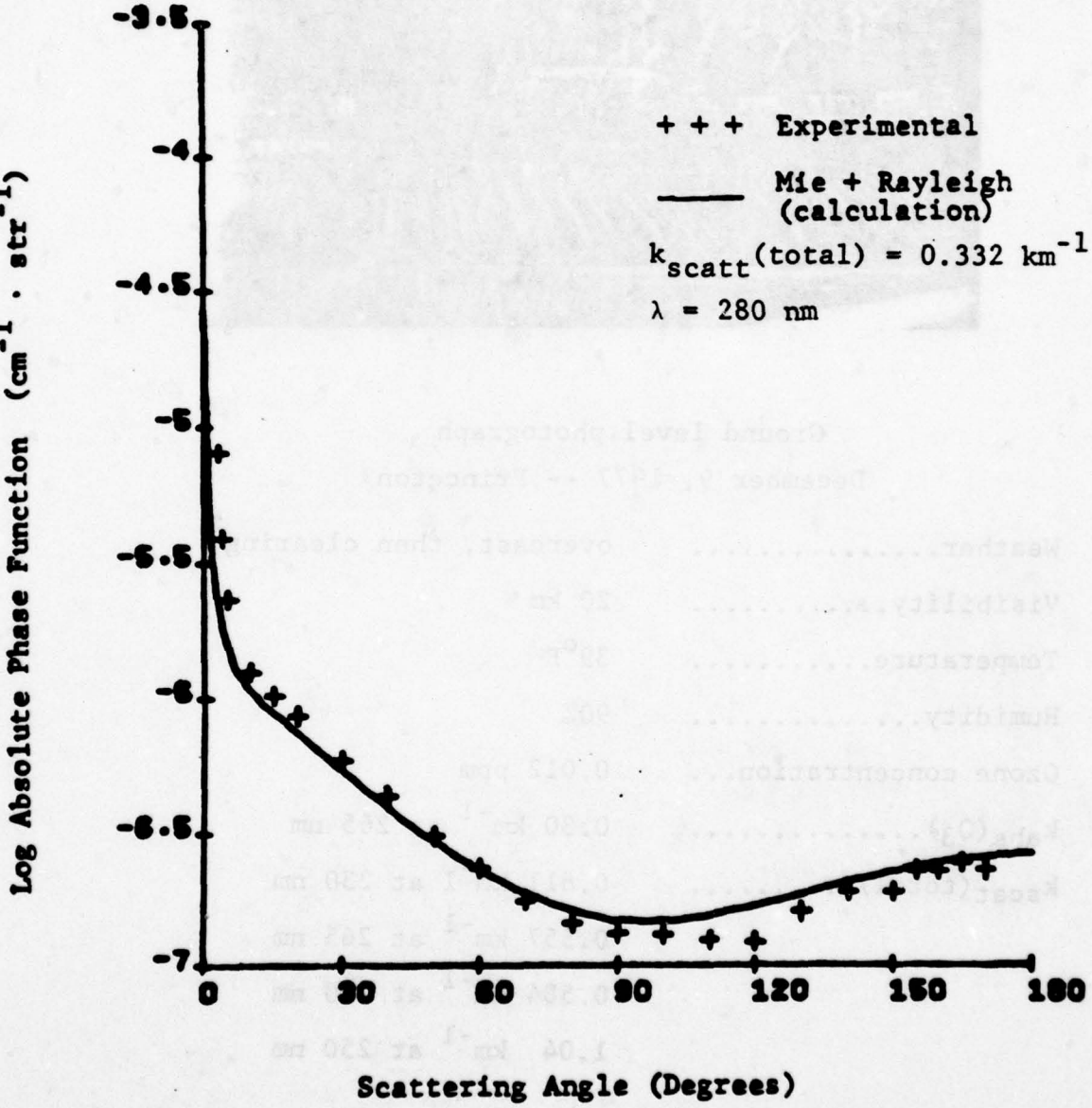

Phase function measured on December 8, 1977.

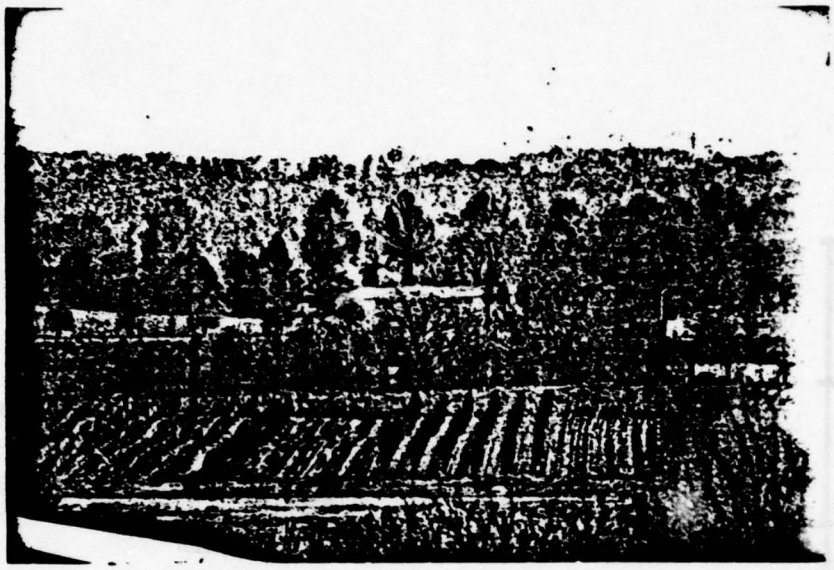

Ground level photograph
December 9, 1977 -- Princeton

Weather.....	overcast, then clearing
Visibility.....	20 km
Temperature.....	$39^{o}F$
Humidity.....	90%
Ozone concentration...	0.012 ppm
$k_{abs}(O_3)$.....	0.30 km^{-1} at 265 nm
k_{scat}(total).....	0.811 km^{-1} at 230 nm
	0.557 km^{-1} at 265 nm
	0.584 km^{-1} at 280 nm
	1.04 km^{-1} at 250 nm

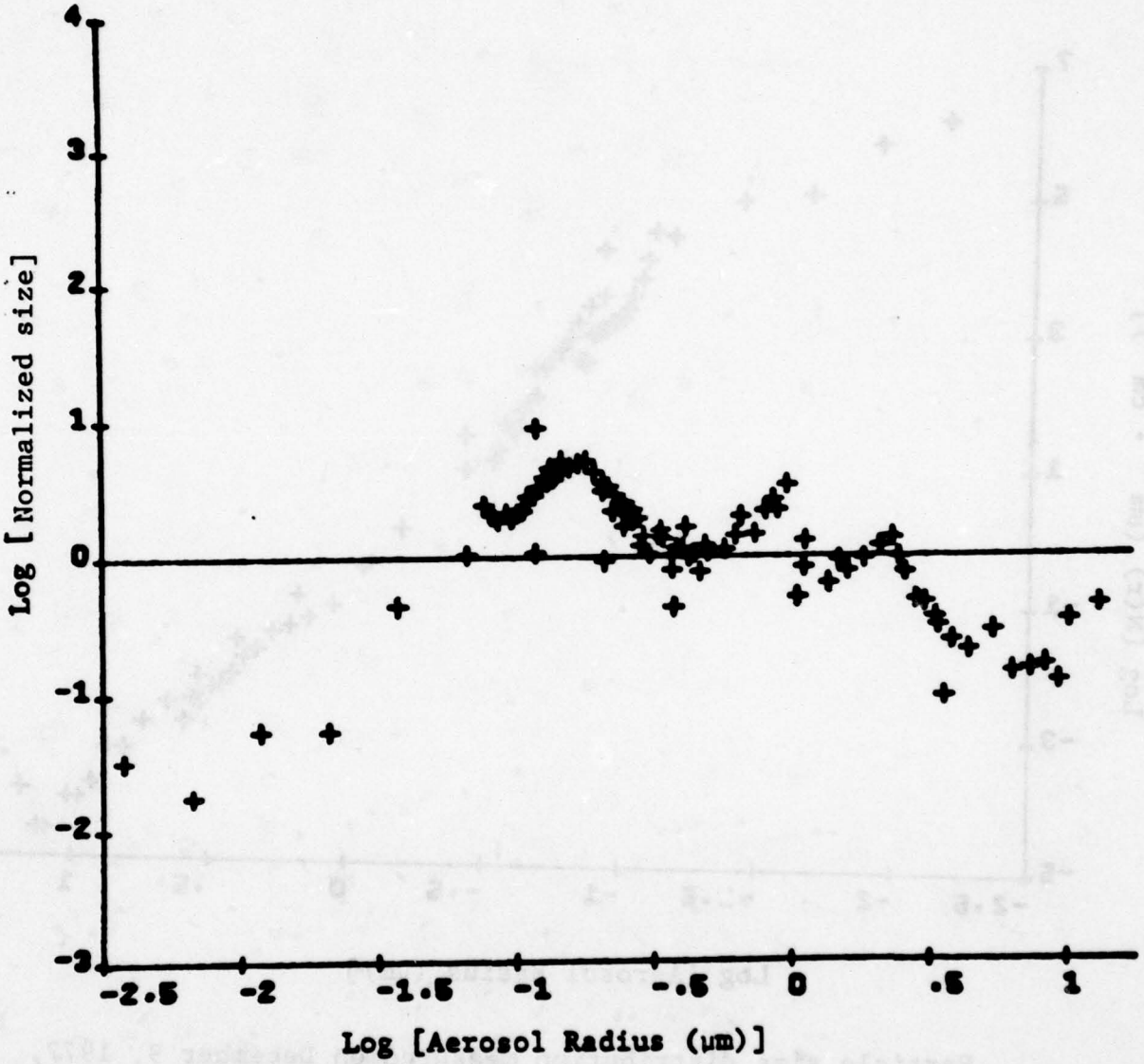

Normalized size distribution measured on December 9, 1977.

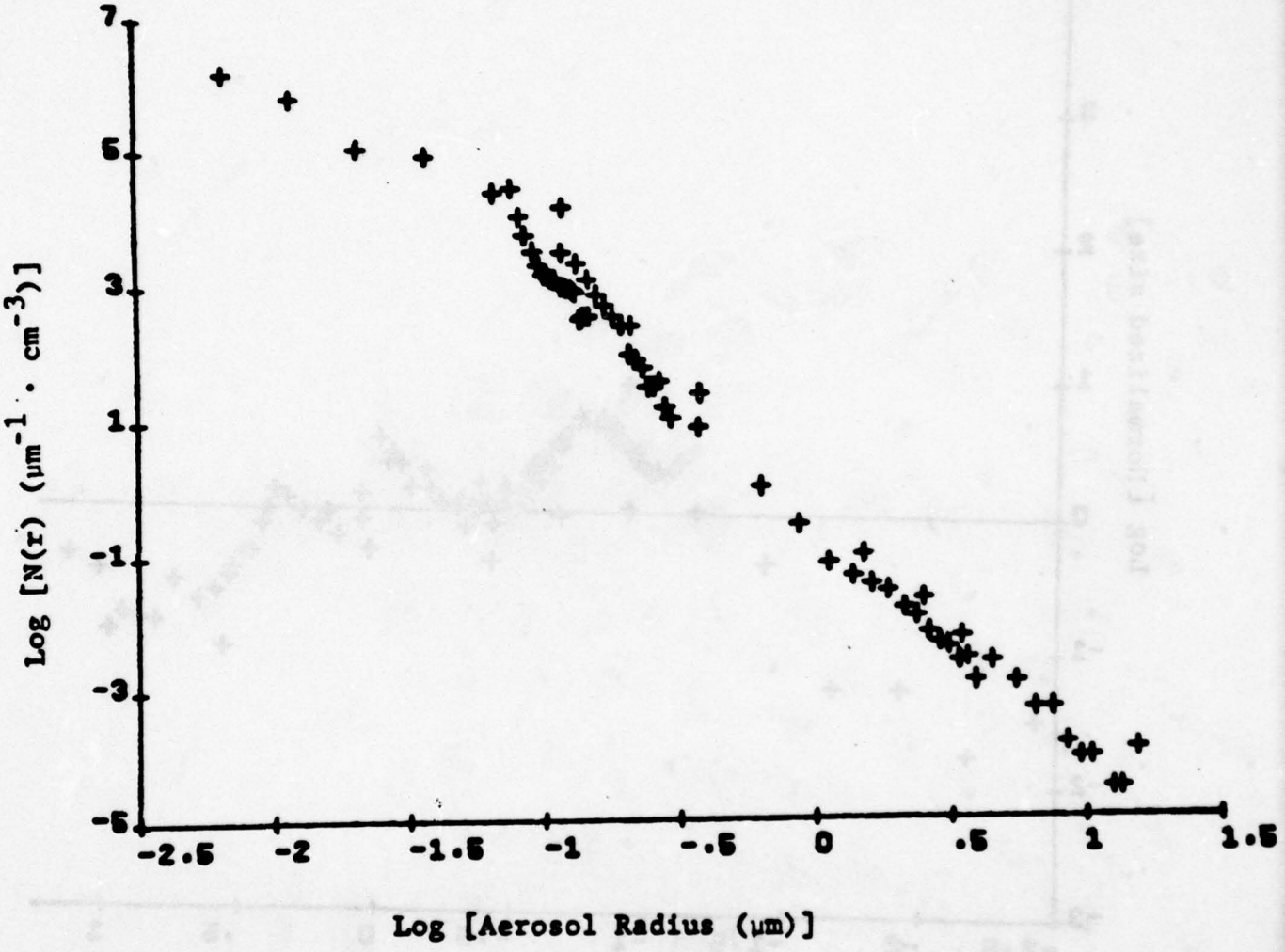

Particle size distribution measured on December 9, 1977.

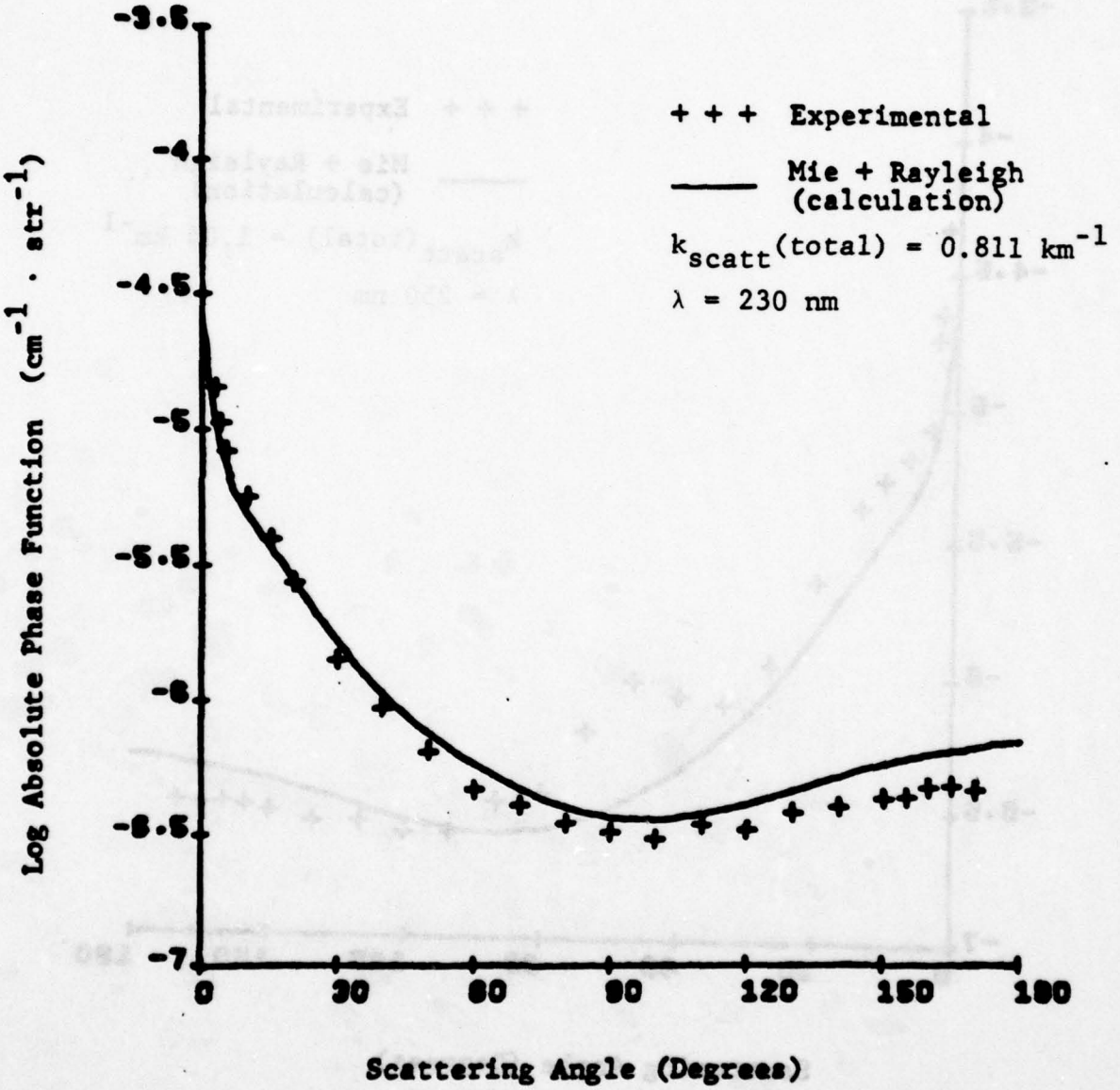

Phase function measured on December 9, 1977.

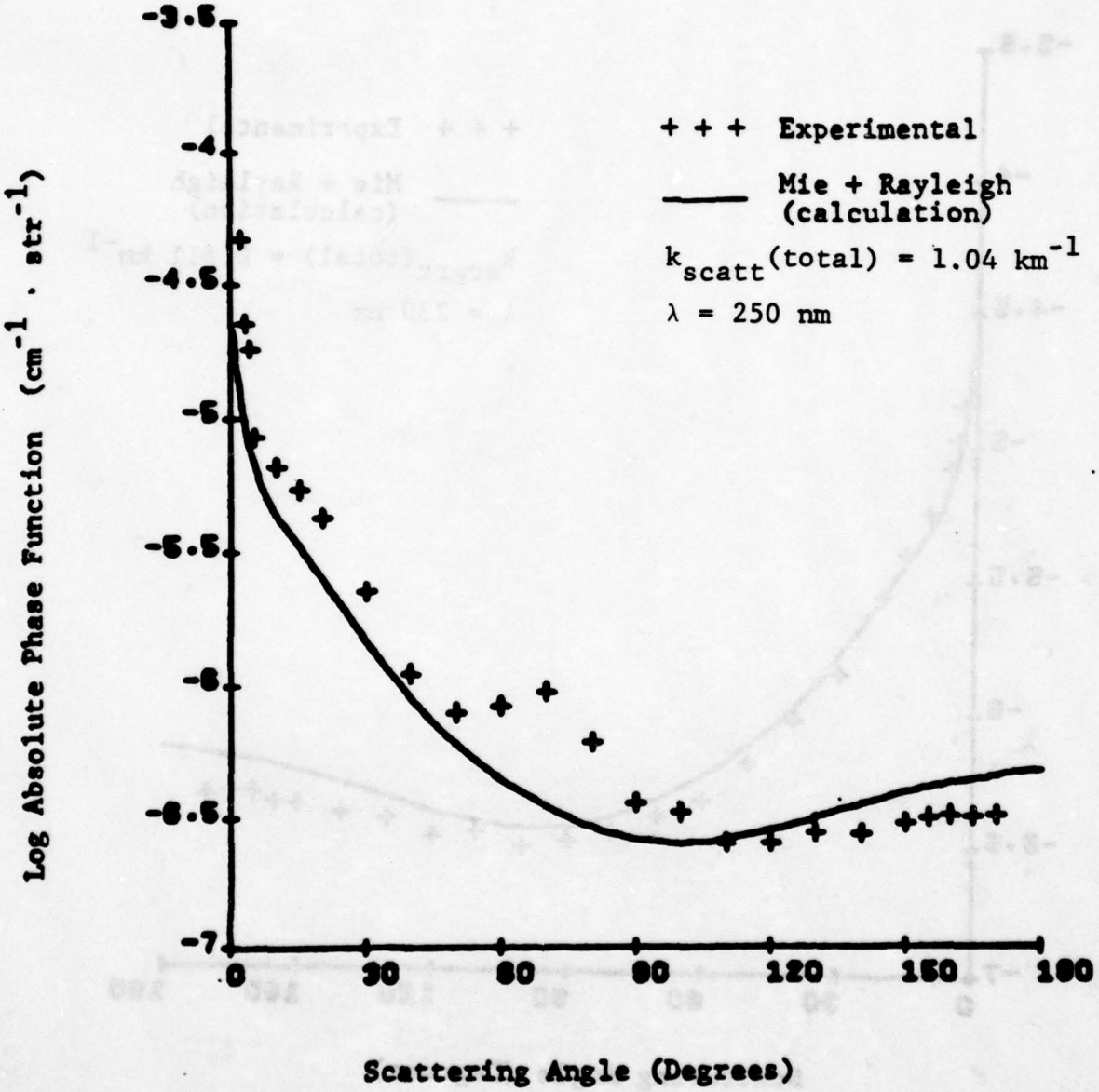

Phase function measured on December 9, 1977.

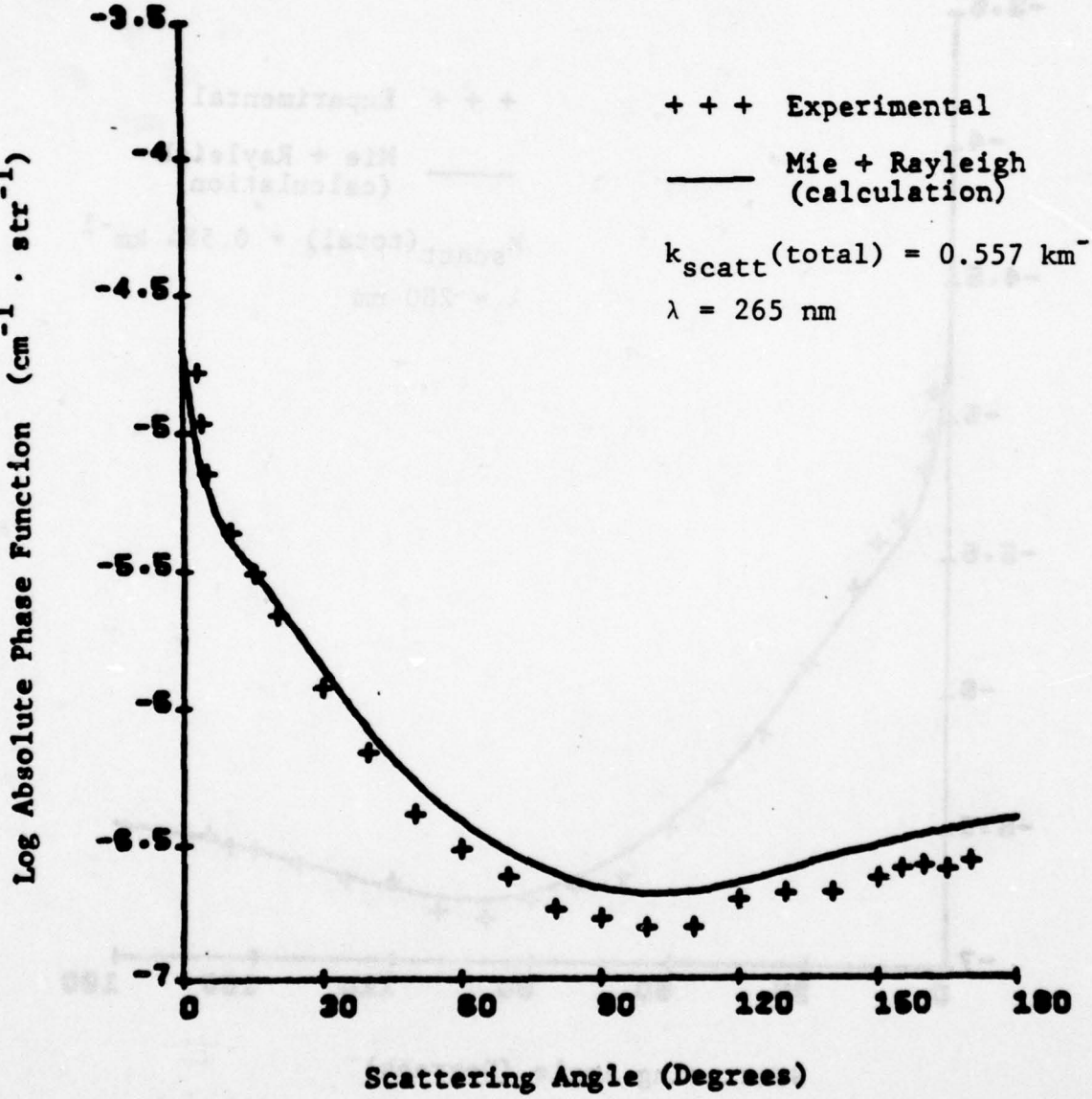

Phase function measured on December 9, 1977.

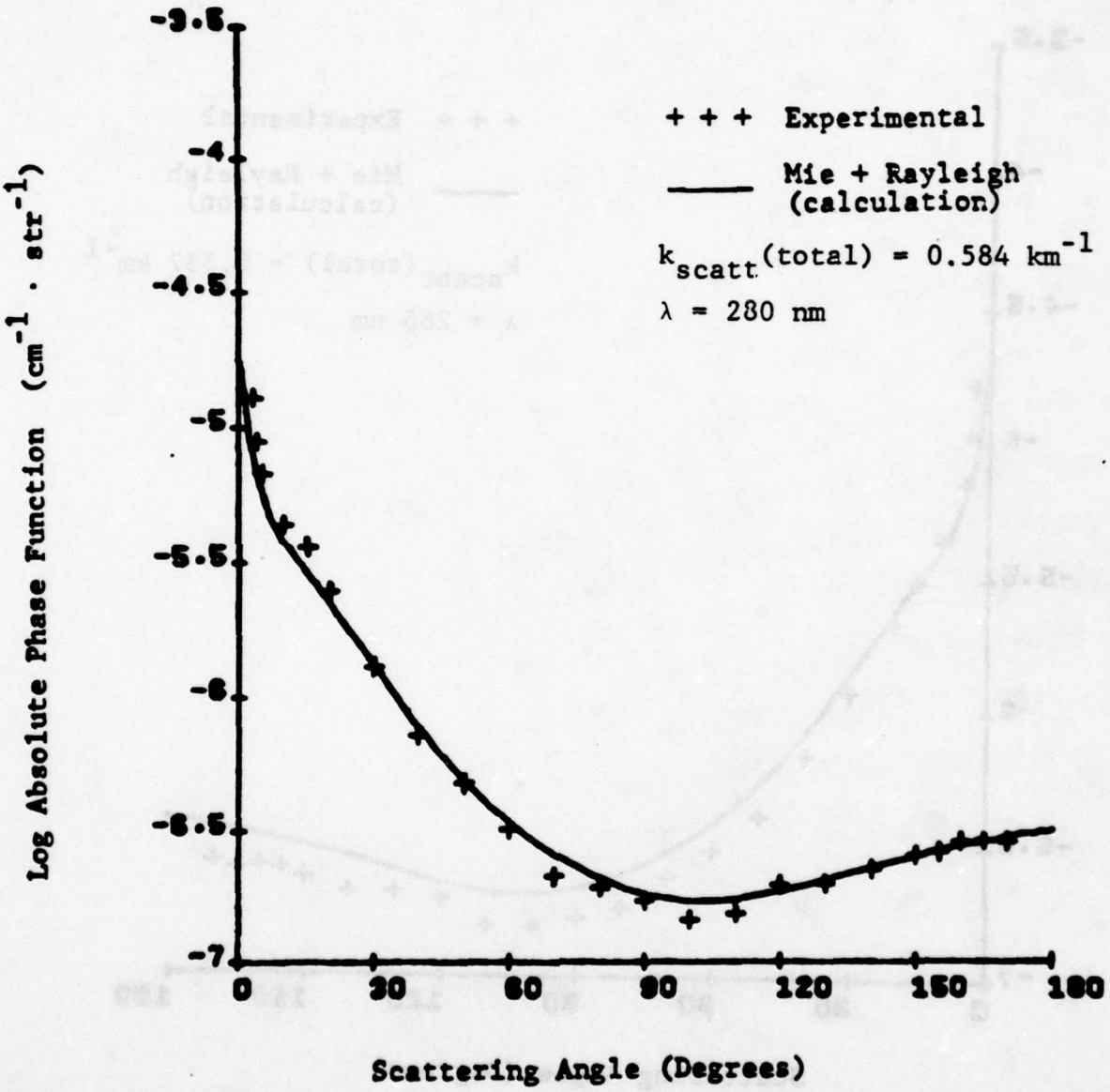

Phase function measured on December 9, 1977.

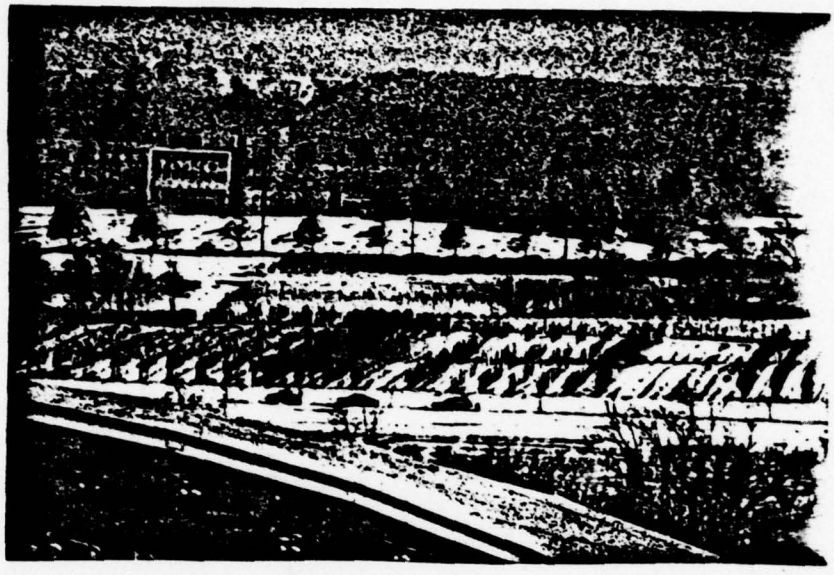

Ground level photograph
January 19, 1978 -- Princeton

Weather.....	overcast, thermal inversion, snow on ground
Visibility.....	10 km
Temperature.....	27°F
Humidity.....	-
Ozone concentration...	0.002 ppm
$k_{abs}(O_3)$.....	0.05 km^{-1} at 265 nm
k_{scat}(total).....	0.607 km^{-1} at 230 nm
	0.455 km^{-1} at 250 nm
	0.483 km^{-1} at 265 nm
	0.317 km^{-1} at 275 nm

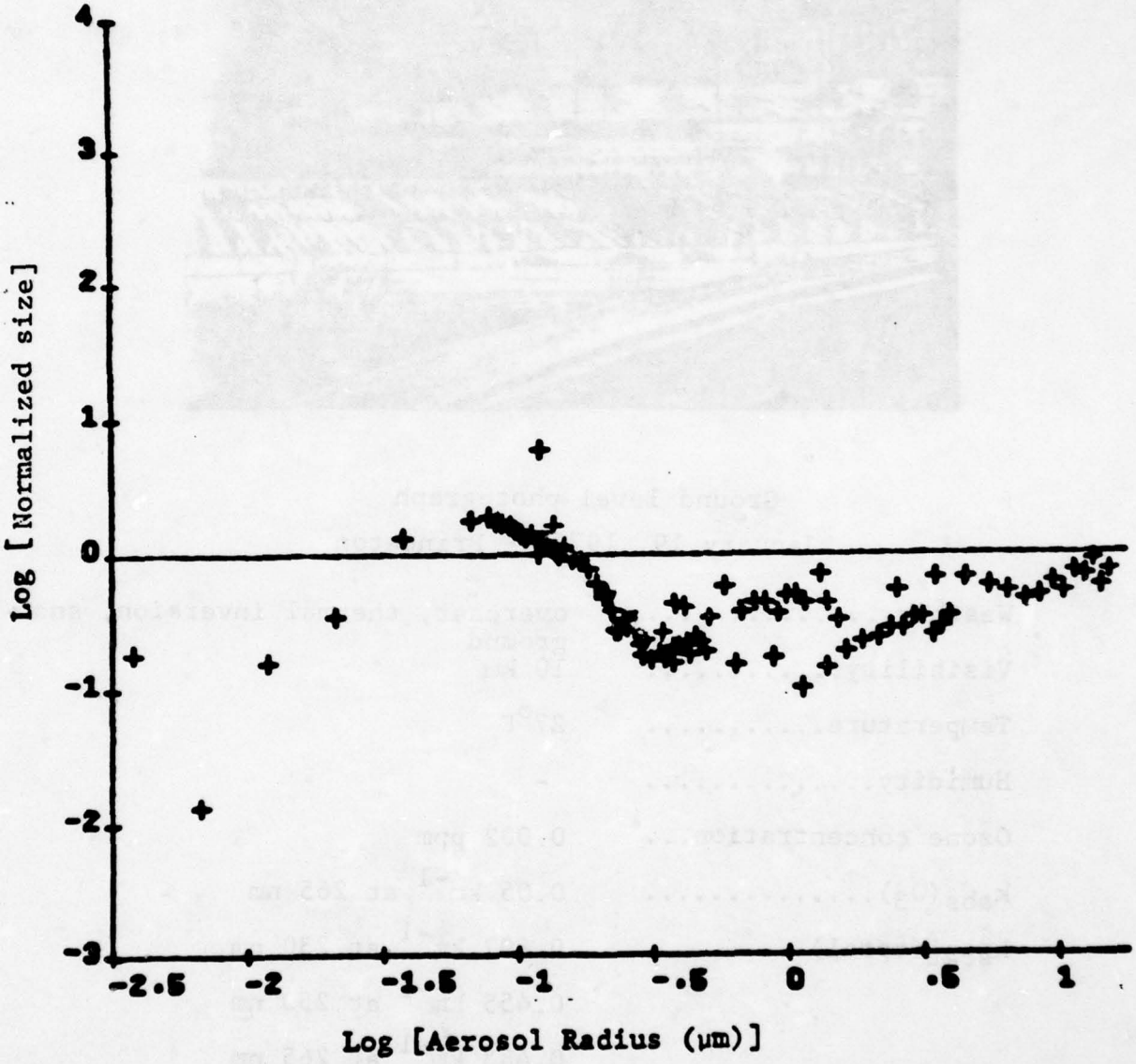

Normalized size distribution measured on January 19, 1978.

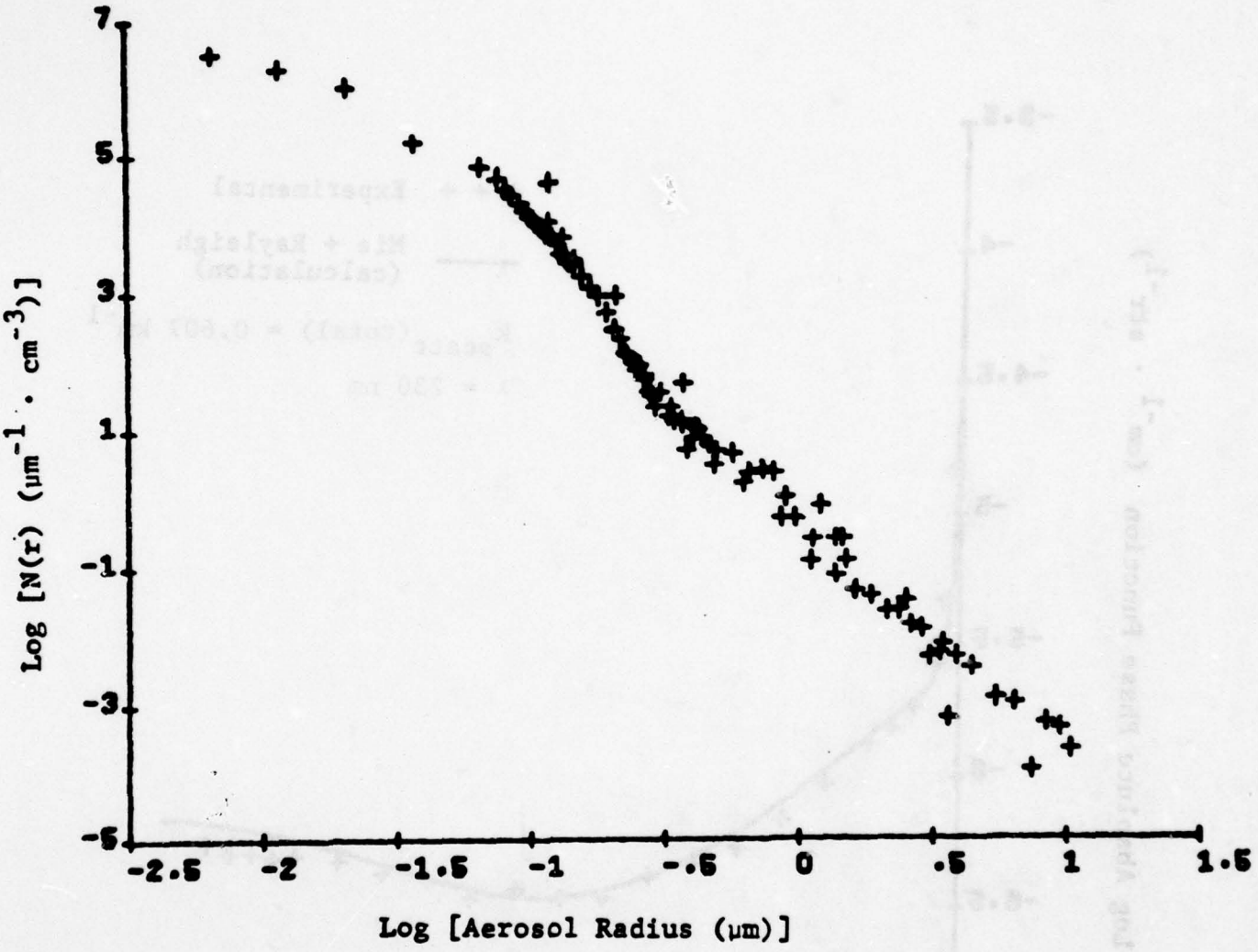

Particle size distribution measured on January 19, 1978.

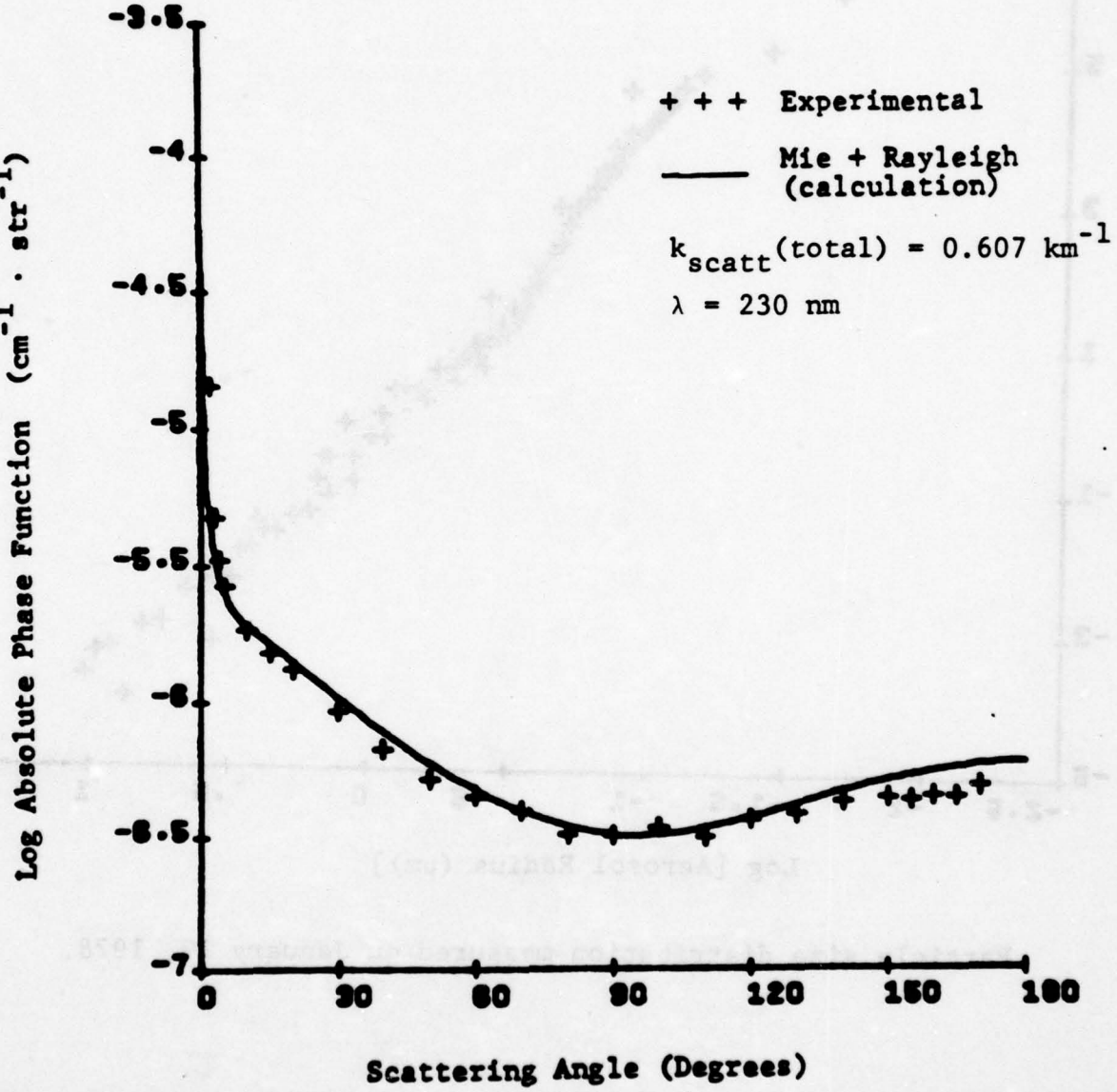

Phase function measured on January 19, 1978.

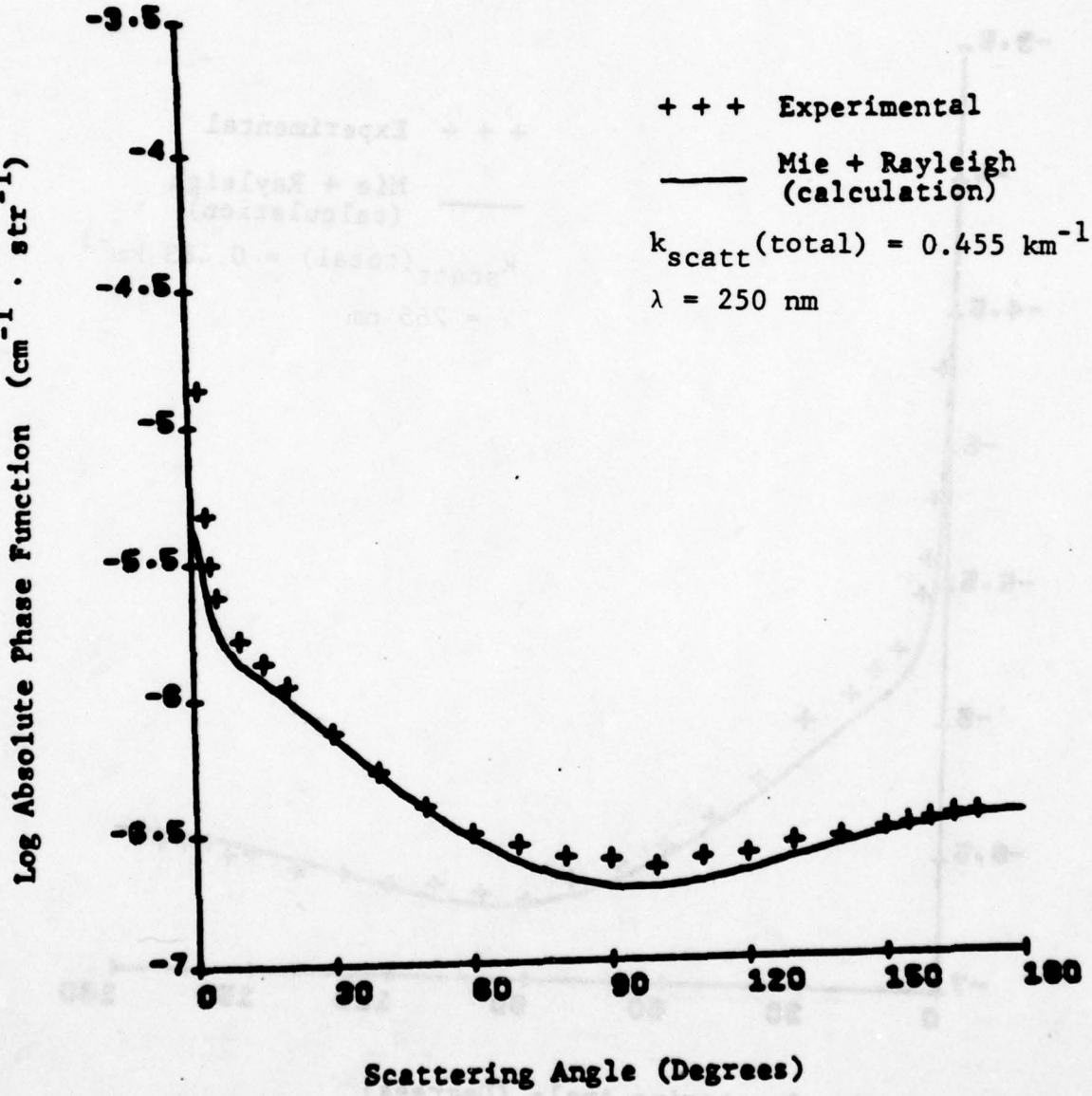

Phase function measured on January 19, 1978.

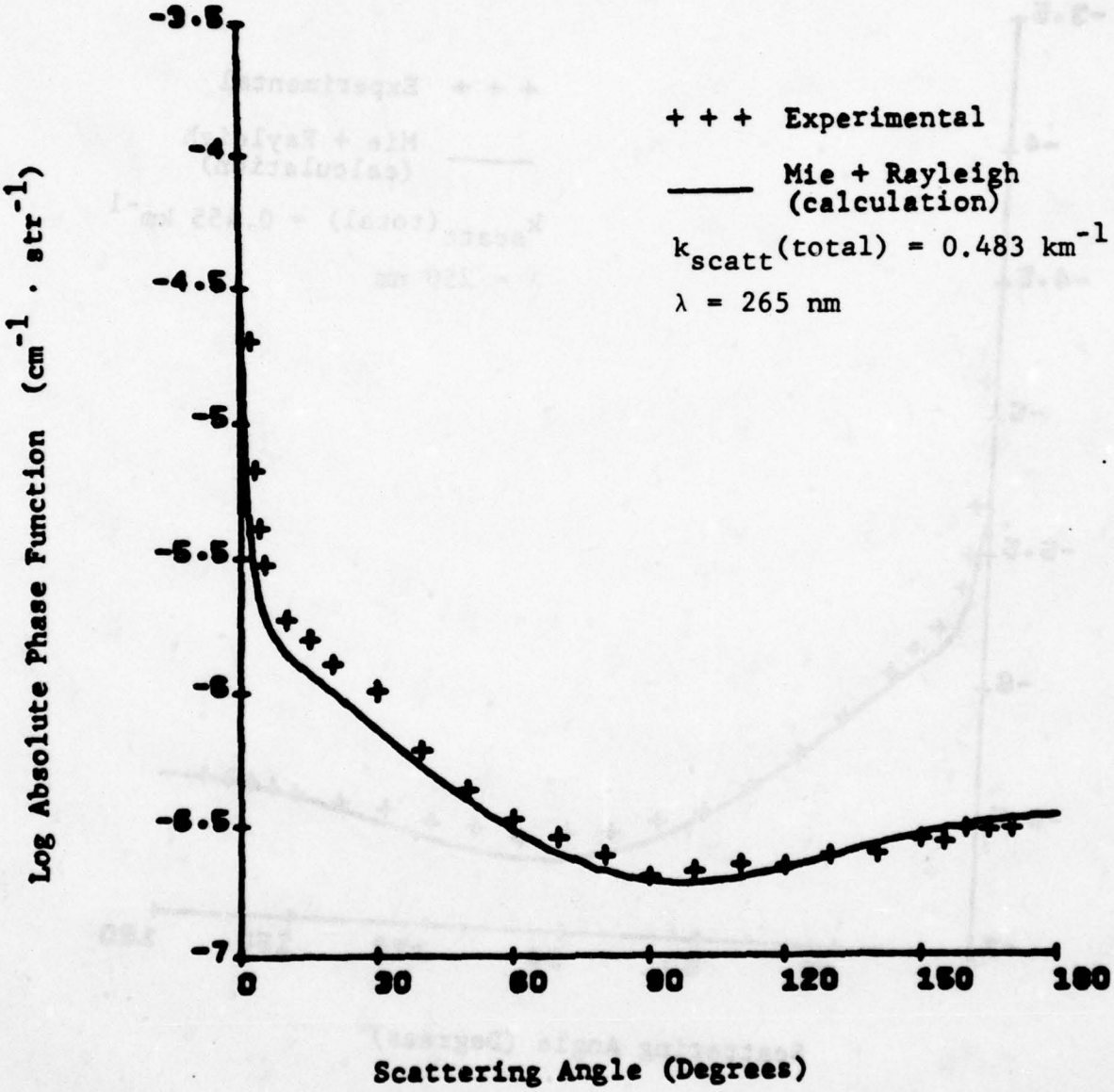

Phase function measured on January 19, 1978.

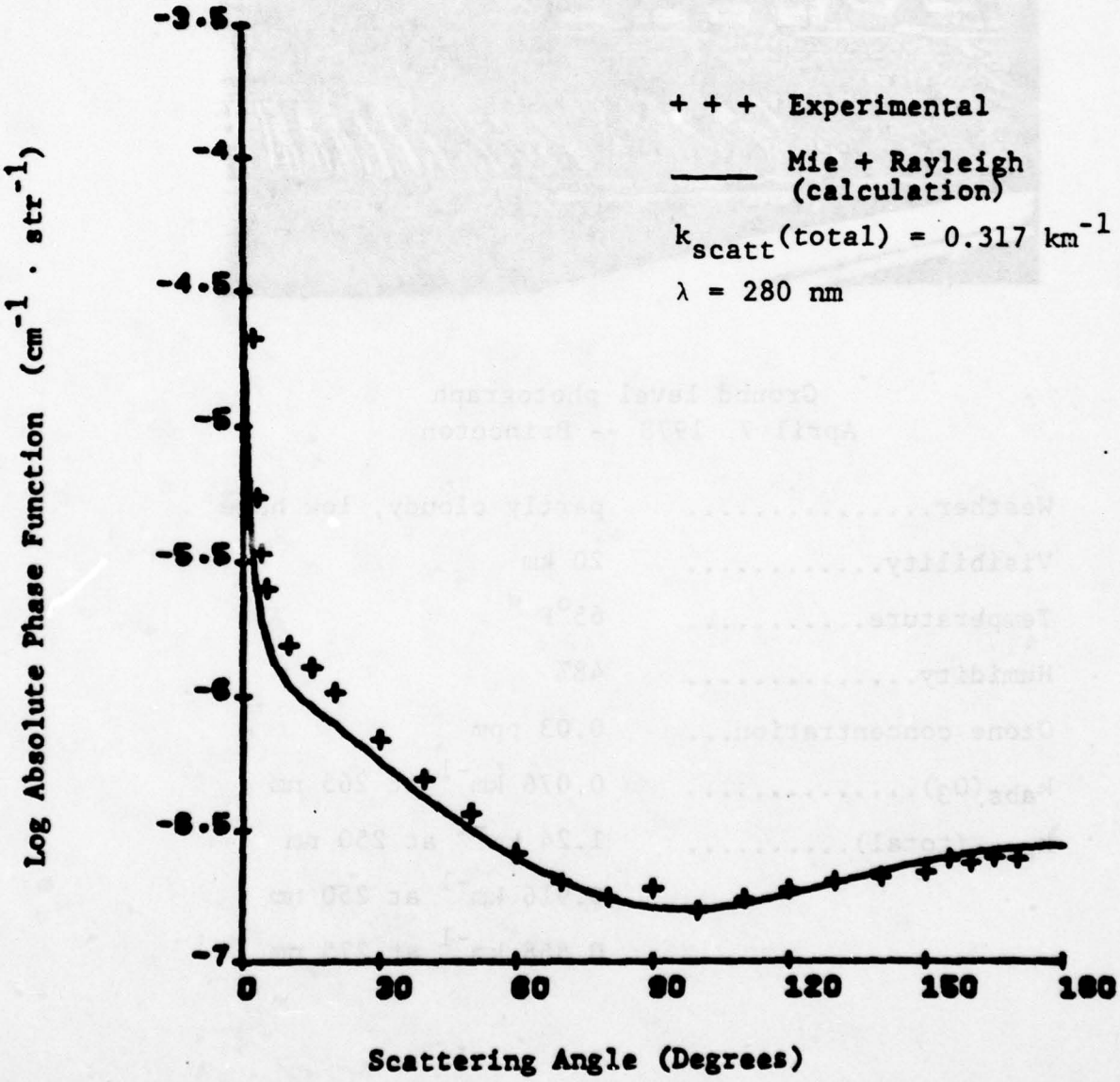

Phase function measured on January 19, 1978.

Ground level photograph
April 7, 1978 -- Princeton

Weather.....	partly cloudy, low haze
Visibility.....	20 km
Temperature.....	65°F
Humidity.....	48%
Ozone concentration...	0.03 ppm
$k_{abs}(O_3)$.....	0.076 km^{-1} at 265 nm
k_{scat}(total).....	1.24 km^{-1} at 250 nm
	0.916 km^{-1} at 250 nm
	0.868 km^{-1} at 275 nm

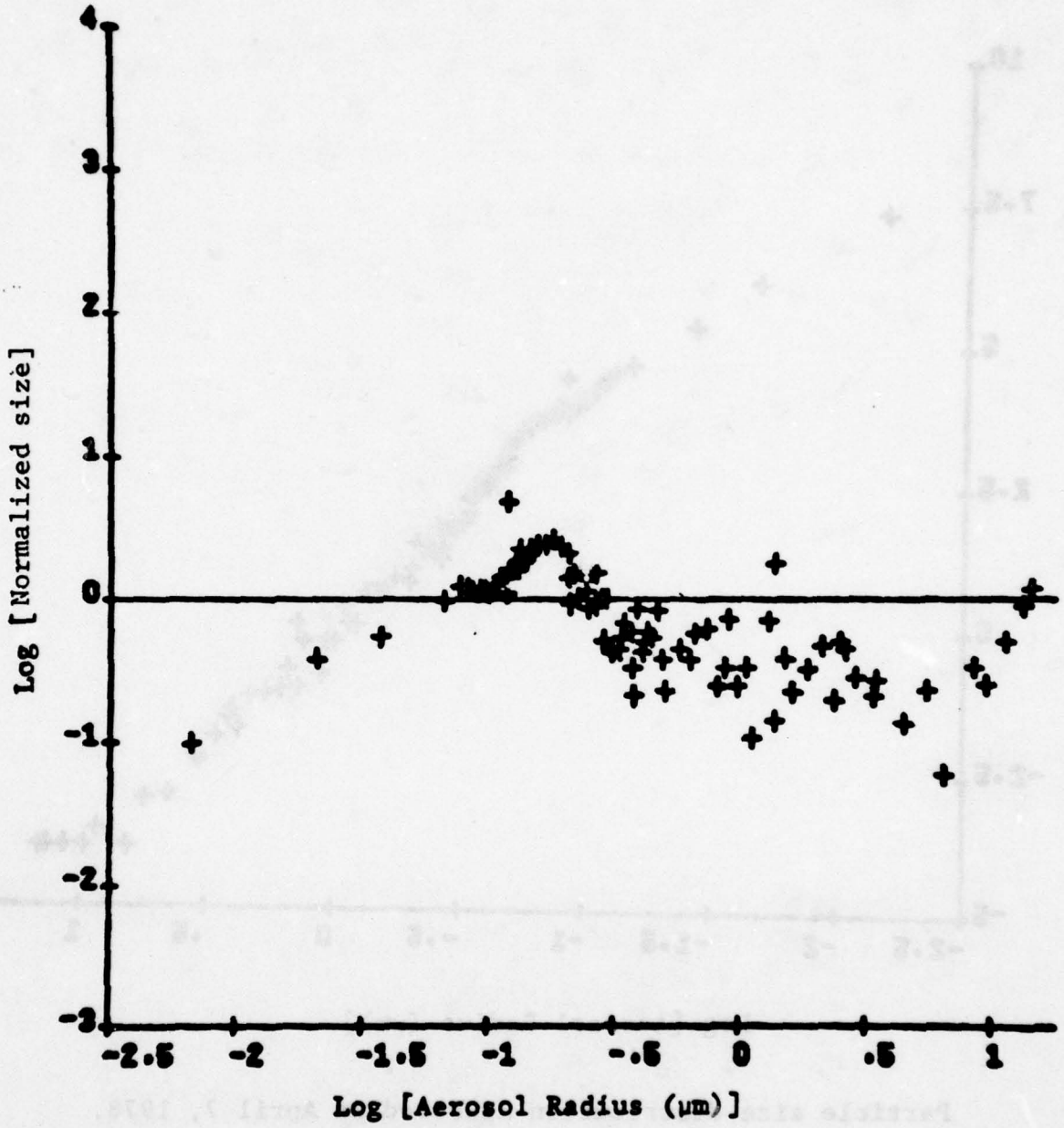

Normalized size distribution measured on April 7, 1978.

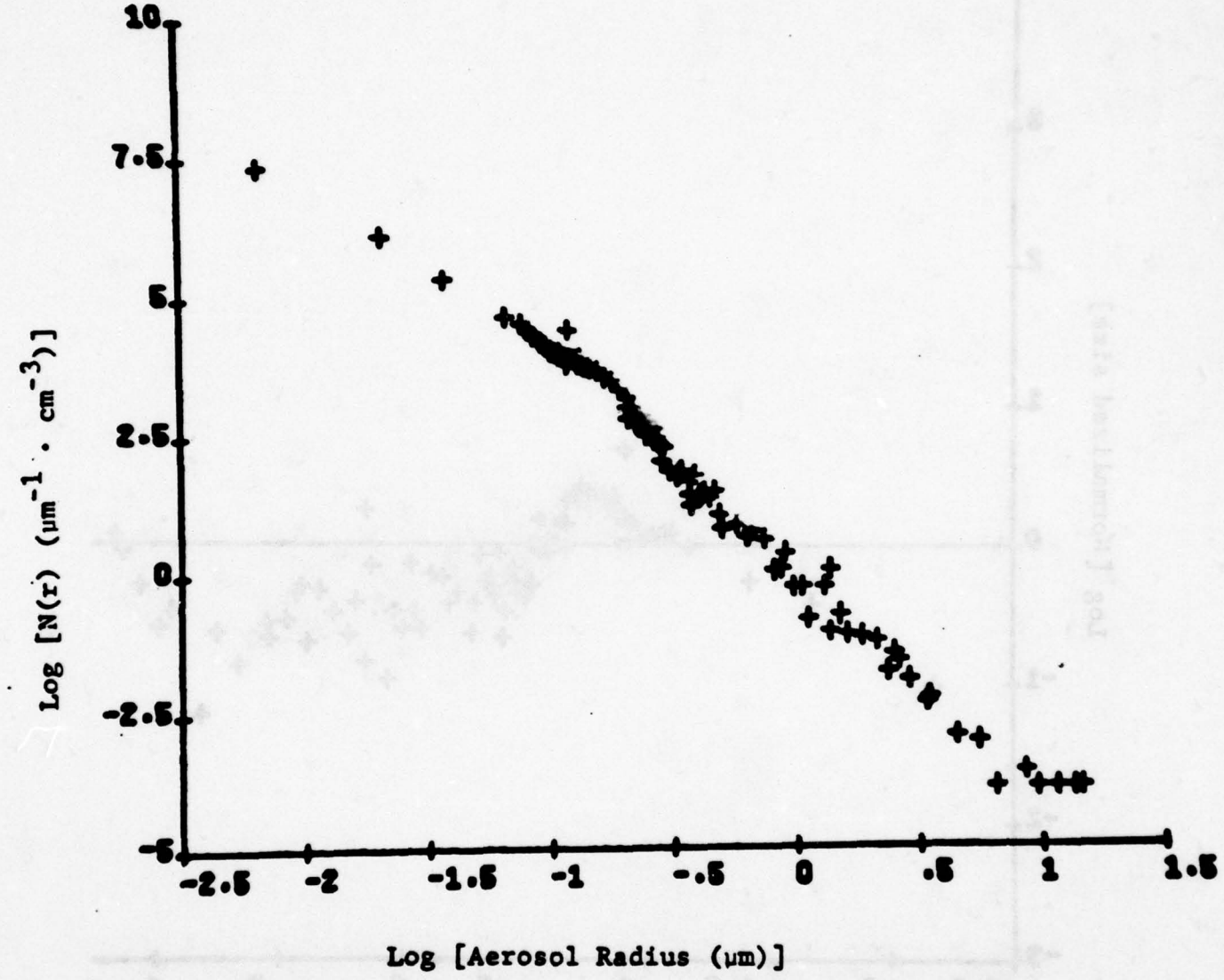

Particle size distribution measured on April 7, 1978.

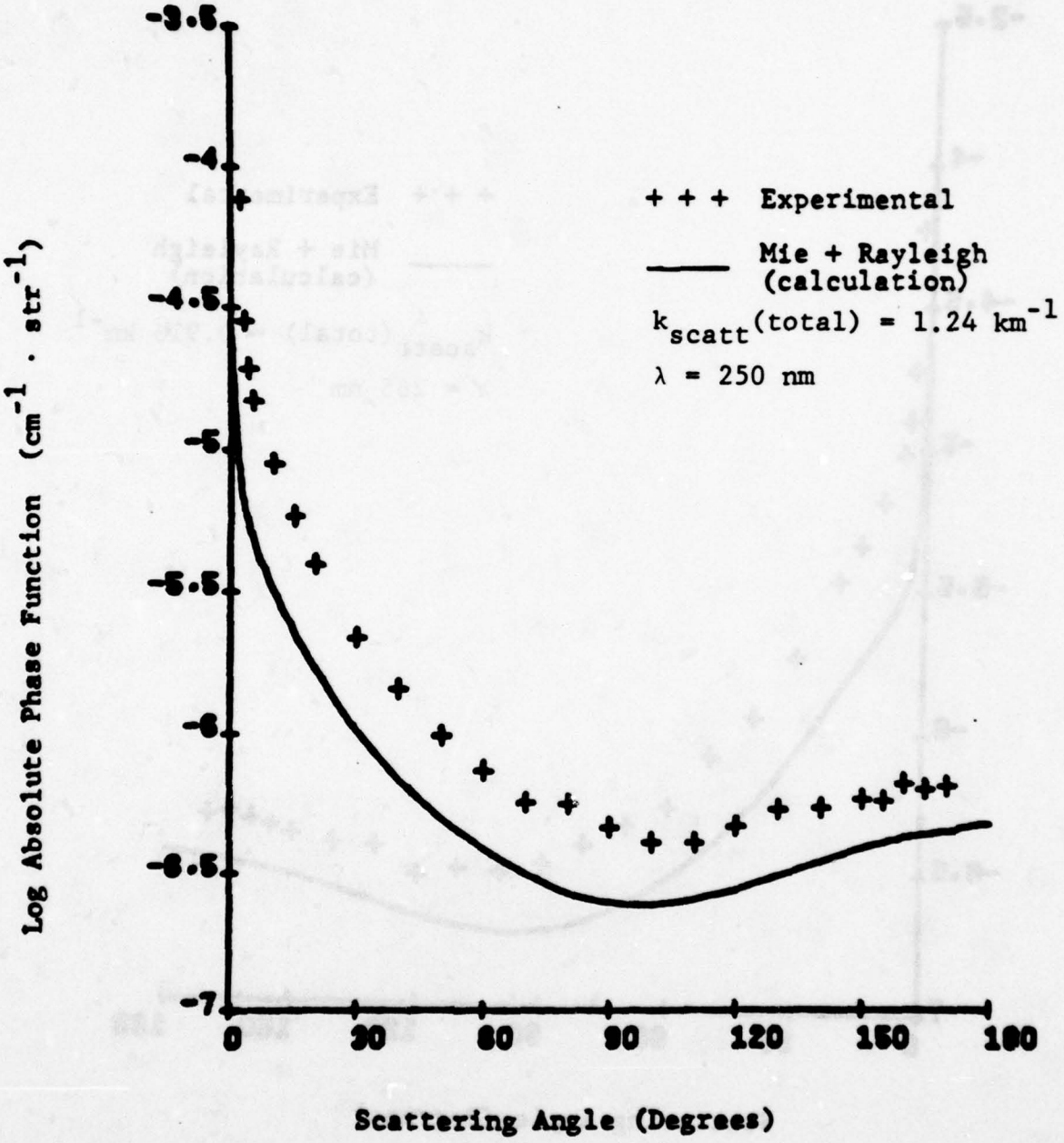

Phase function measured on April 7, 1978.

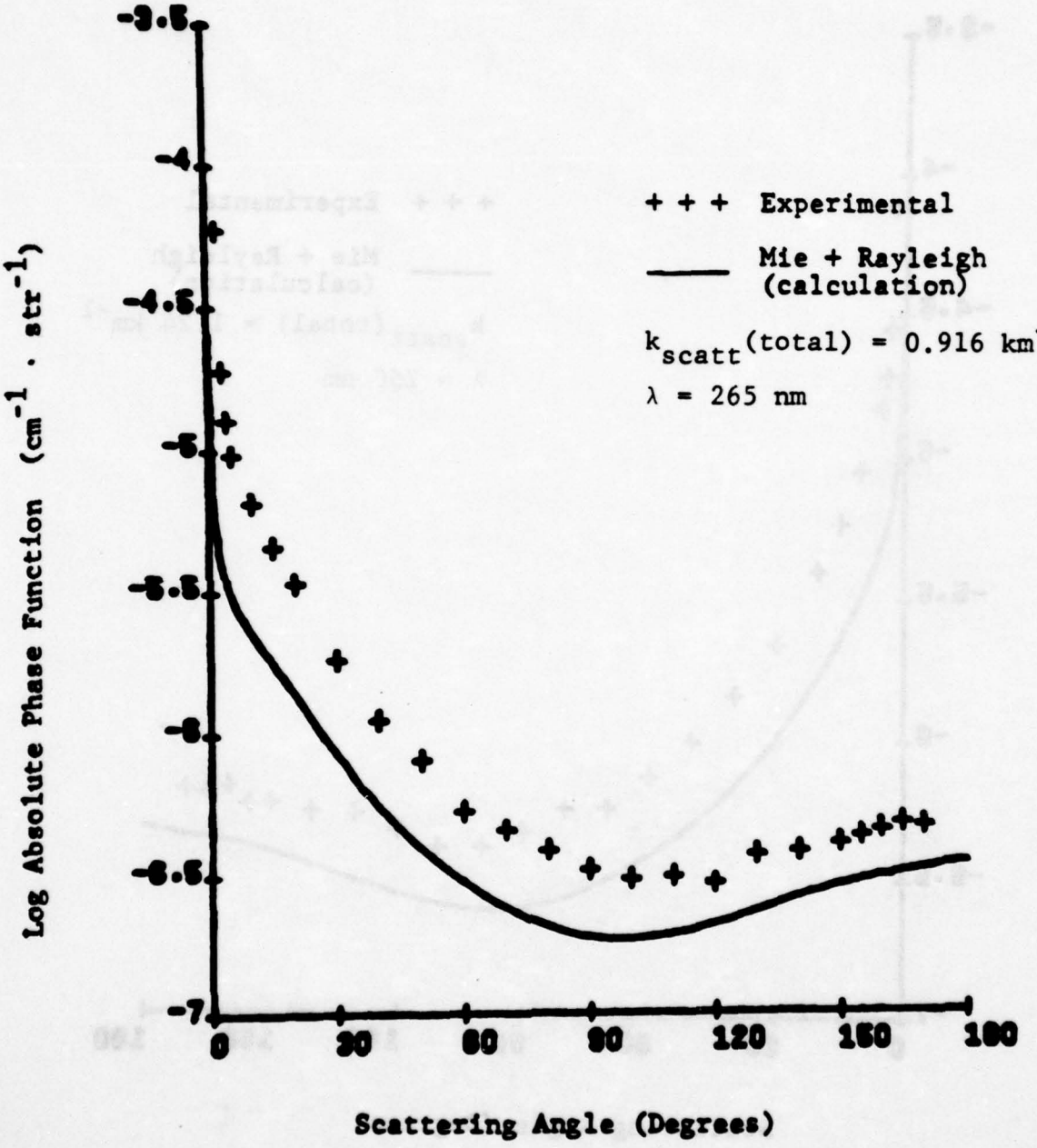

Phase function measured on April 7, 1978.

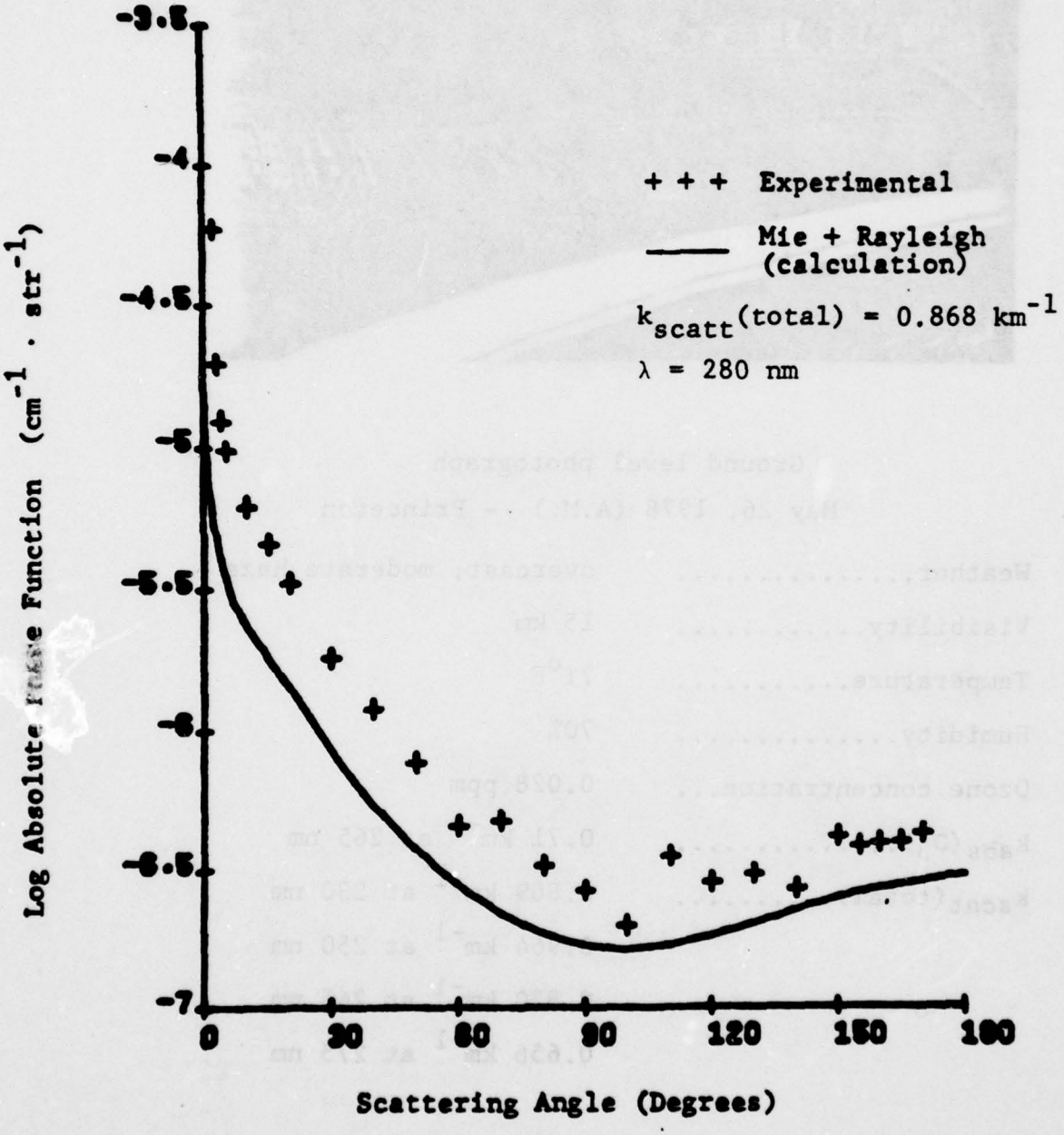

Phase function measured on April 7, 1978.

Ground level photograph

May 26, 1978 (A.M.) -- Princeton

Weather.....	overcast, moderate haze
Visibility.....	15 km
Temperature.....	$71^{o}F$
Humidity.....	70%
Ozone concentration...	0.028 ppm
$k_{abs}(O_3)$.....	0.71 km^{-1} at 265 nm
k_{scat}(total).....	0.869 km^{-1} at 230 nm
	0.964 km^{-1} at 250 nm
	0.820 km^{-1} at 265 nm
	0.656 km^{-1} at 275 nm

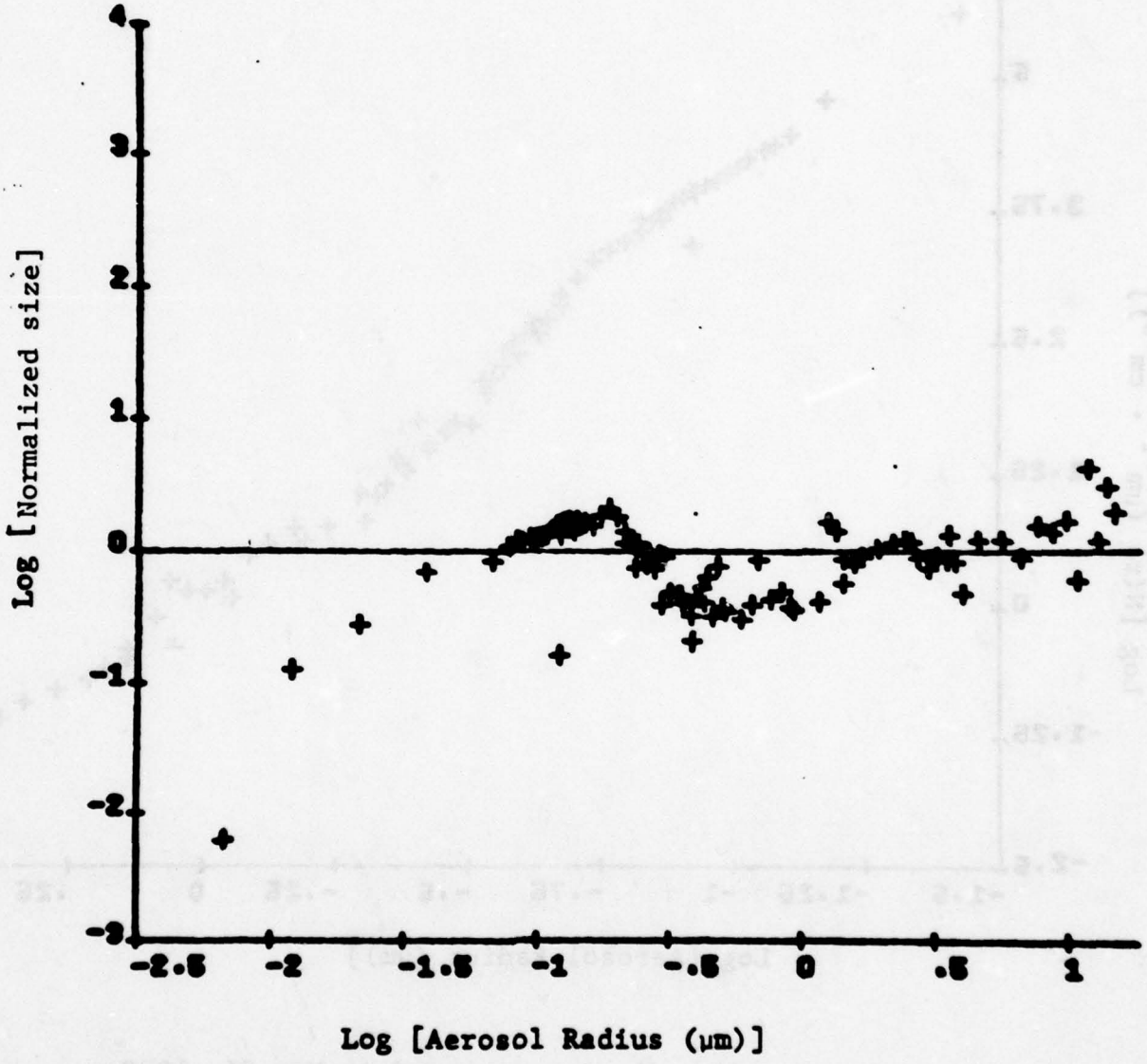

Normalized size distribution measured on May 26, 1978.

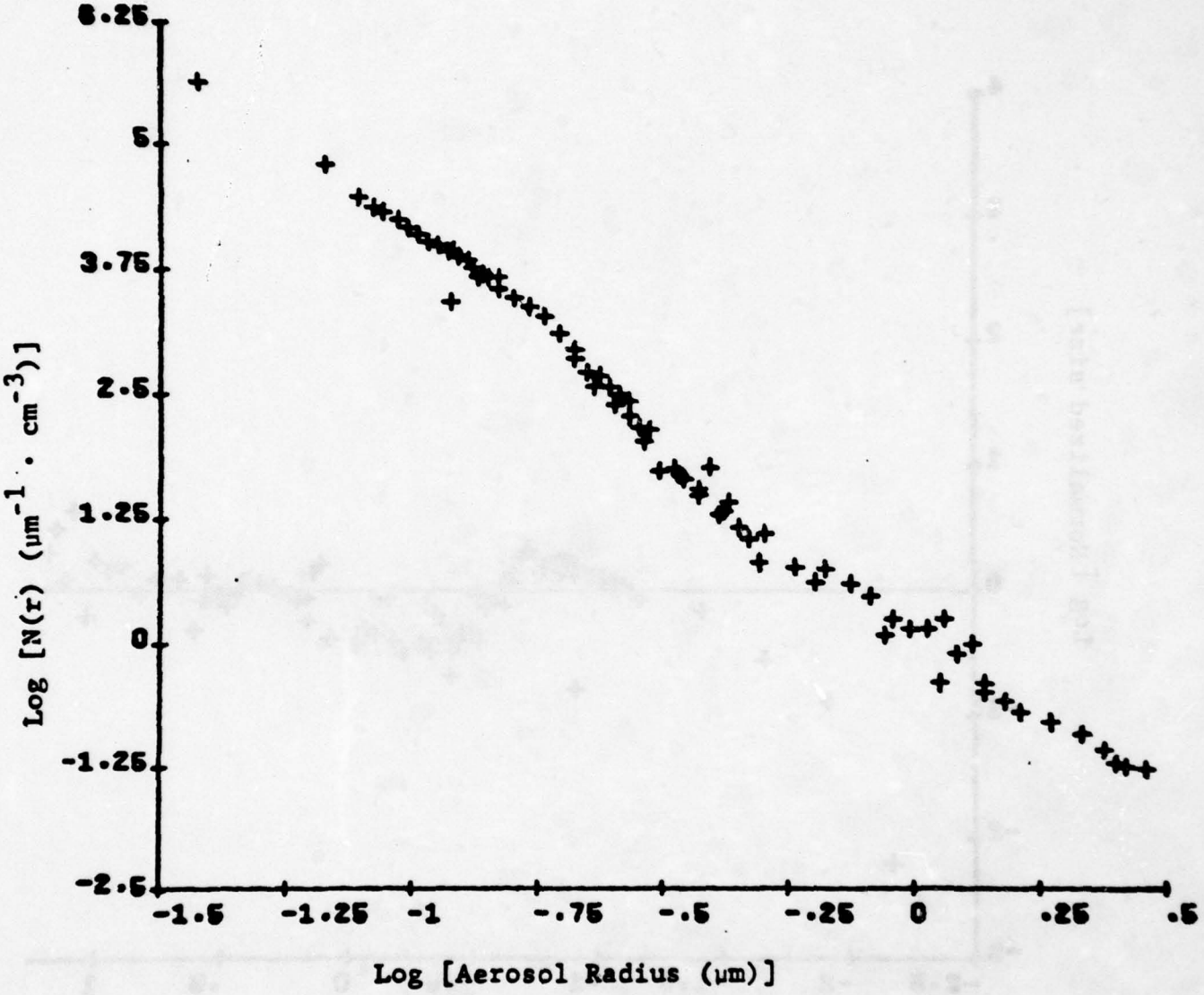

Particle size distribution measured on May 26, 1978.

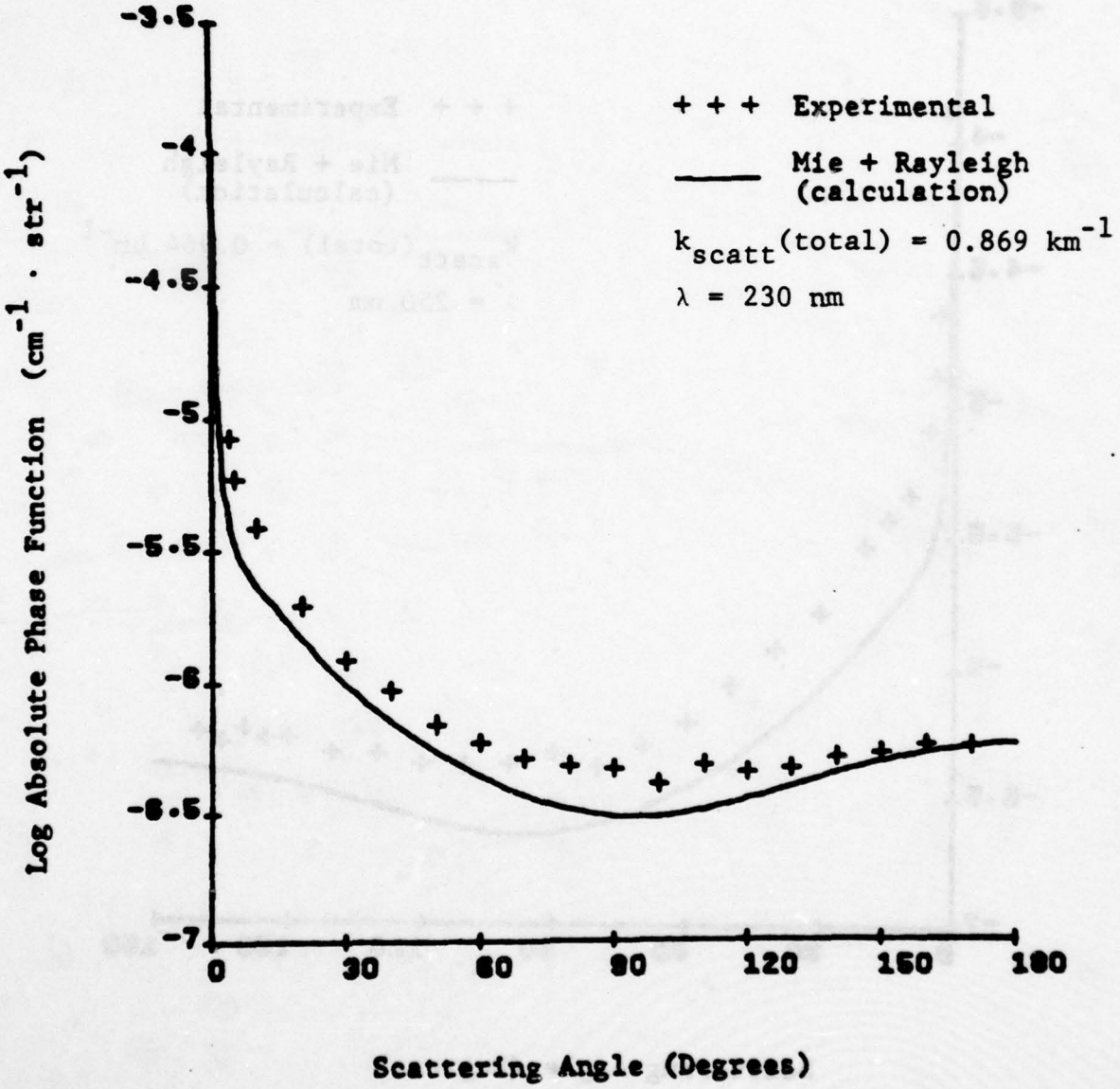

Phase function measured on May 26, 1978.

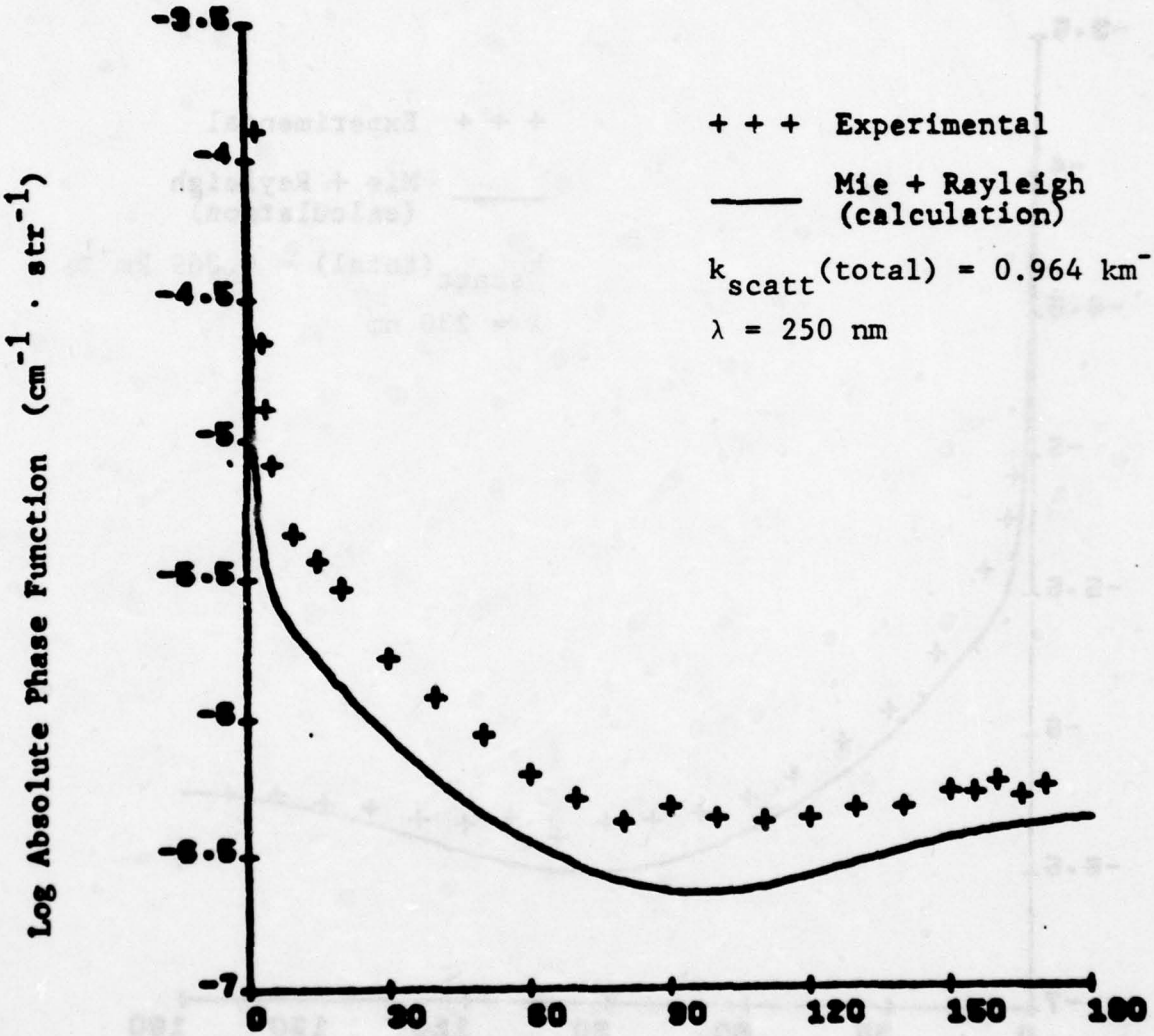

Phase function measured on May 26, 1978.

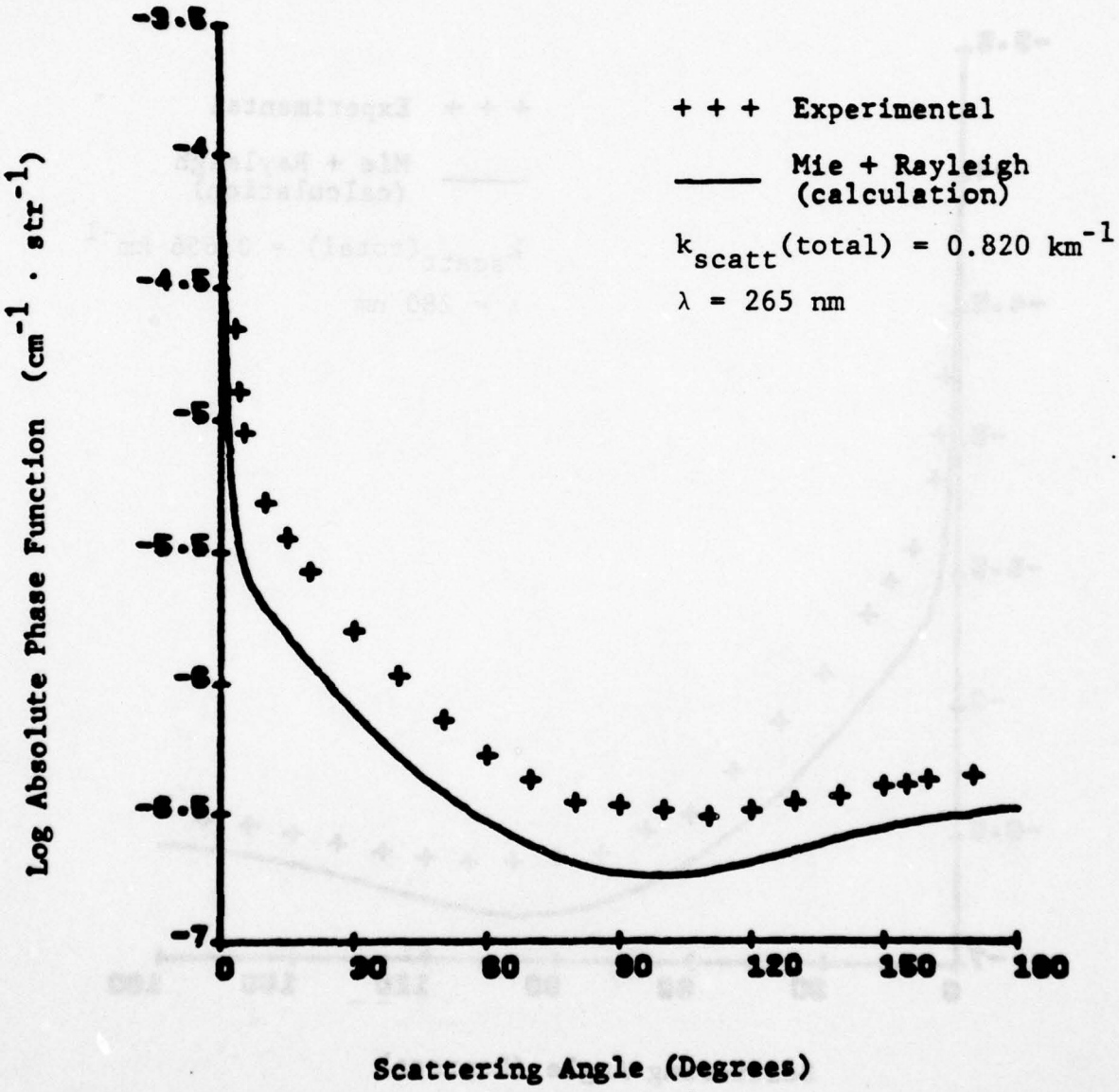

Phase function measured on May 26, 1978.

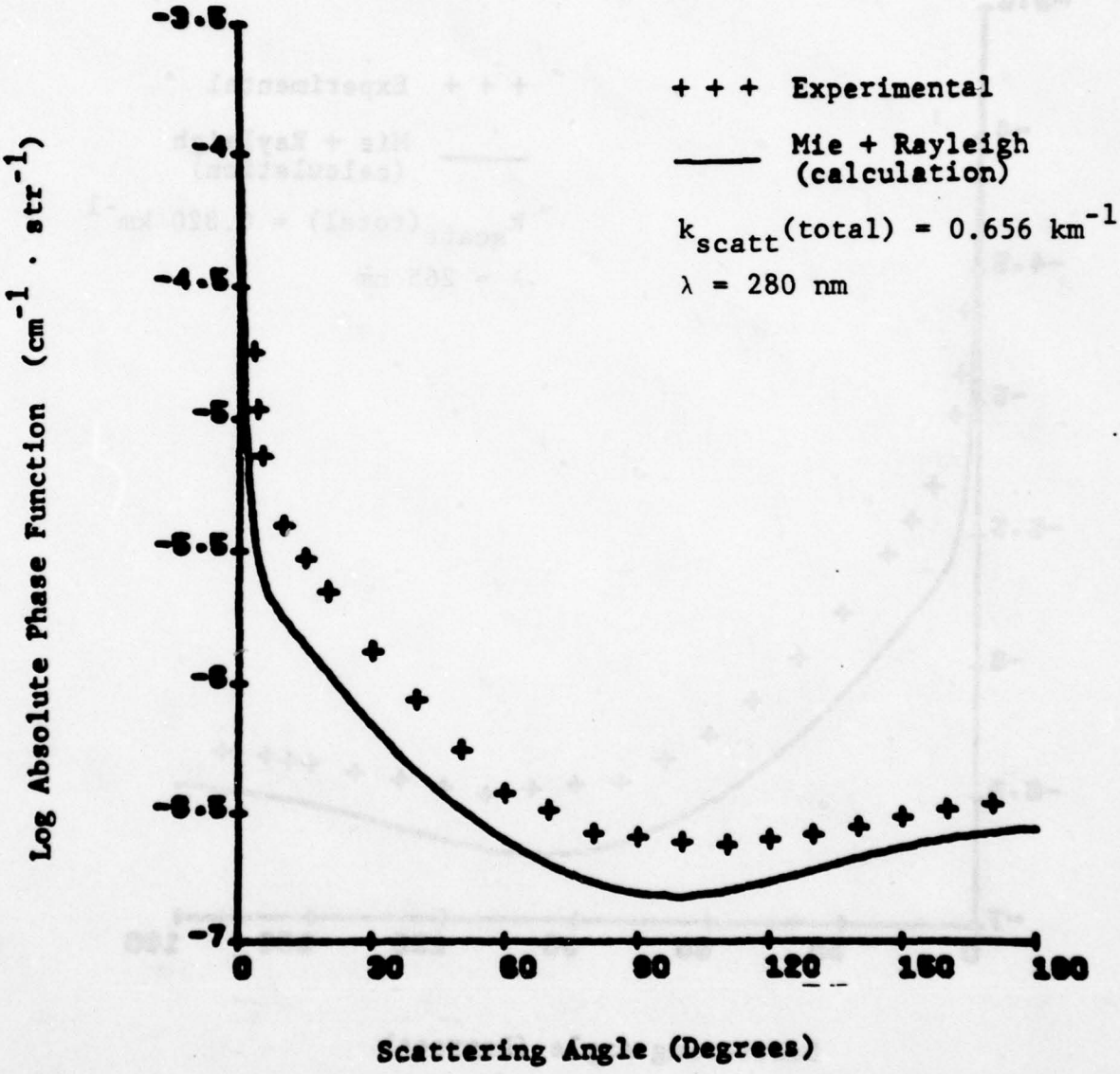

Phase function measured on May 26, 1978.

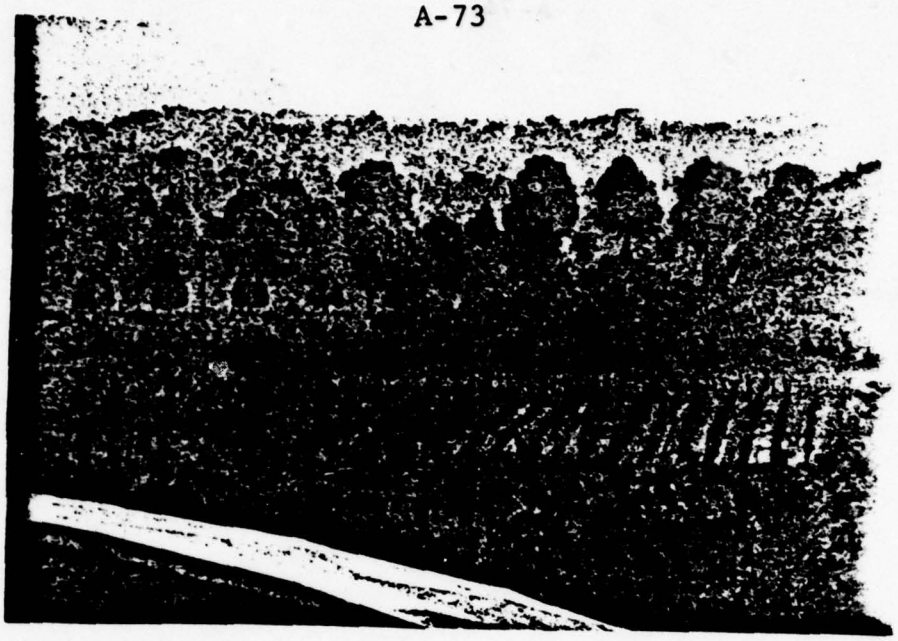

Ground level photograph
May 31, 1978 (A.M.) -- Princeton

Weather.....	overcast, high haze
Visibility.....	10 km
Temperature.....	76°F
Humidity.....	70%
Ozone concentration...	0.10 ppm
$k_{abs}(O_3)$.....	2.53 km^{-1} at 265 nm
k_{scat}(total).....	1.05 km^{-1} at 250 nm

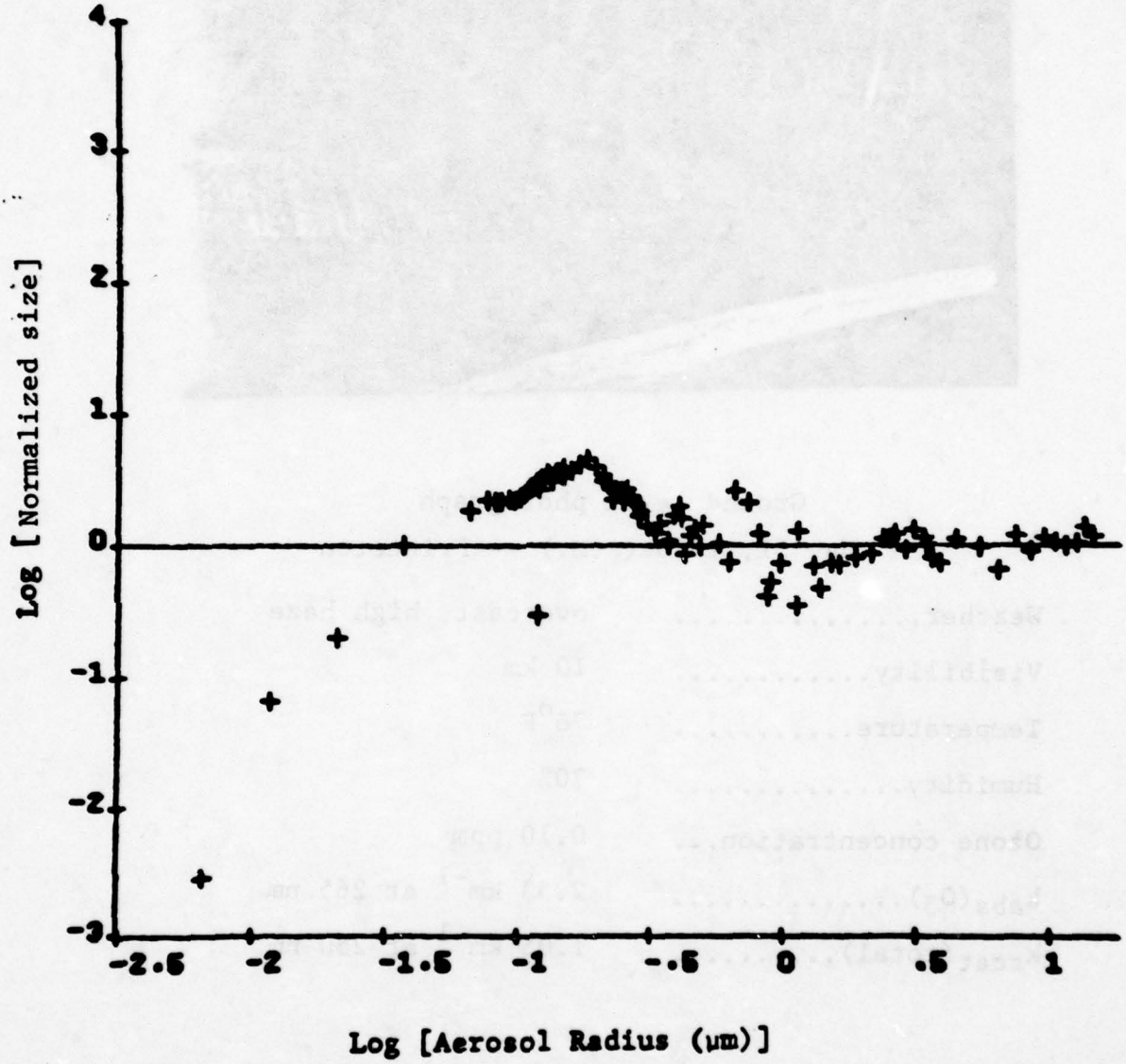

Normalized size distribution measured on May 31, 1978.

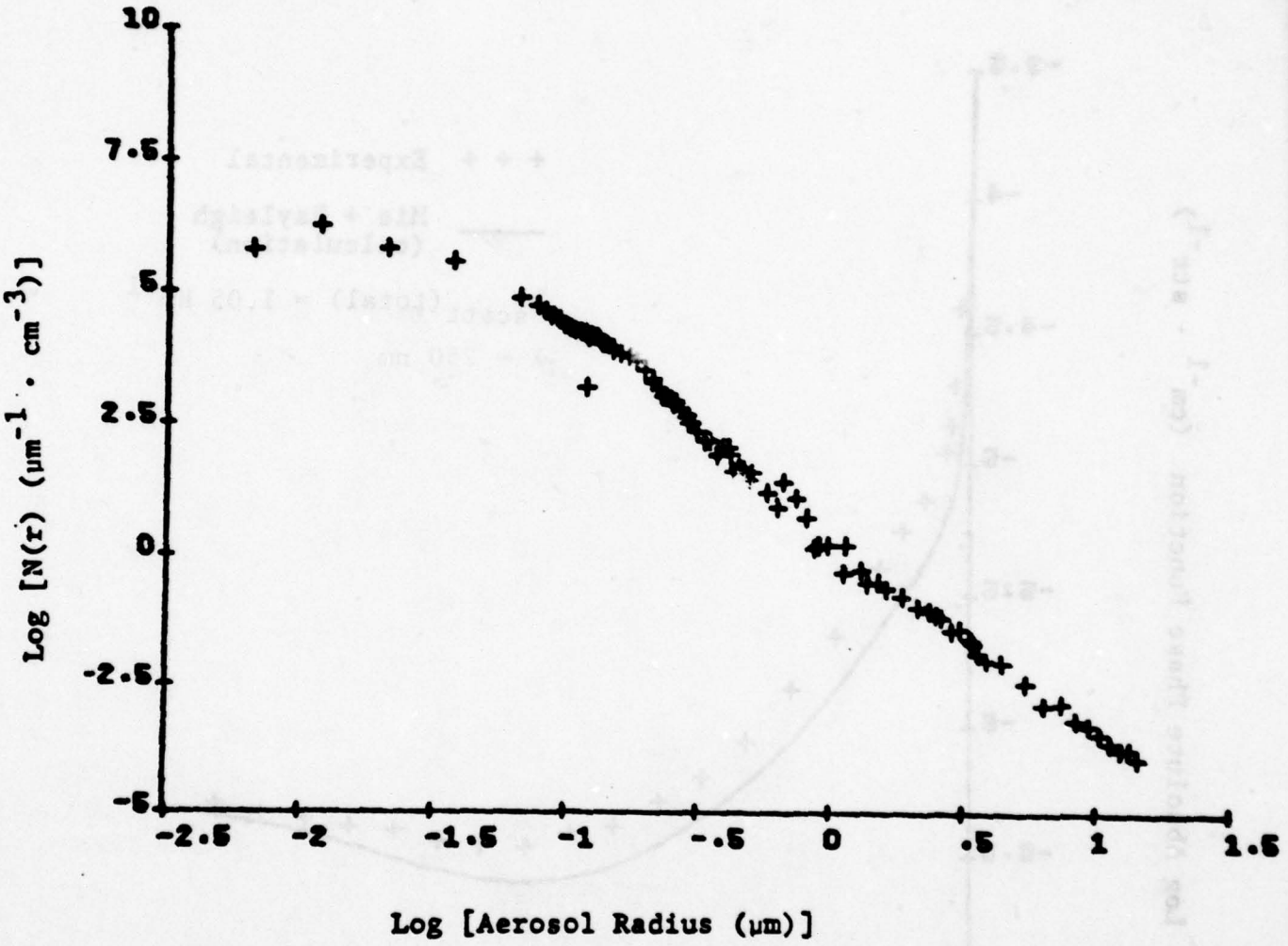

Particle size distribution measured on May 31, 1978.

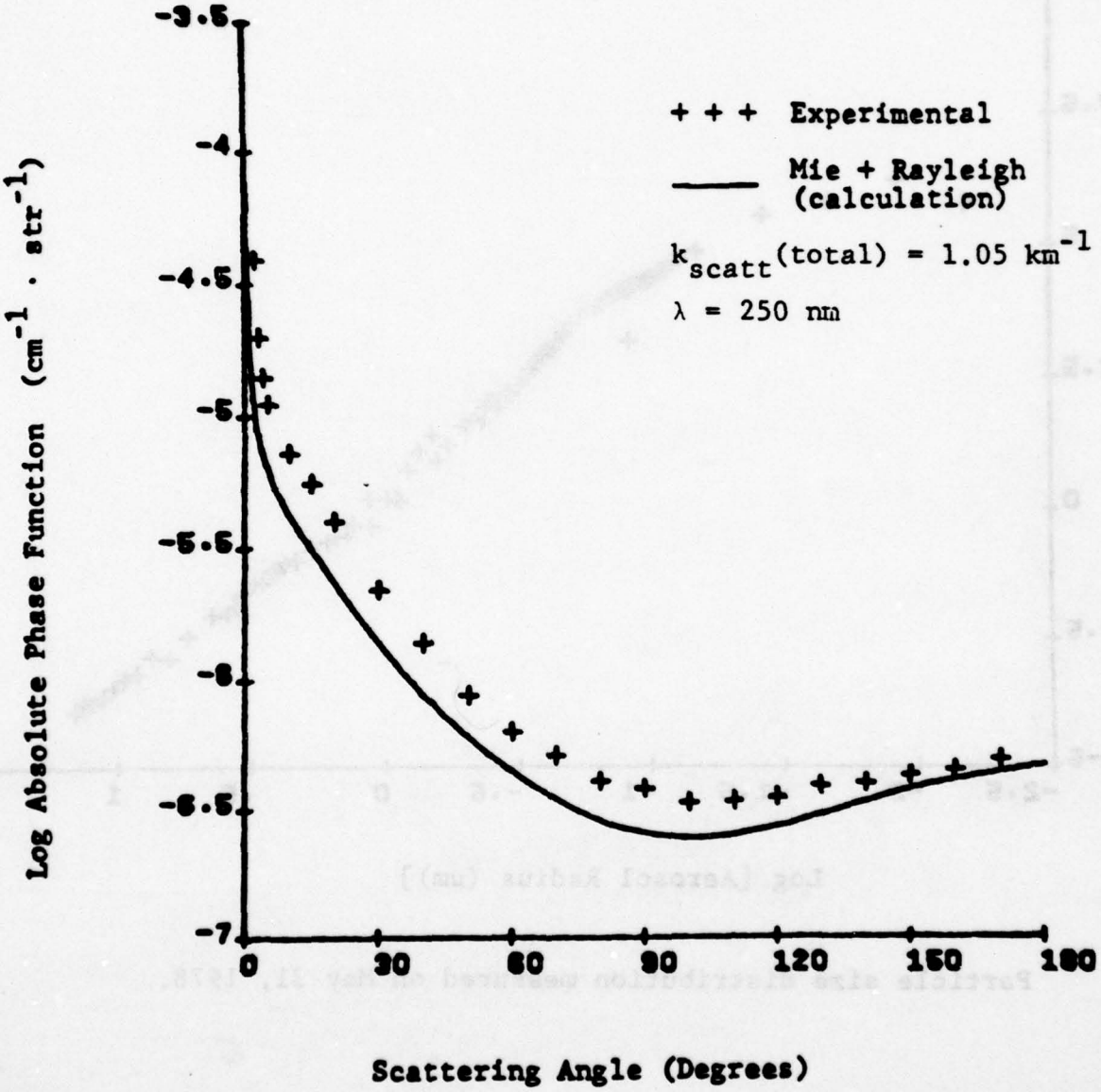

Phase function measured on May 31, 1978.

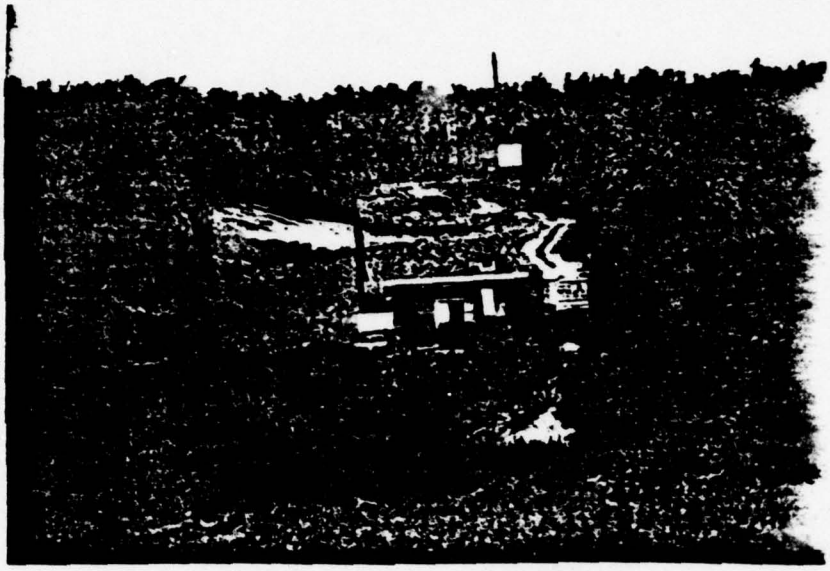

Ground level photograph
July 26, 1978 -- Ft. Monmouth

Weather.....	clear
Visibility.....	25 km
Temperature.....	75°F
Humidity.....	71%
Ozone concentration...	0.007
$k_{abs}(O_3)$.....	0.18 km^{-1} at 265 nm
k_{scat}(total).....	0.623 km^{-1} at 250 nm
	0.597 km^{-1} at 265 nm

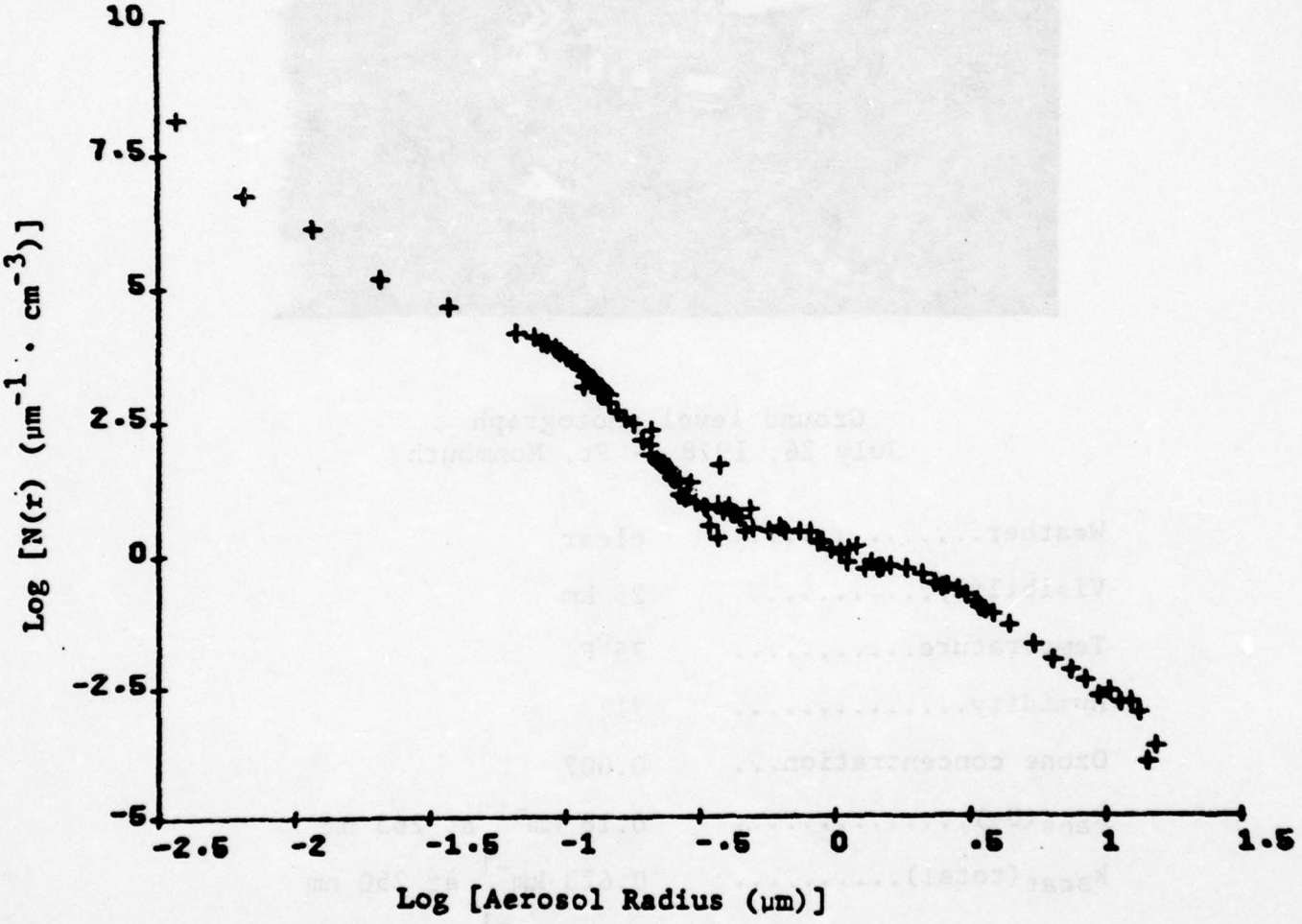

Particle size distribution measured on July 26, 1978.

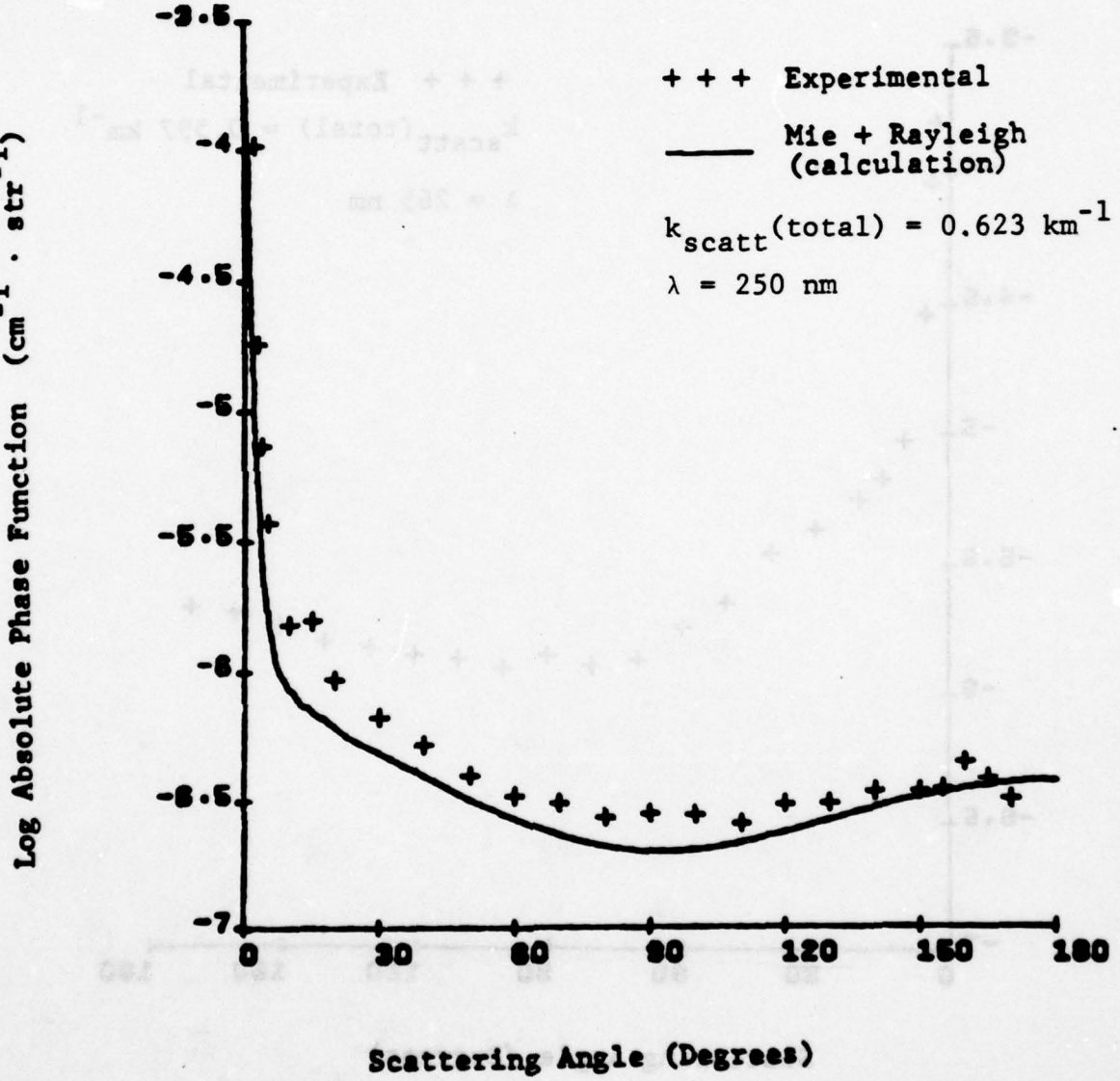

Phase function measured on July 26, 1978.

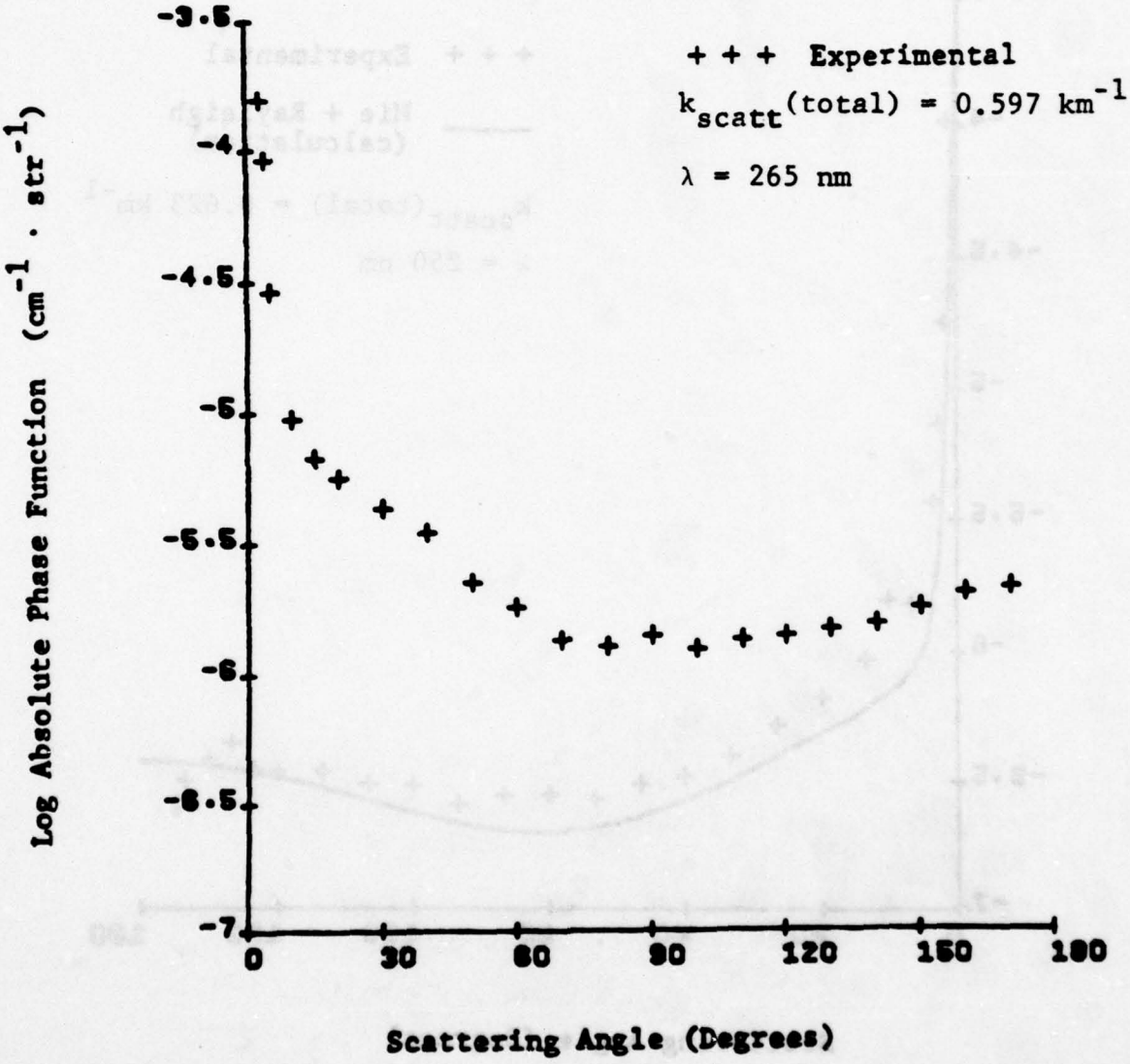

Phase function measured on July 26, 1978.

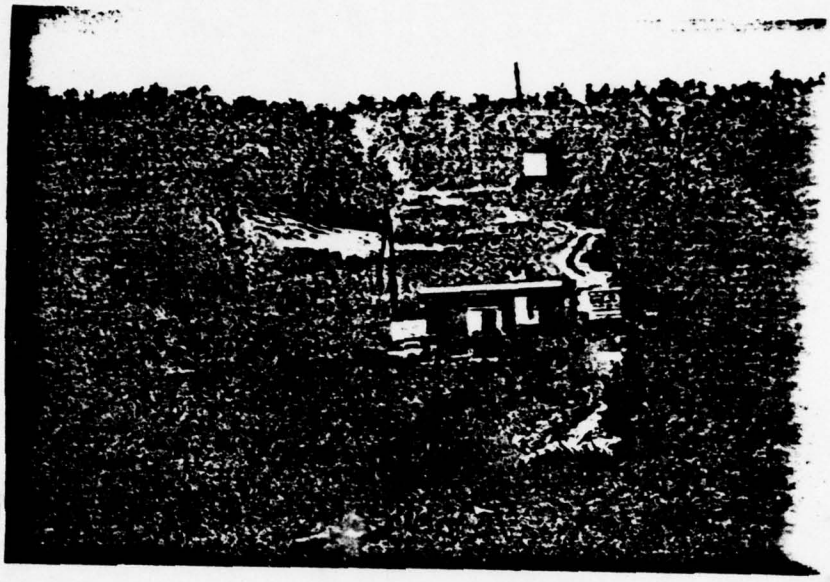

Ground level photograph
July 28, 1978 -- Ft. Monmouth

Weather.....	rain, haze
Visibility.....	8 km
Temperature.....	79°F
Humidity.....	73%
Ozone concentration...	0.02 ppm
$k_{abs}(O_3)$.....	0.50 km^{-1} at 265 nm
k_{scat}(total).....	1.34 km^{-1} at 265 nm

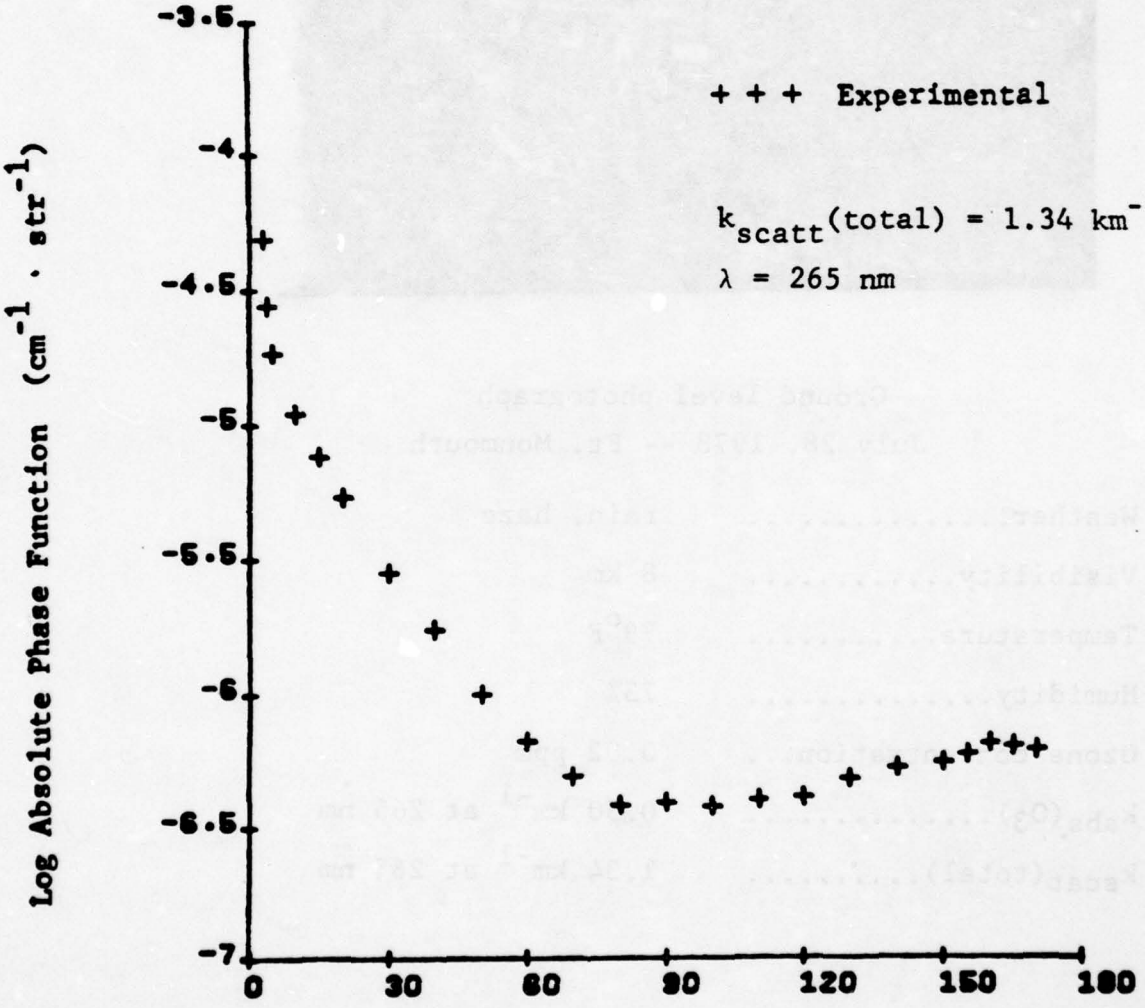

Phase function measured on July 28, 1978.

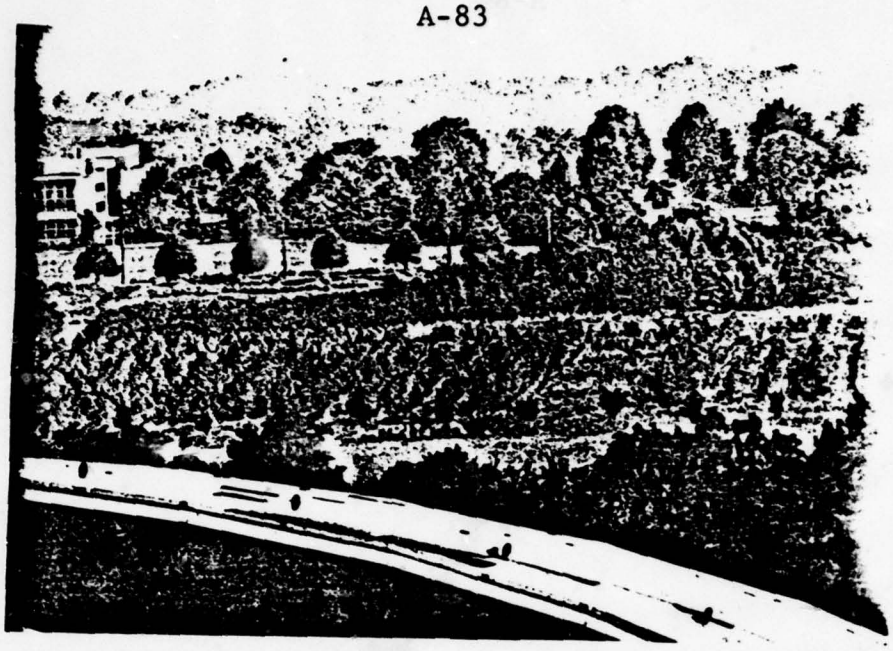

Ground level photograph
August 31, 1978 -- Princeton

Weather.....	rainy day, high mist
Visibility.....	8 km
Temperature.....	78°F
Humidity.....	83%
Ozone concentration...	0.04 ppm
$k_{abs}(O_3)$.....	1.00 km^{-1} at 265 nm
k_{scat}(total).....	0.94 km^{-1} at 250 nm
	1.30 km^{-1} at 265 nm
	0.71 km^{-1} at 265 nm

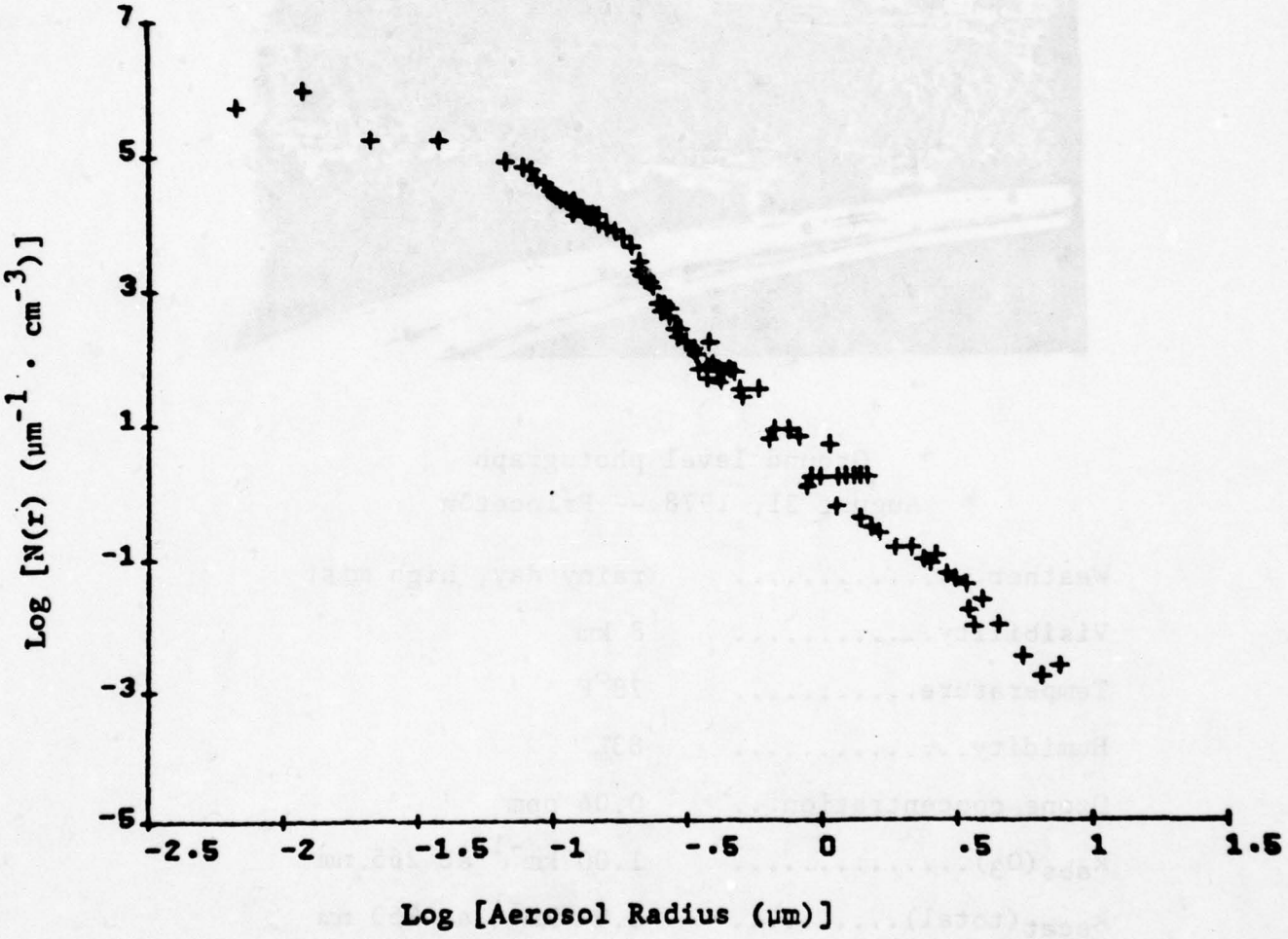

Particle size distribution measured on August 31, 1978.

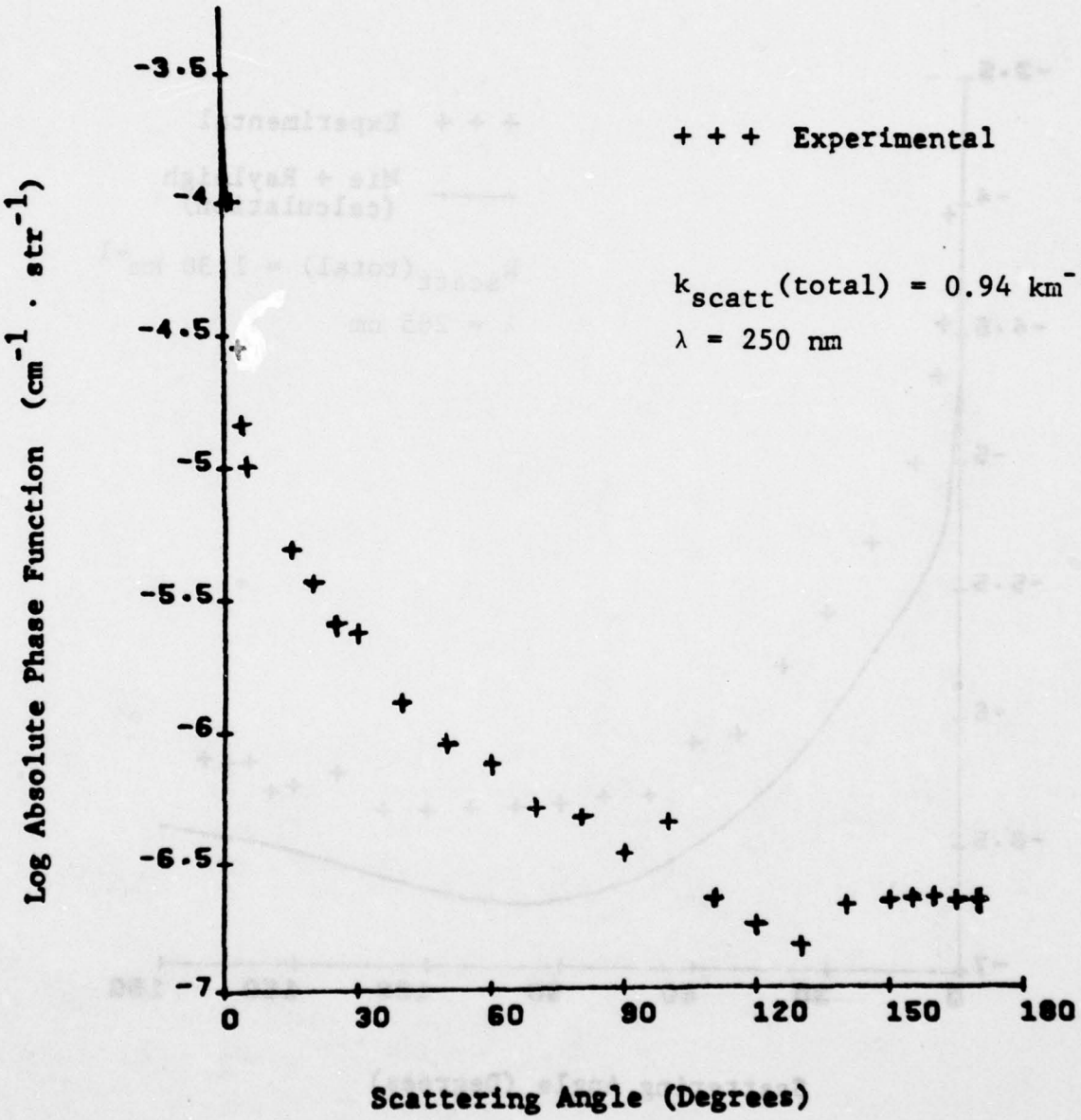

Phase function measured on August 31, 1978.

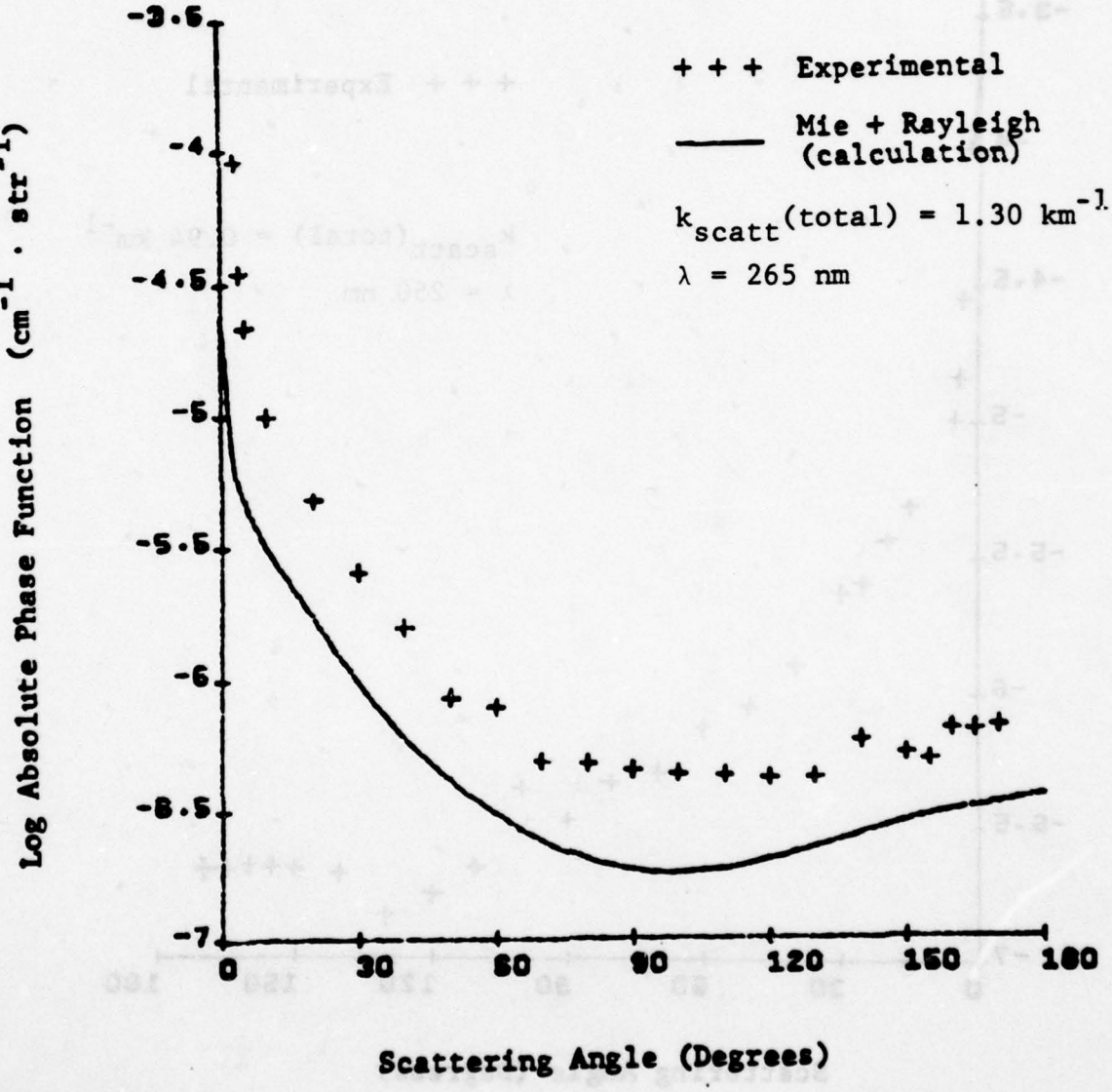

Phase function measured on August 31, 1978.

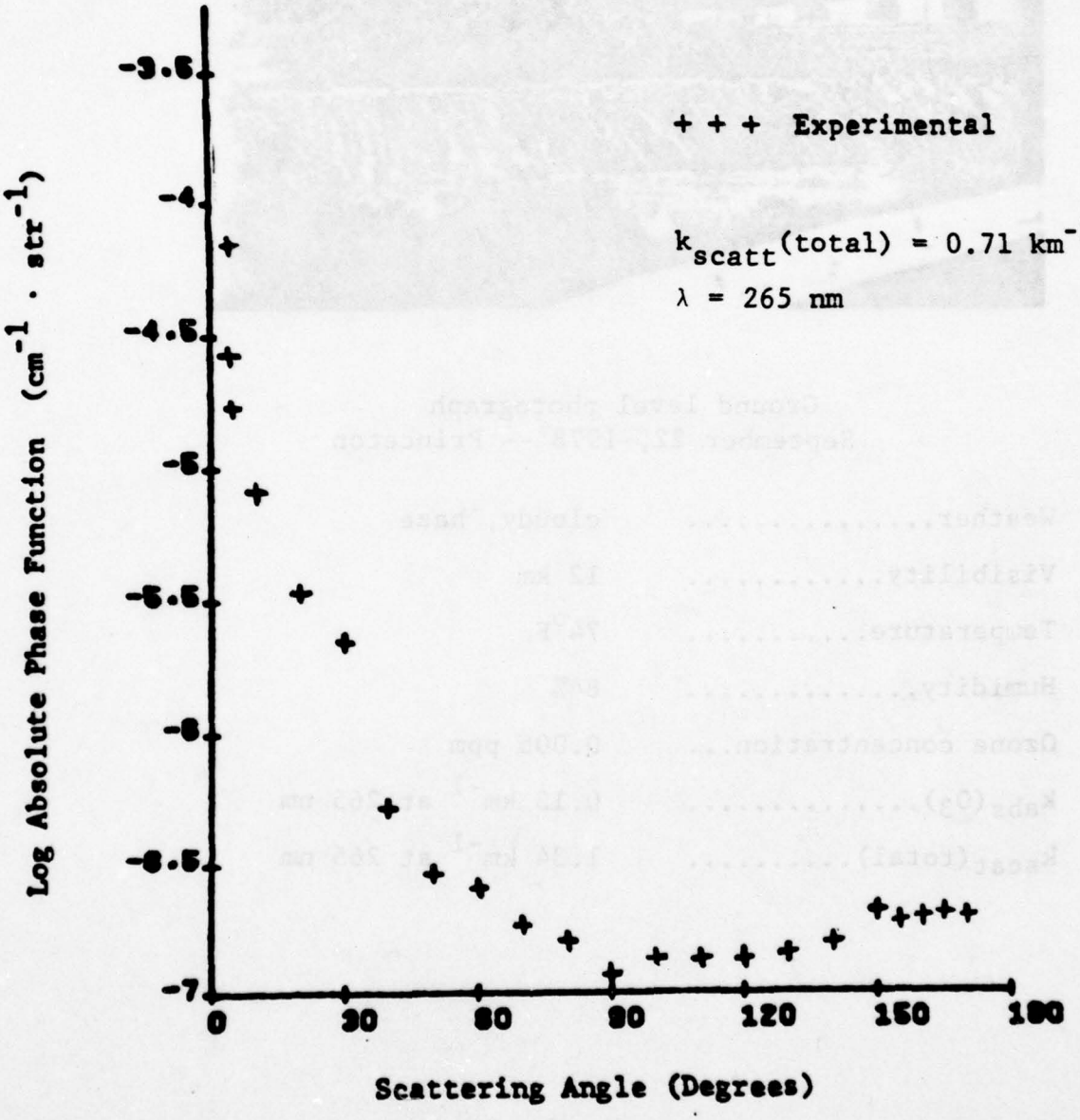

Phase function measured on August 31, 1978.

Ground level photograph
September 22, 1978 -- Princeton

Weather.....	cloudy, haze
Visibility.....	12 km
Temperature.....	$74^{o}F$
Humidity.....	84%
Ozone concentration...	0.005 ppm
$k_{abs}(O_3)$.....	0.13 km^{-1} at 265 nm
k_{scat}(total).....	1.34 km^{-1} at 265 nm

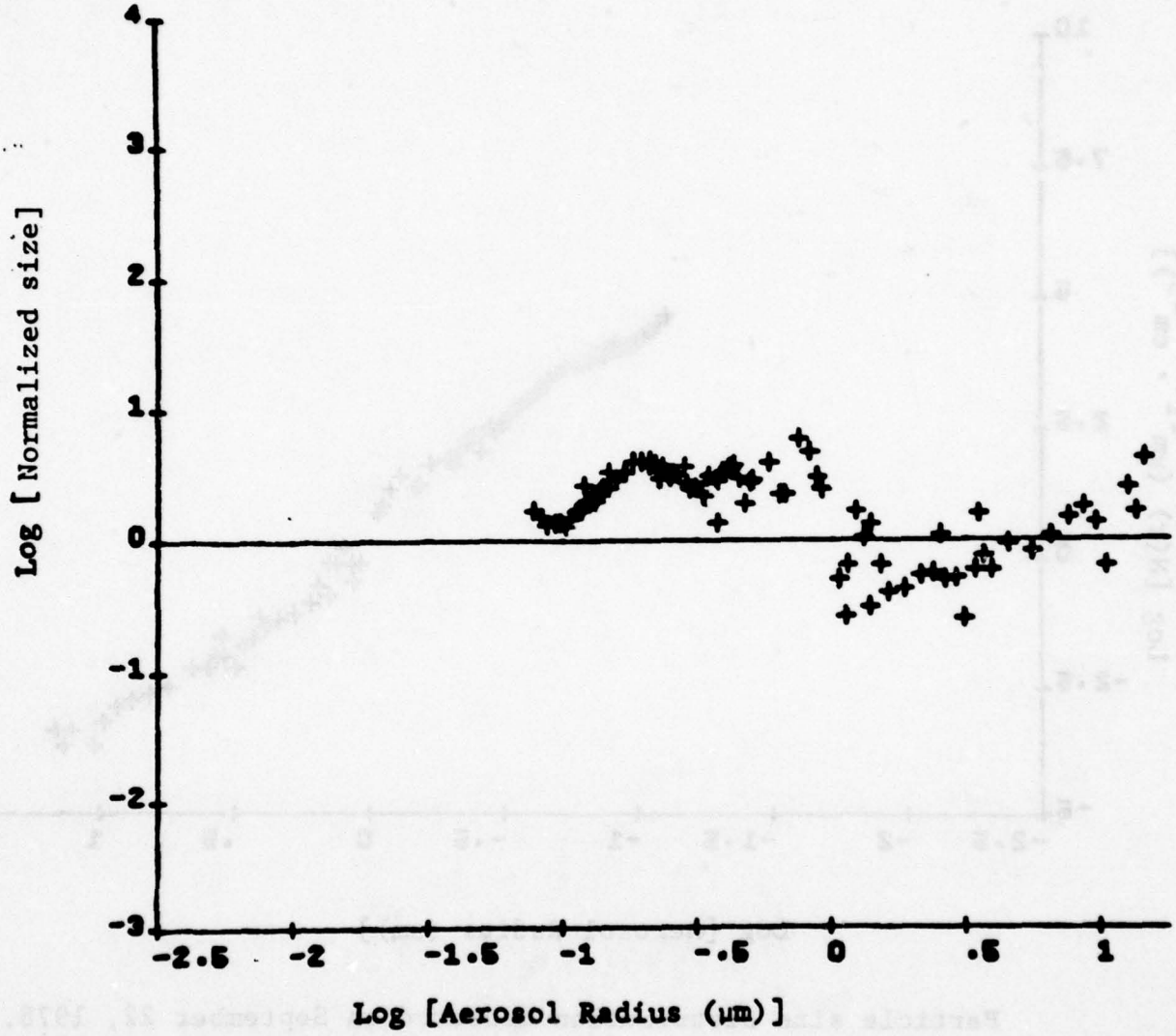

Normalized size distribution measured on September 22, 1978.

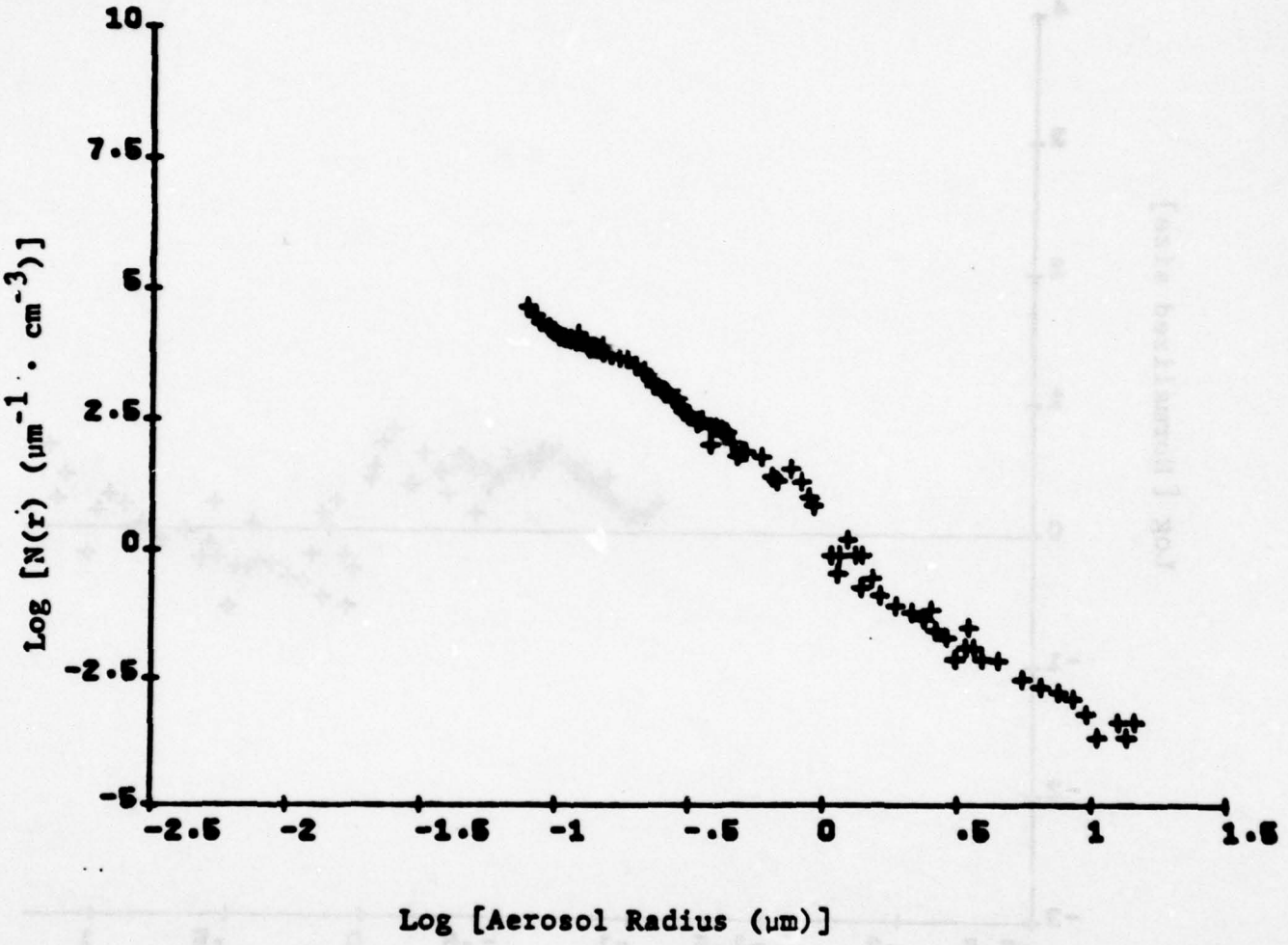

Particle size distribution measured on September 22, 1978.

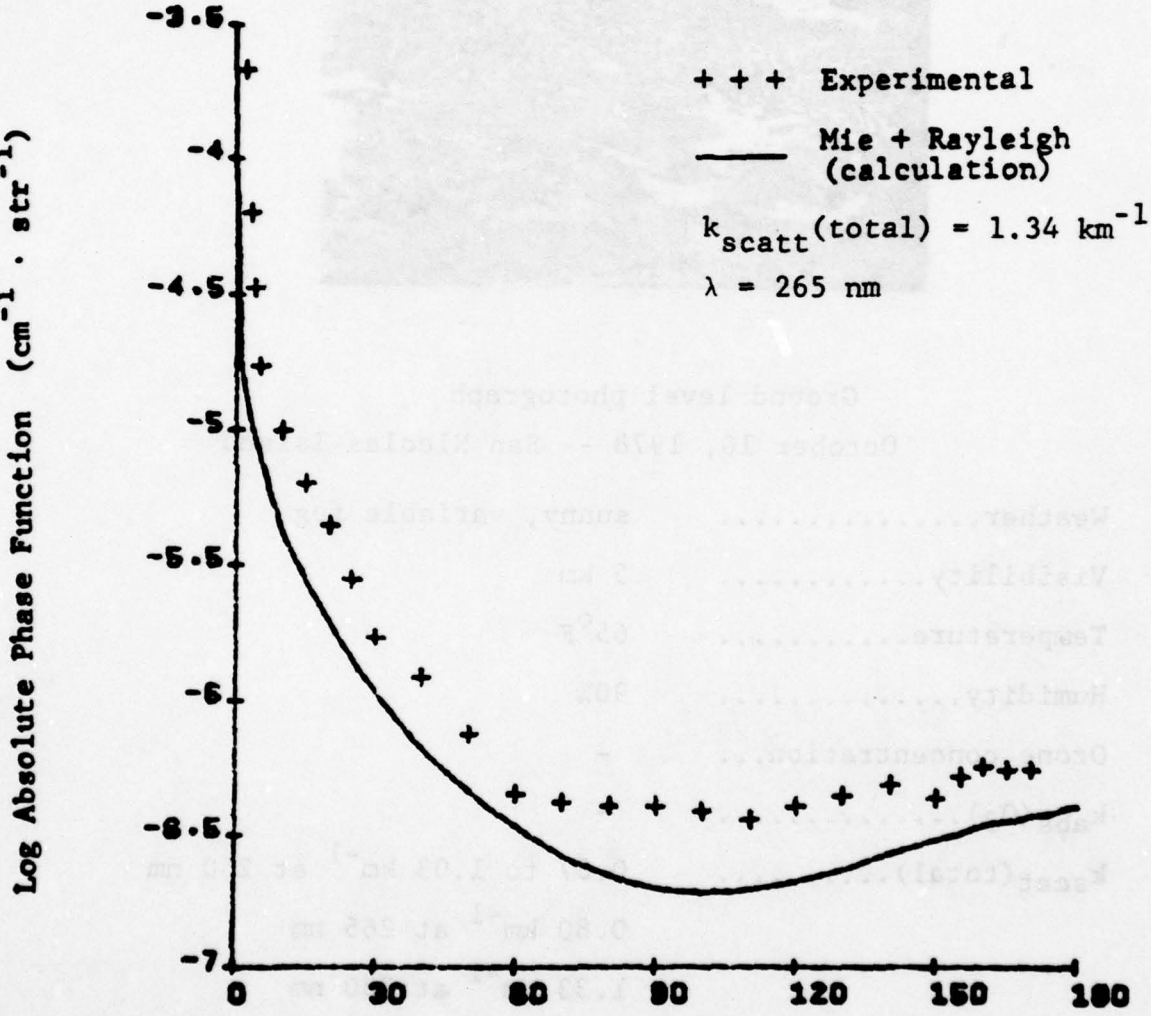

Phase function measured on September 22, 1978.

Ground level photograph

October 10, 1978 -- San Nicolas Island

Weather.....	sunny, variable fog
Visibility.....	5 km
Temperature.....	65°F
Humidity.....	90%
Ozone concentration...	-
$k_{abs}(O_3)$.....	-
k_{scat}(total).....	0.87 to 1.03 km^{-1} at 250 nm
	0.80 km^{-1} at 265 nm
	1.33 km^{-1} at 280 nm

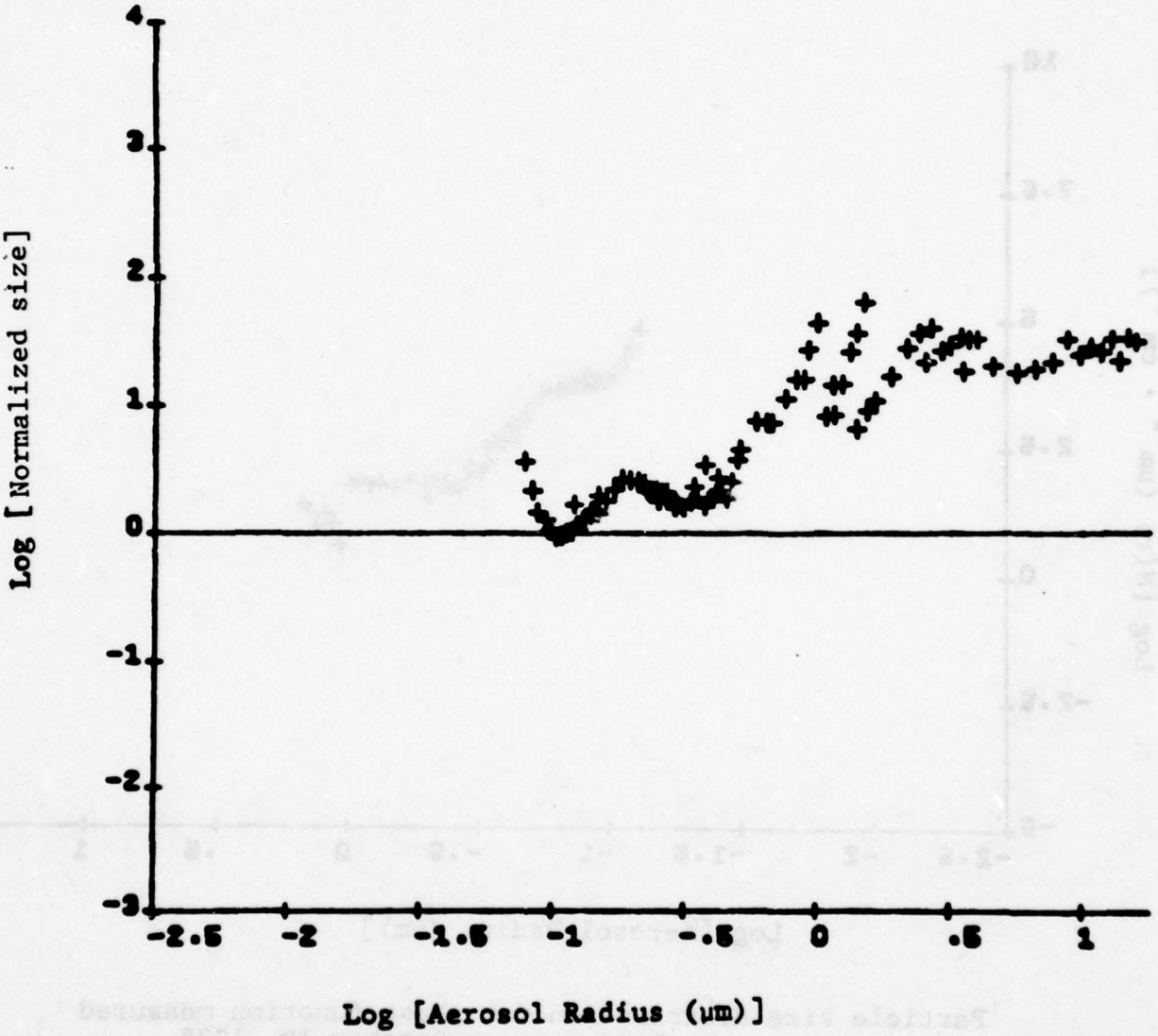

Typical normalized size distribution measured on October 10, 1978.

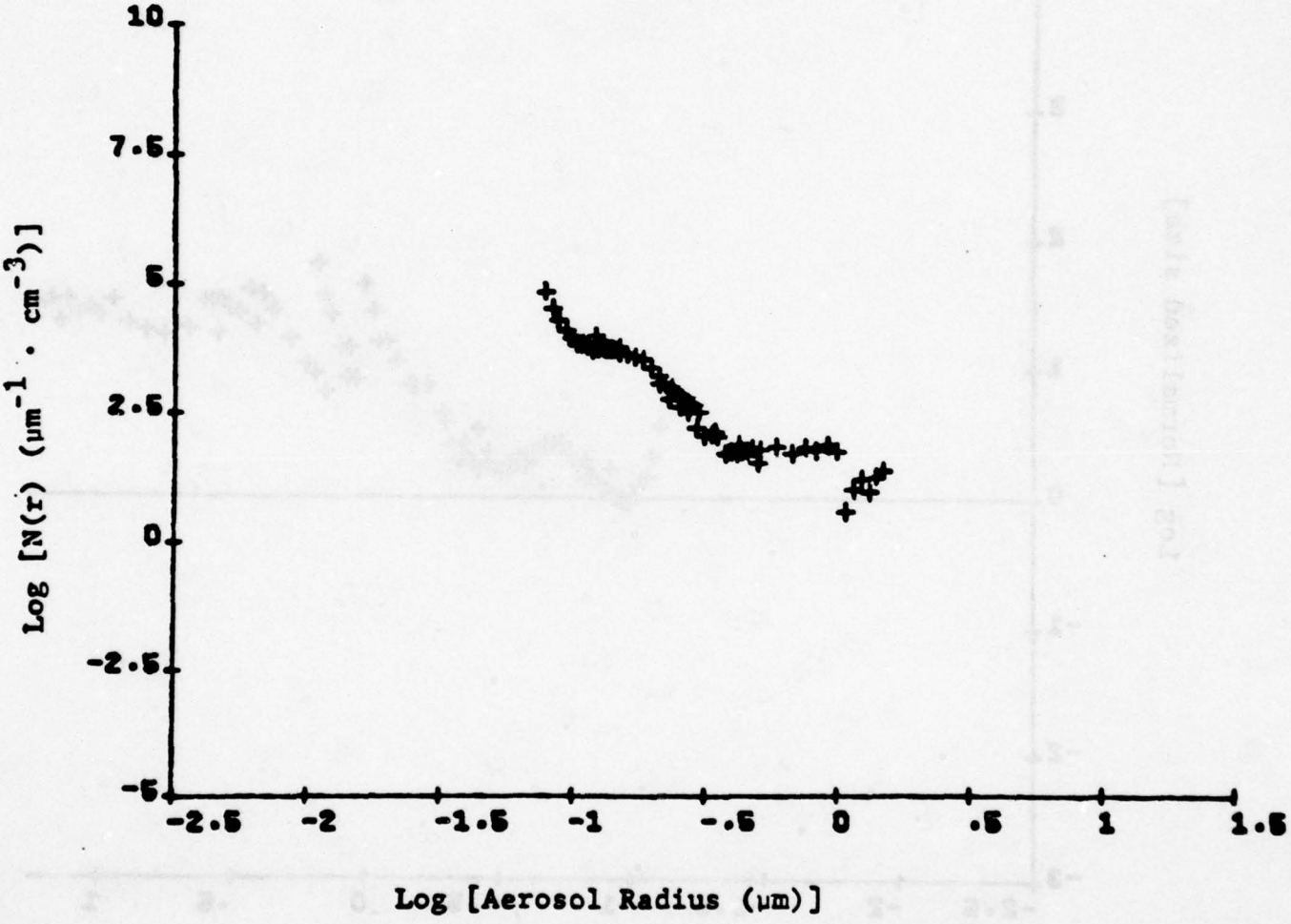

Particle size distribution for phase function measured at 5:30 p.m. on October 10, 1978.

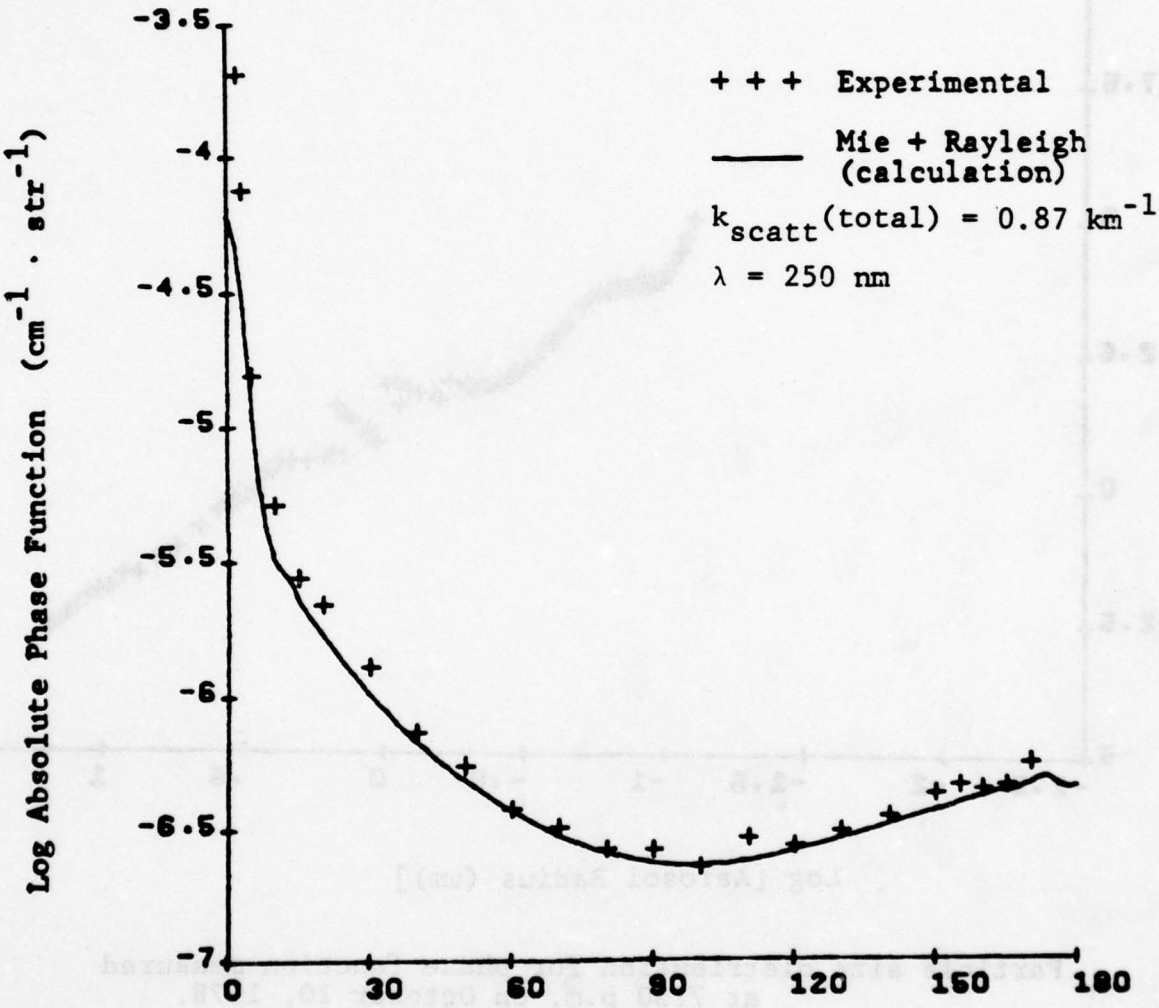

Phase function measured on October 10, 1978 at 5:30 p.m.

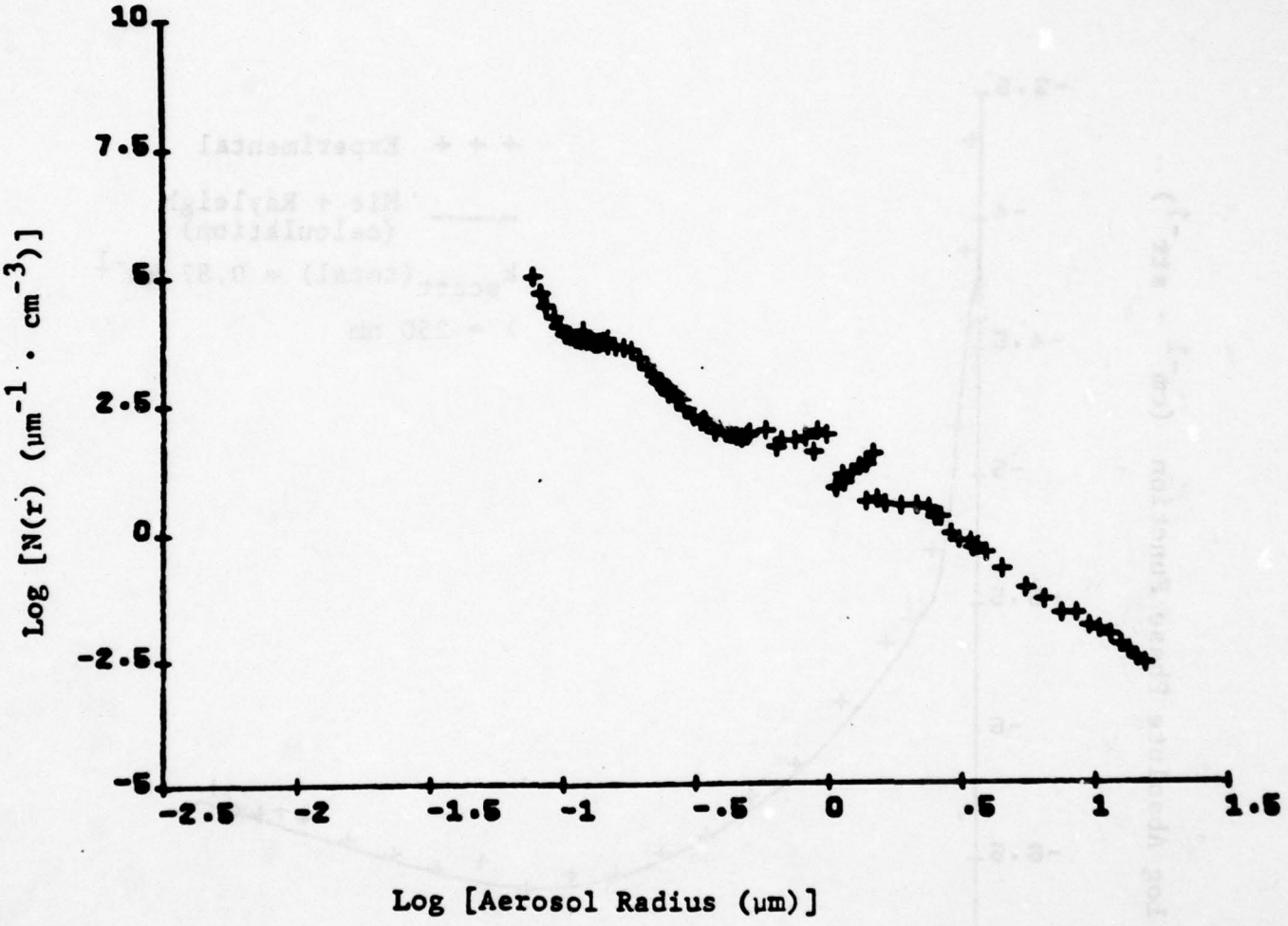

Particle size distribution for phase function measured at 7:30 p.m. on October 10, 1978.

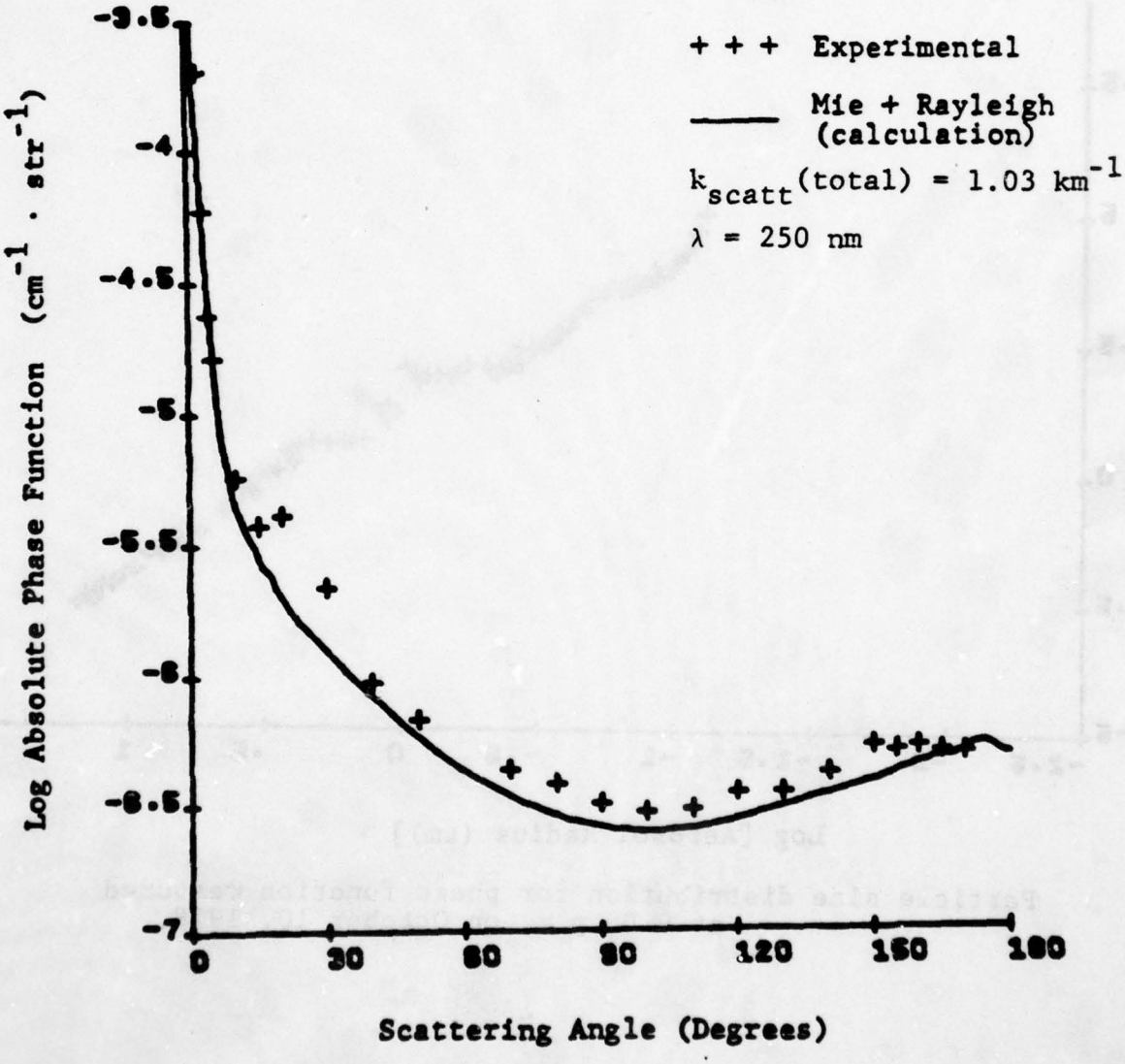

Phase function measured on October 10, 1978 at 7:30 p.m.

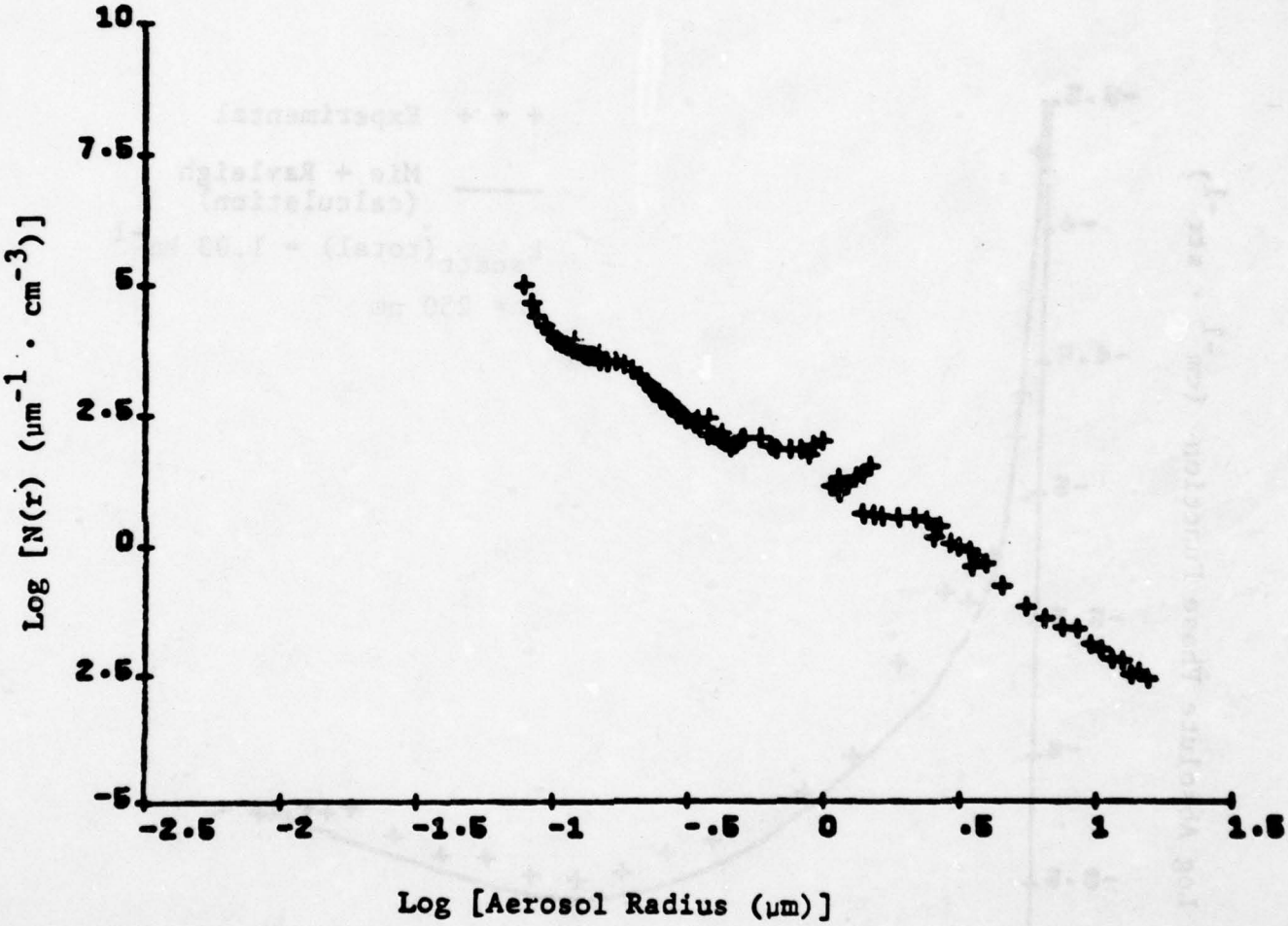

Particle size distribution for phase function measured at 9:00 p.m. on October 10, 1978.

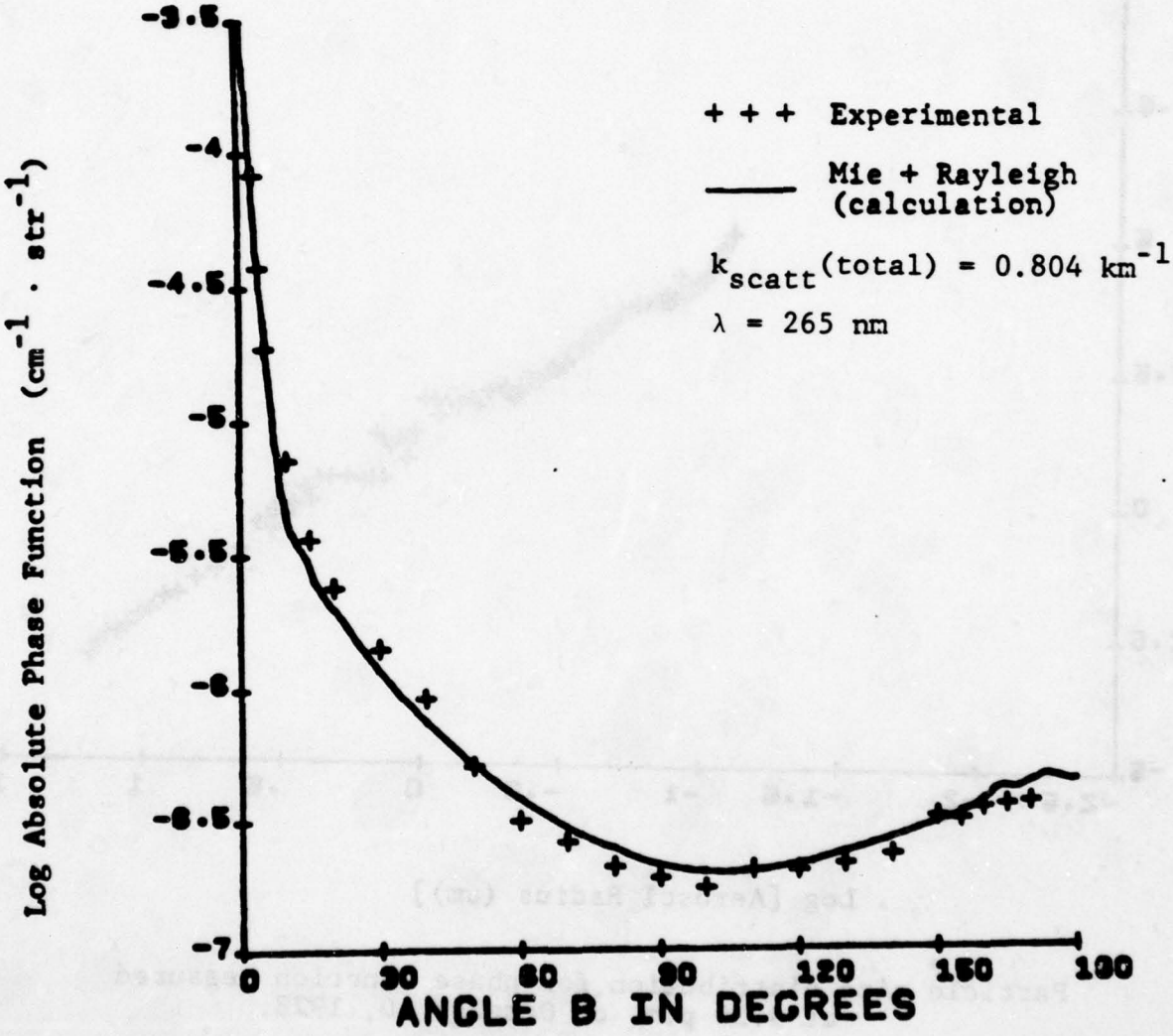

Phase function measured on October 10, 1978 at 9:00 p.m.

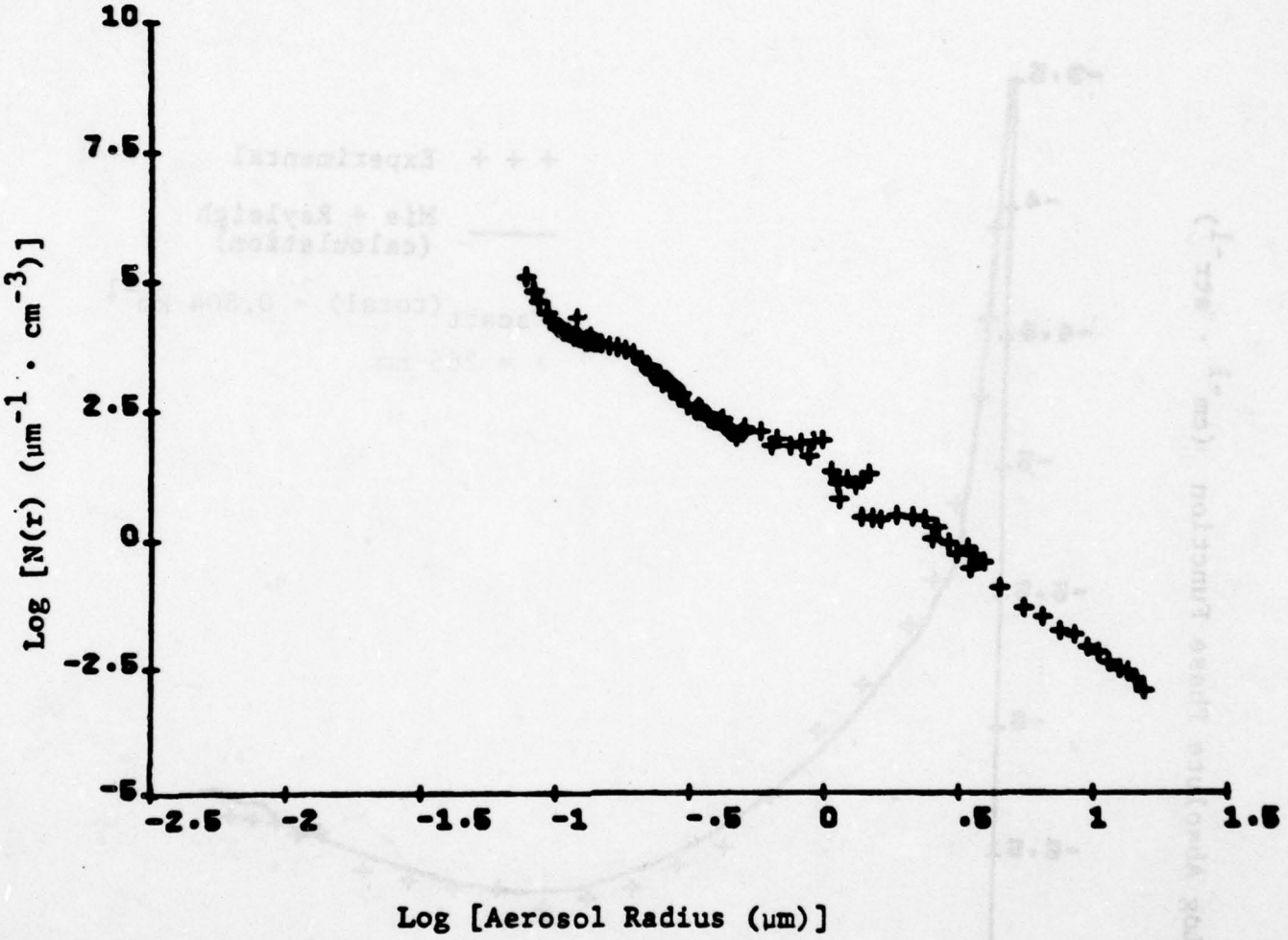

Particle size distribution for phase function measured at 9:50 p.m. on October 10, 1978.

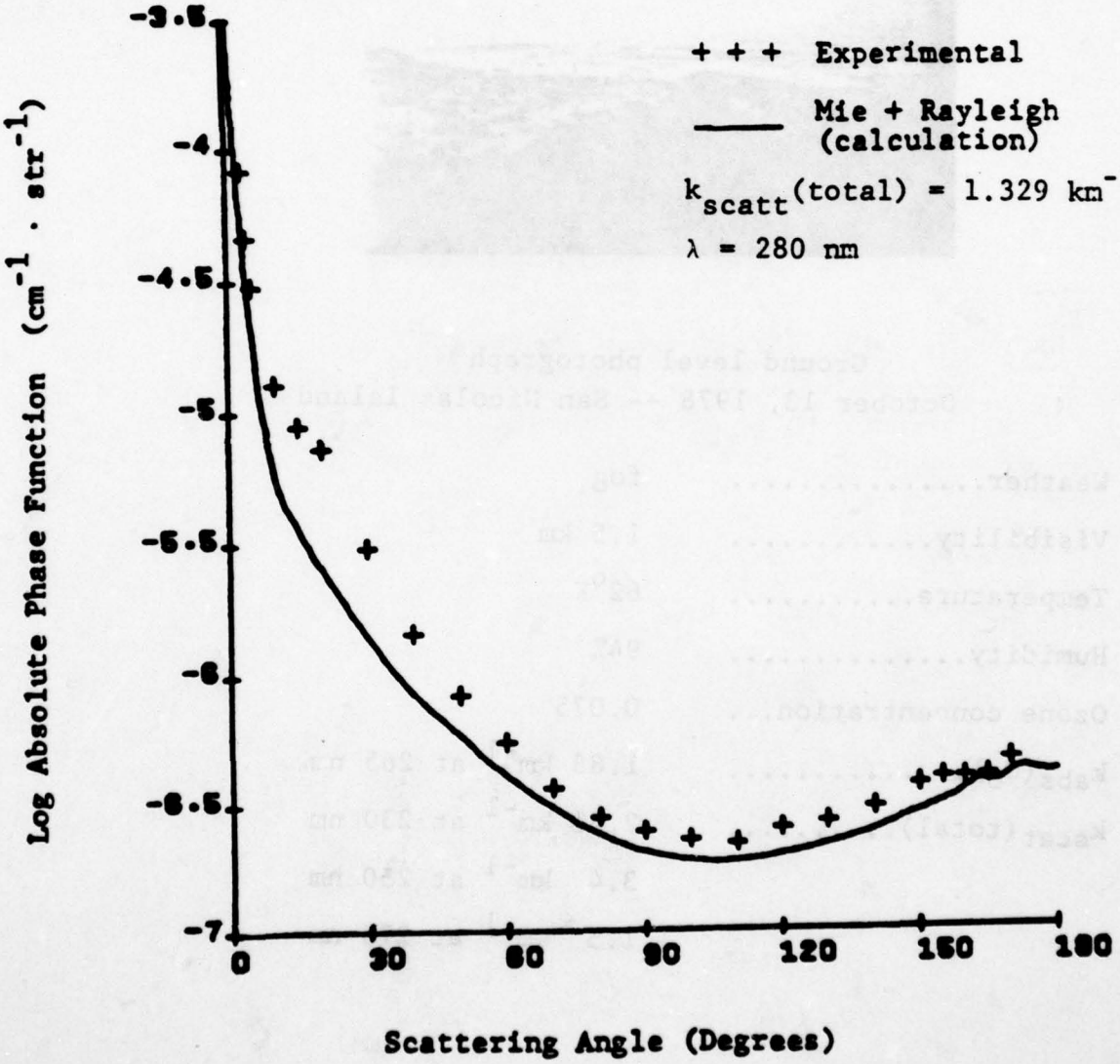

Phase function measured on October 10, 1978 at 9:50 p.m.

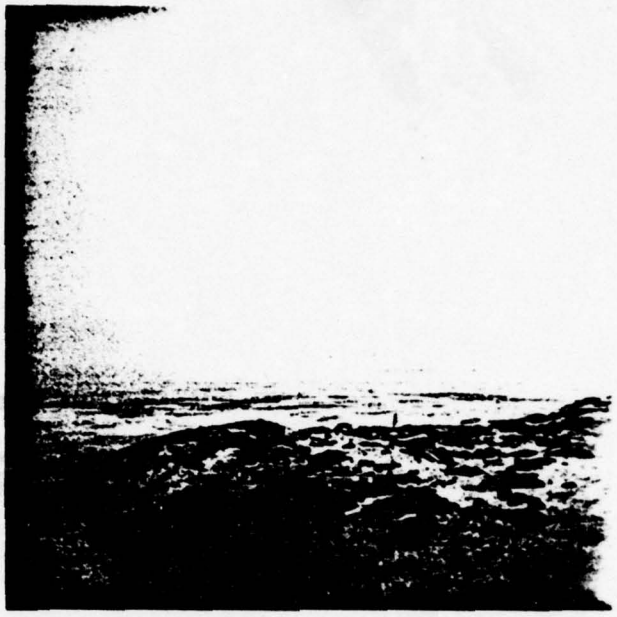

Ground level photograph
October 13, 1978 -- San Nicolas Island

Weather.....	fog
Visibility.....	1.5 km
Temperature.....	$62^{o}F$
Humidity.....	94%
Ozone concentration...	0.075
$k_{abs}(O_3)$.....	1.88 km^{-1} at 265 nm
k_{scat}(total).....	2.31 km^{-1} at 230 nm
	3.4 km^{-1} at 250 nm
	1.5 km^{-1} at 275 nm

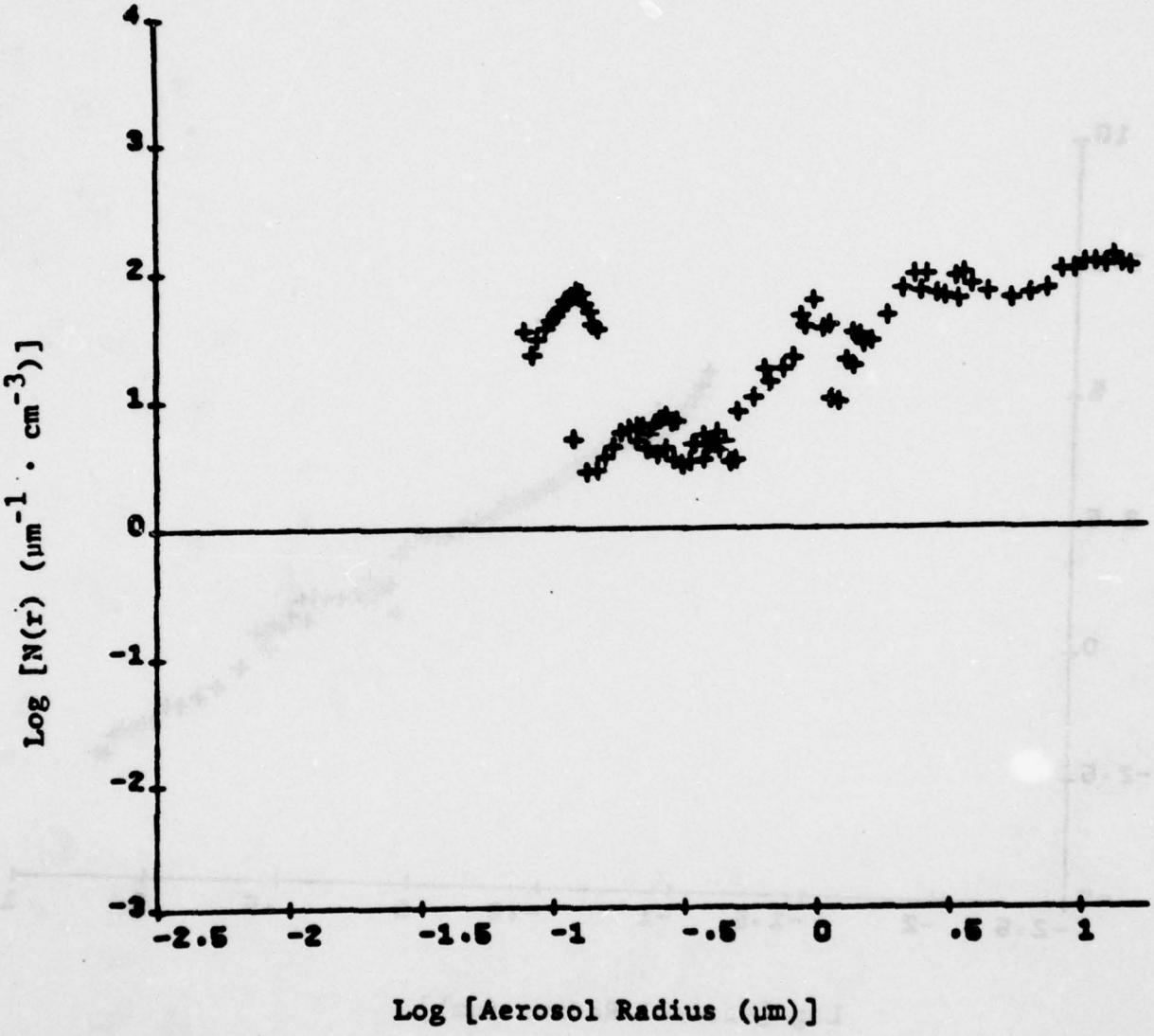

Typical normalized particle size distribution on October 13, 1978.

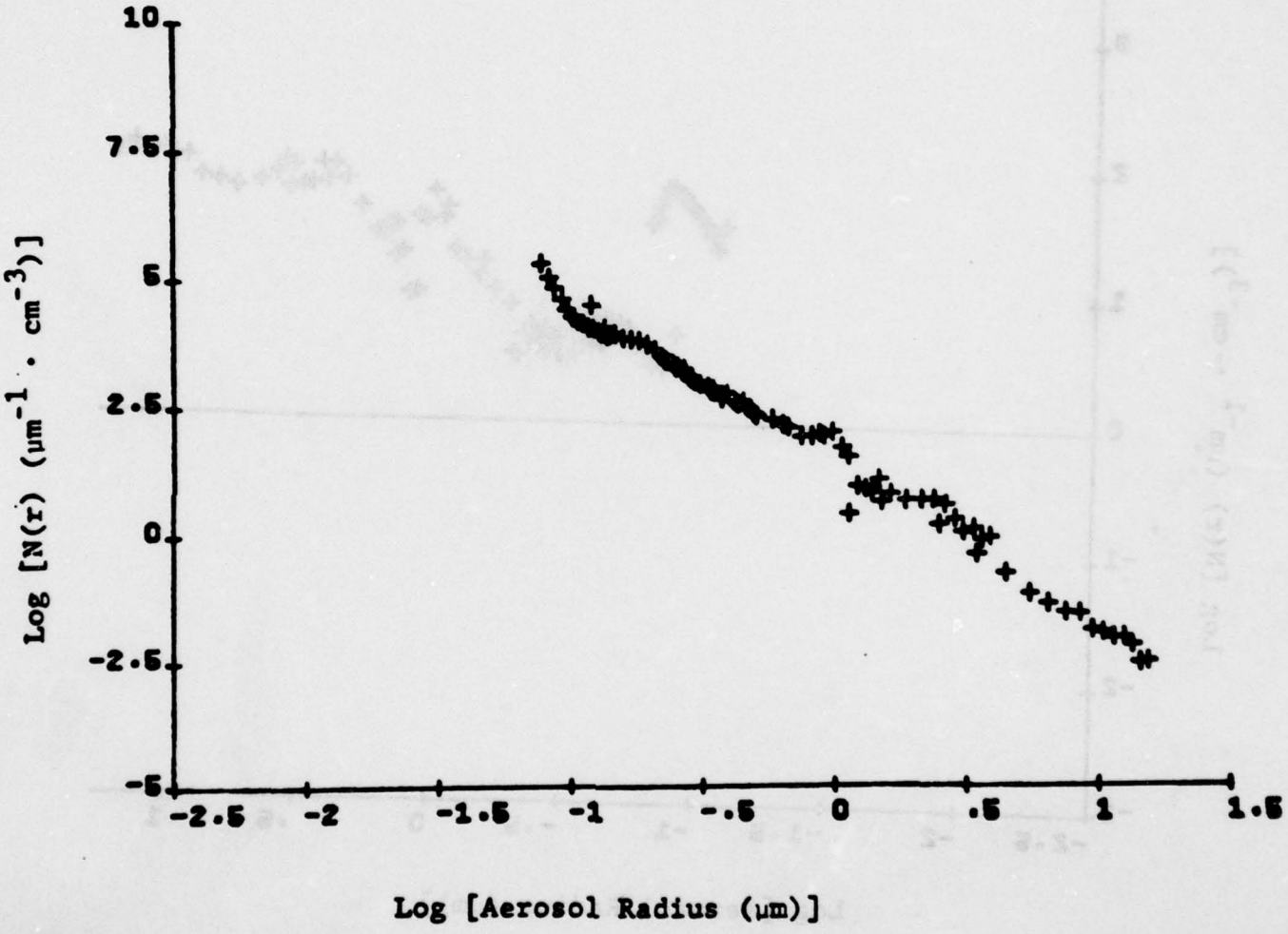

Particle size distribution for the phase function measured at 8:25 a.m. on October 13, 1978.

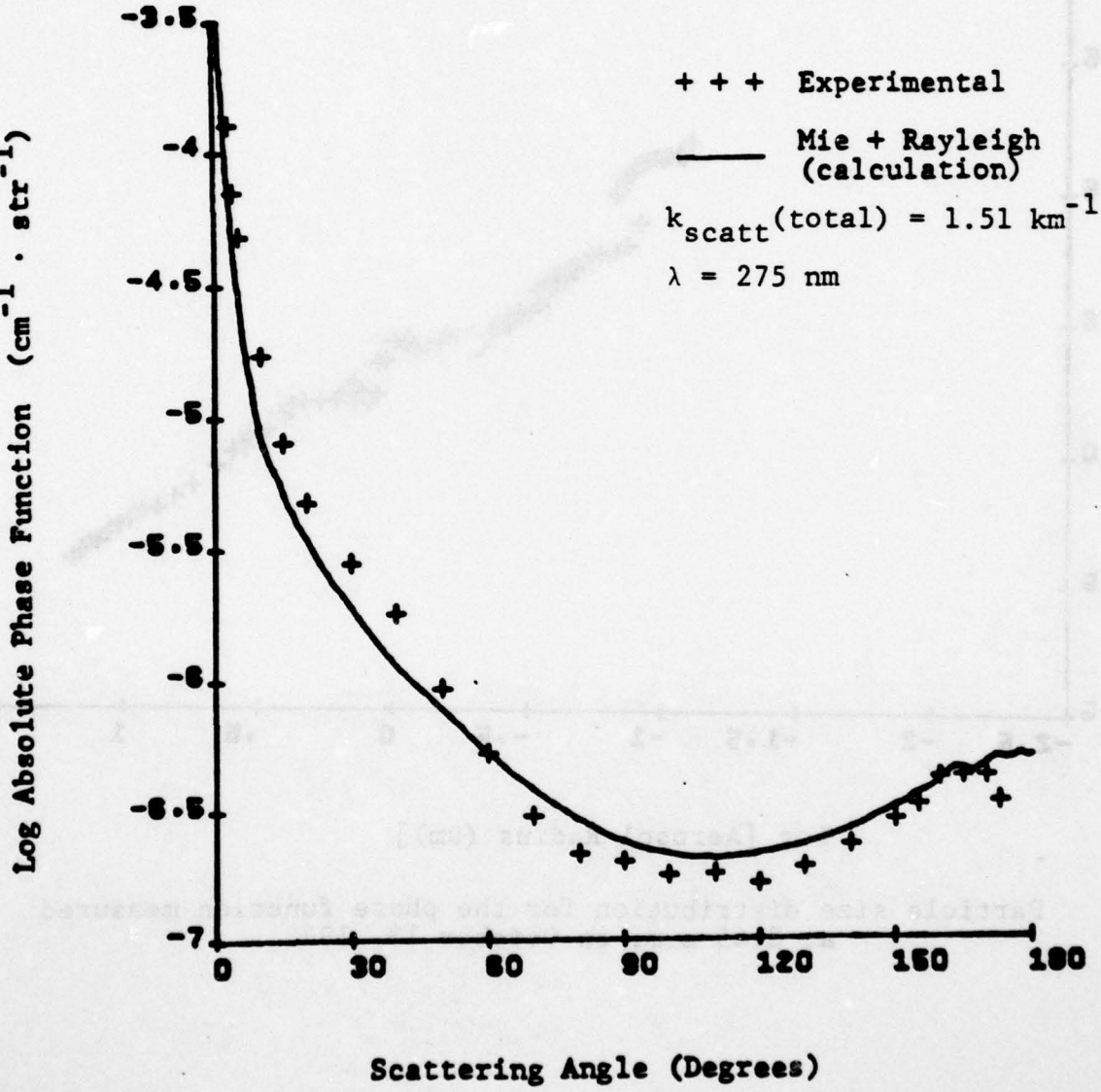

Phase function measured on October 13, 1978 at 8:25 a.m.

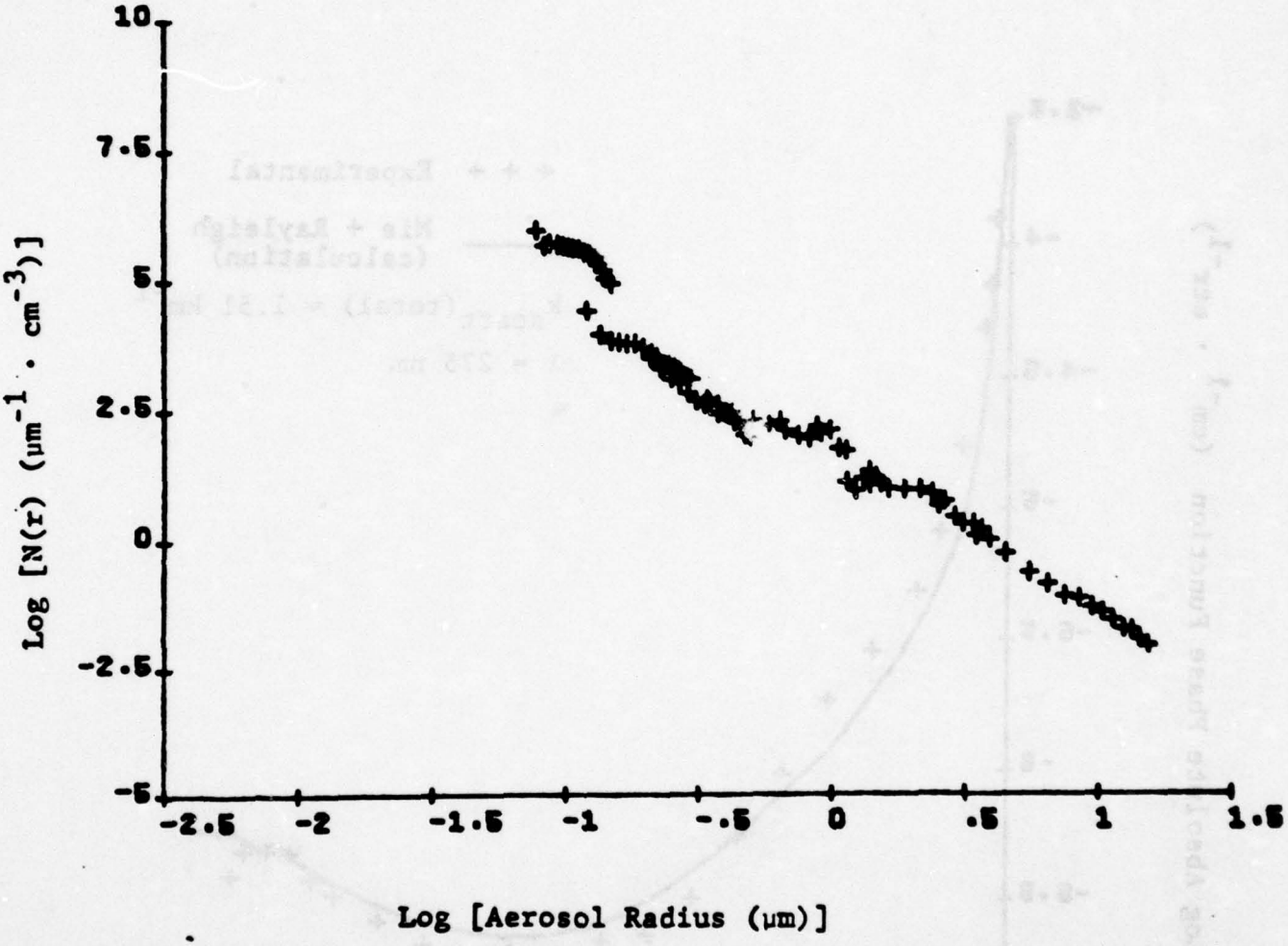

Particle size distribution for the phase function measured at 8:45 a.m. on October 13, 1978.

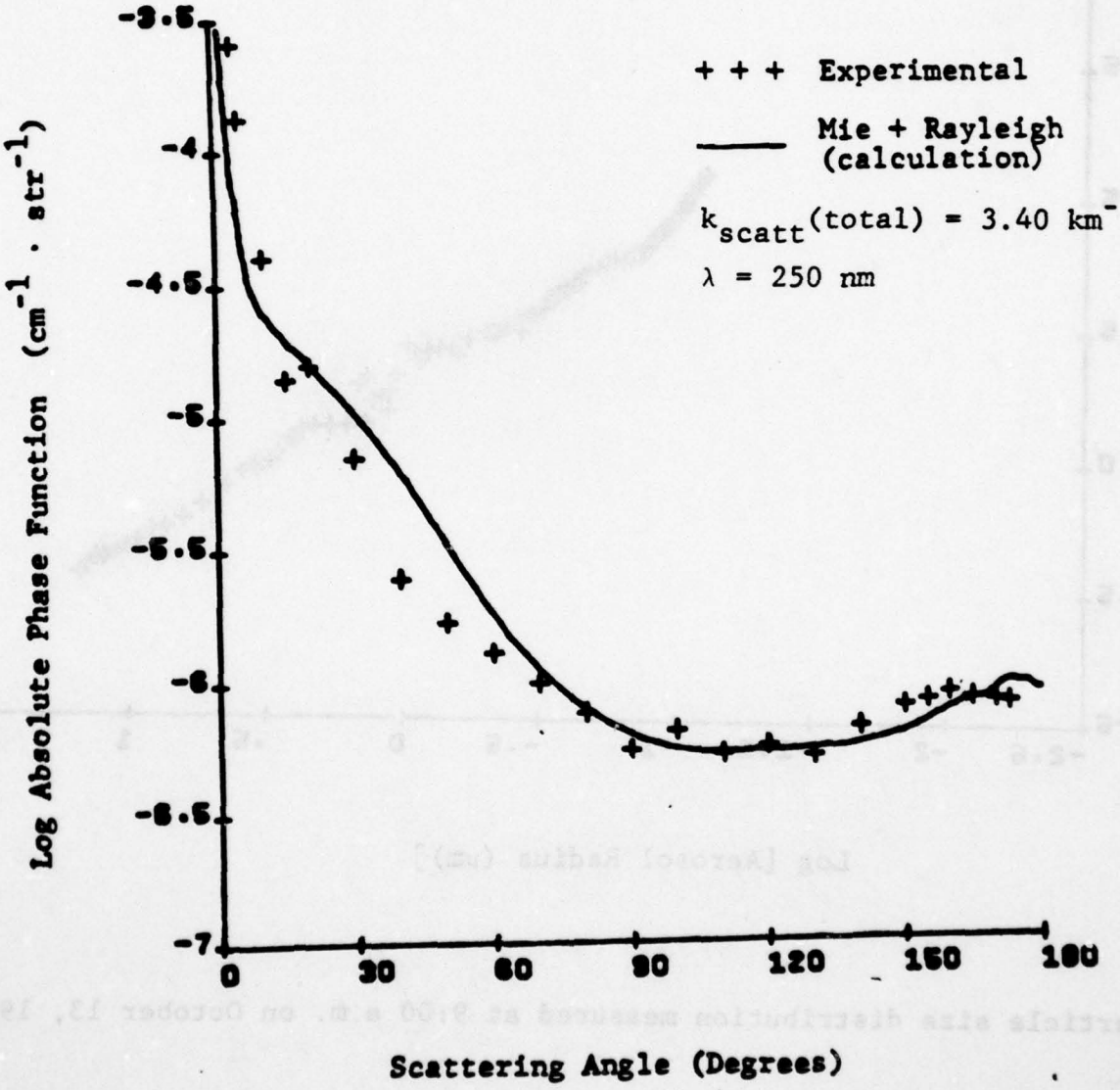

Phase function measured on October 13, 1978 at 8:45 a.m.

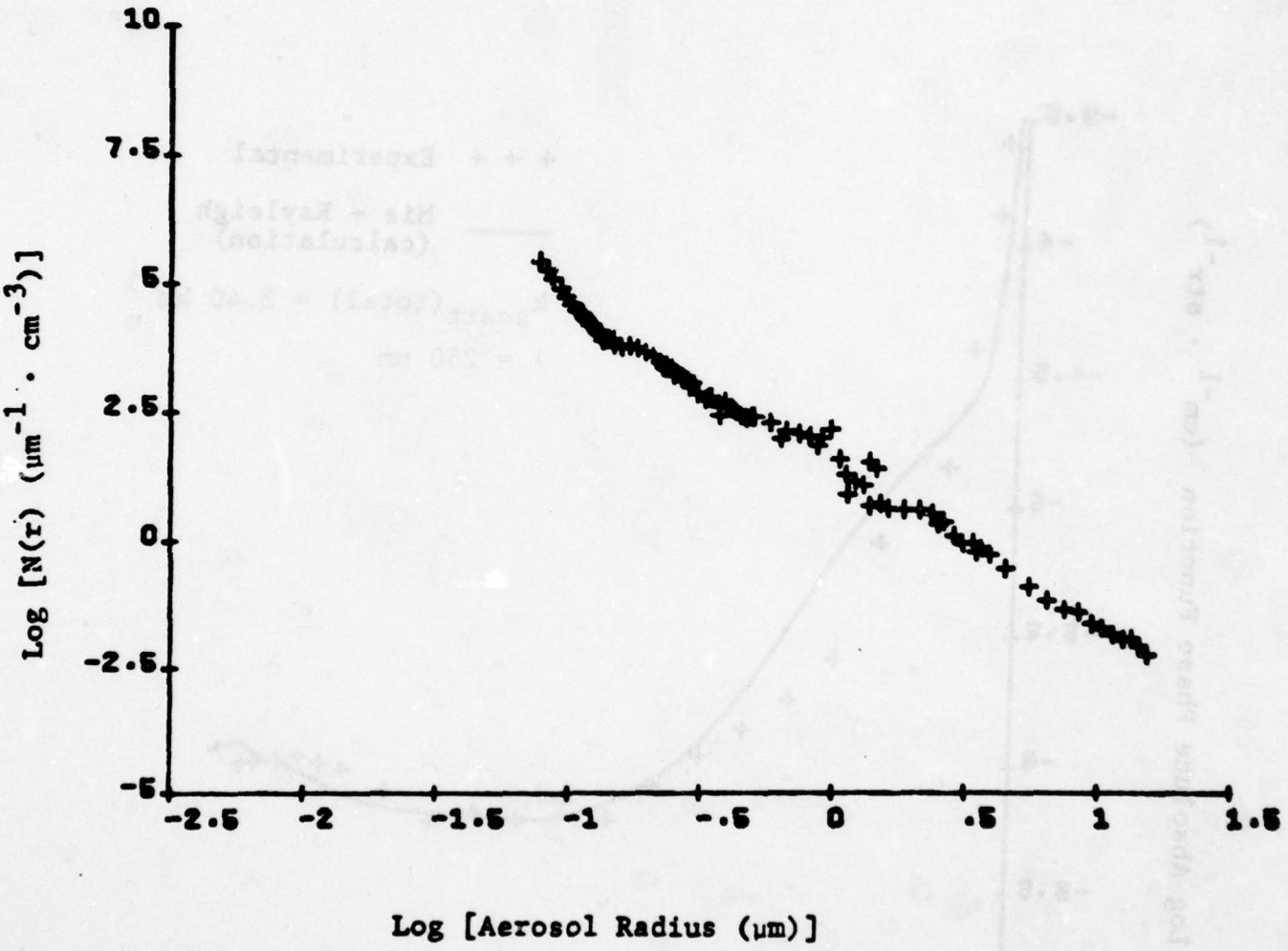

Particle size distribution measured at 9:00 a.m. on October 13, 1978.

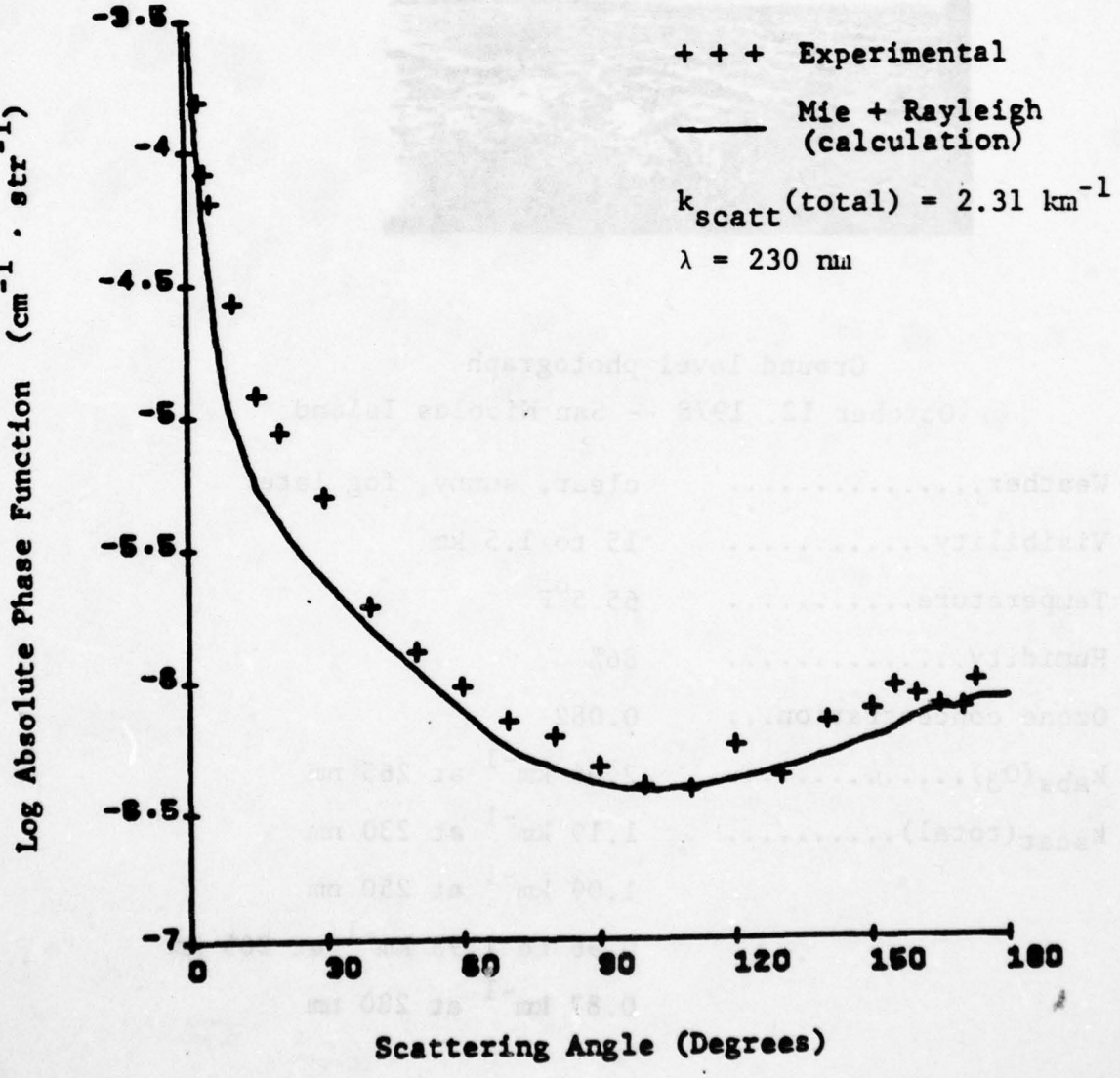

Phase function measured on October 13, 1978 at 9:00 a.m.

Ground level photograph
October 12, 1978 -- San Nicolas Island

Weather.....	clear, sunny, fog later
Visibility.....	15 to 1.5 km
Temperature.....	65.5°F
Humidity.....	86%
Ozone concentration...	0.082
$k_{abs}(O_3)$.....	2.06 km^{-1} at 265 nm
k_{scat}(total).....	1.19 km^{-1} at 230 nm
	1.09 km^{-1} at 250 nm
	0.96 to 1.98 km^{-1} at 265 nm
	0.87 km^{-1} at 280 nm

AD-A066 160 AERONAUTICAL RESEARCH ASSOCIATES OF PRINCETON INC N J F/G 4/1
SEASONAL VARIATIONS IN ULTRAVIOLET SINGLE SCATTERING PHASE FUNC--ETC(U)
FEB 79 J M SCHLUPF, C R DICKSON, M E NEER N00014-76-C-1094

UNCLASSIFIED ARAP-383 NL

3 OF 3
ADA
066160

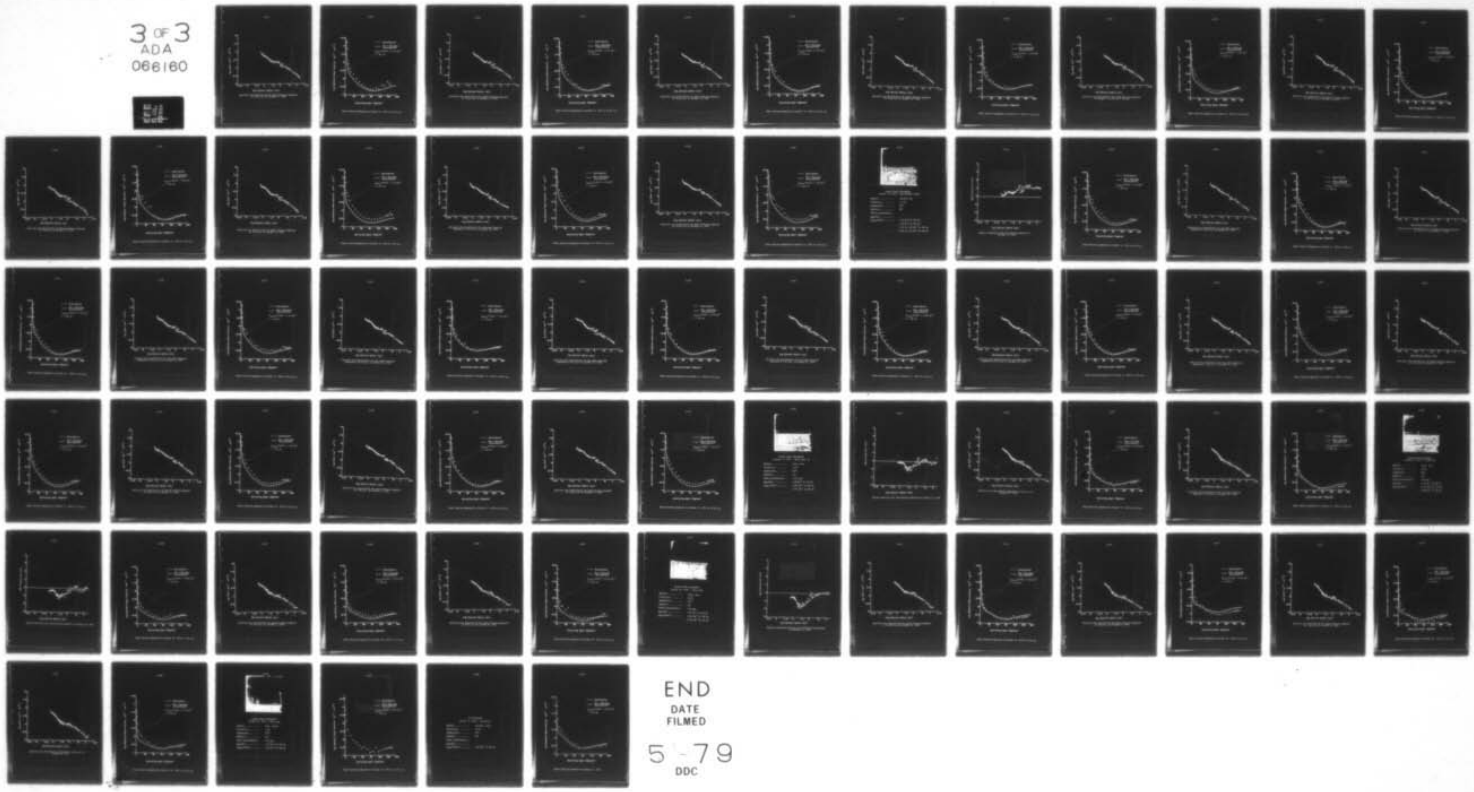

END
DATE
FILMED
5-79
DDC

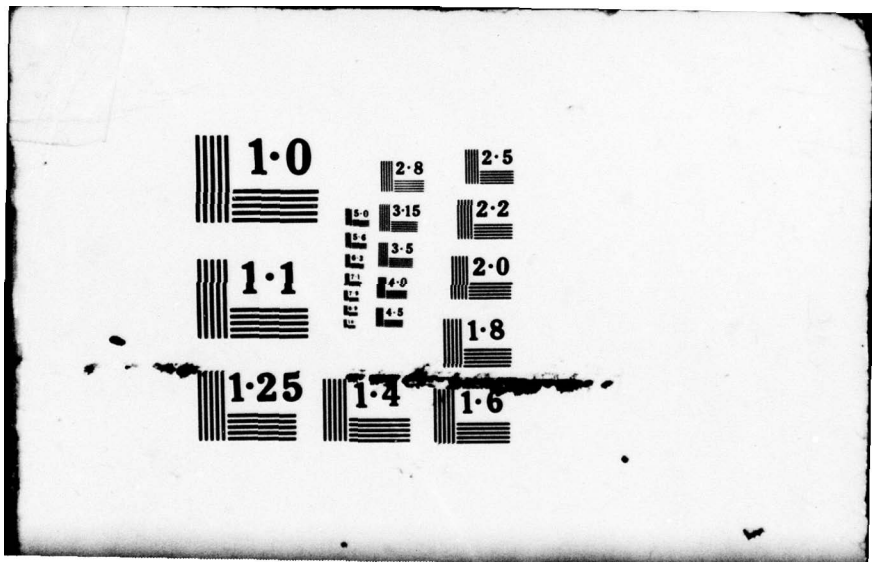
1·0
1·1
1·25
2·8
3·15
3·5
4·0
4·5
2·5
2·2
2·0
1·8
1·4
1·6

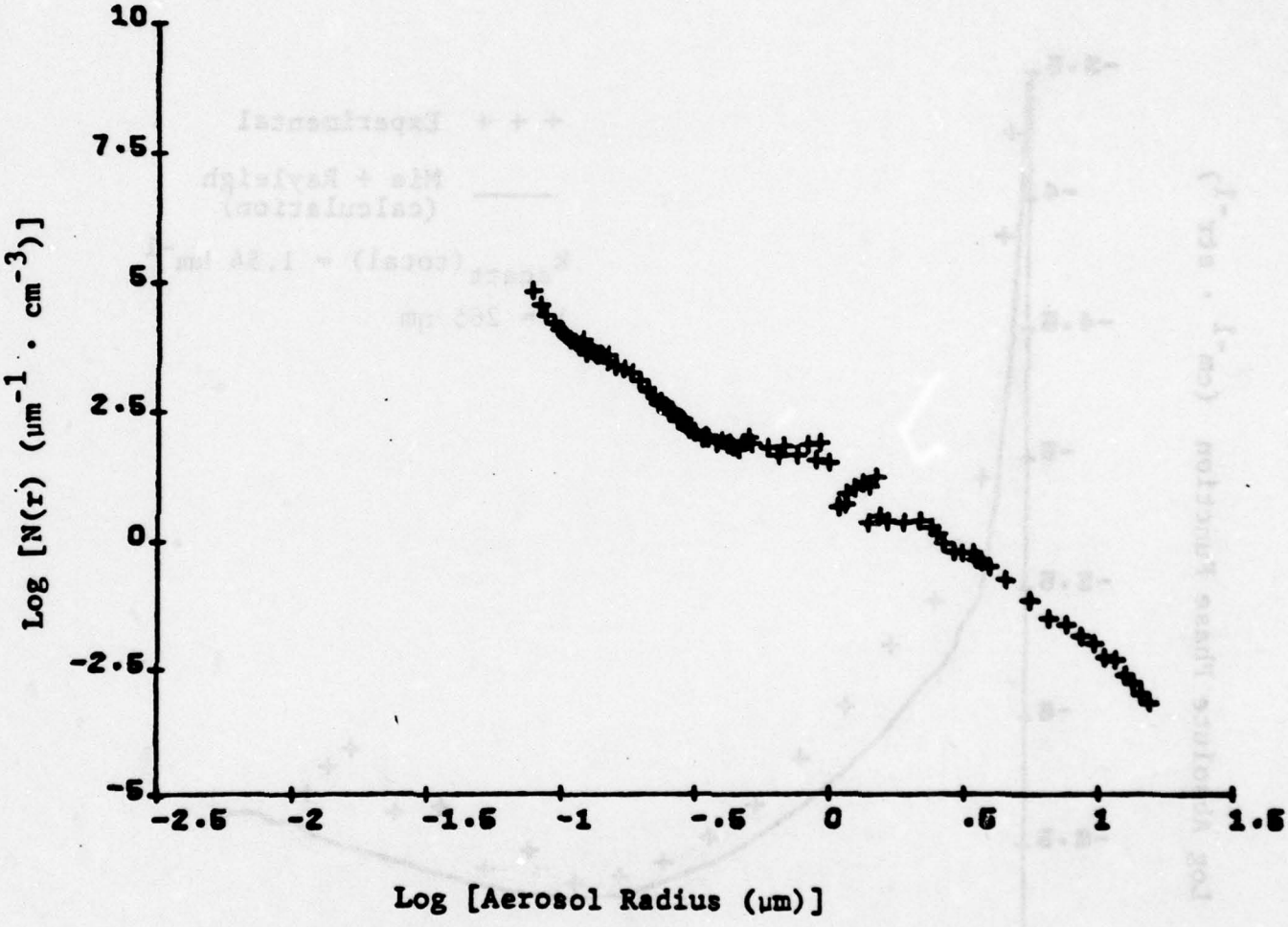

Particle size distribution for phase function measured at 9:05 a.m. on October 12, 1978.

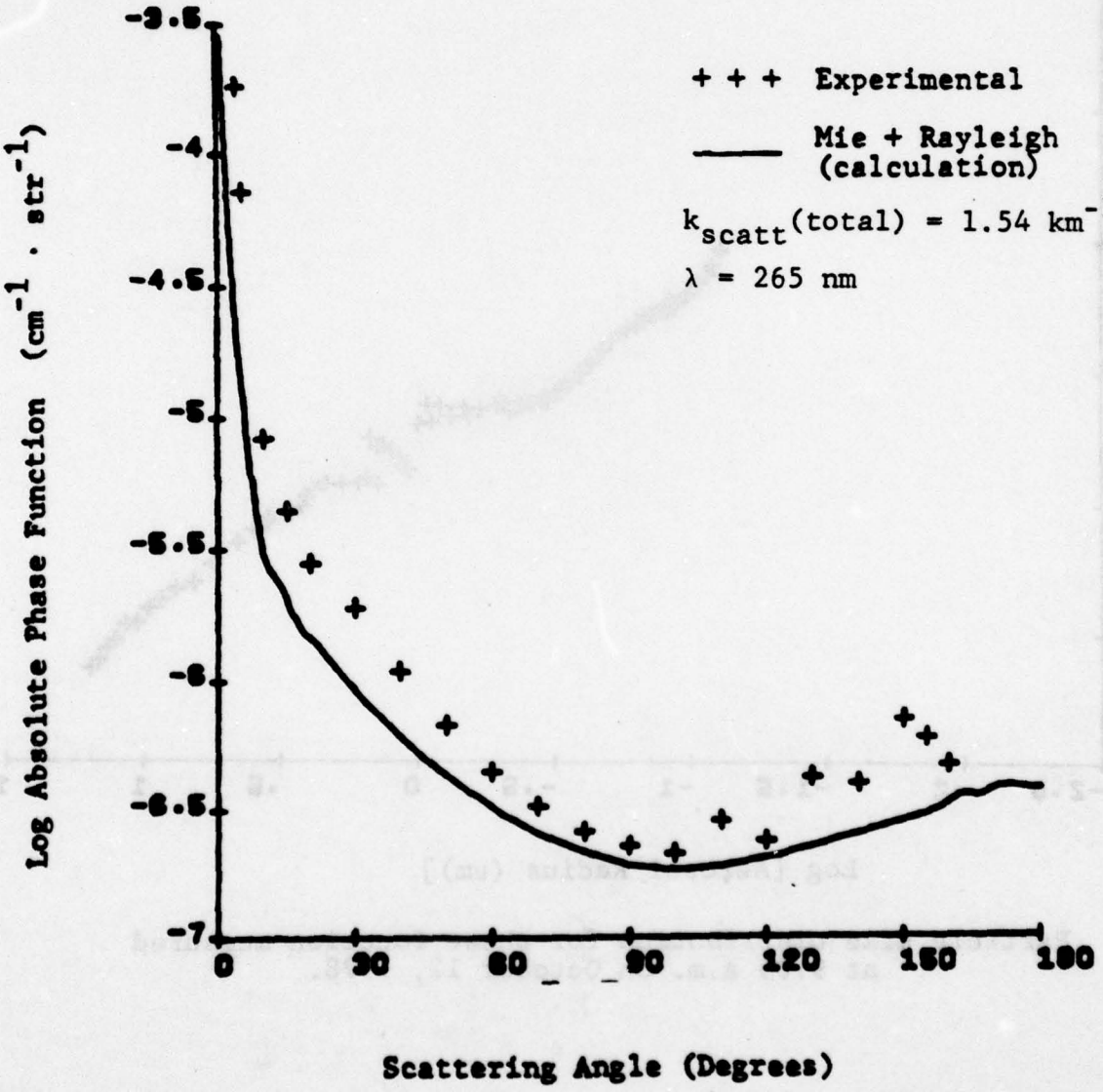

Phase function measured on October 12, 1978 at 9:05 a.m.

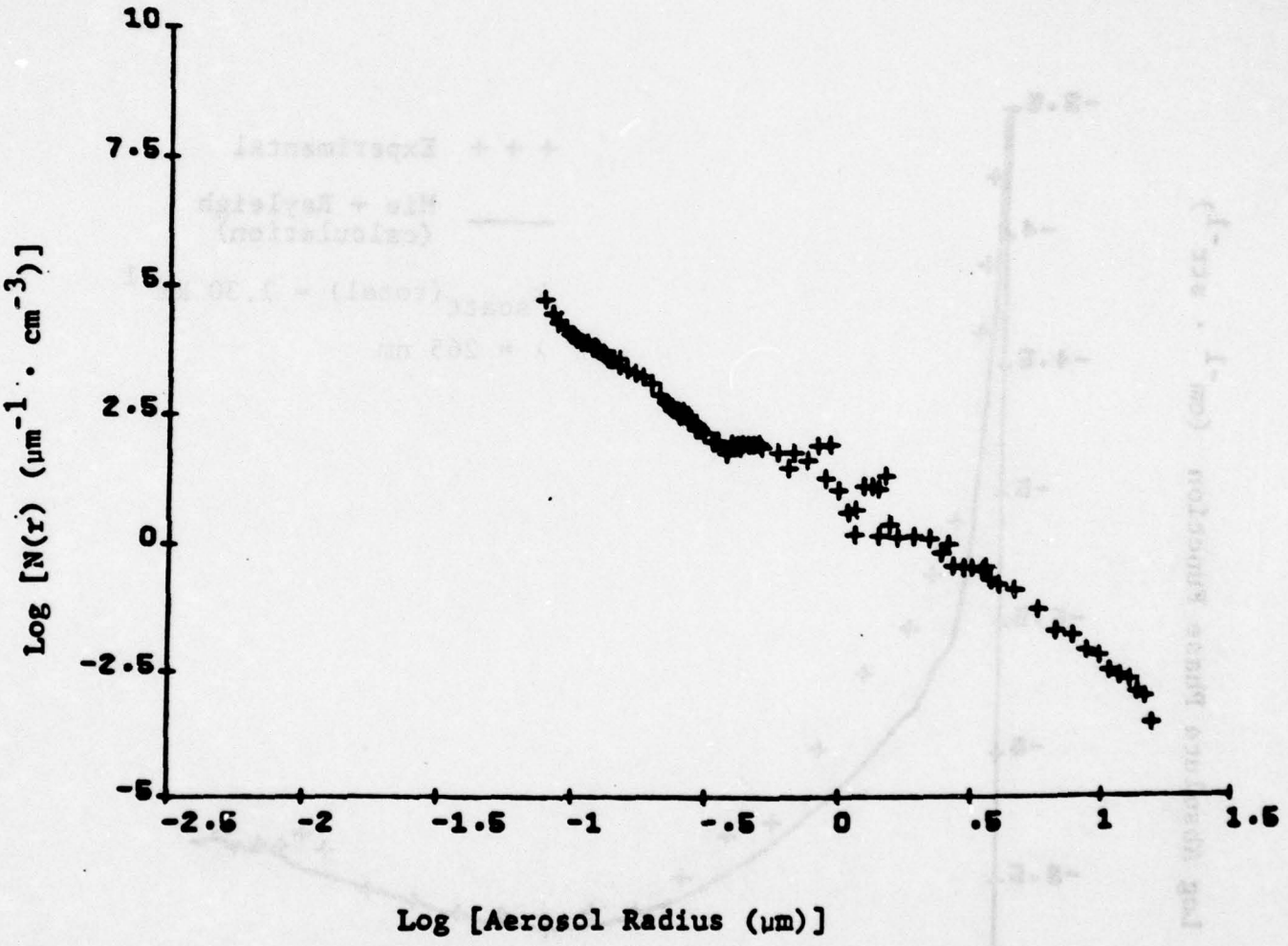

Particle size distribution for phase function measured at 10:00 a.m. on October 12, 1978.

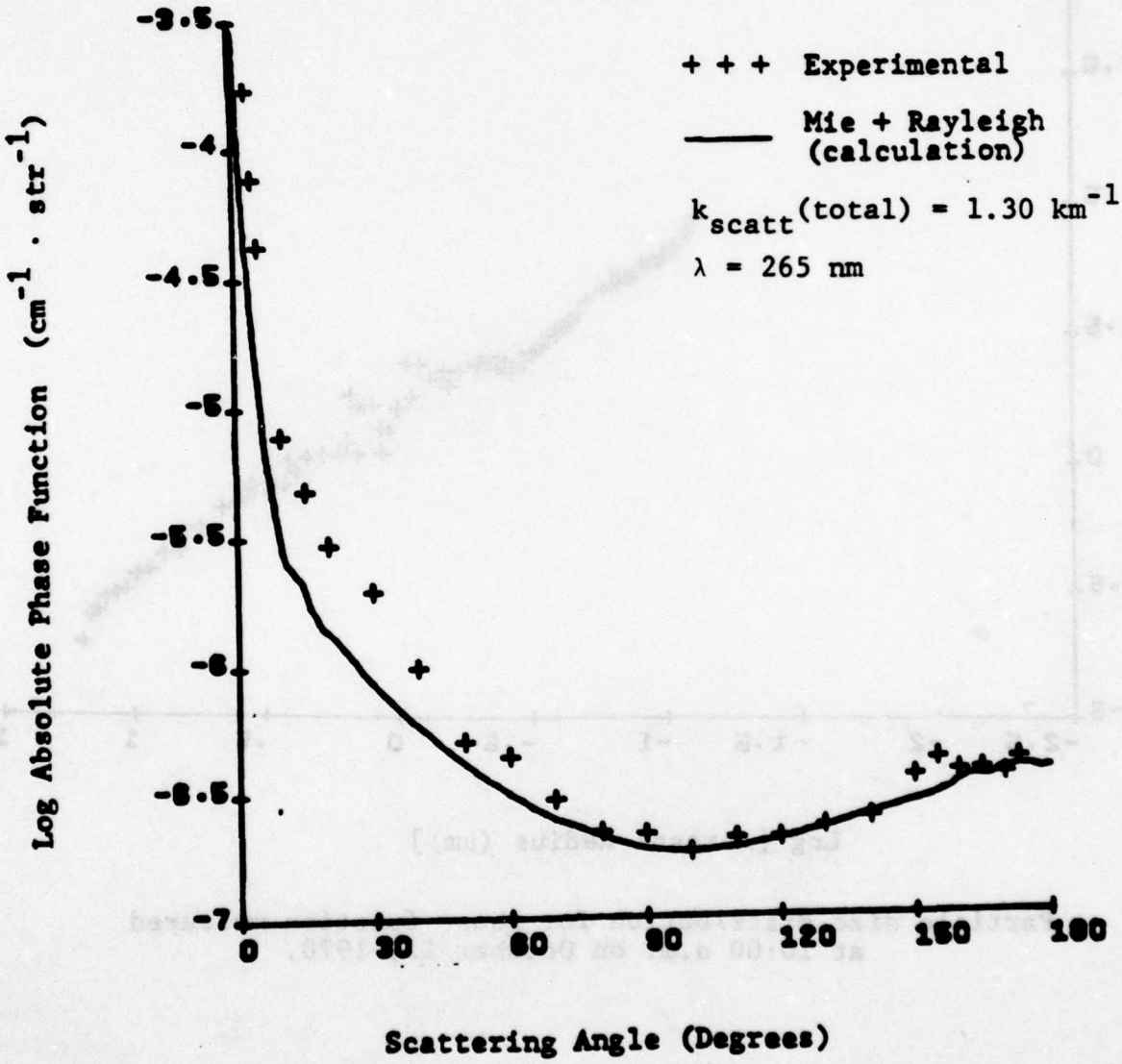

Phase function measured on October 12, 1978 at 10:00 a.m.

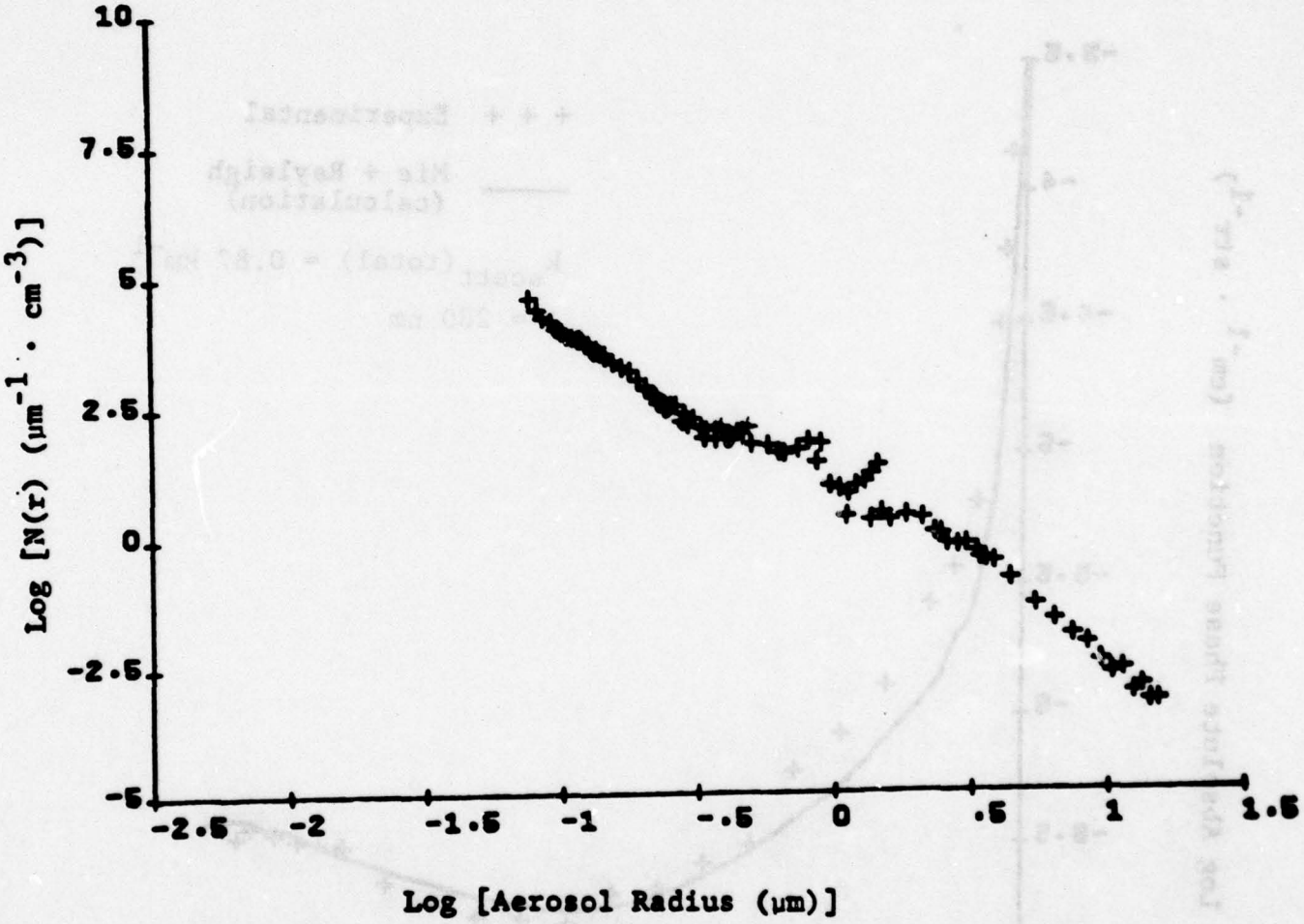

Particle size distribution for phase function measured at 10:40 a.m. on October 12, 1978.

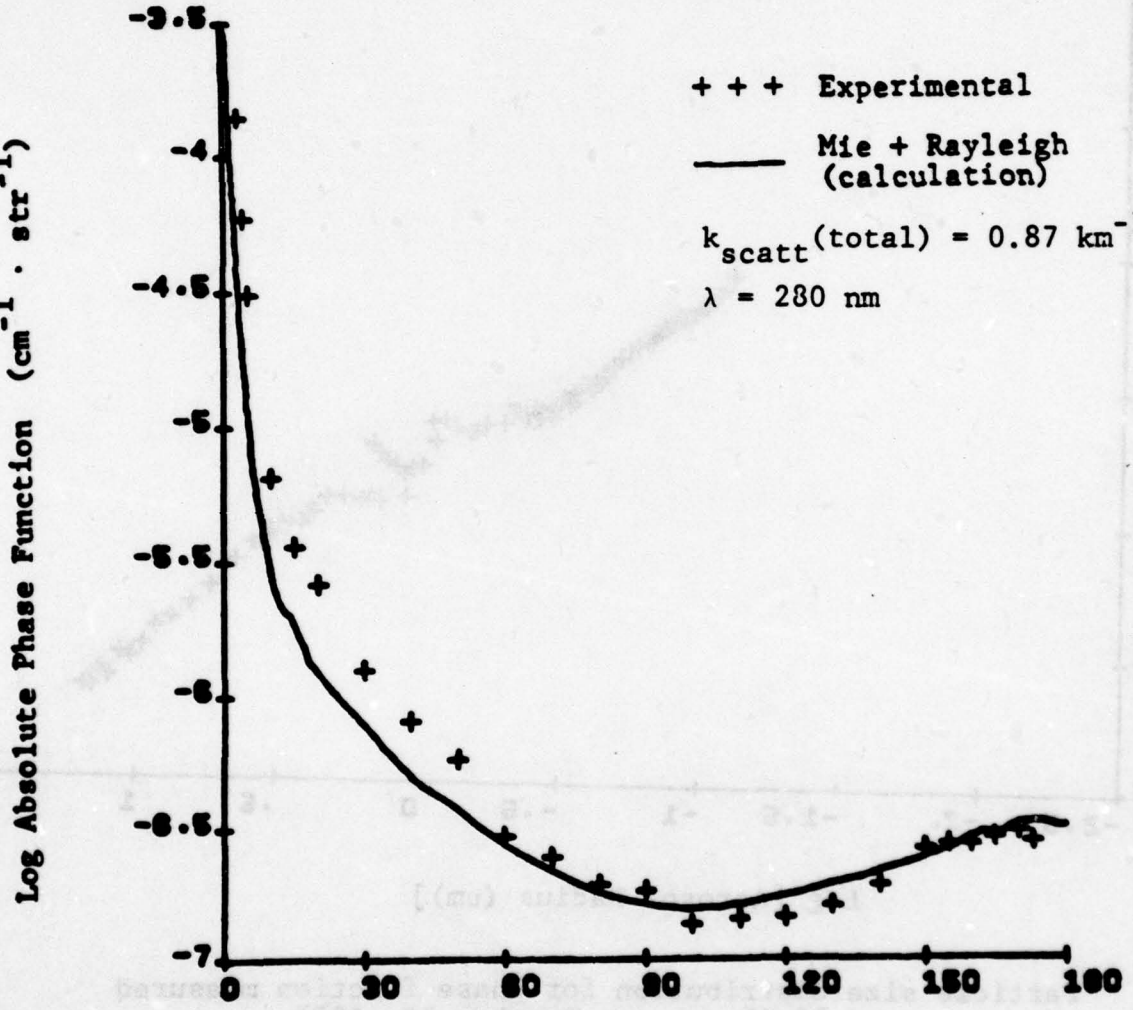

Phase function measured on October 12, 1978 at 10:40 a.m.

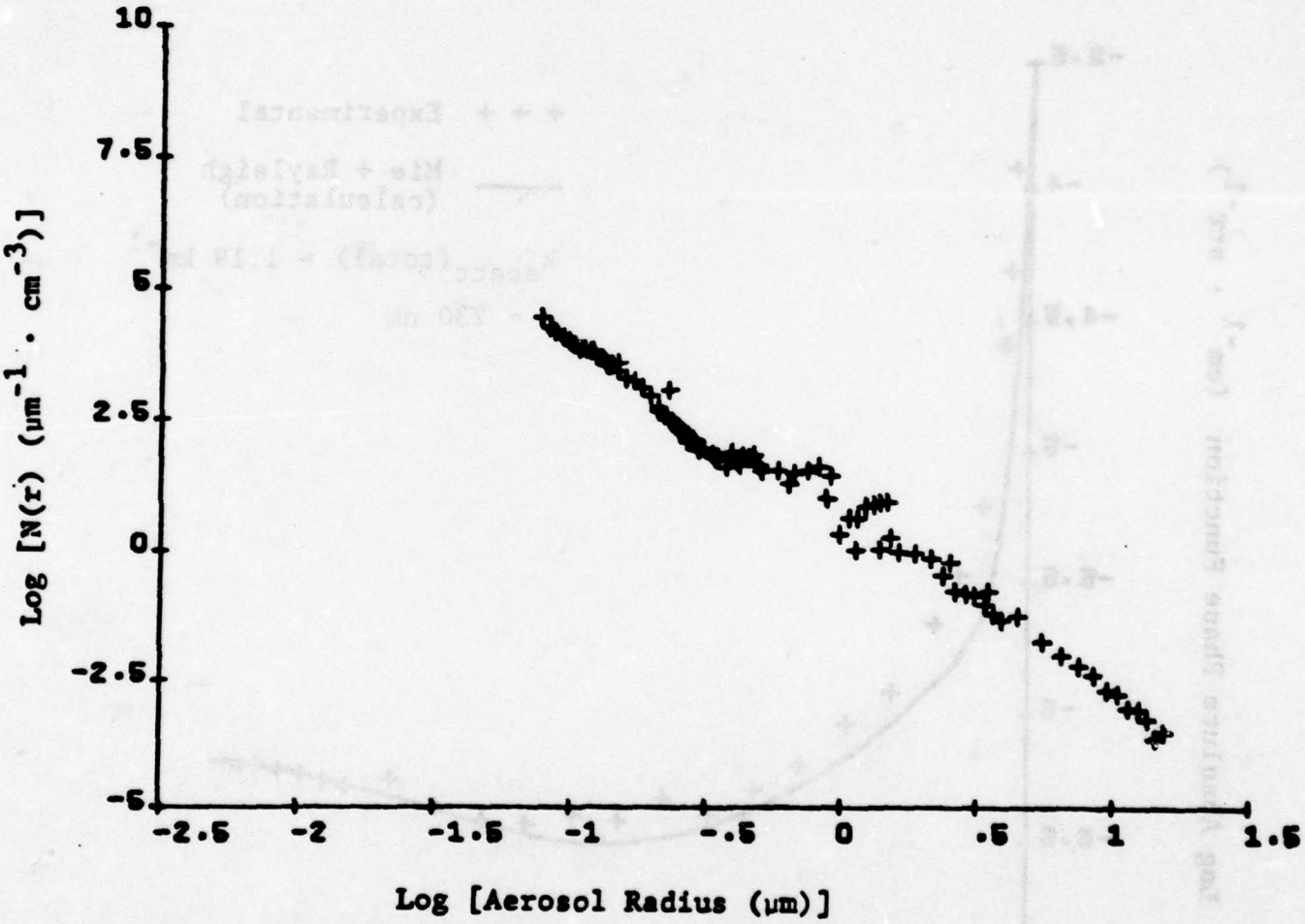

Particle size distribution for phase function measured at 11:30 a.m. on October 12, 1978.

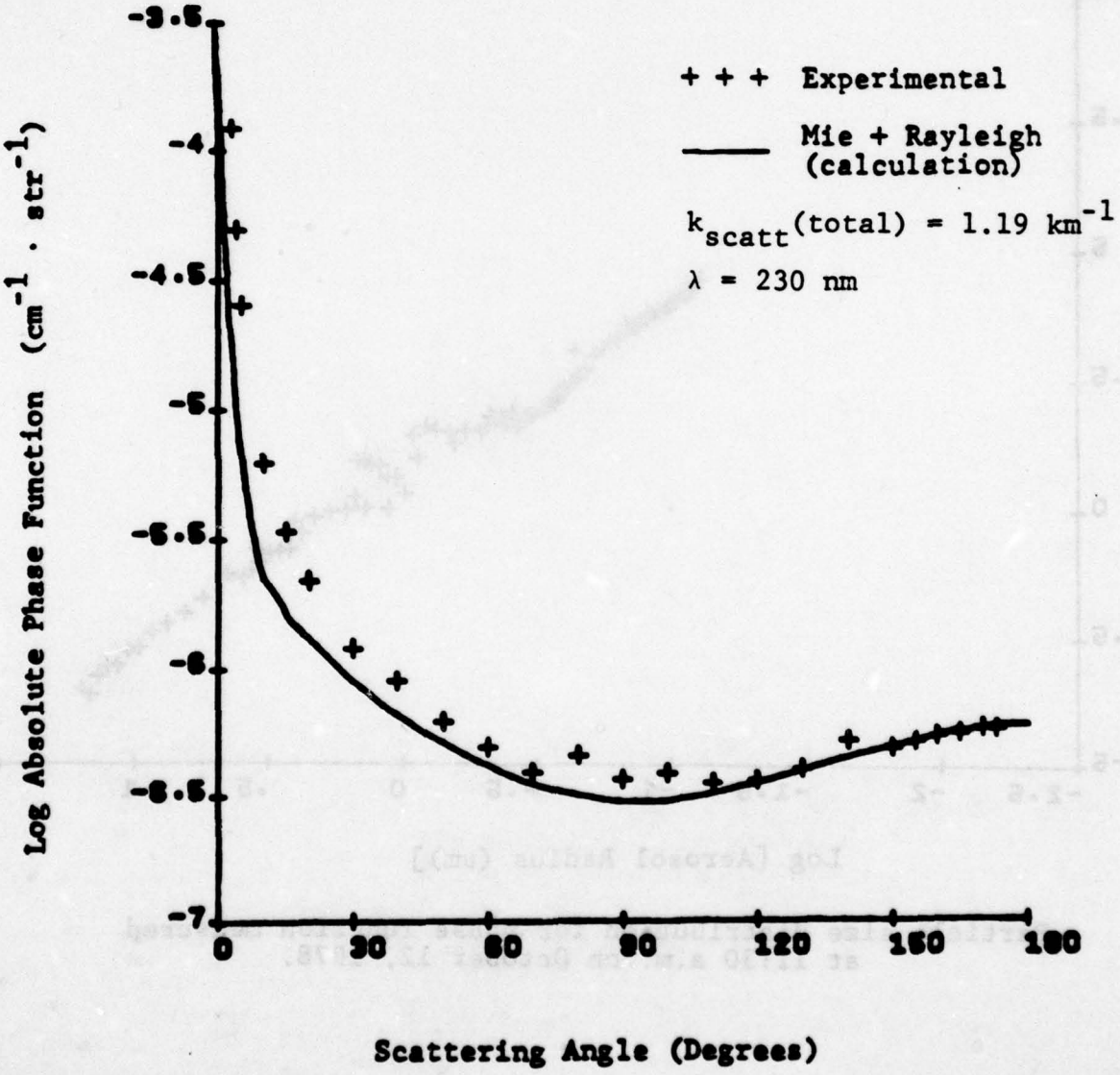

Phase function measured on October 12, 1978 at 11:30 a.m.

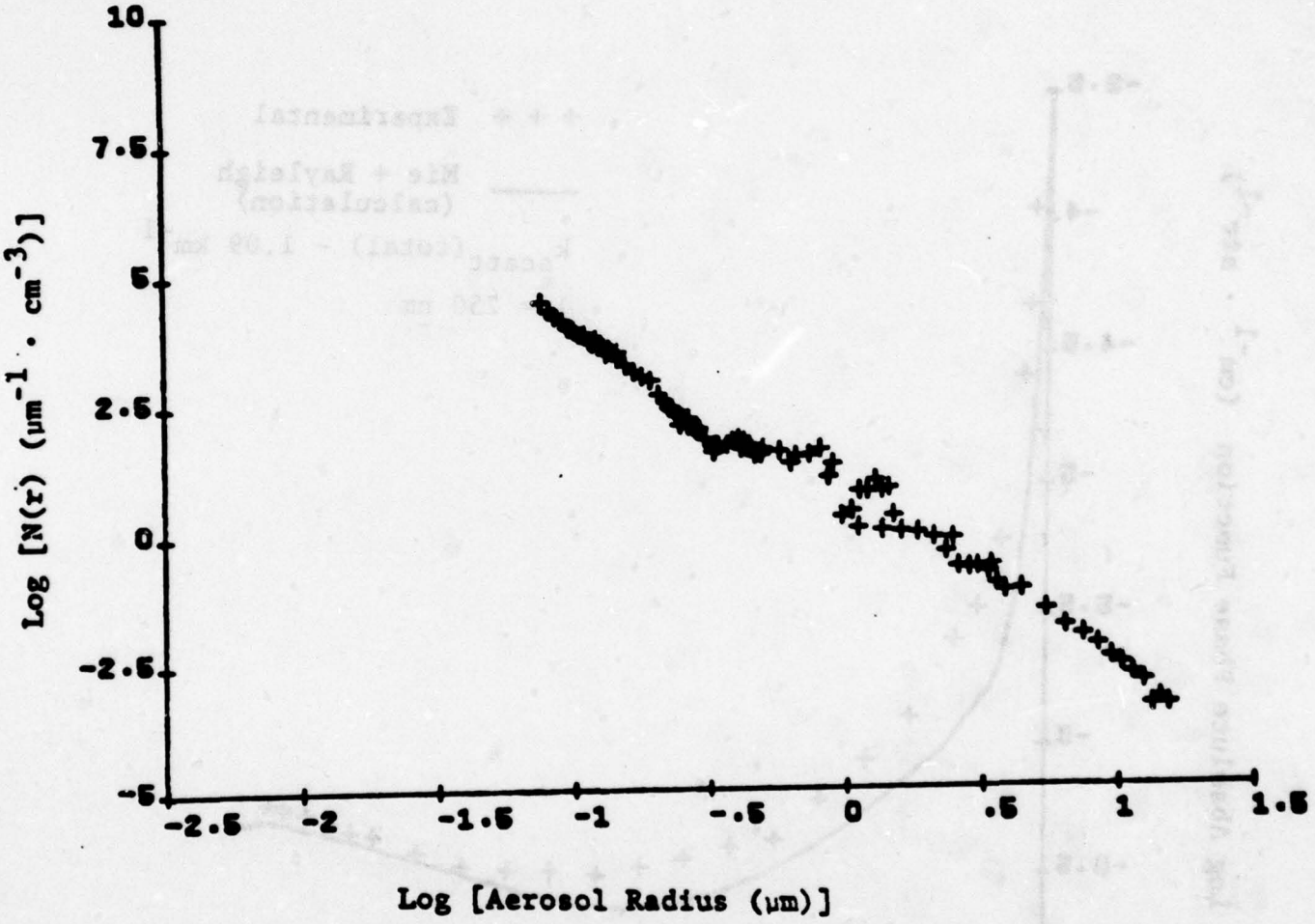

Particle size distribution for phase function measured on October 12, 1978 at 12:00 noon.

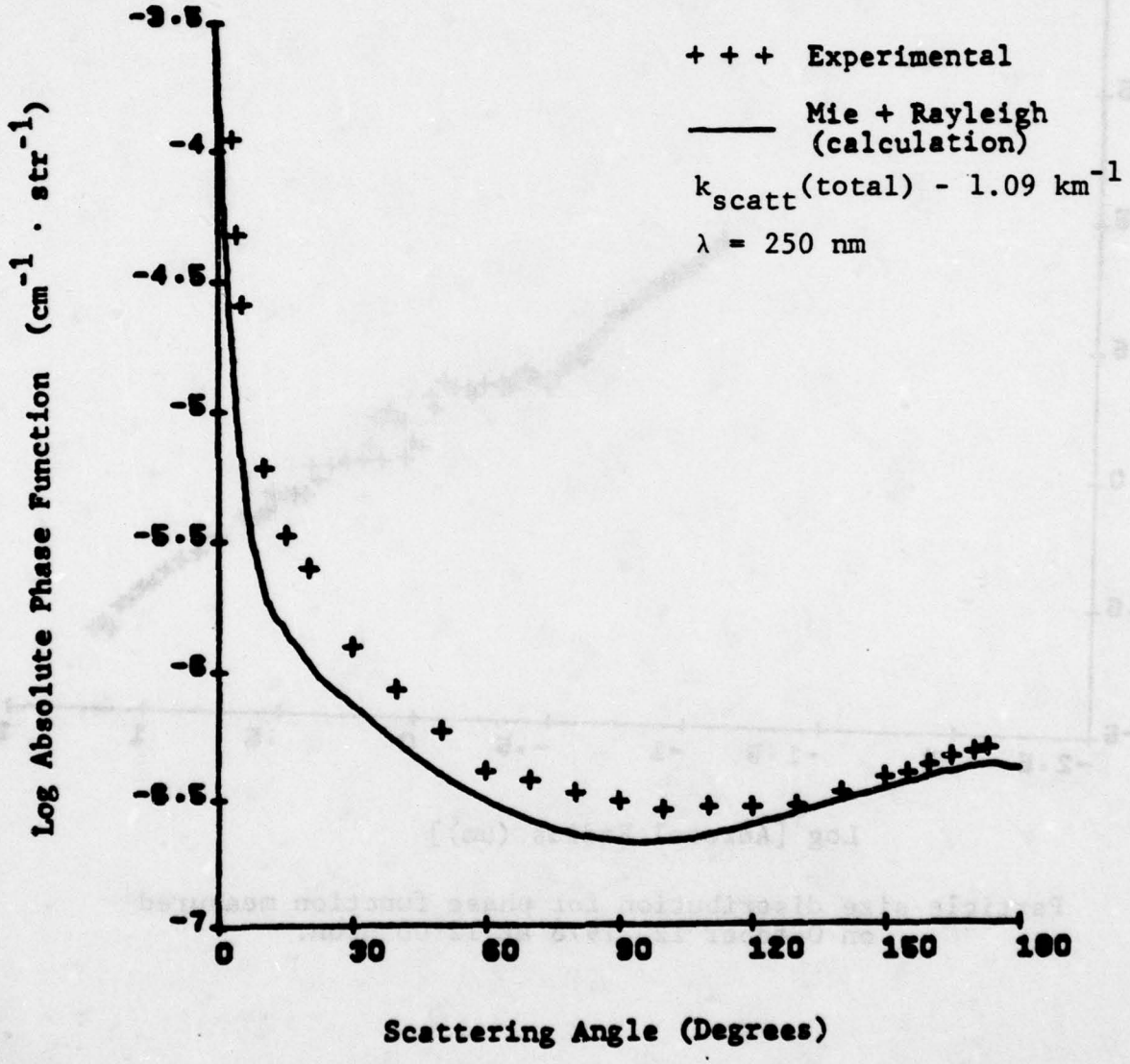

Phase function measured on October 12, 1978 at 12:00 noon.

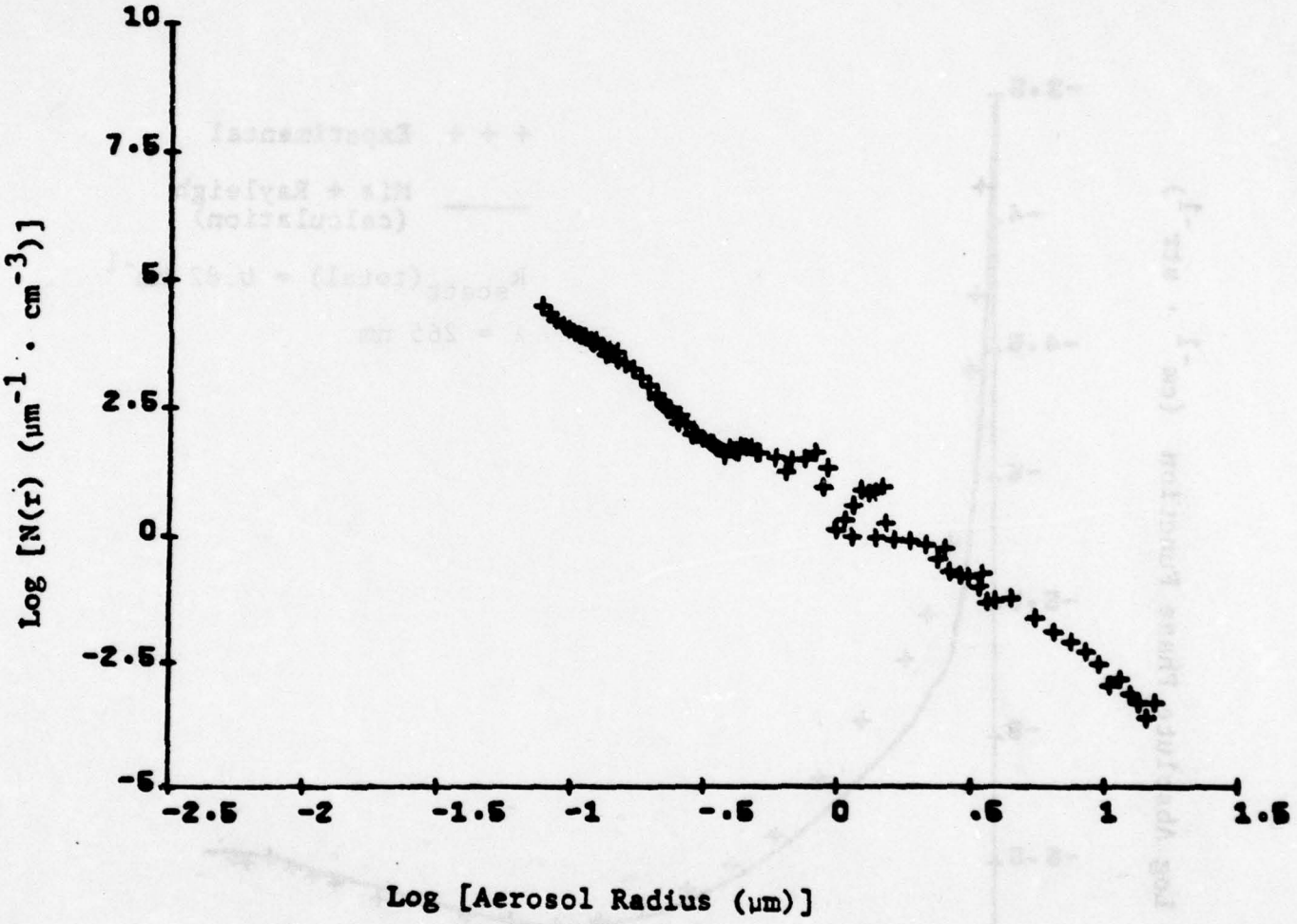

Particle size distribution for phase function measured at 12:35 p.m. on October 12, 1978.

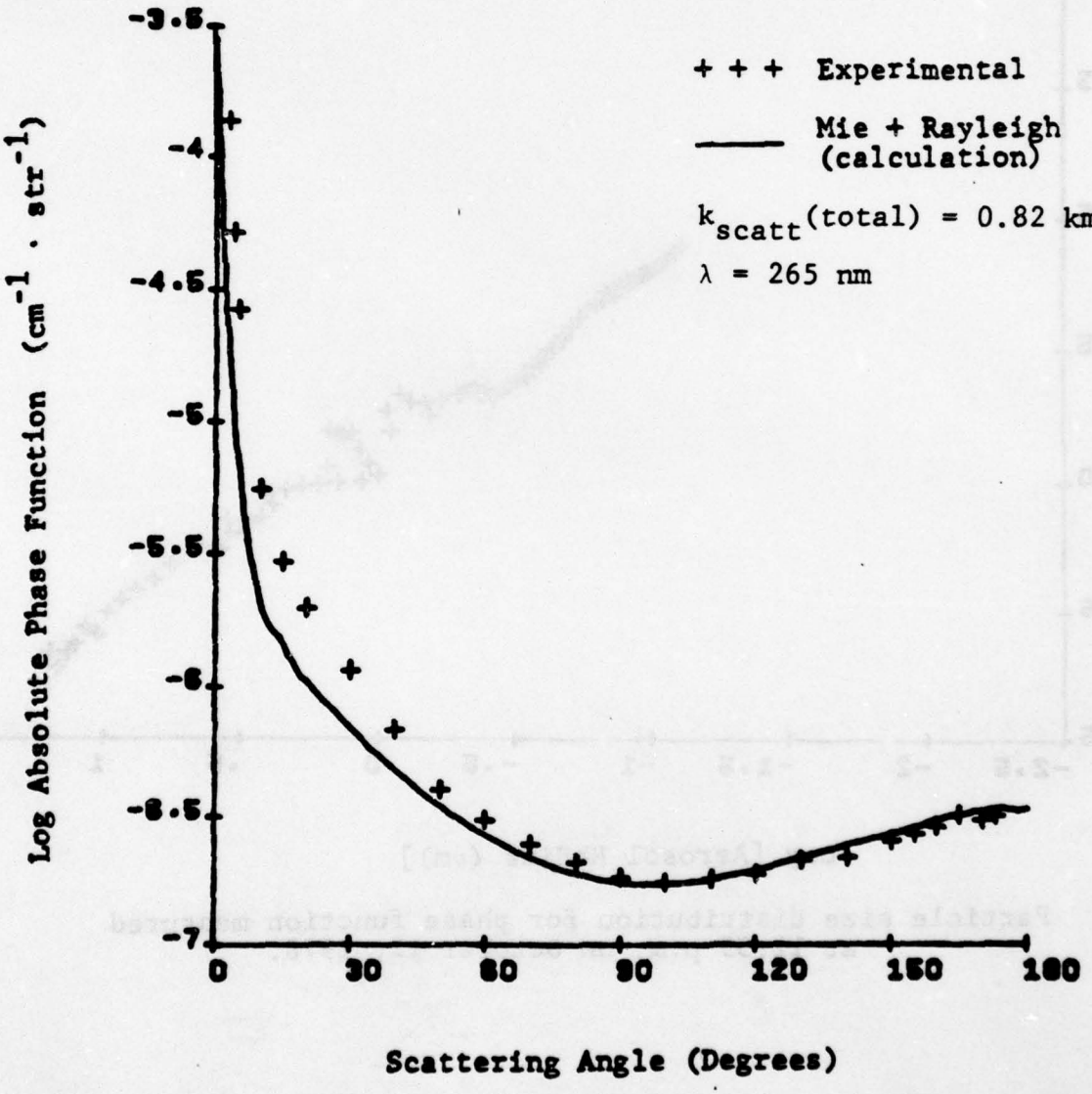

Phase function measured on October 12, 1978 at 12:35 p.m.

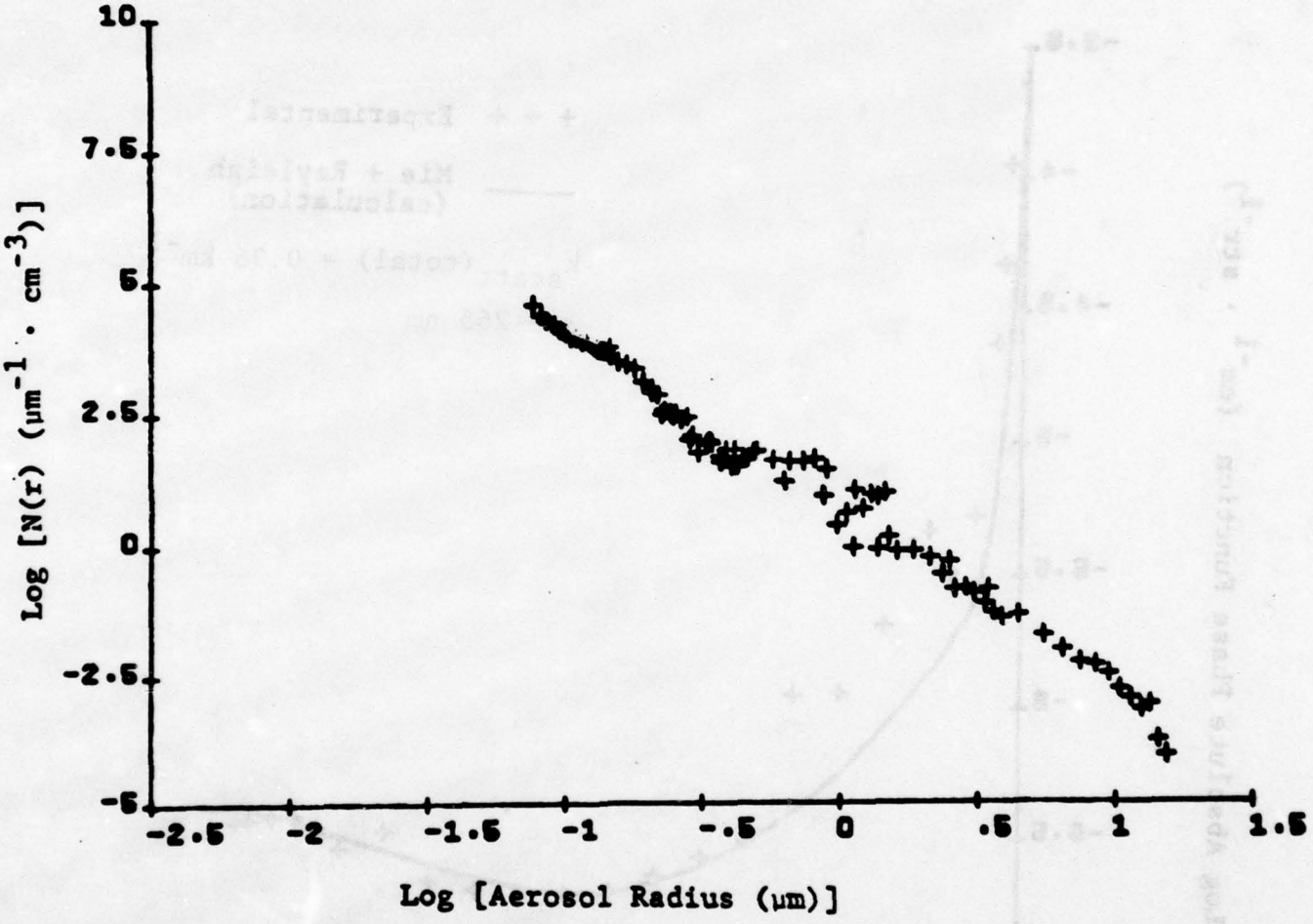

Particle size distribution for phase function measured at 2:30 p.m. on October 12, 1978.

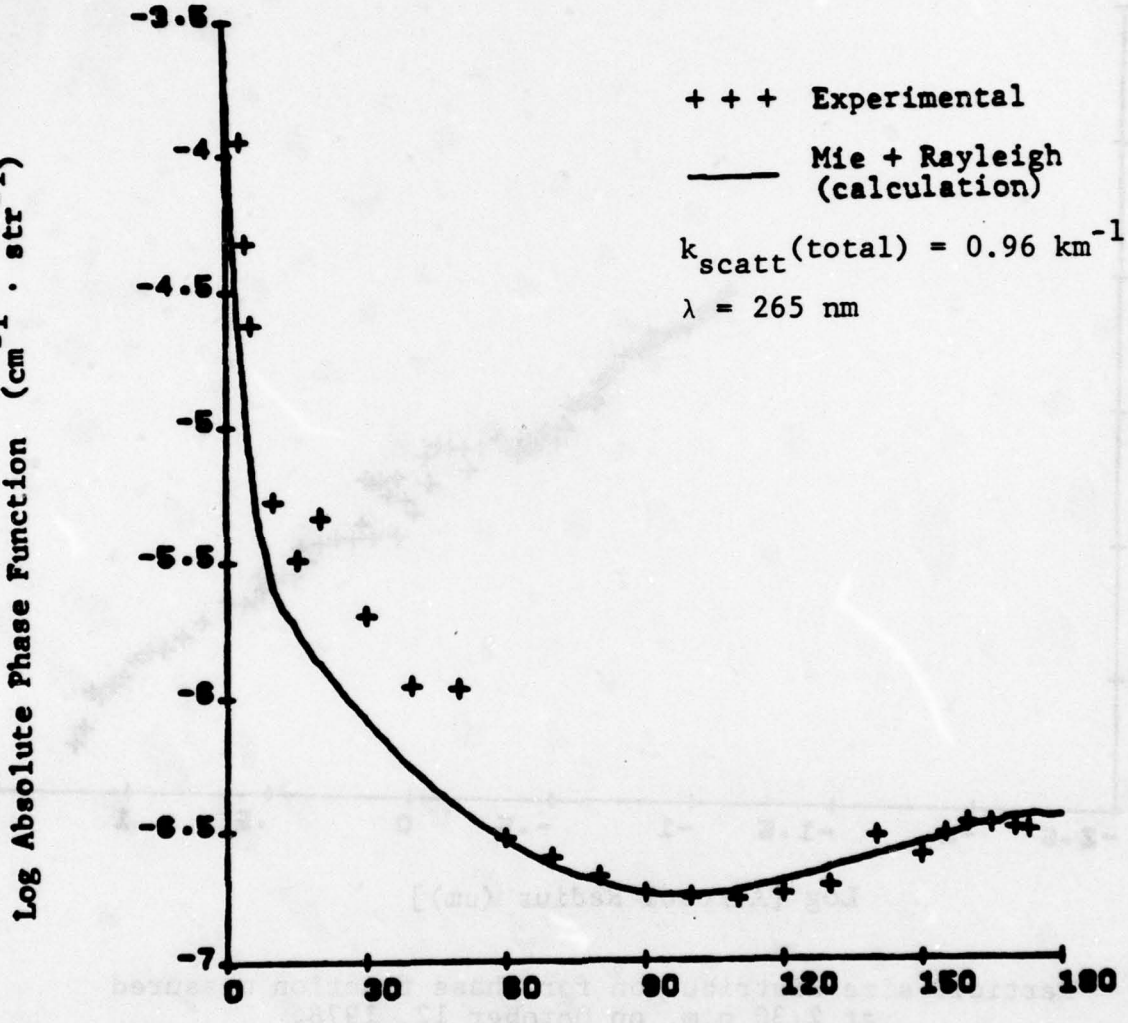

Phase function measured on October 12, 1978 at 2:30 p.m.

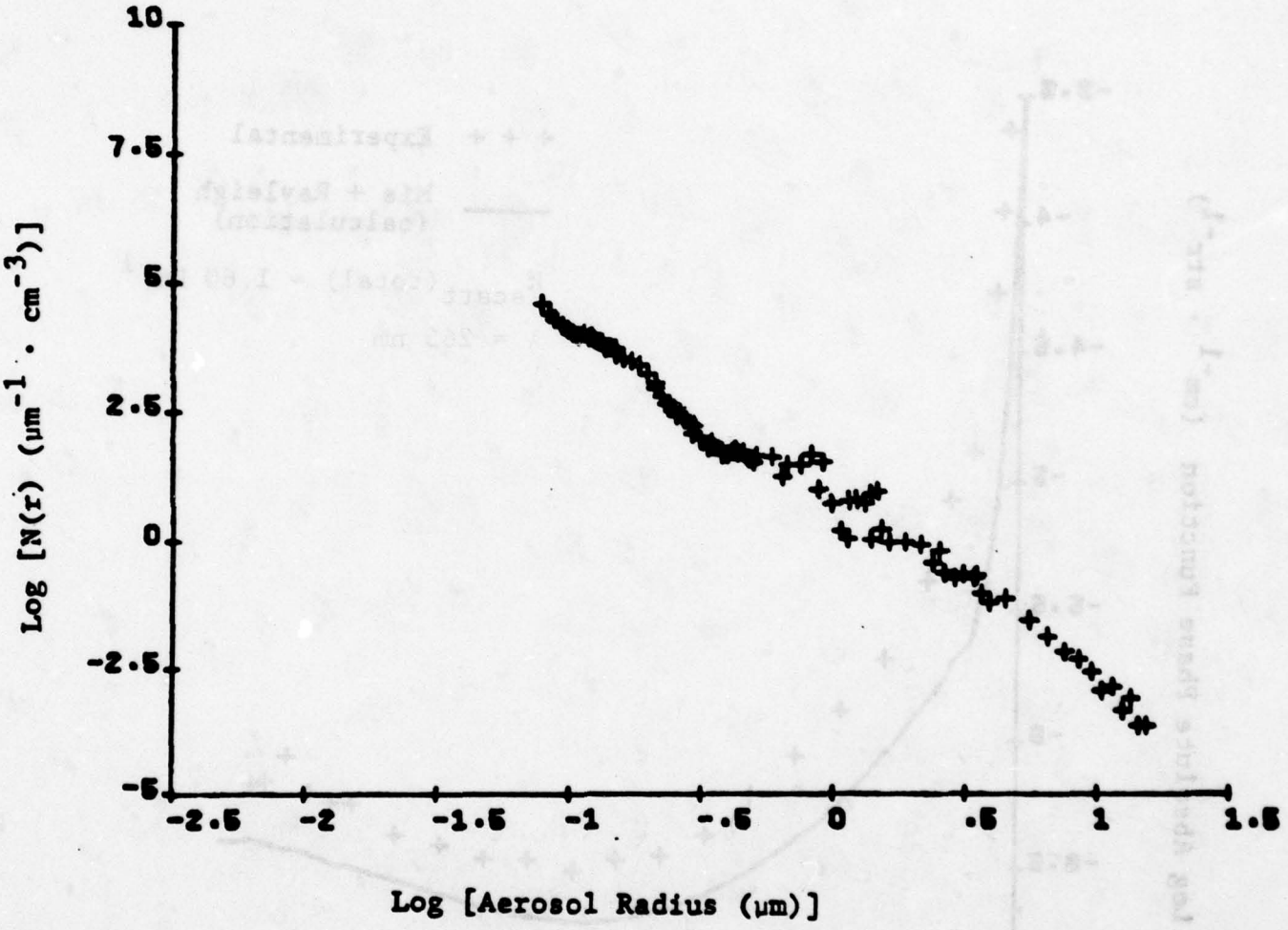

Particle size distribution for phase function measured at 3:25 p.m. on October 12, 1978.

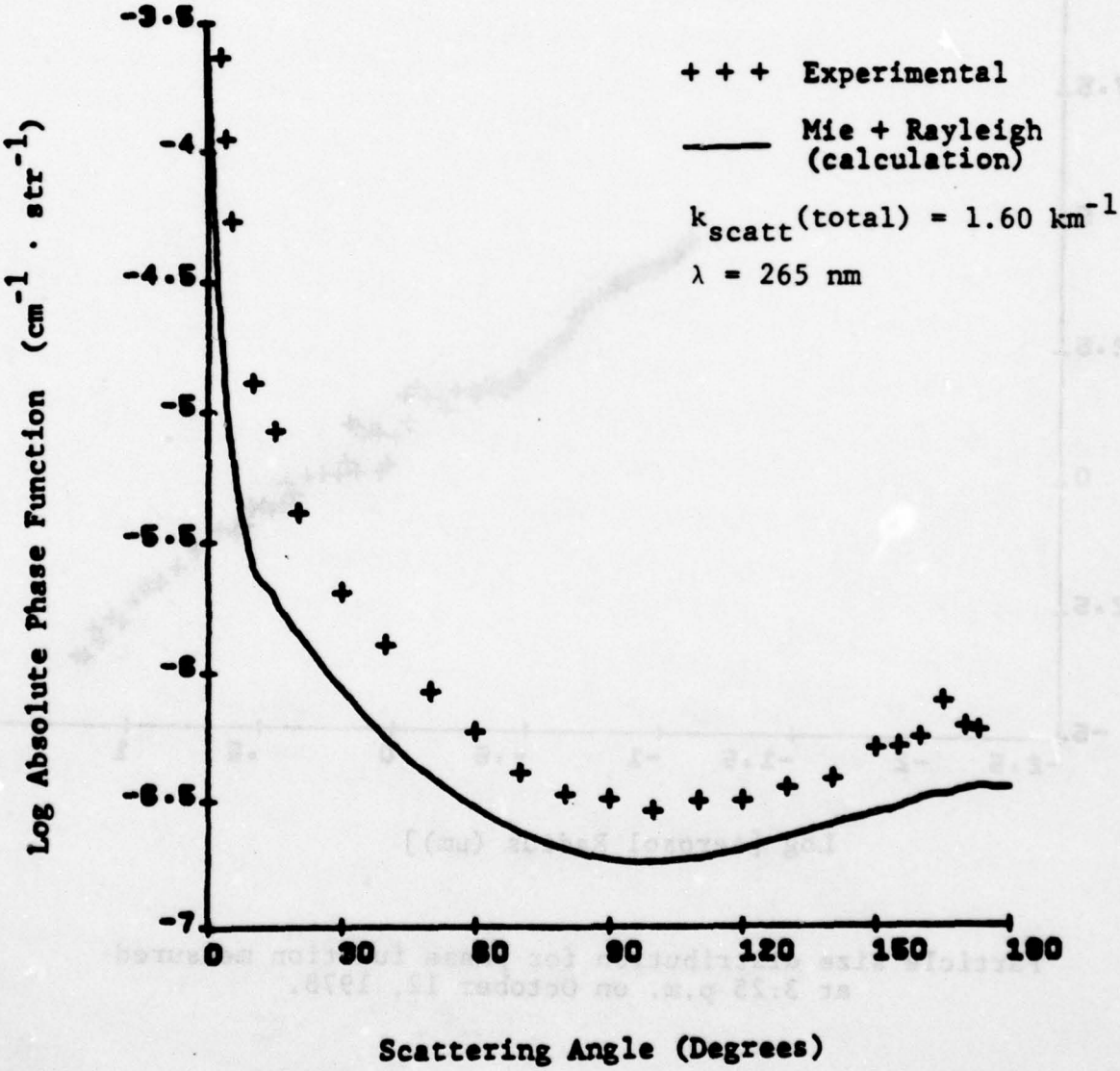

Phase function measured on October 12, 1978 at 3:25 p.m.

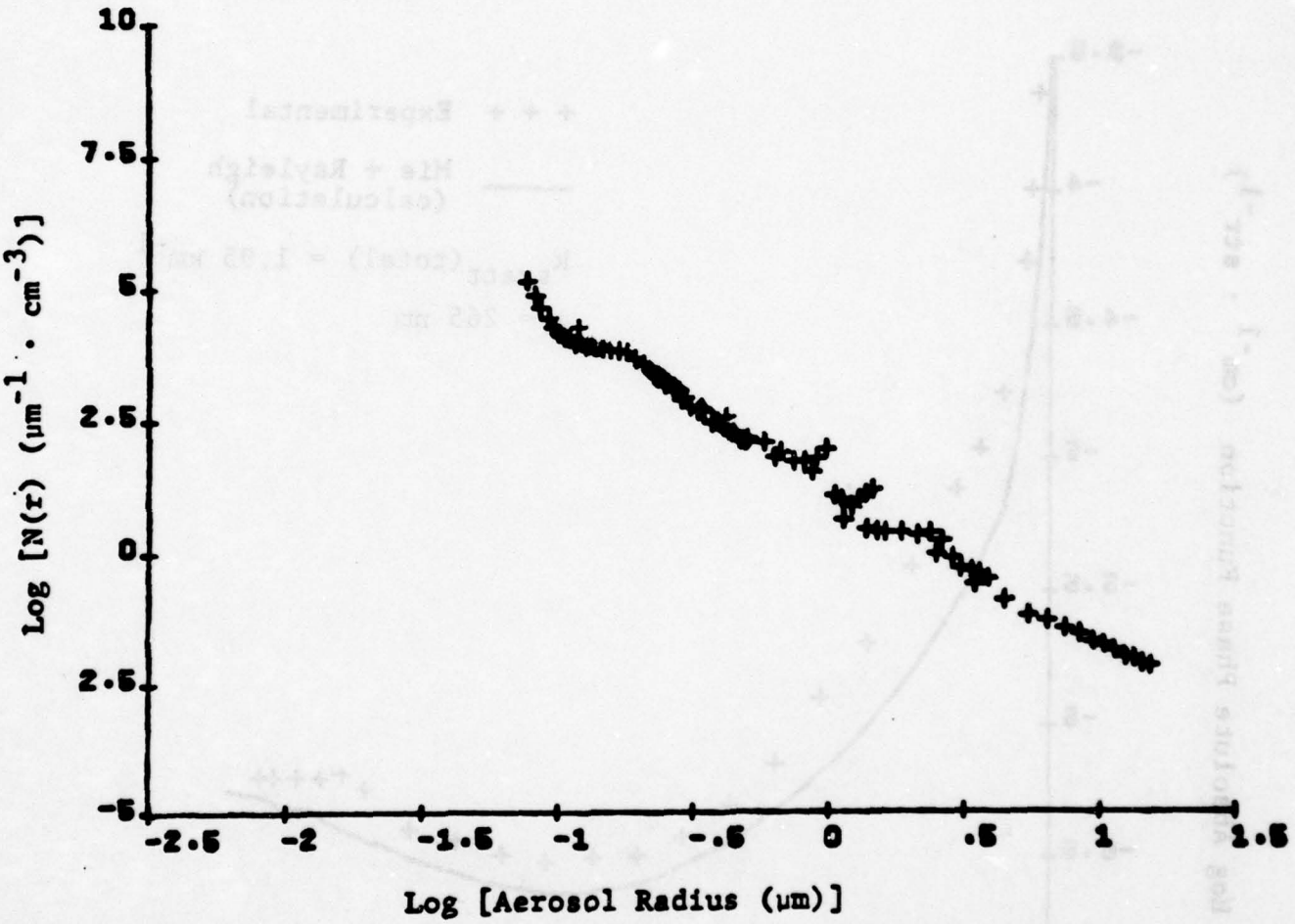

Particle size distribution for the phase function measured at 7:20 p.m. on October 12, 1978.

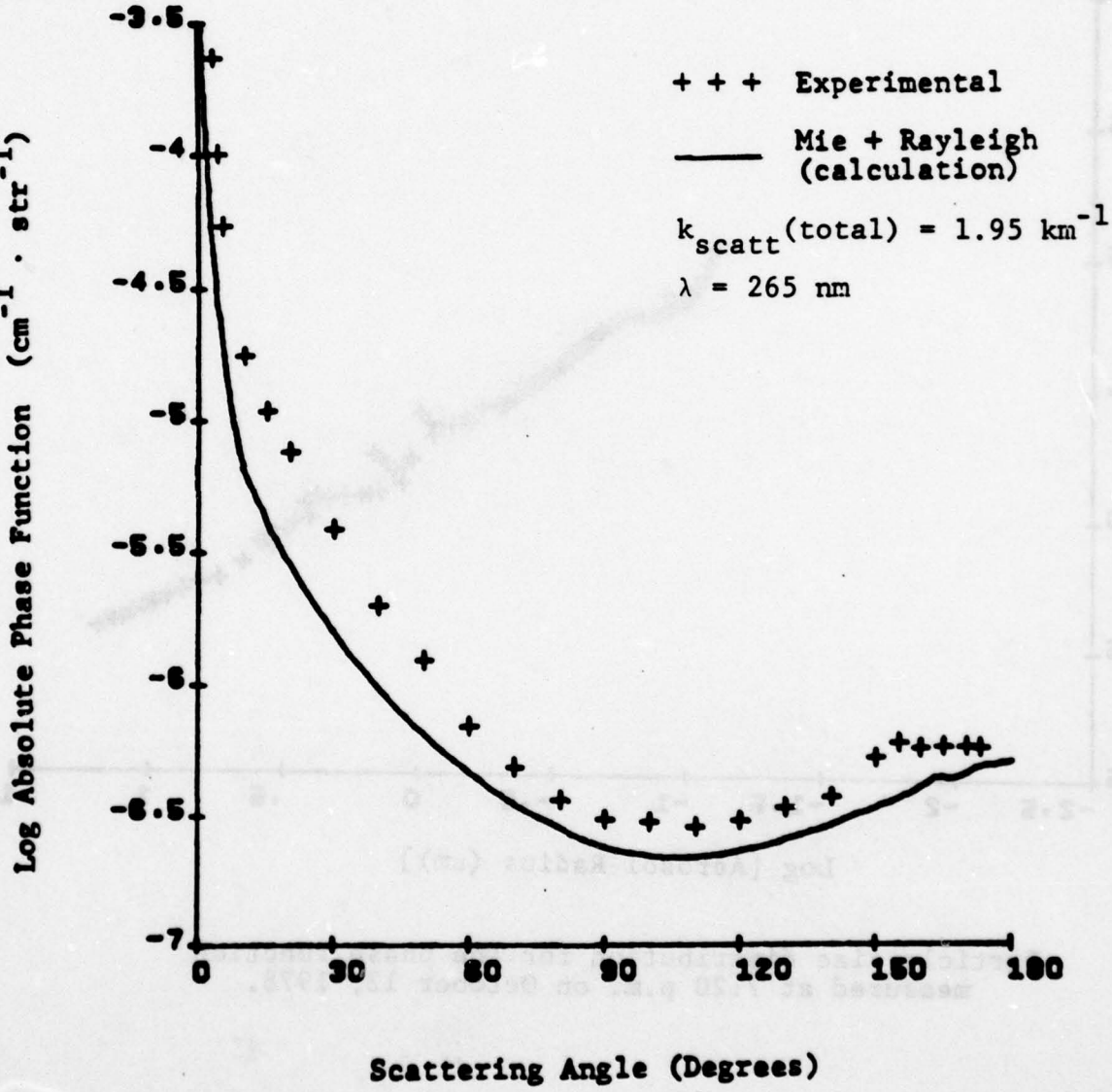

Phase function measured on October 12, 1978 at 7:20 p.m.

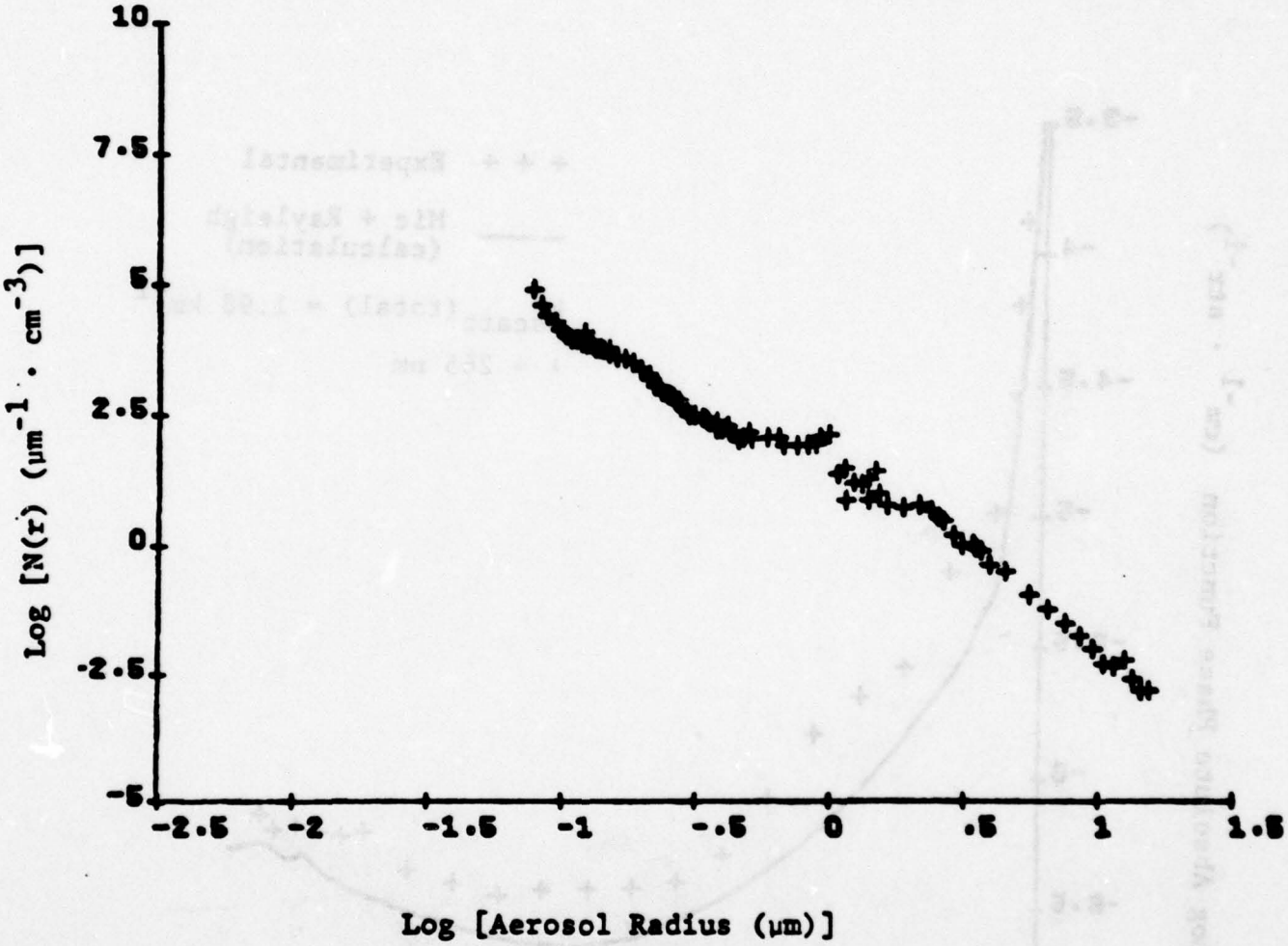

Particle size distribution for phase function measured at 11:00 p.m. on October 12, 1978.

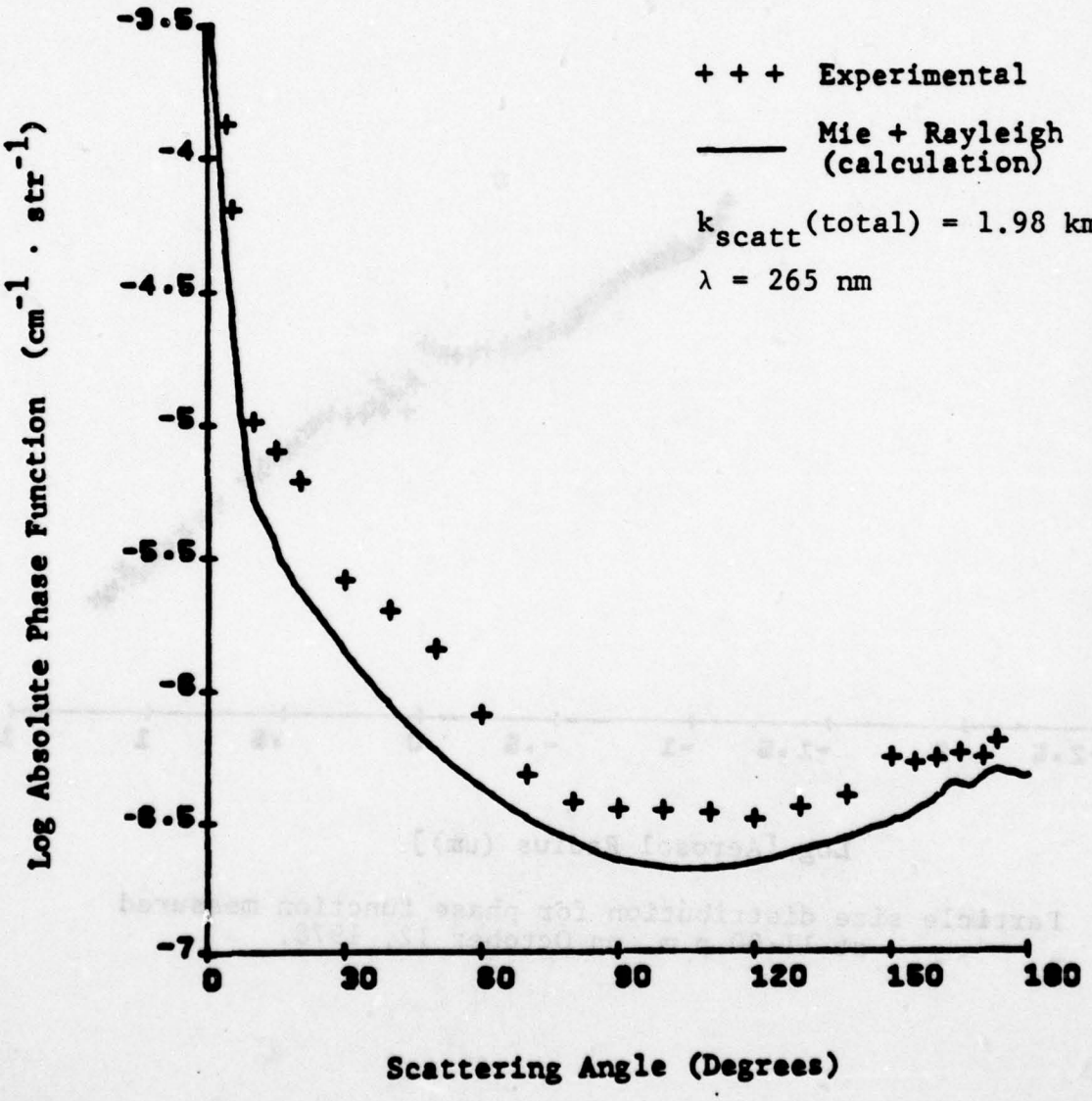

Phase function measured on October 12, 1978 at 11:00 p.m.

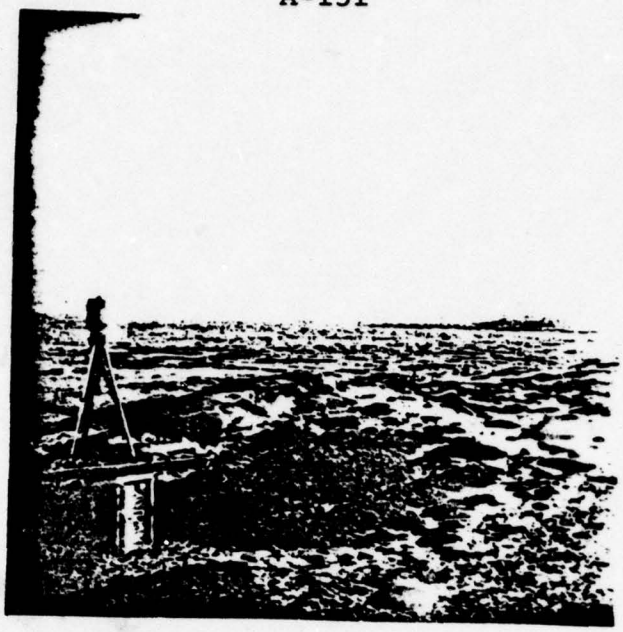

Ground level photograph
October 11, 1978 -- San Nicolas Island

Weather.....	variable fog
Visibility.....	1.5 km
Temperature.....	$63^{o}F$
Humidity.....	89%
Ozone concentration...	-
$k_{abs}(O_3)$.....	-
k_{scat}(total).....	1.19 km^{-1} at 230 nm
	1.42 km^{-1} at 250 nm
	1.20 to 1.66 km^{-1} at 265 nm
	0.98 to 1.15 km^{-1} at 280 nm

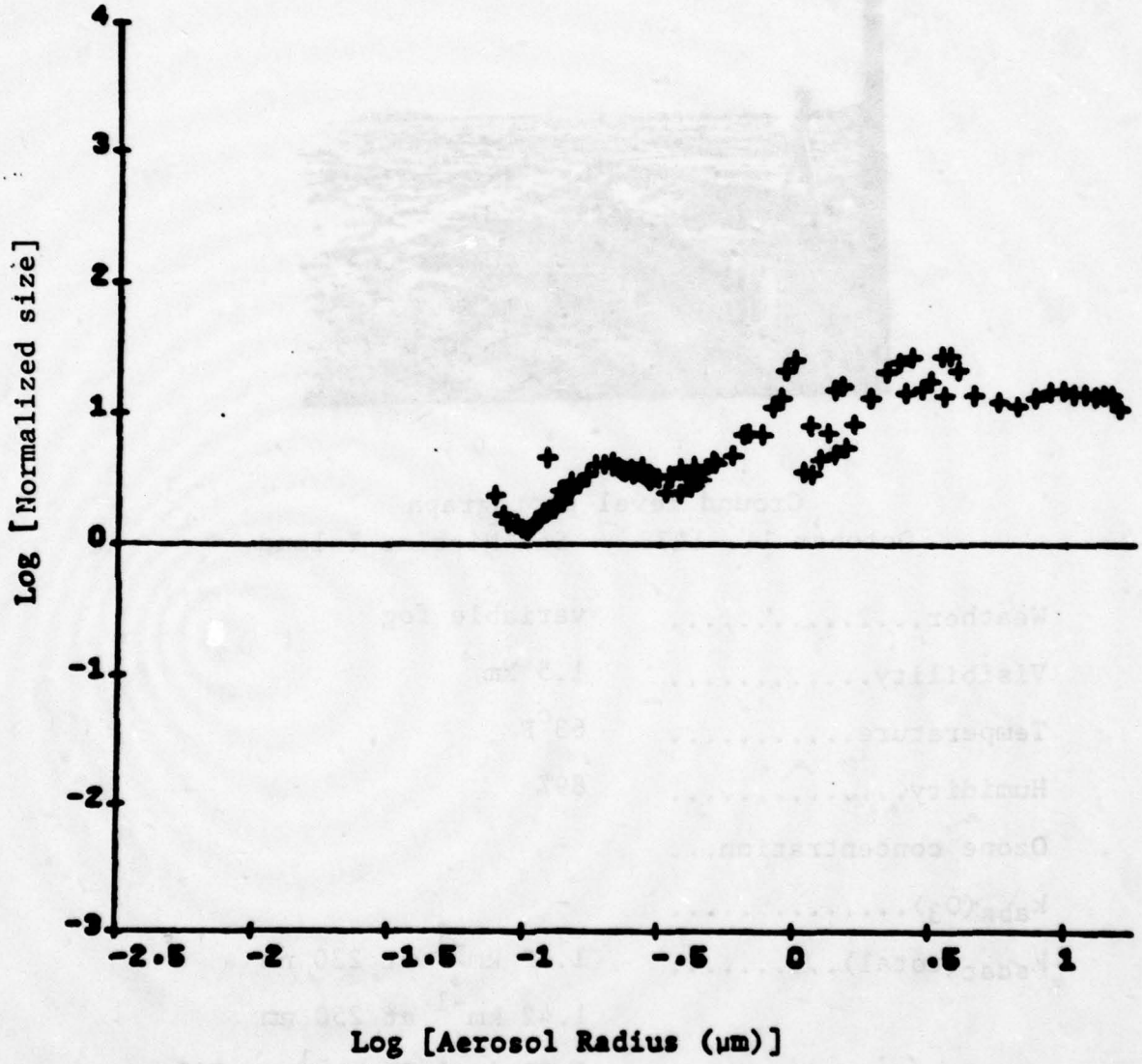

Typical normalized size distribution measured on October 11, 1978.

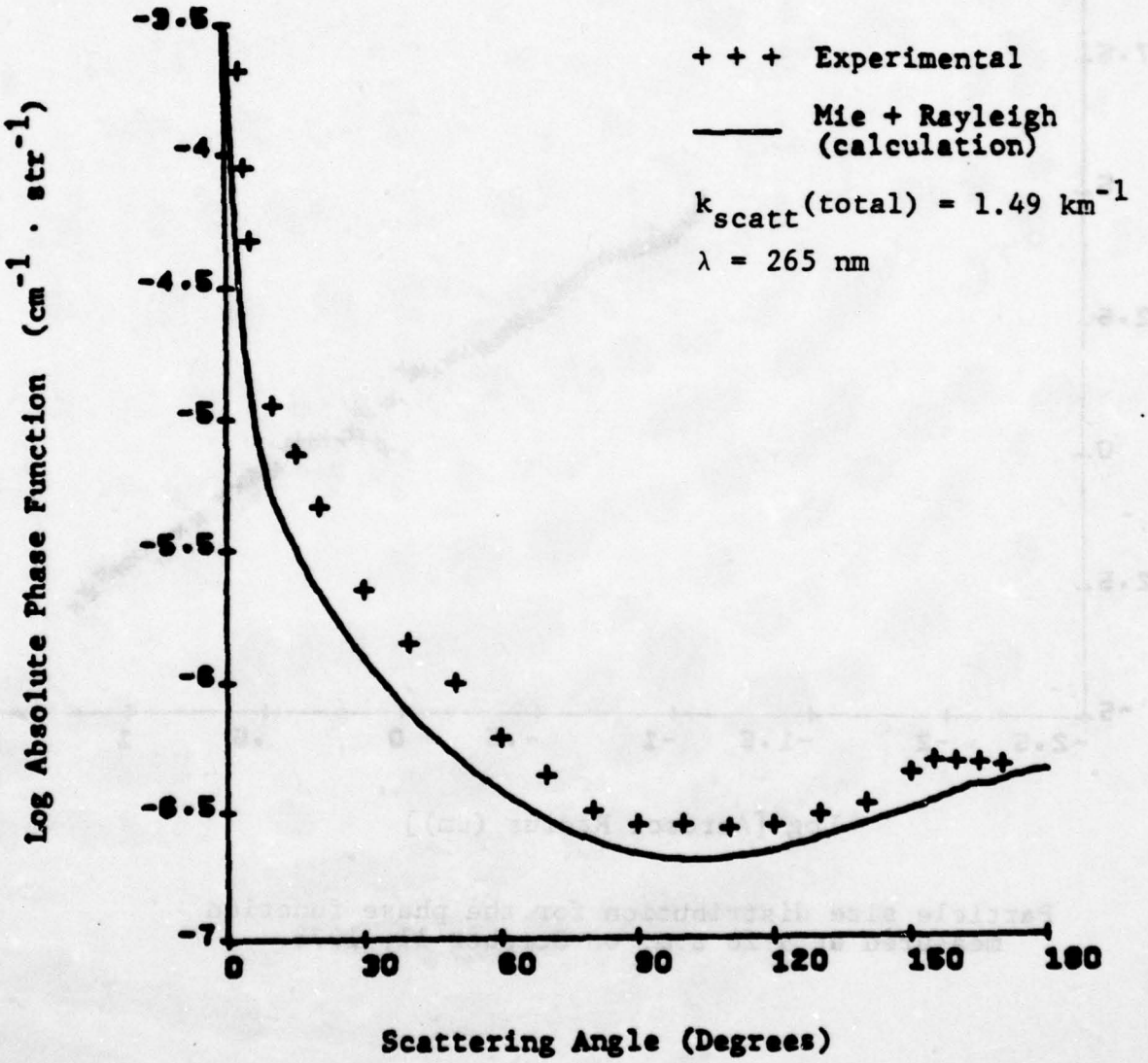

Phase function measured on October 11, 1978 at 8:45 a.m.

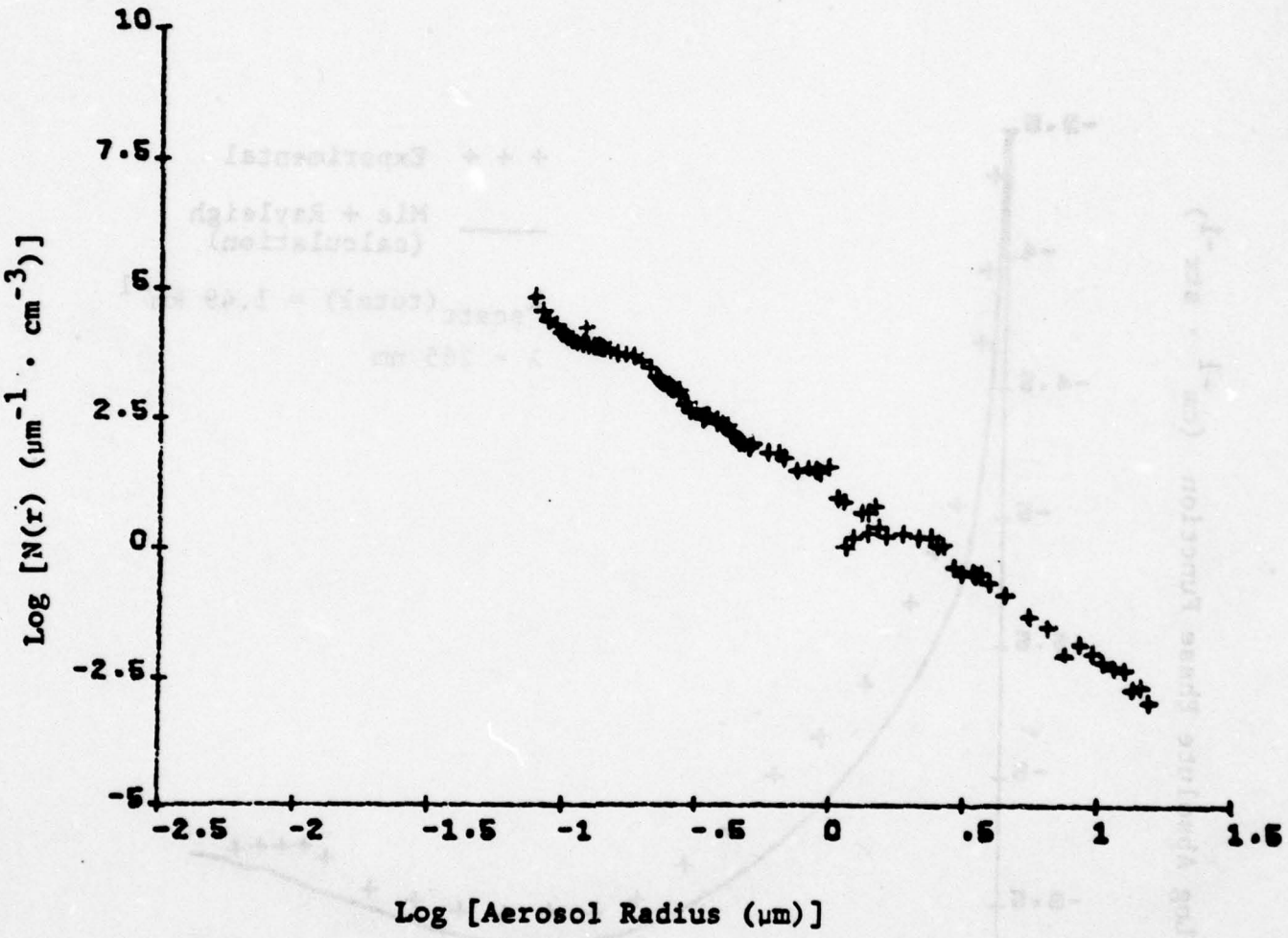

Particle size distribution for the phase function measured at 9:20 a.m. on October 11, 1978.

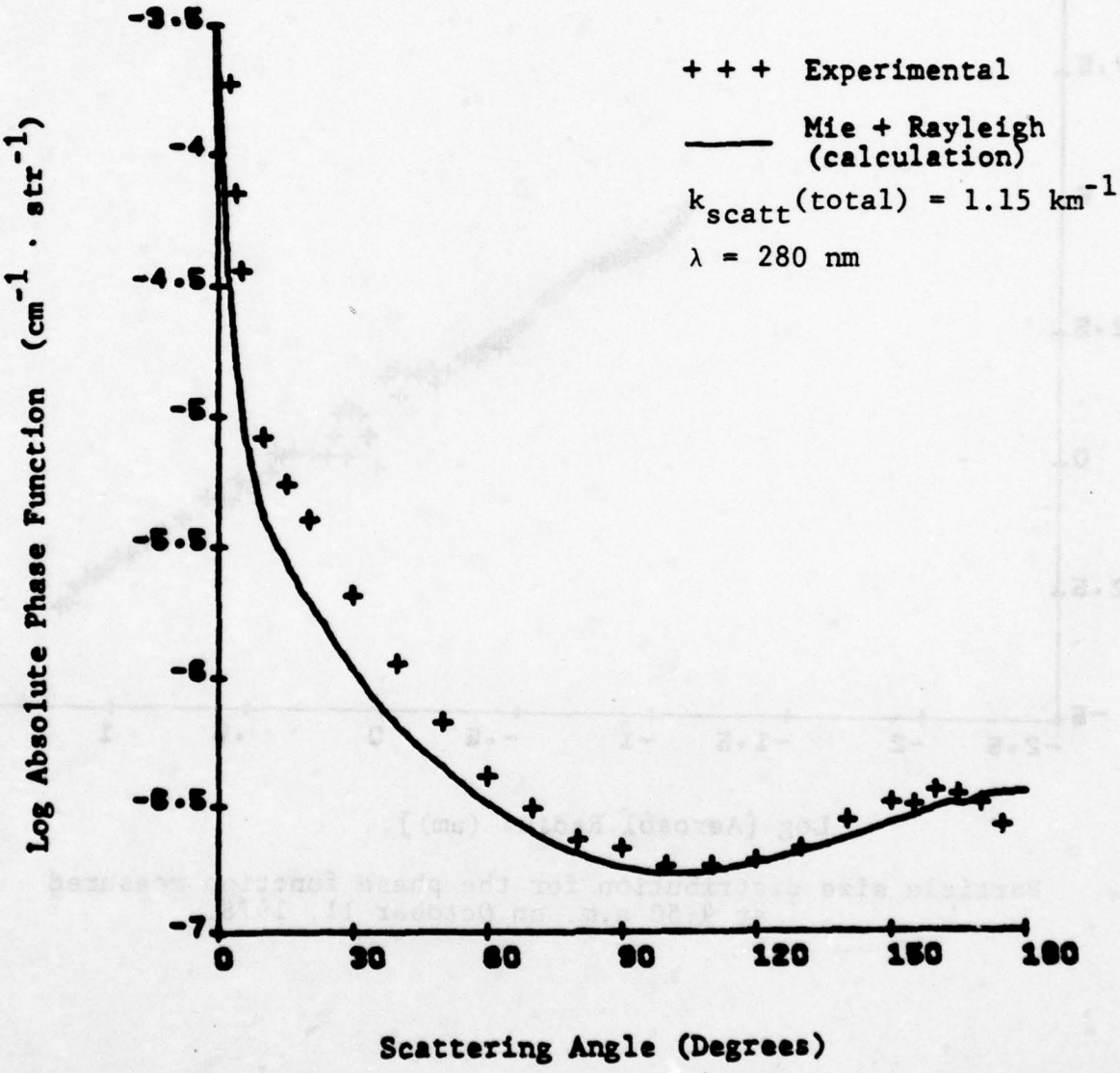

Phase function measured on October 11, 1978 at 9:20 a.m.

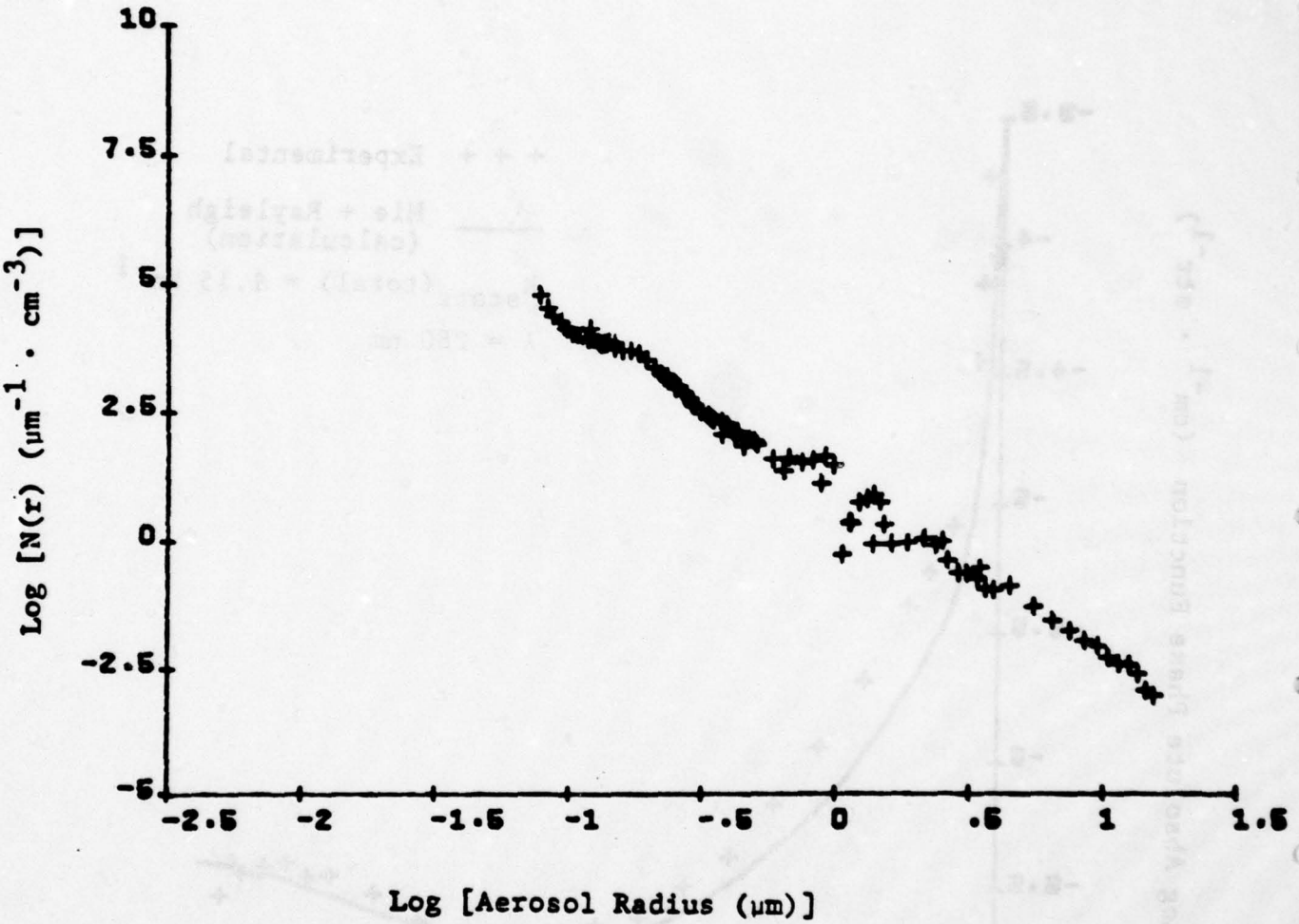

Particle size distribution for the phase function measured at 9:50 a.m. on October 11, 1978.

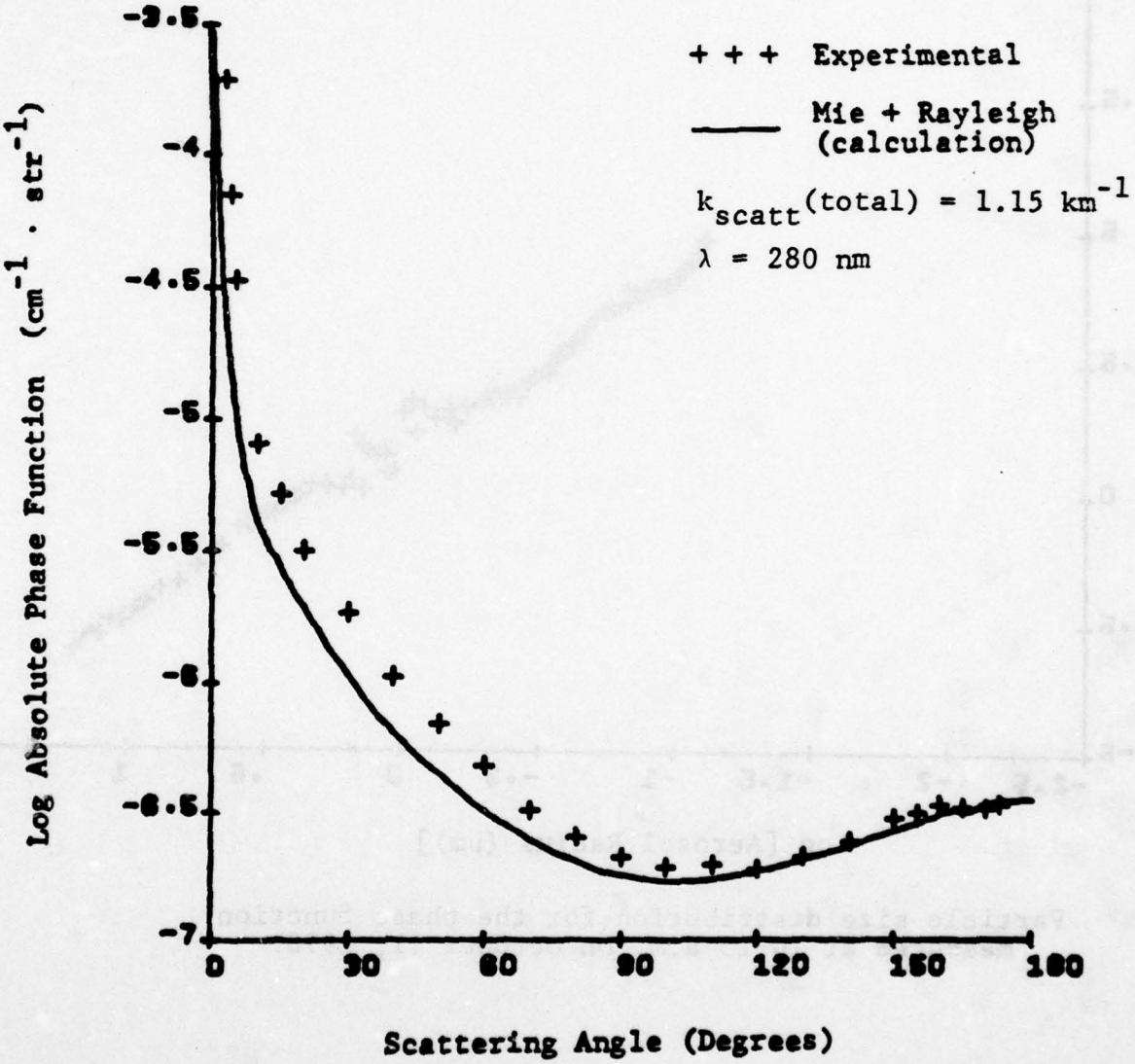

Phase function measured on October 11, 1978 at 9:50 a.m.

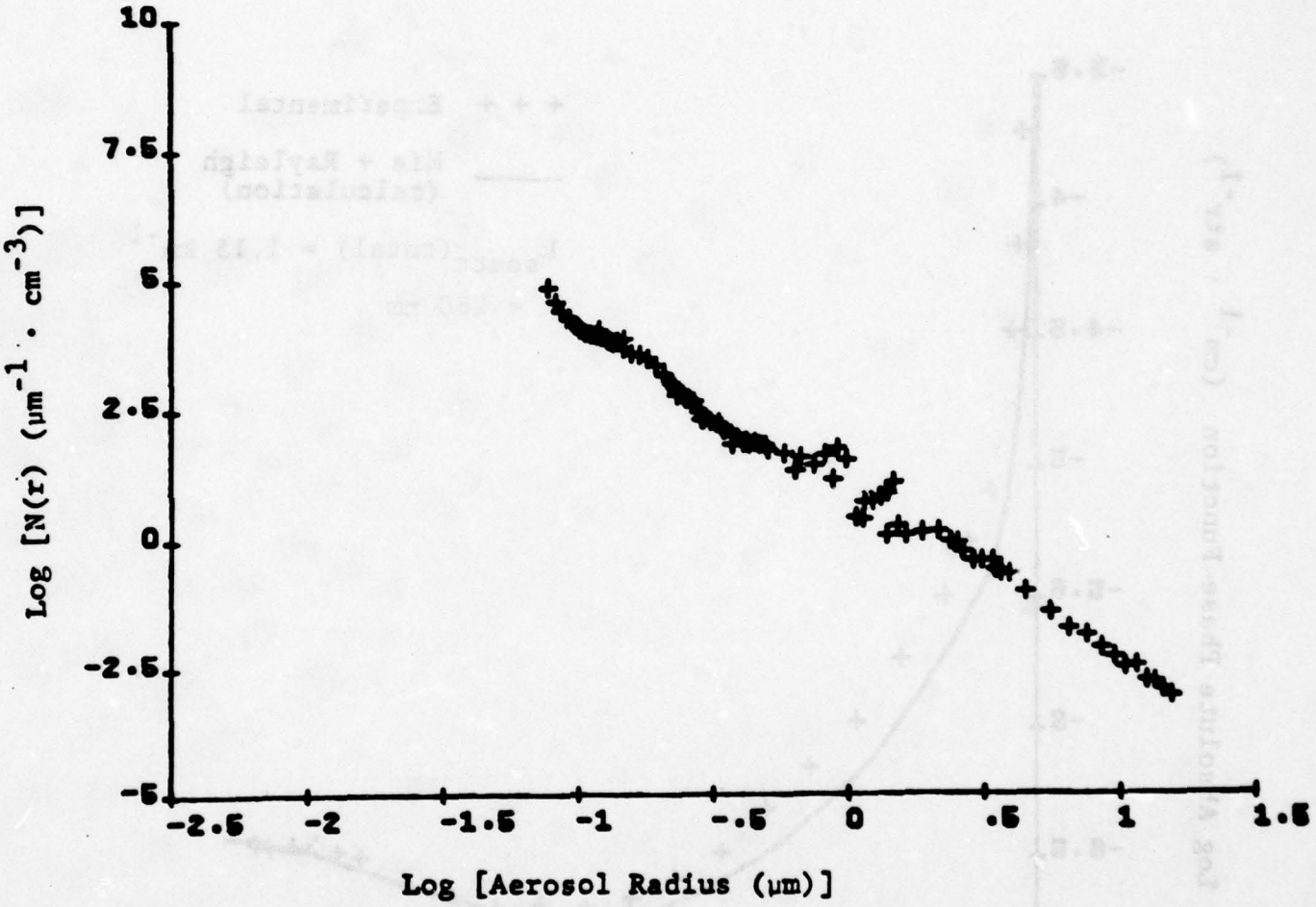

Particle size distribution for the phase function measured at 10:15 a.m. on October 11, 1978.

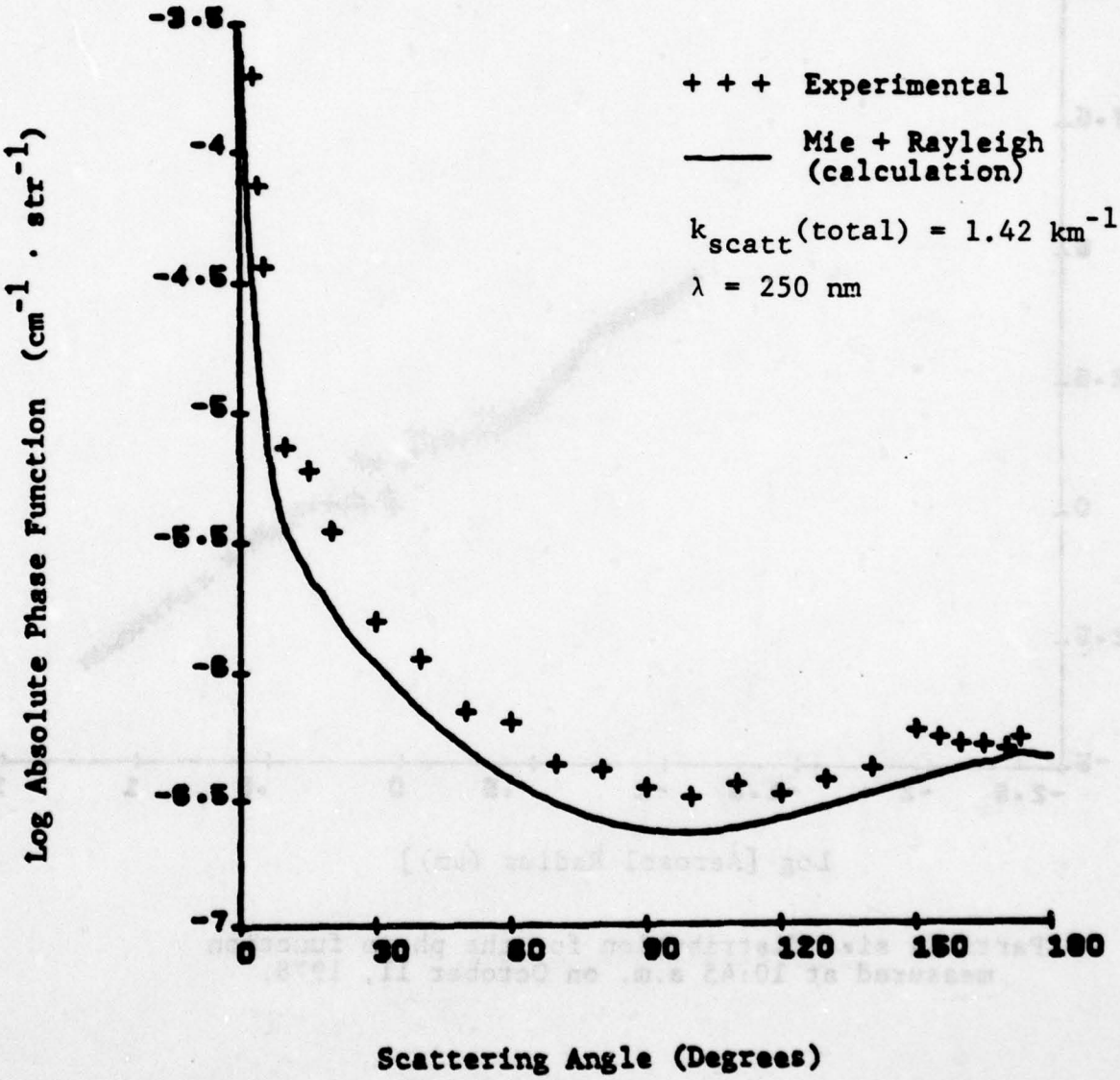

Phase function measured on October 11, 1978 at 10:15 a.m.

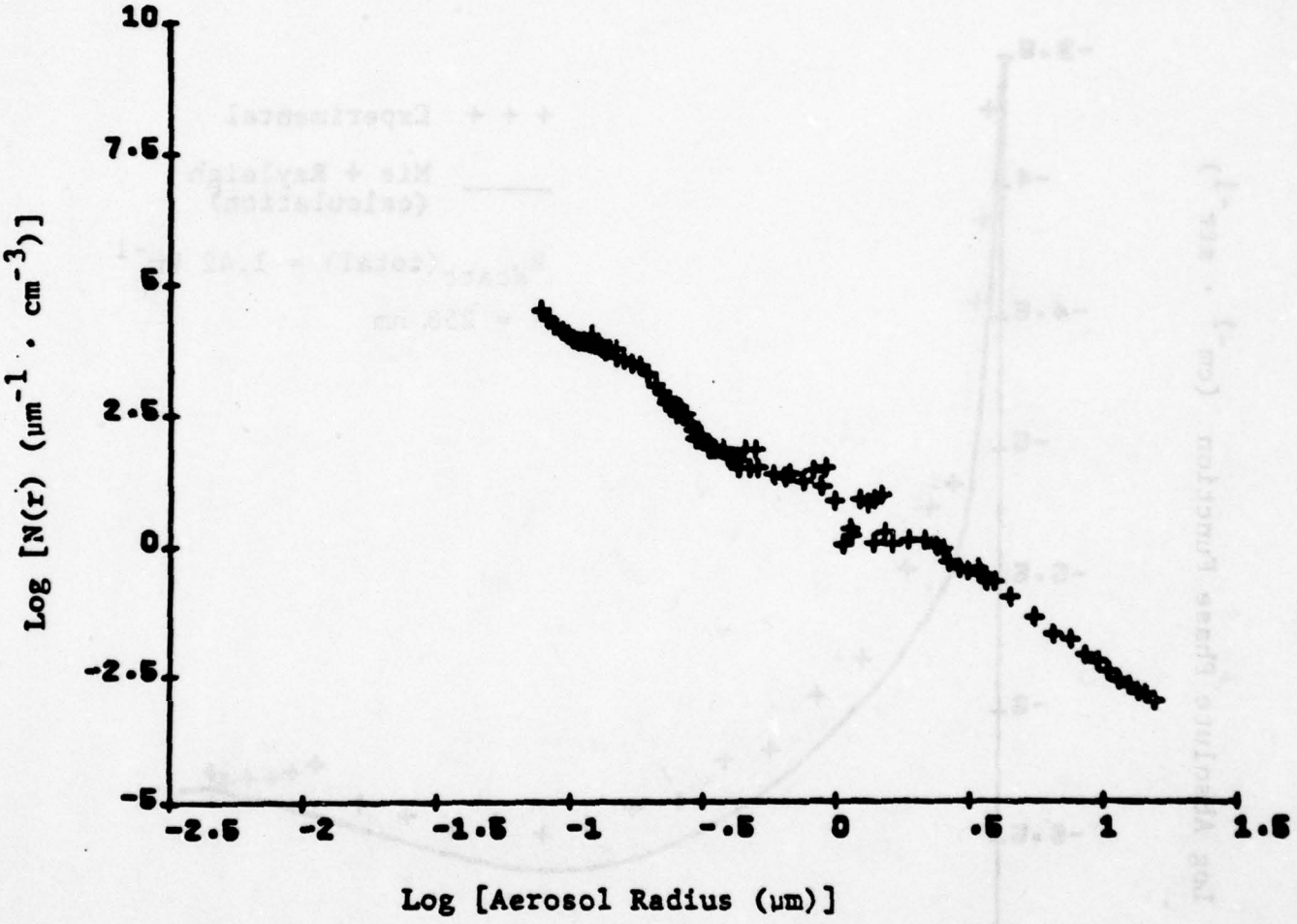

Particle size distribution for the phase function measured at 10:45 a.m. on October 11, 1978.

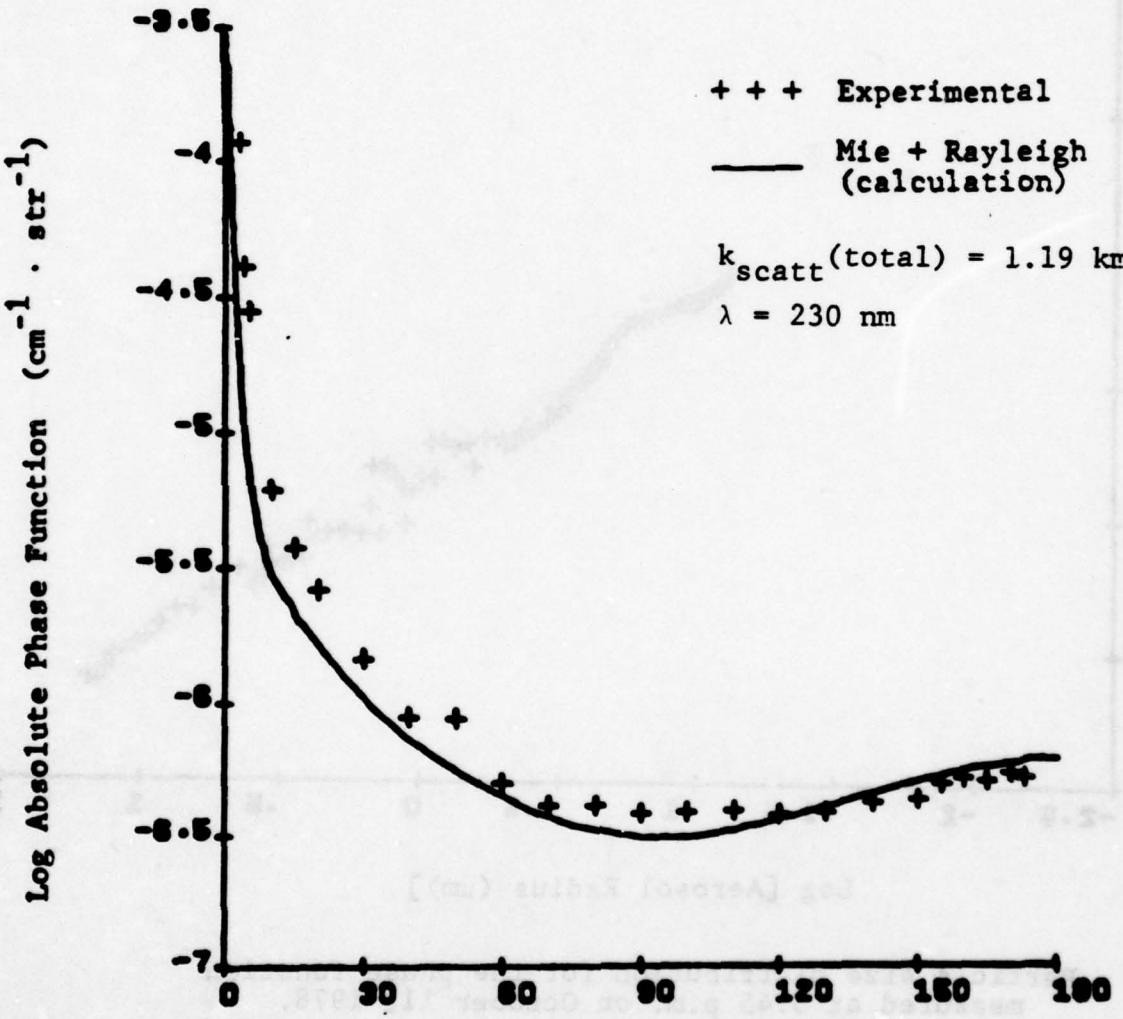

Phase function measured on October 11, 1978 at 10:45 a.m.

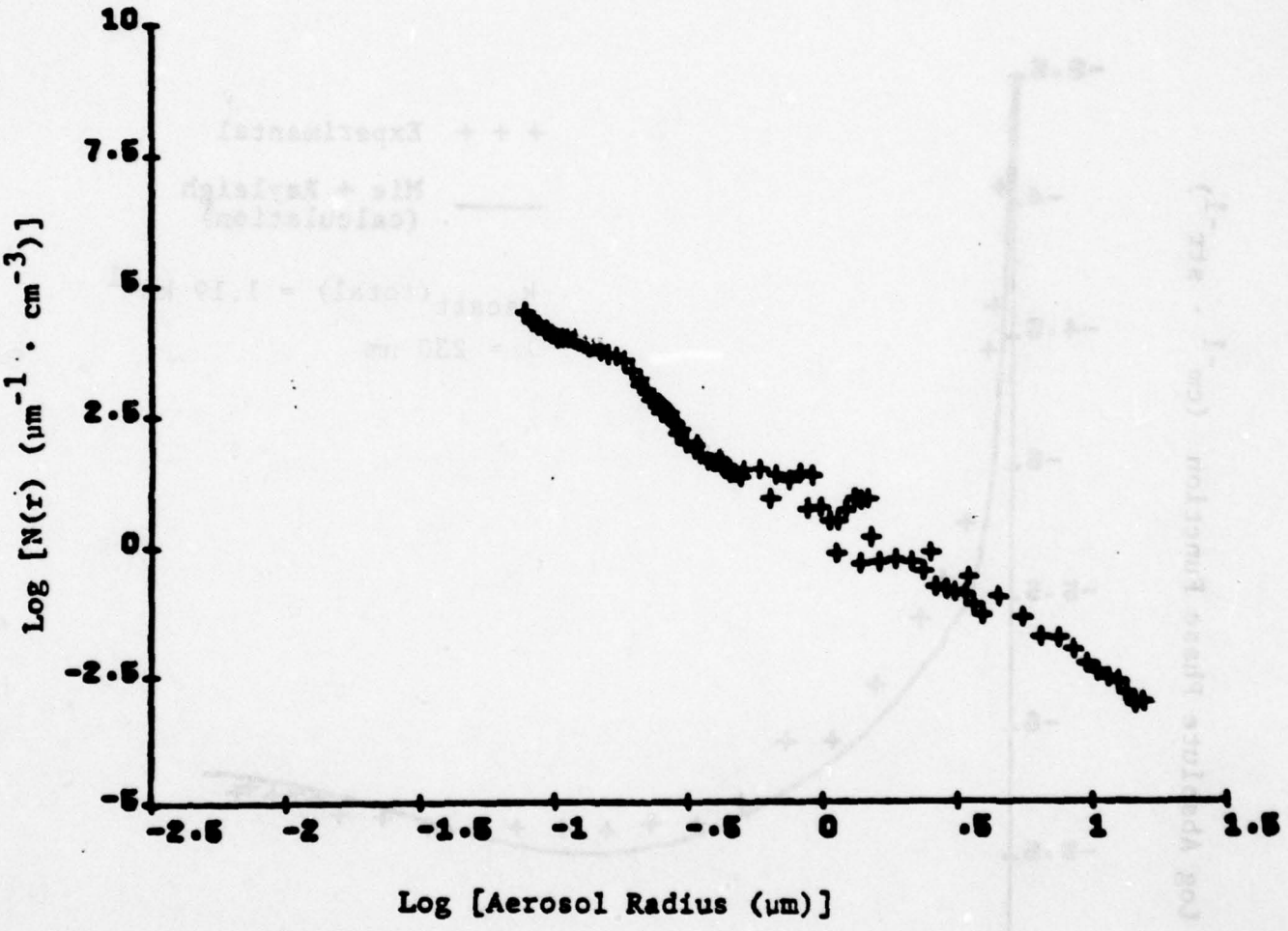

Particle size distribution for the phase function measured at 3:45 p.m. on October 11, 1978.

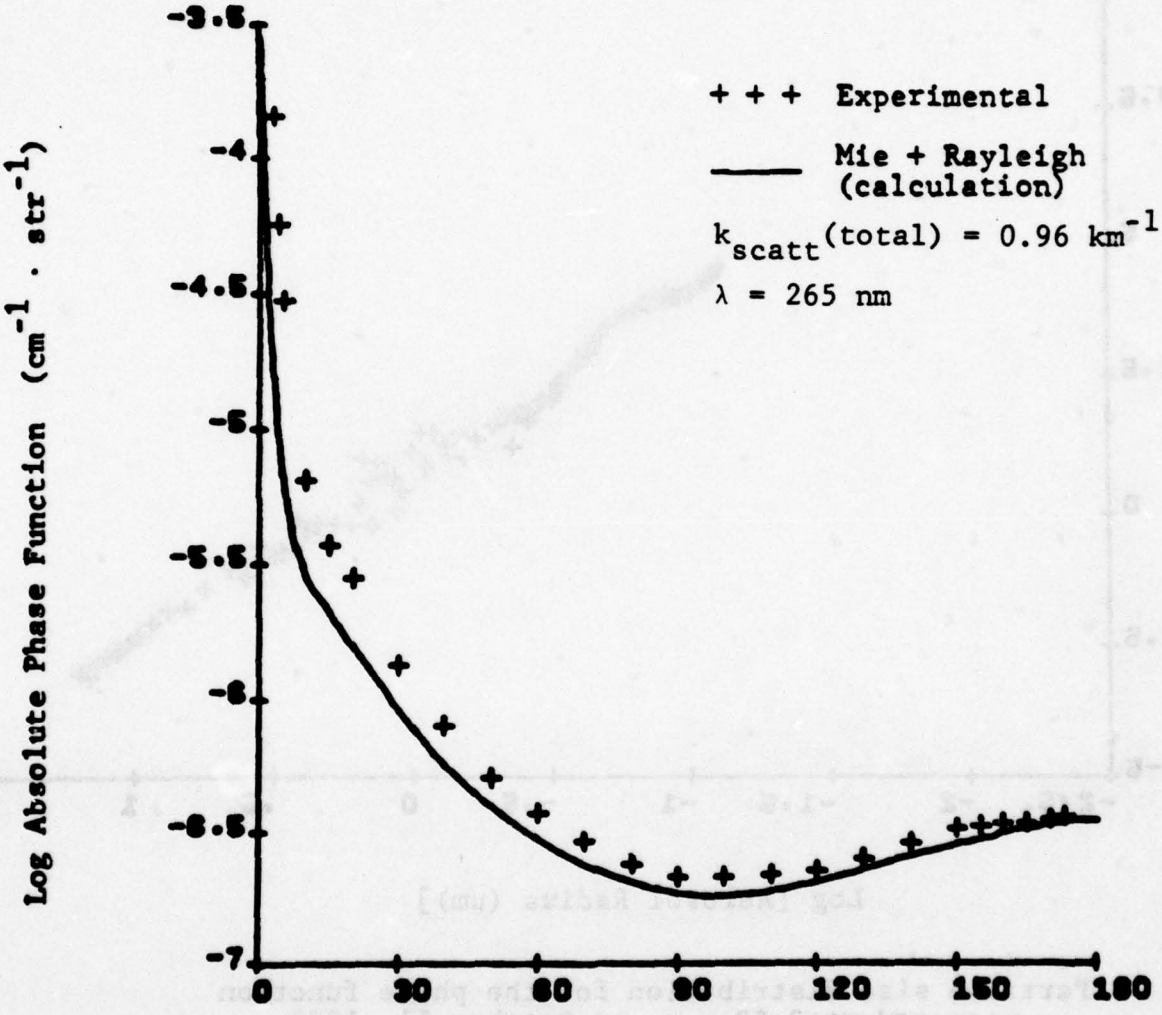

Phase function measured on October 11, 1978 at 3:15 p.m.

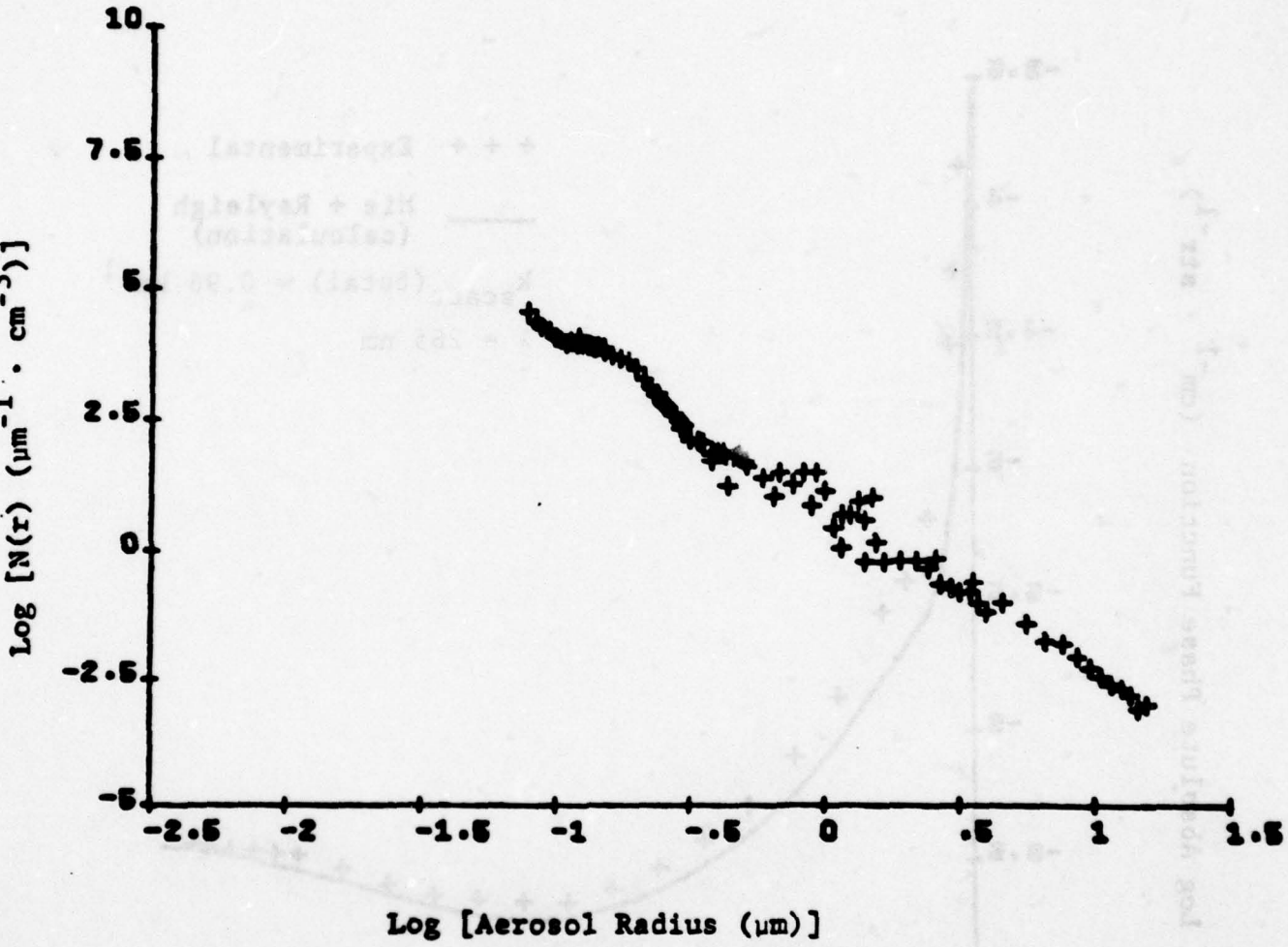

Particle size distribution for the phase function measured at 3:50 p.m. on October 11, 1978.

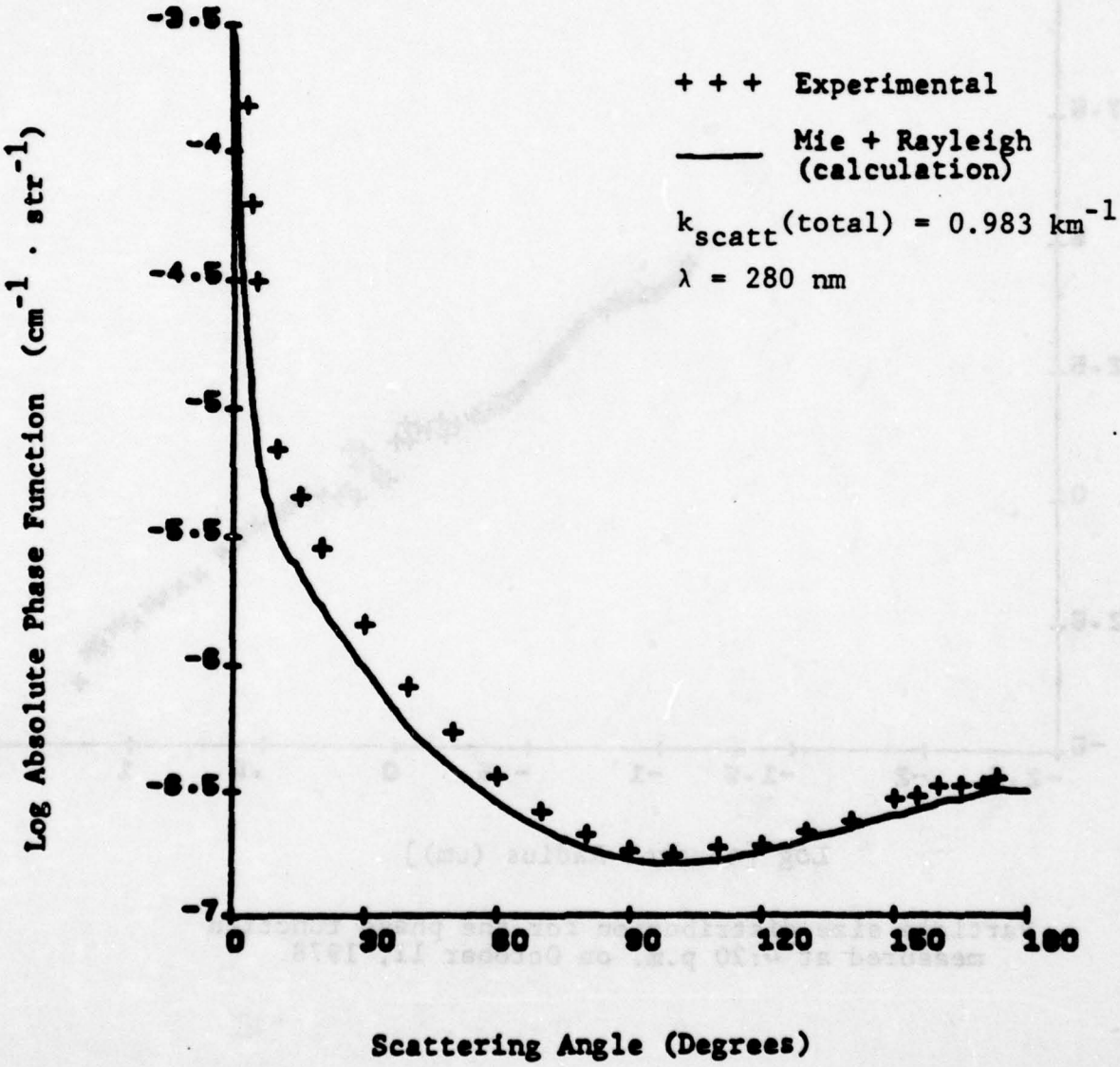

Phase function measured on October 11, 1978 at 3:50 p.m.

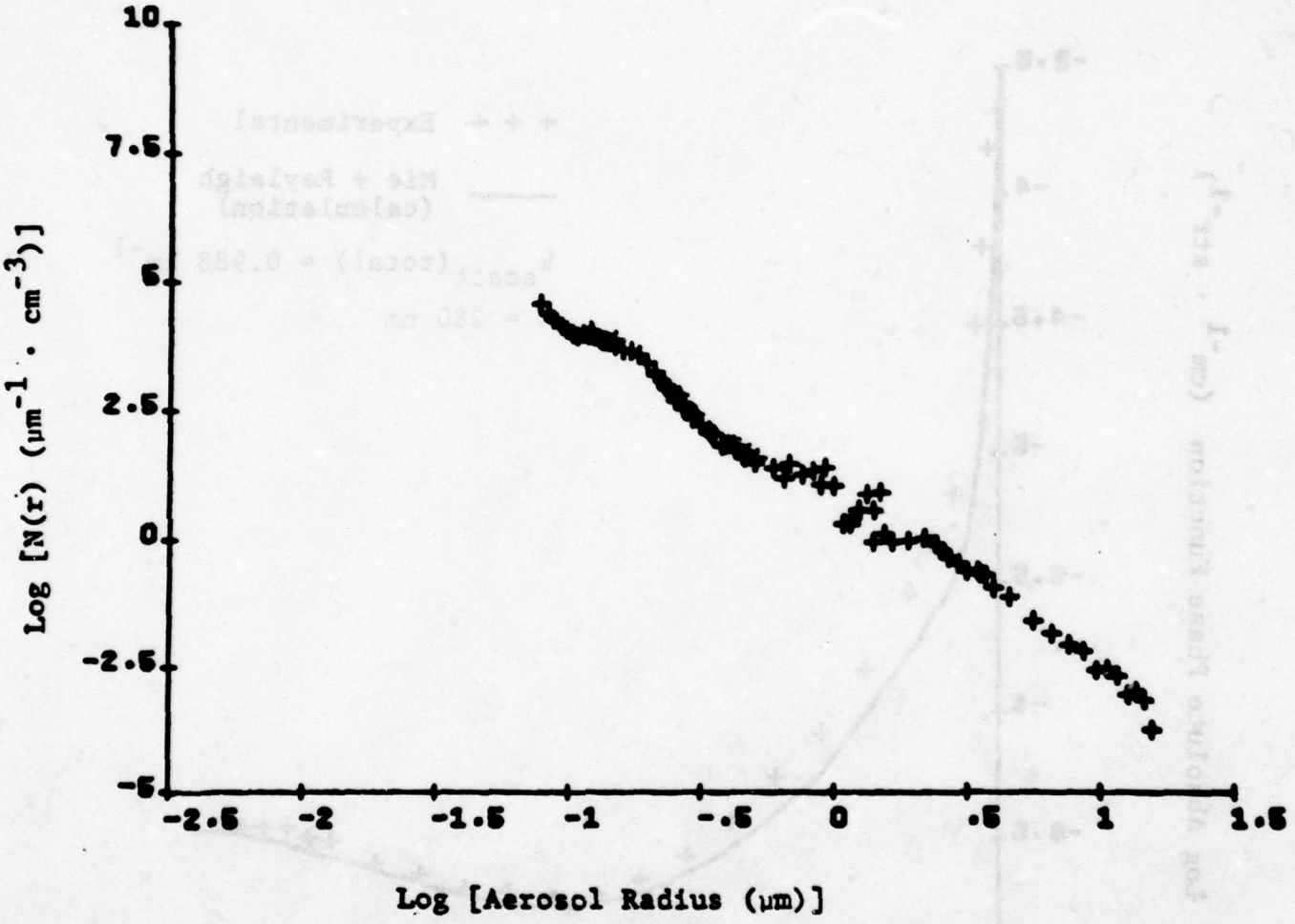

Particle size distribution for the phase function measured at 4:20 p.m. on October 11, 1978.

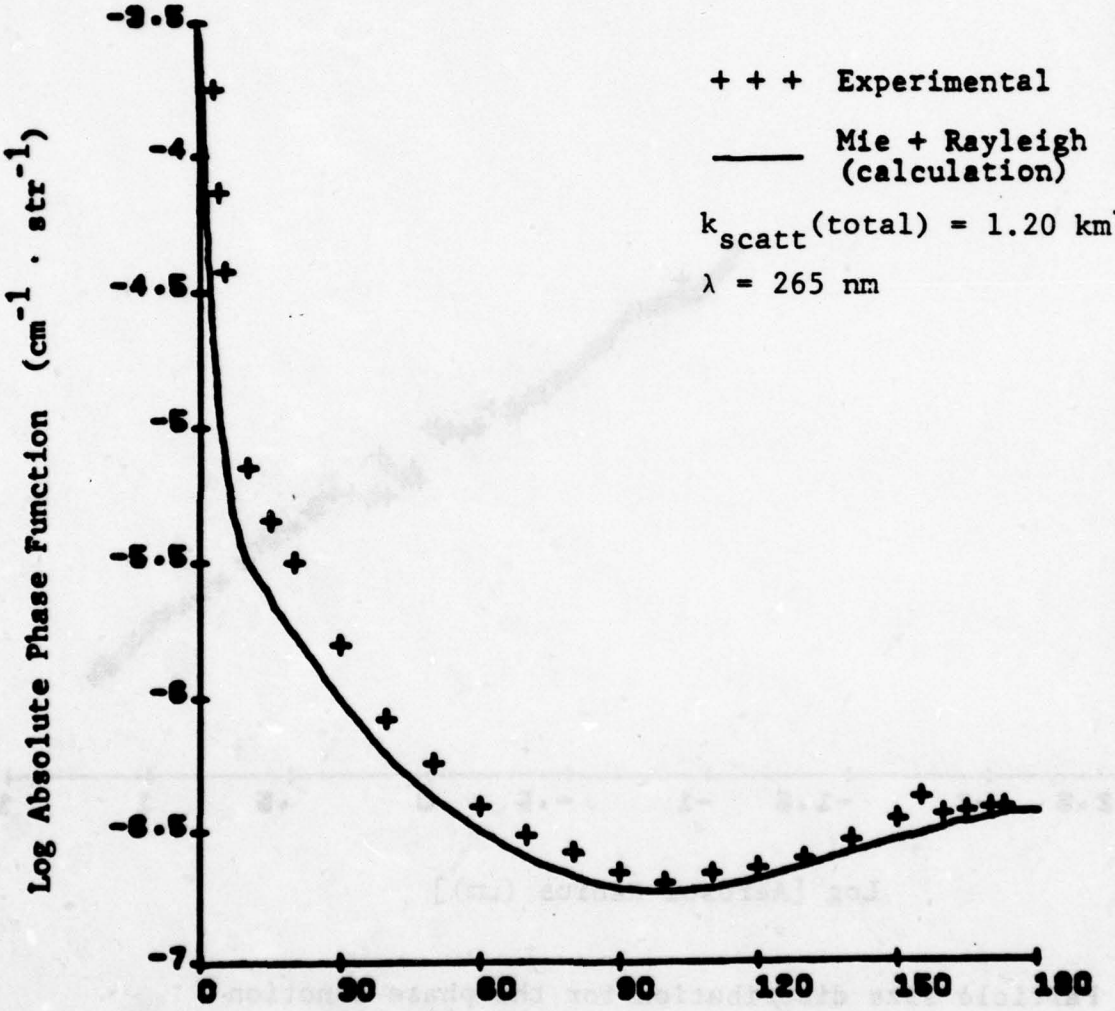

Phase function measured on October 11, 1978 at 4:20 p.m.

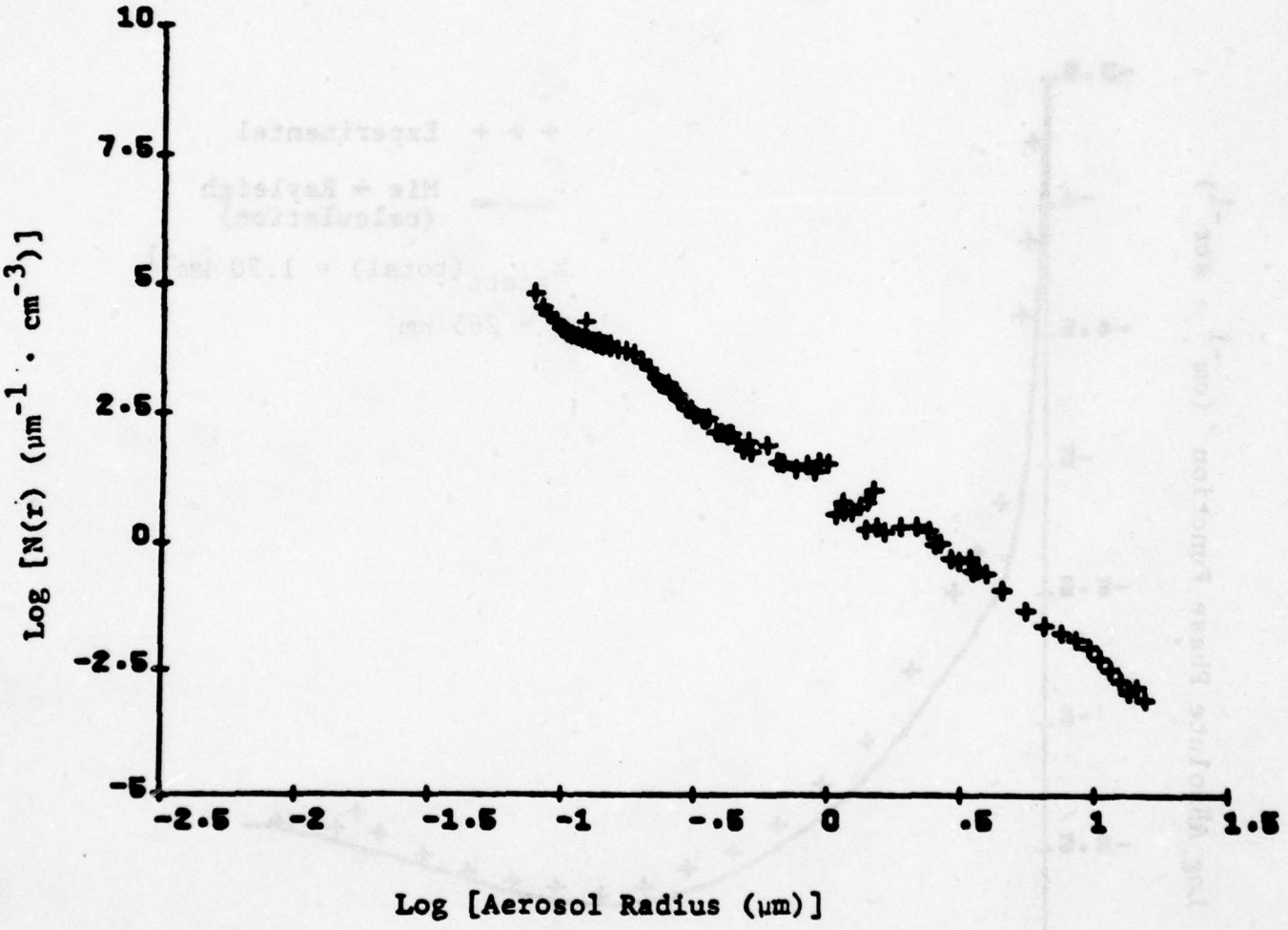

Particle size distribution for the phase function measured at 7:00 p.m. on October 11, 1978.

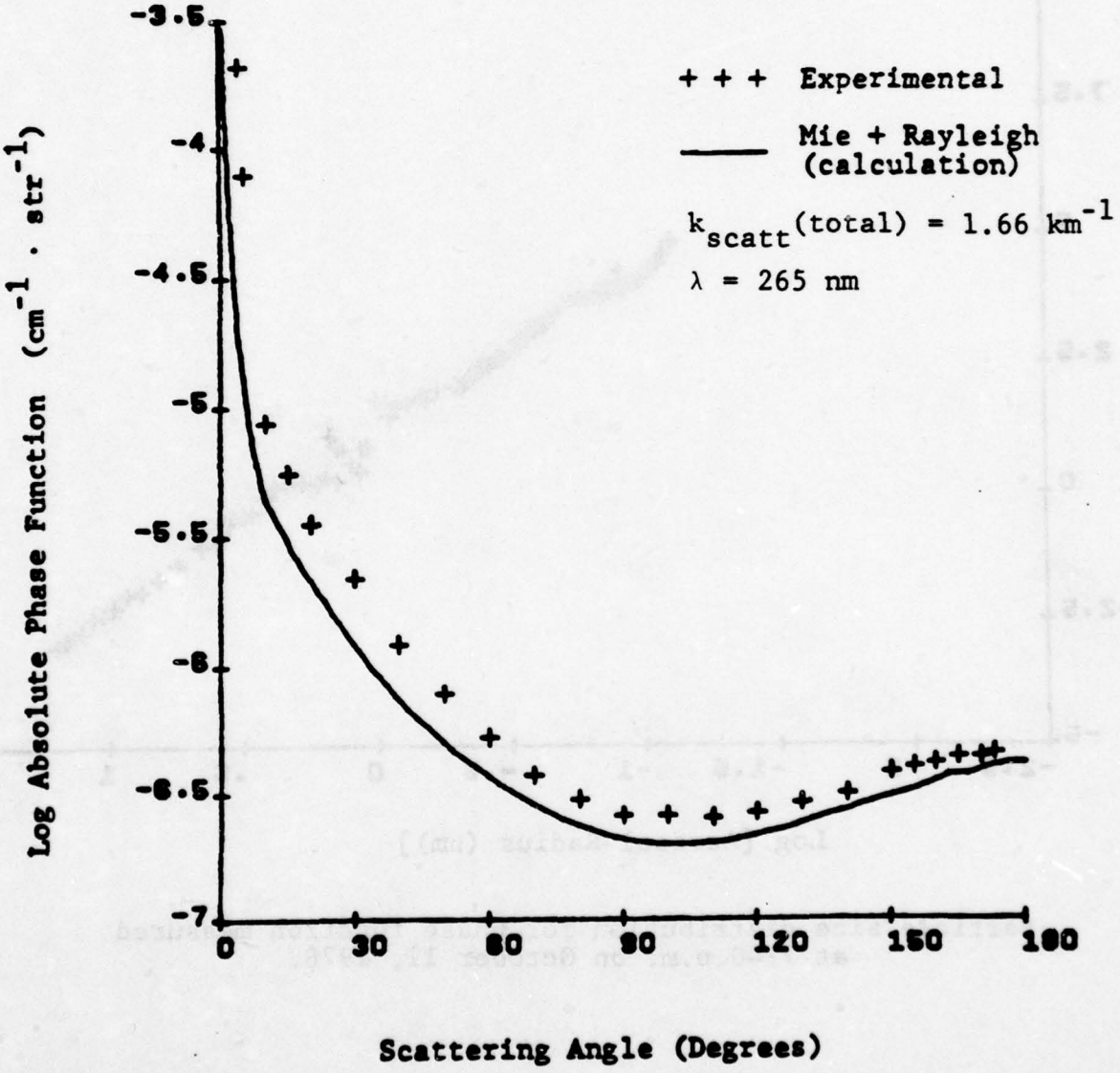

Phase function measured on October 11, 1978 at 7:00 p.m.

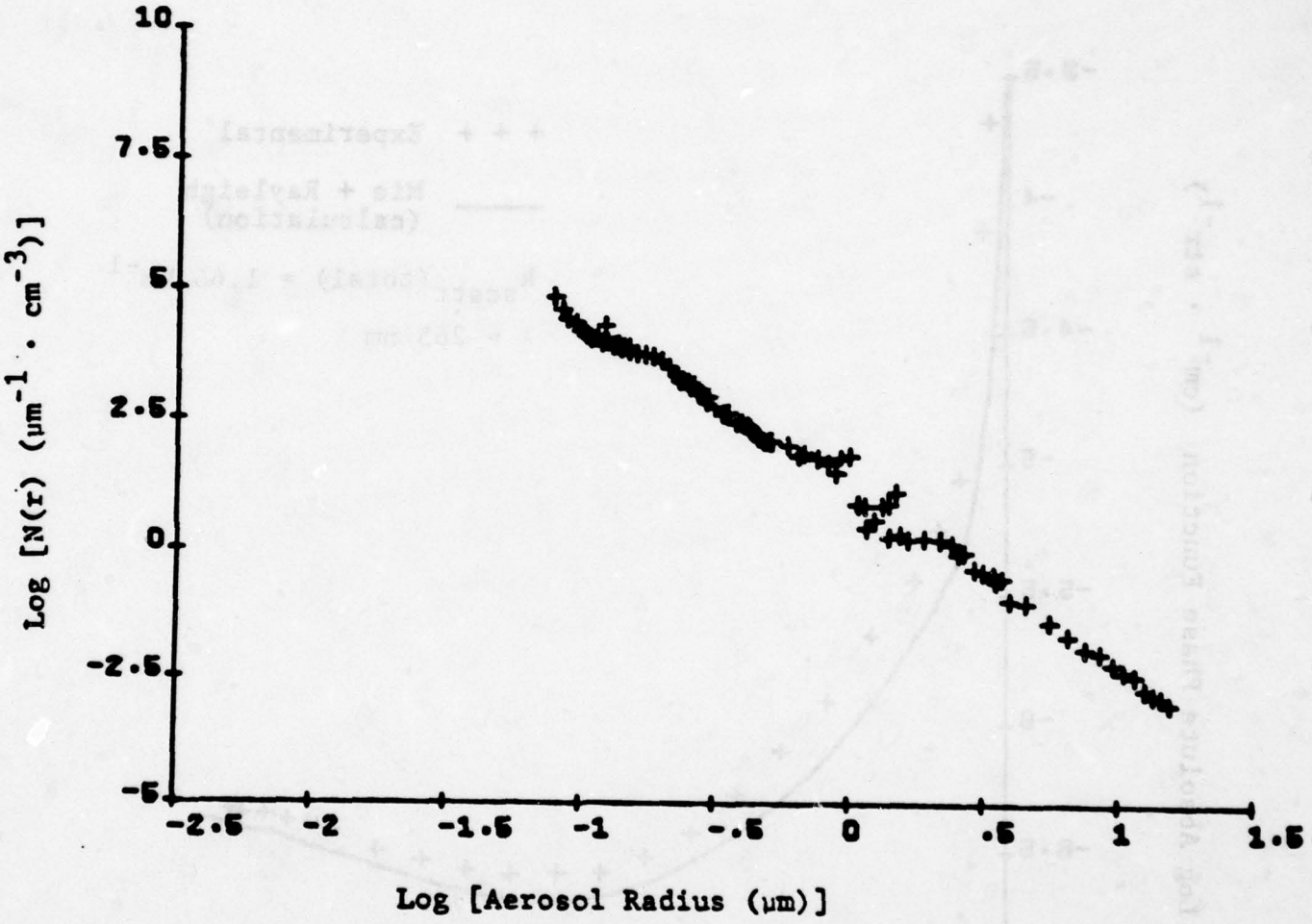

Particle size distribution for phase function measured at 7:40 p.m. on October 11, 1978.

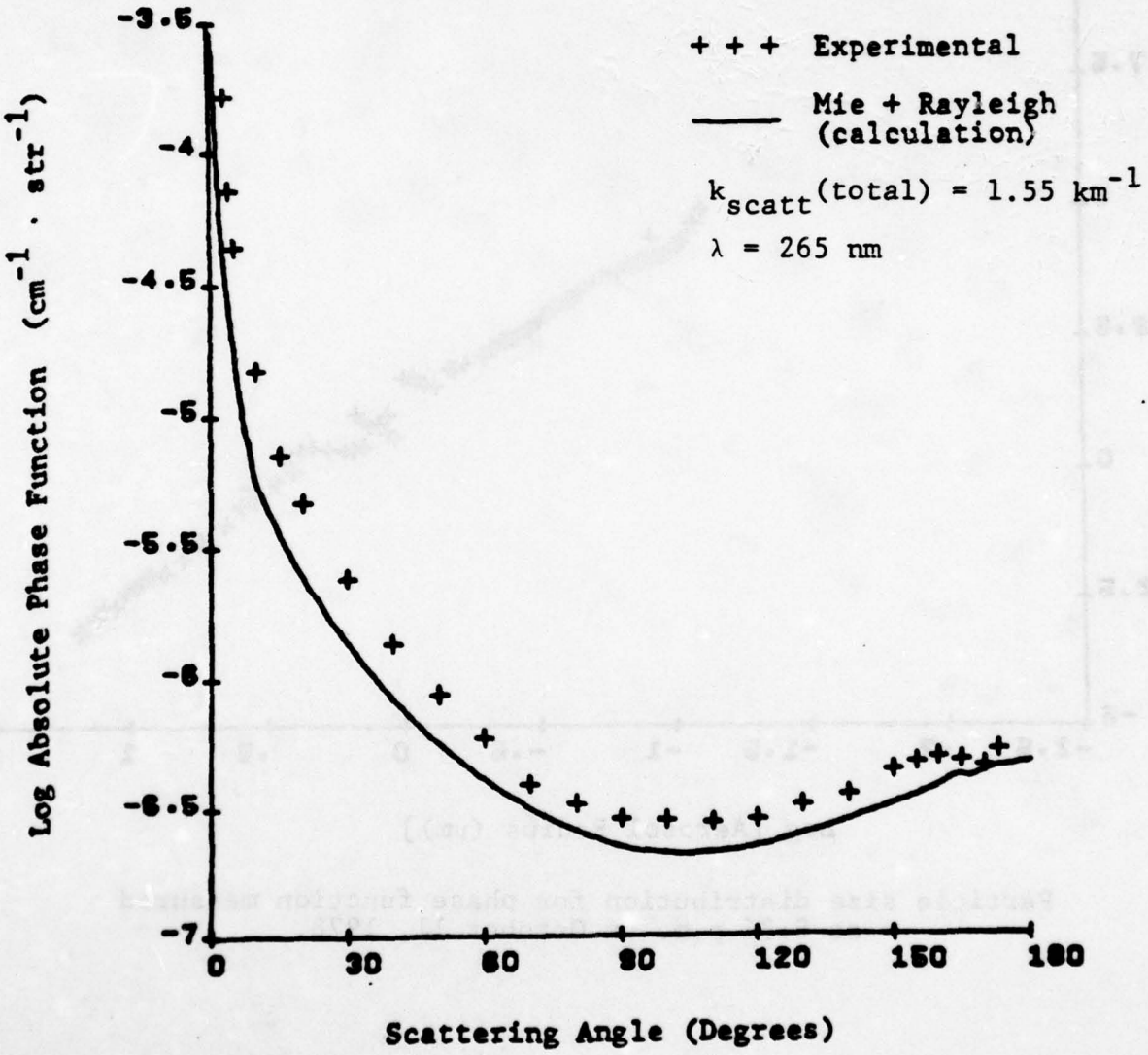

Phase function measured on October 11, 1978 at 7:40 p.m.

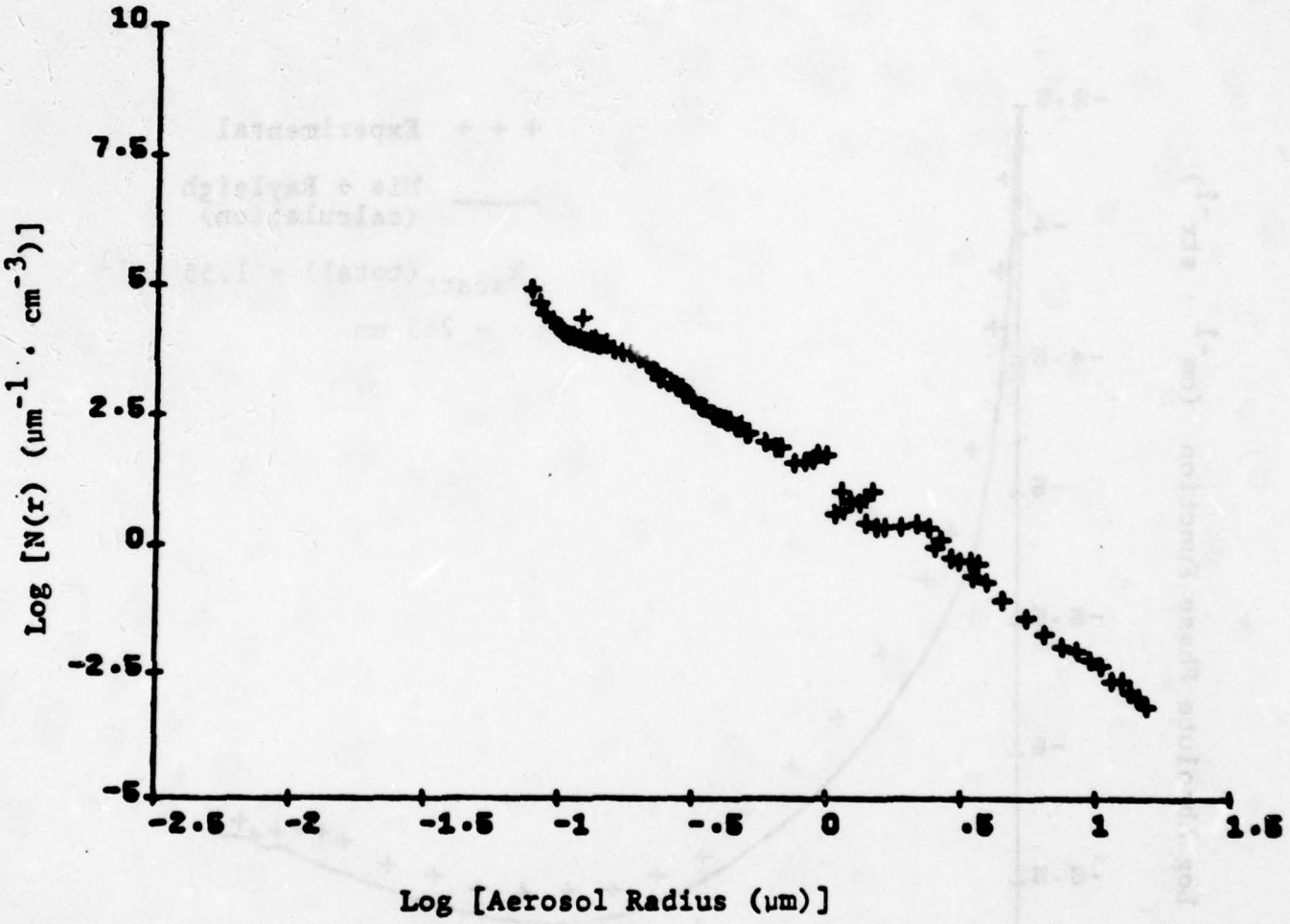

Particle size distribution for phase function measured at 8:35 p.m. on October 11, 1978.

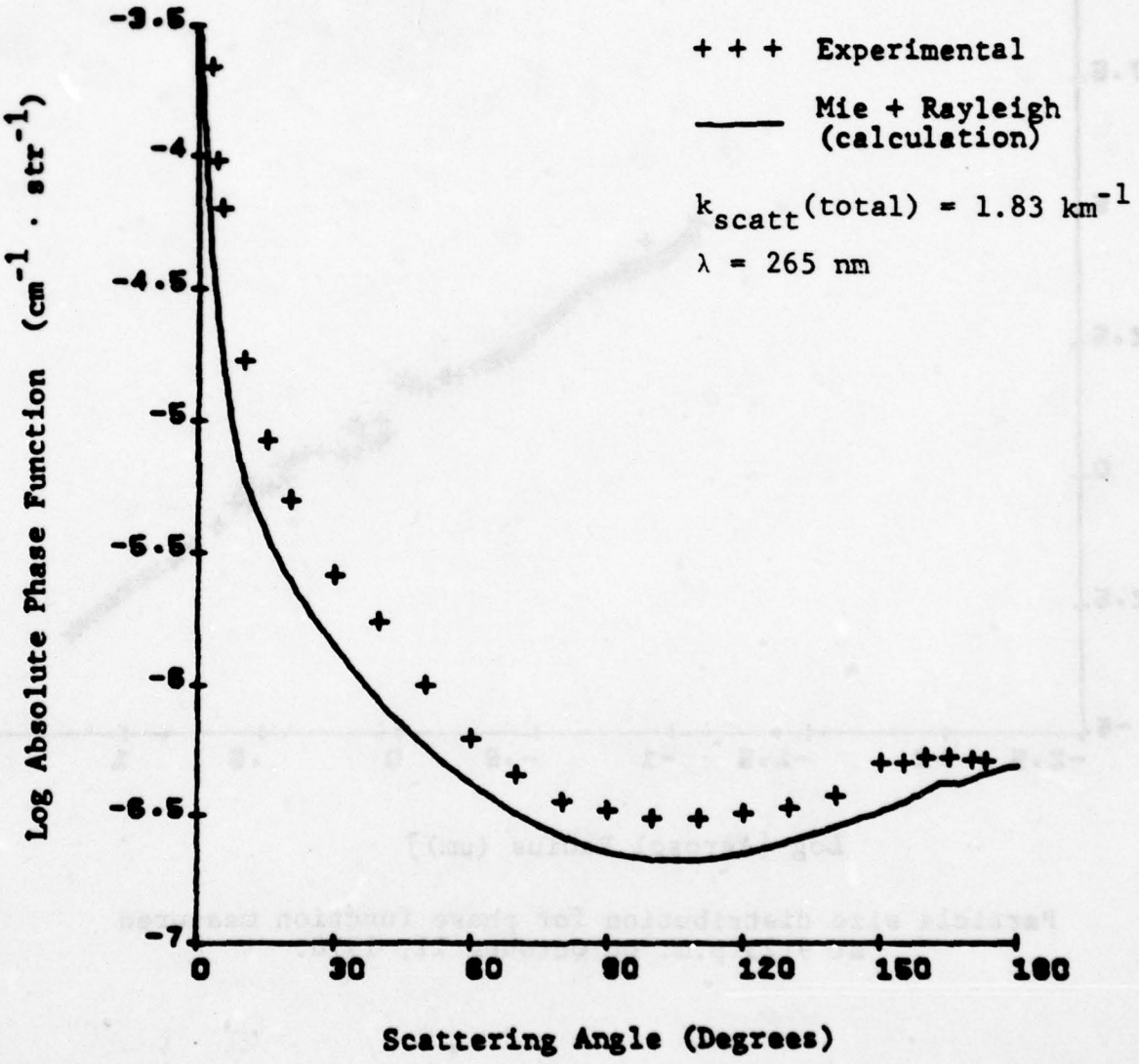

Phase function measured on October 11, 1978 at 8:35 p.m.

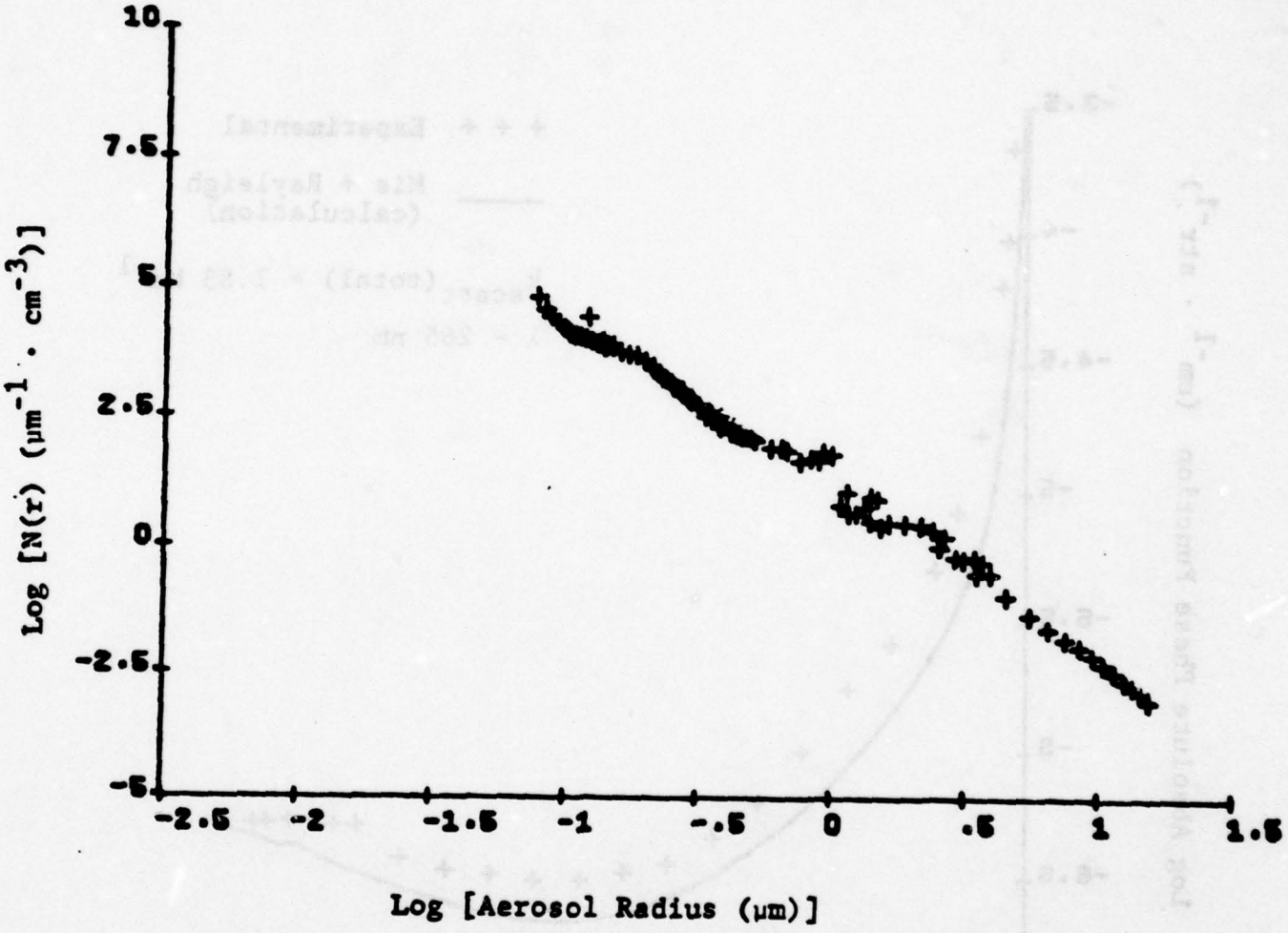

Particle size distribution for phase function measured at 9:25 p.m. on October 11, 1978.

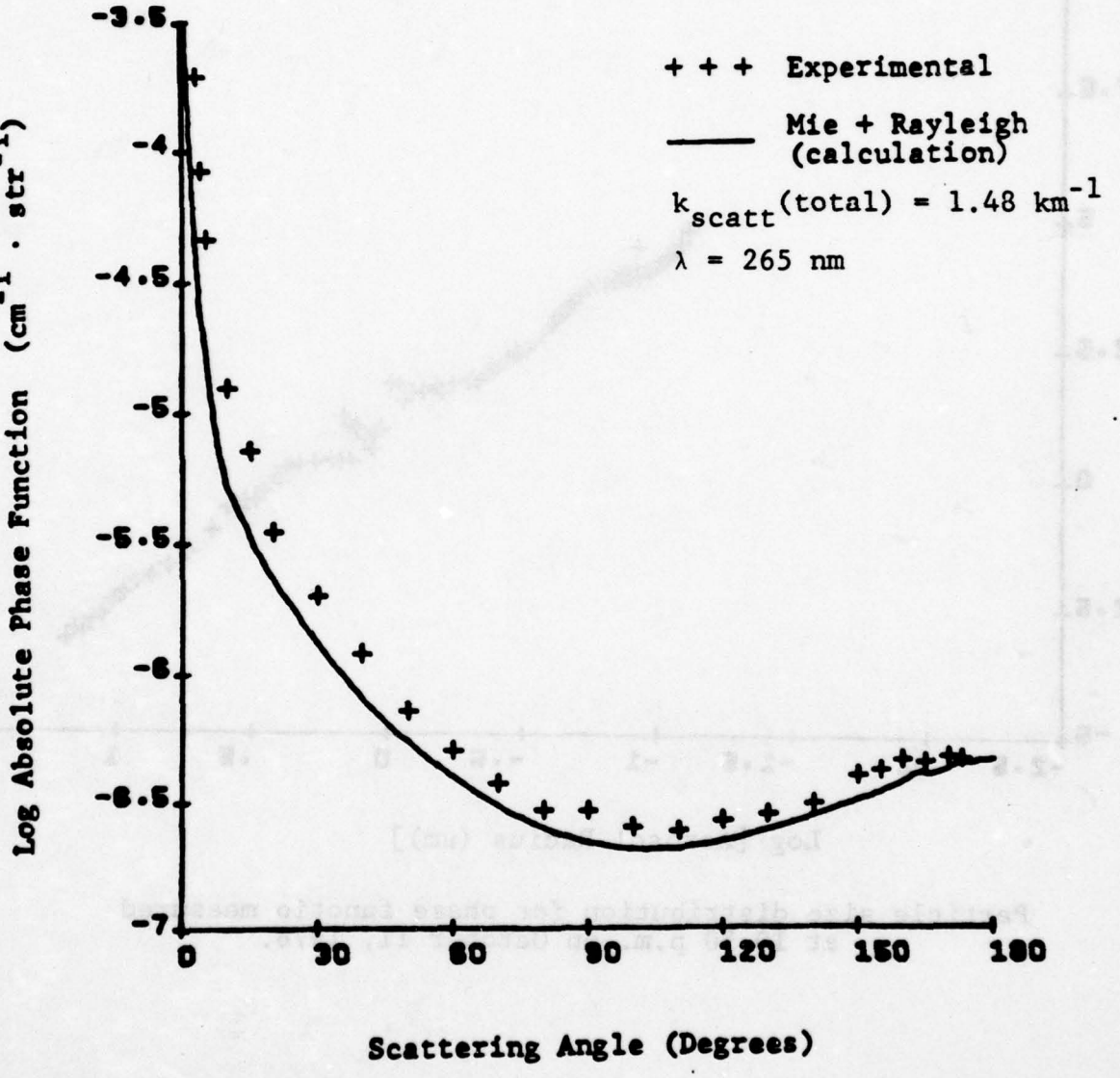

Phase function measured on October 11, 1978 at 9:25 p.m.

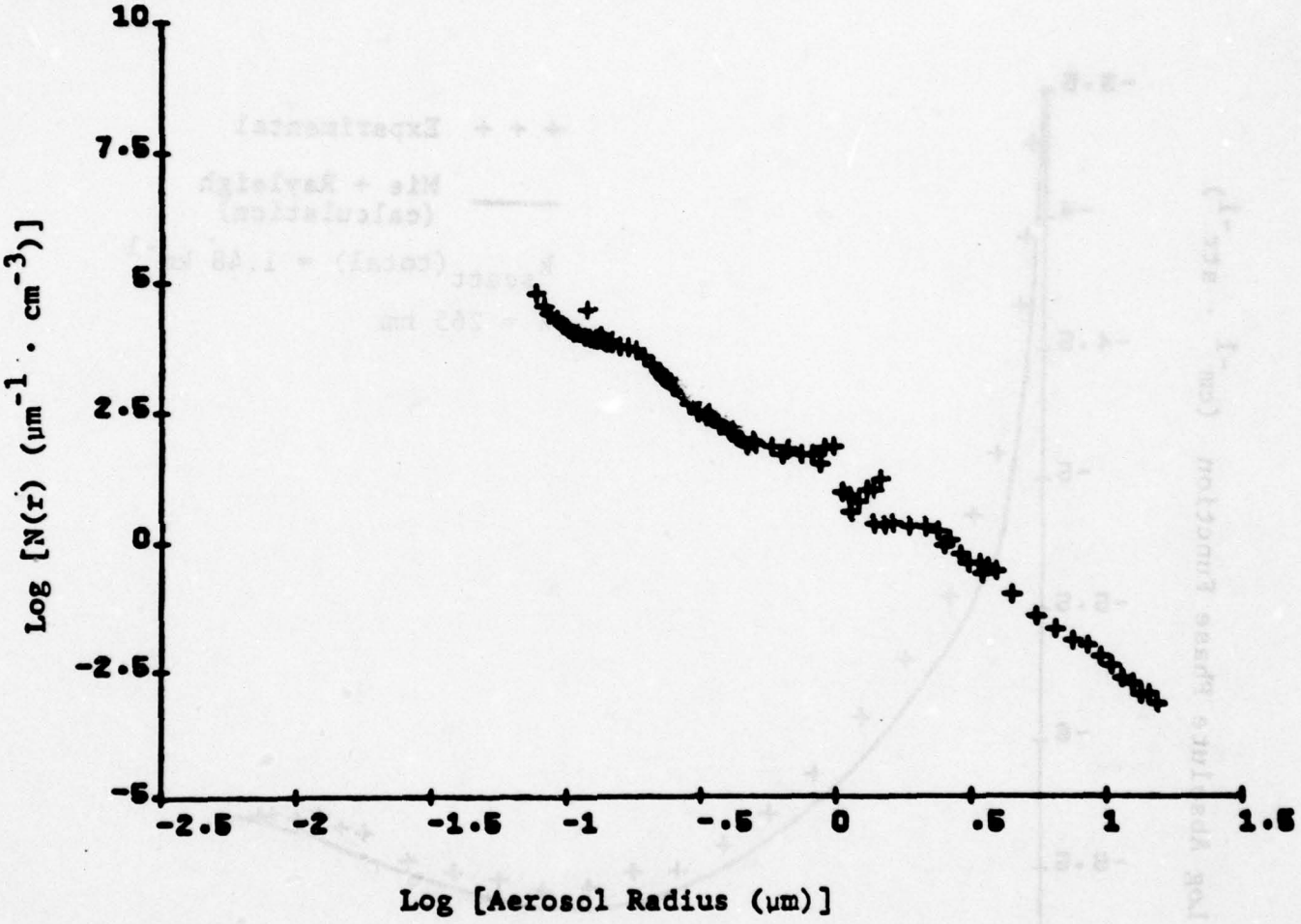

Particle size distribution for phase functio measured at 10:30 p.m. on October 11, 1978.

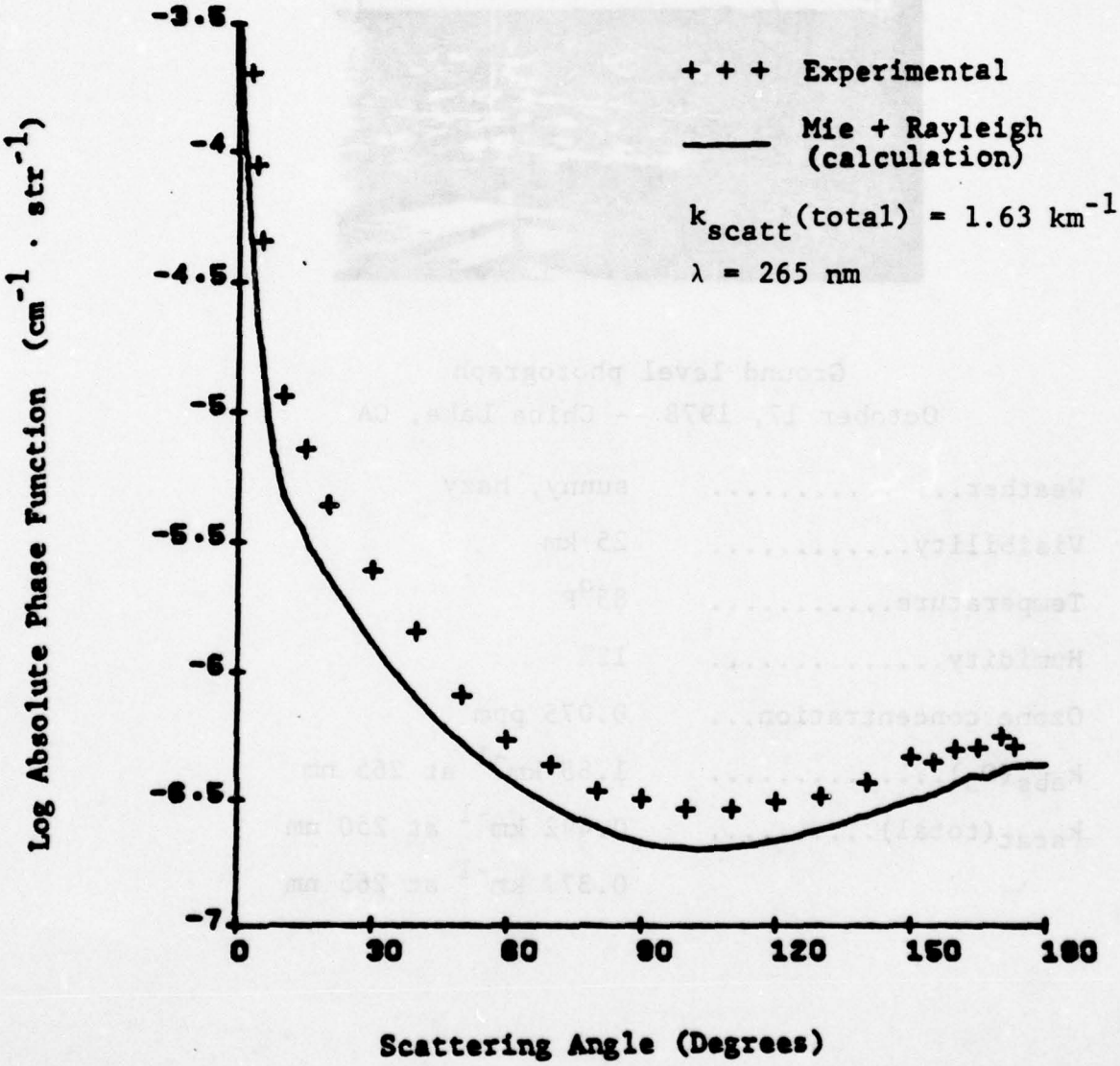

Phase function measured on October 11, 1978 at 10:30 p.m.

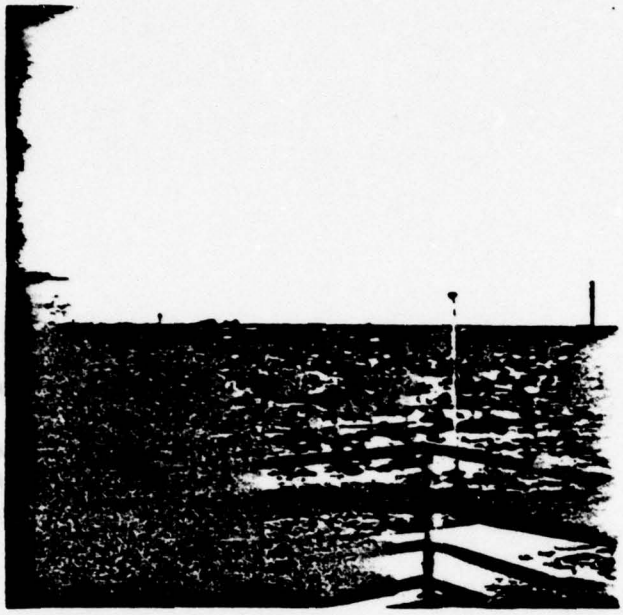

Ground level photograph
October 17, 1978 -- China Lake, CA

Weather.....	sunny, hazy
Visibility.....	25 km
Temperature.....	85°F
Humidity.....	12%
Ozone concentration...	0.075 ppm
$k_{abs}(O_3)$.....	1.88 km^{-1} at 265 nm
k_{scat}(total).....	0.492 km^{-1} at 250 nm
	0.377 km^{-1} at 265 nm

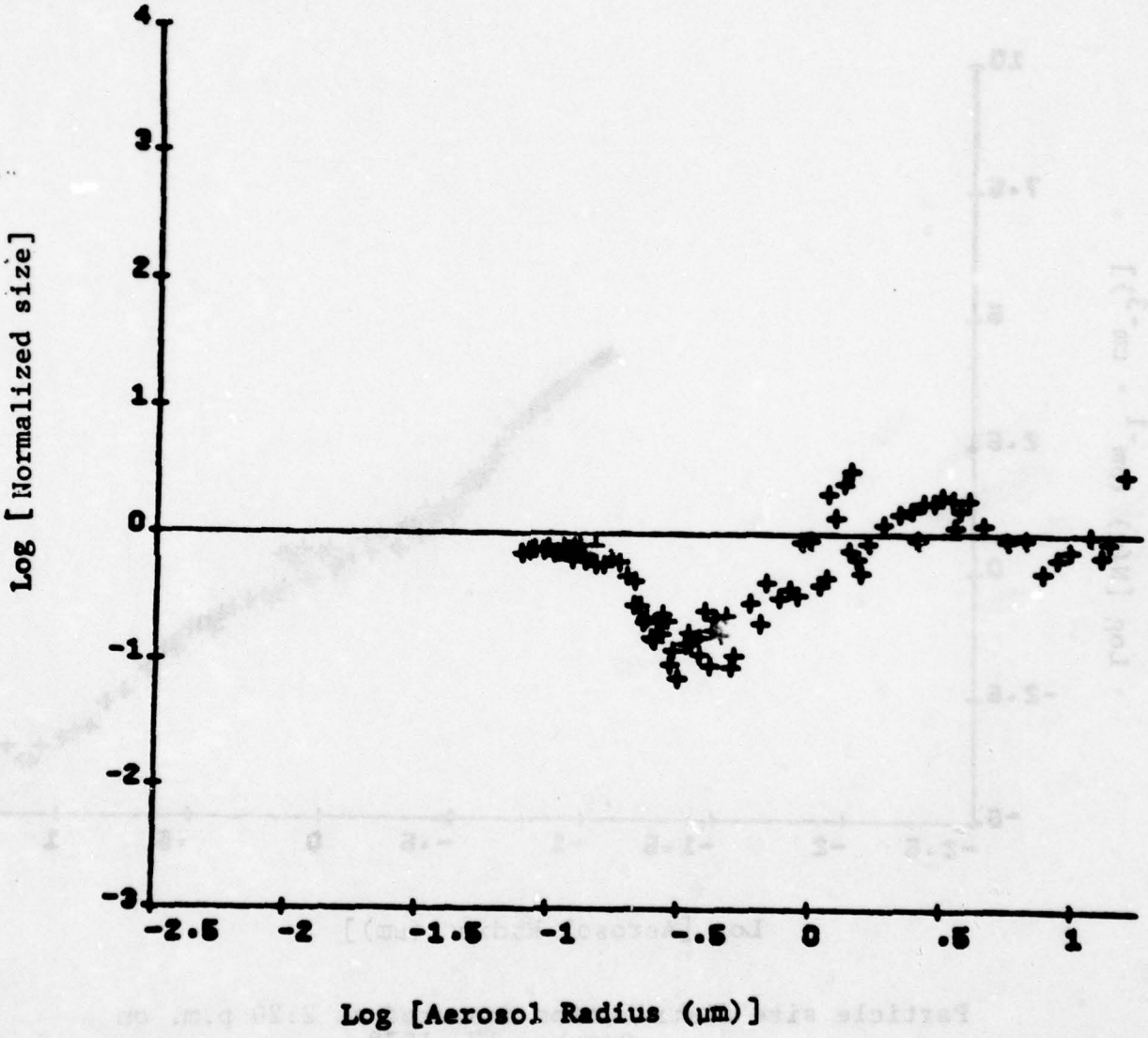

Typical particle size distribution measured on October 17, 1978.

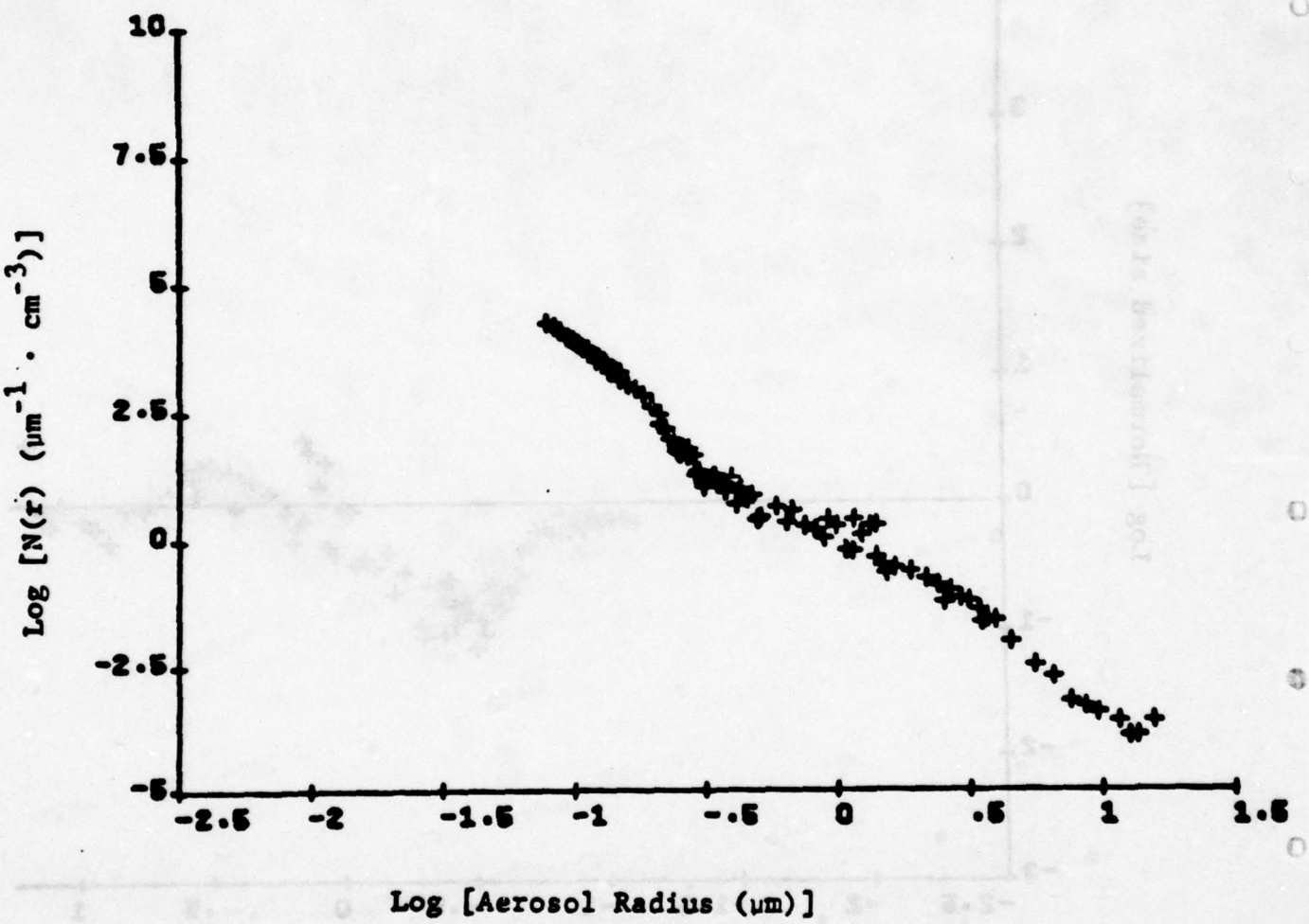

Particle size distribution measured at 2:20 p.m. on October 17, 1978.

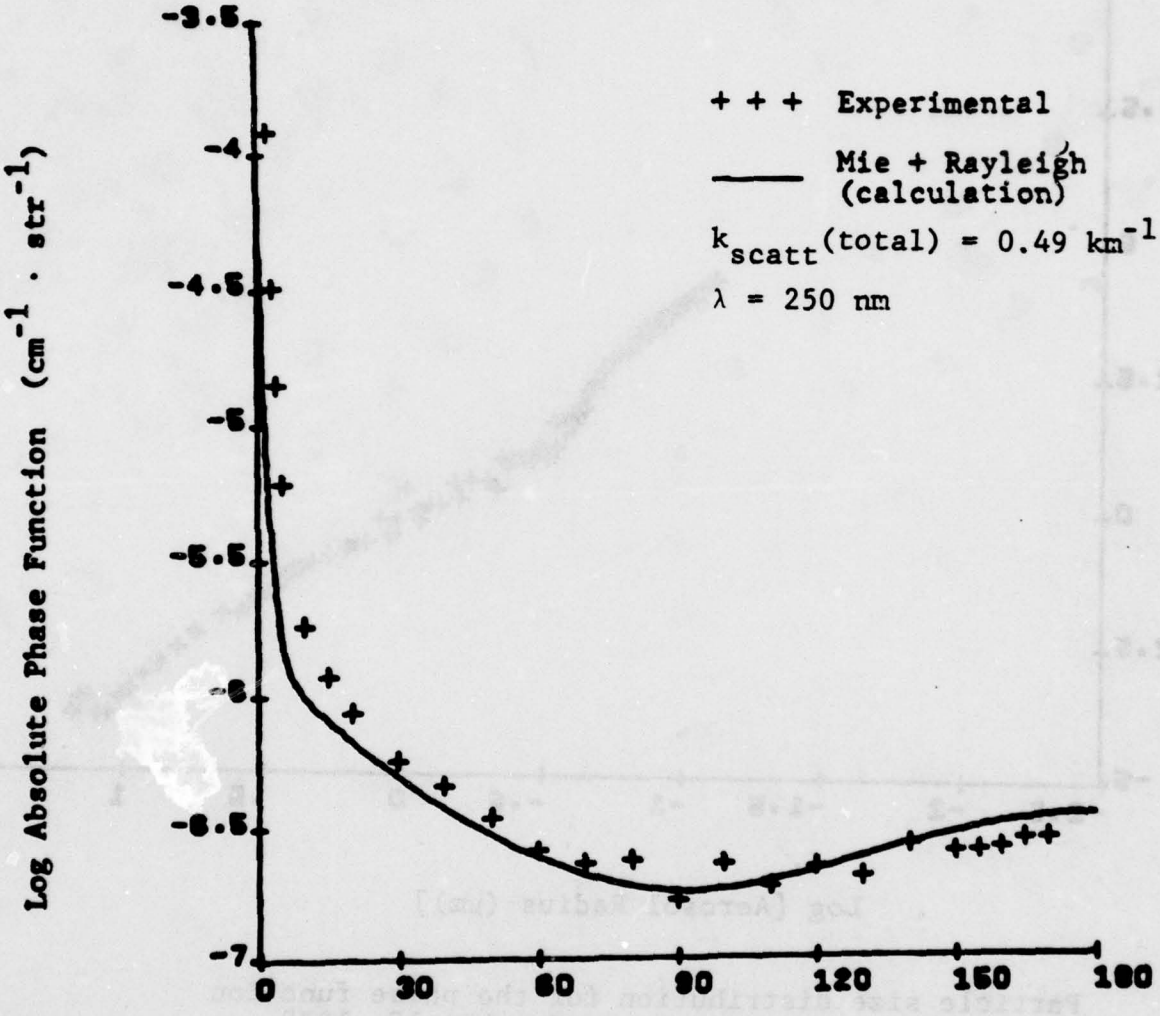

Phase function measured on October 17, 1978 at 2:20 p.m.

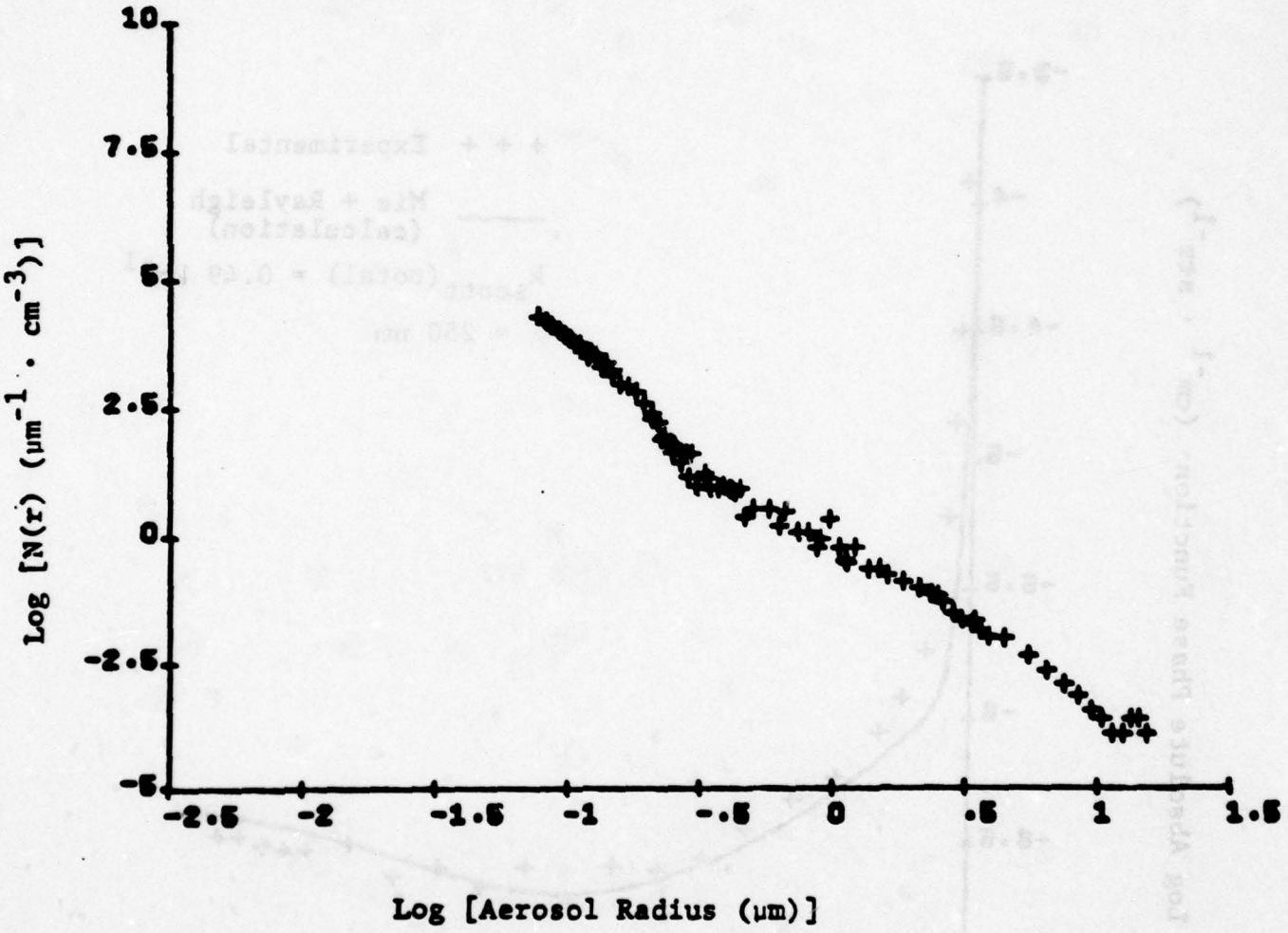

Particle size distribution for the phase function measured at 3:05 p.m. on October 17, 1978.

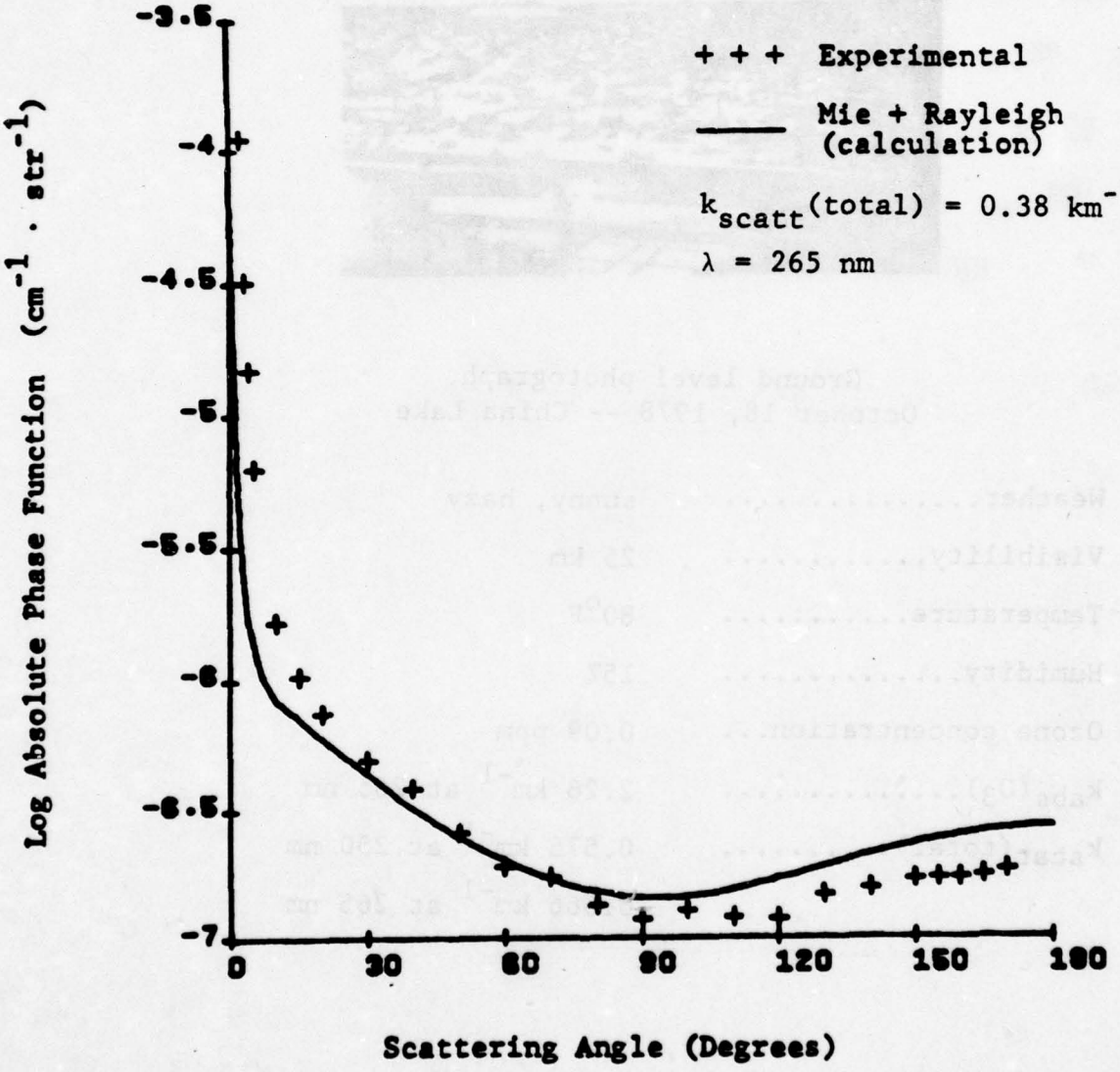

Phase function measured on October 17, 1978 at 3:05 p.m.

Ground level photograph
October 18, 1978 -- China Lake

Weather.....	sunny, hazy
Visibility.....	25 km
Temperature.....	80°F
Humidity.....	15%
Ozone concentration...	0.09 ppm
$k_{abs}(O_3)$.....	2.26 km^{-1} at 265 nm
k_{scat}(total).....	0.575 km^{-1} at 250 nm
	0.566 km^{-1} at 265 nm

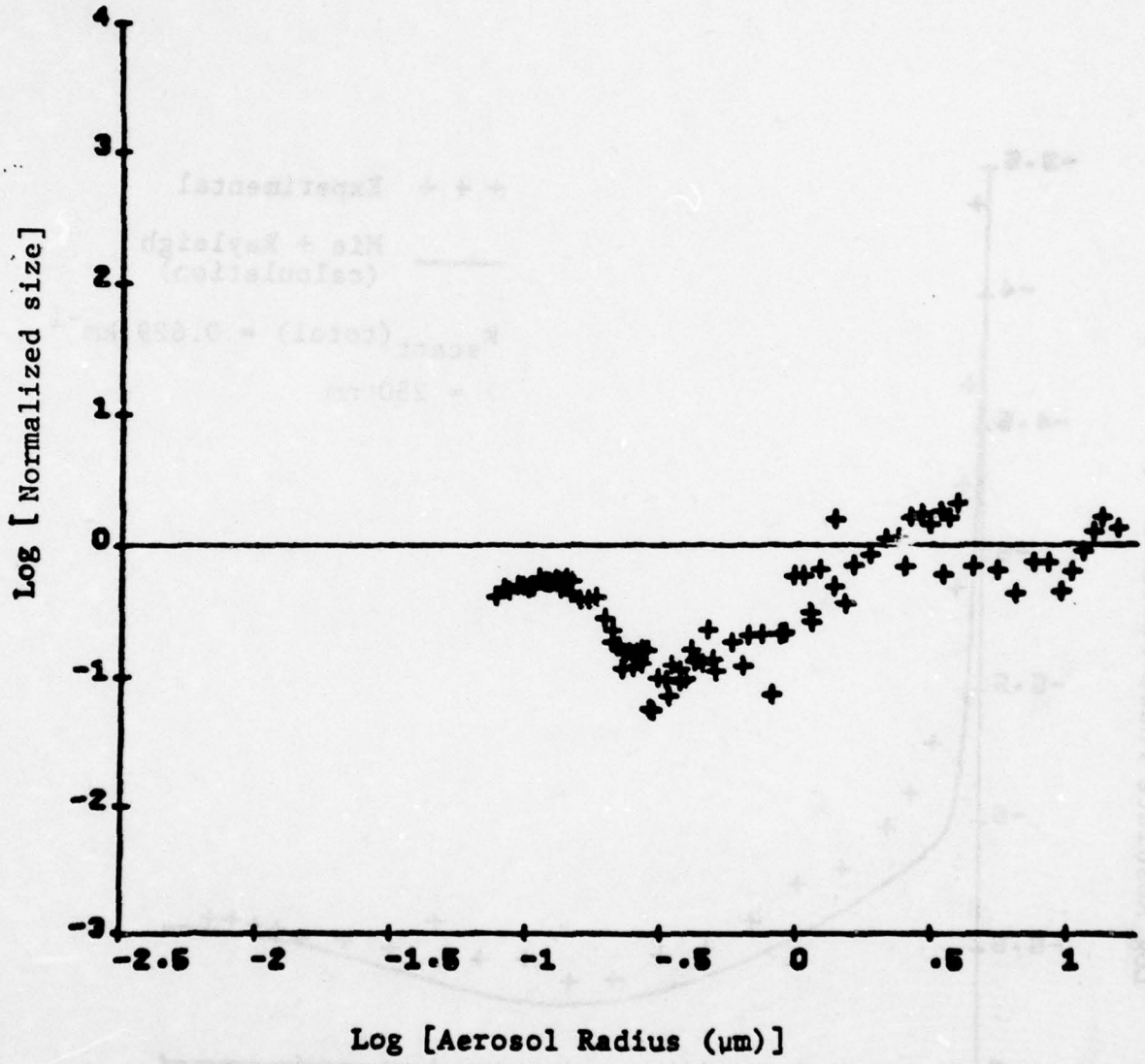

Typical particle size distribution measured on October 18, 1978.

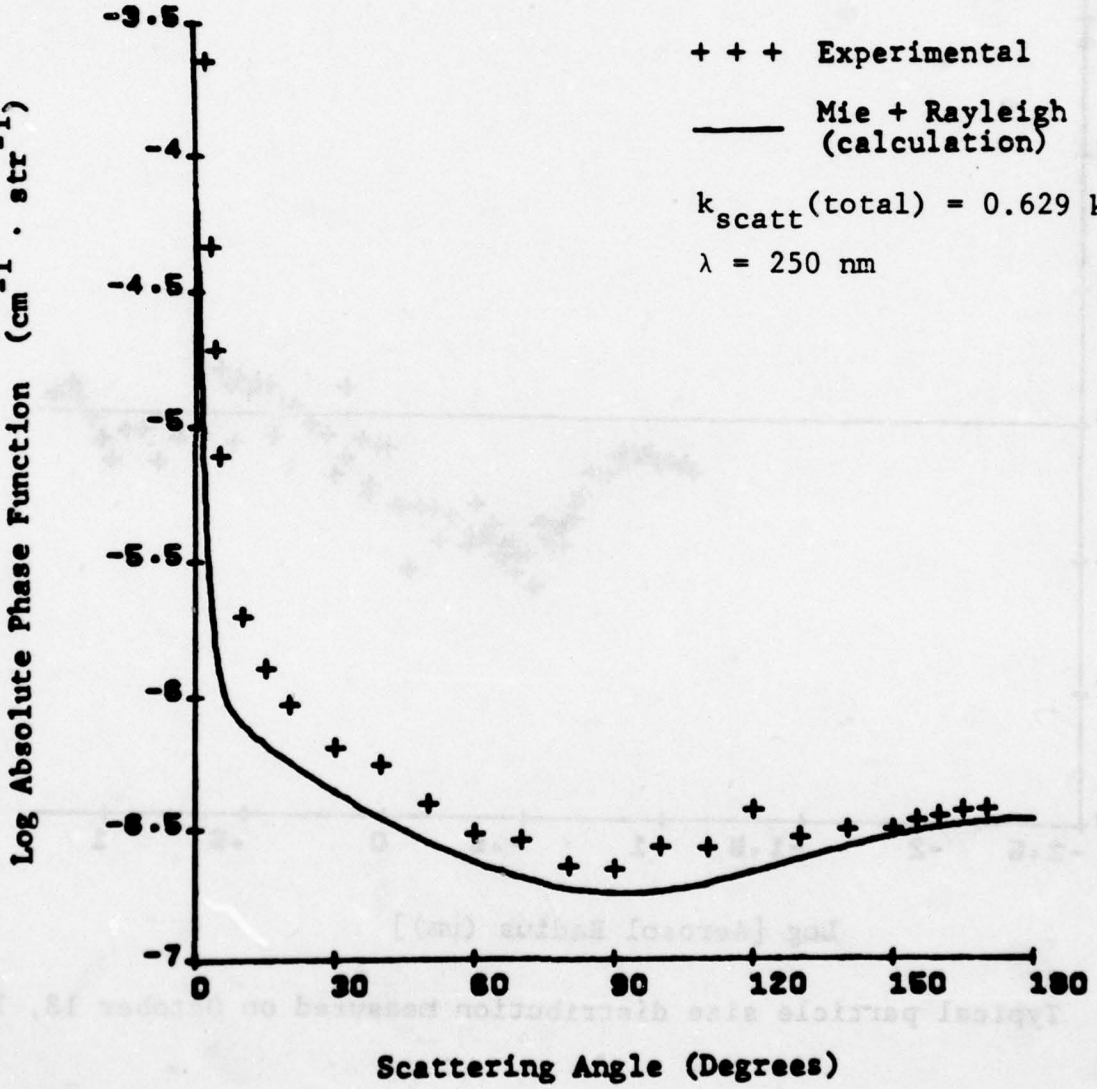

Phase function measured on October 18, 1978 at 1:50 p.m.

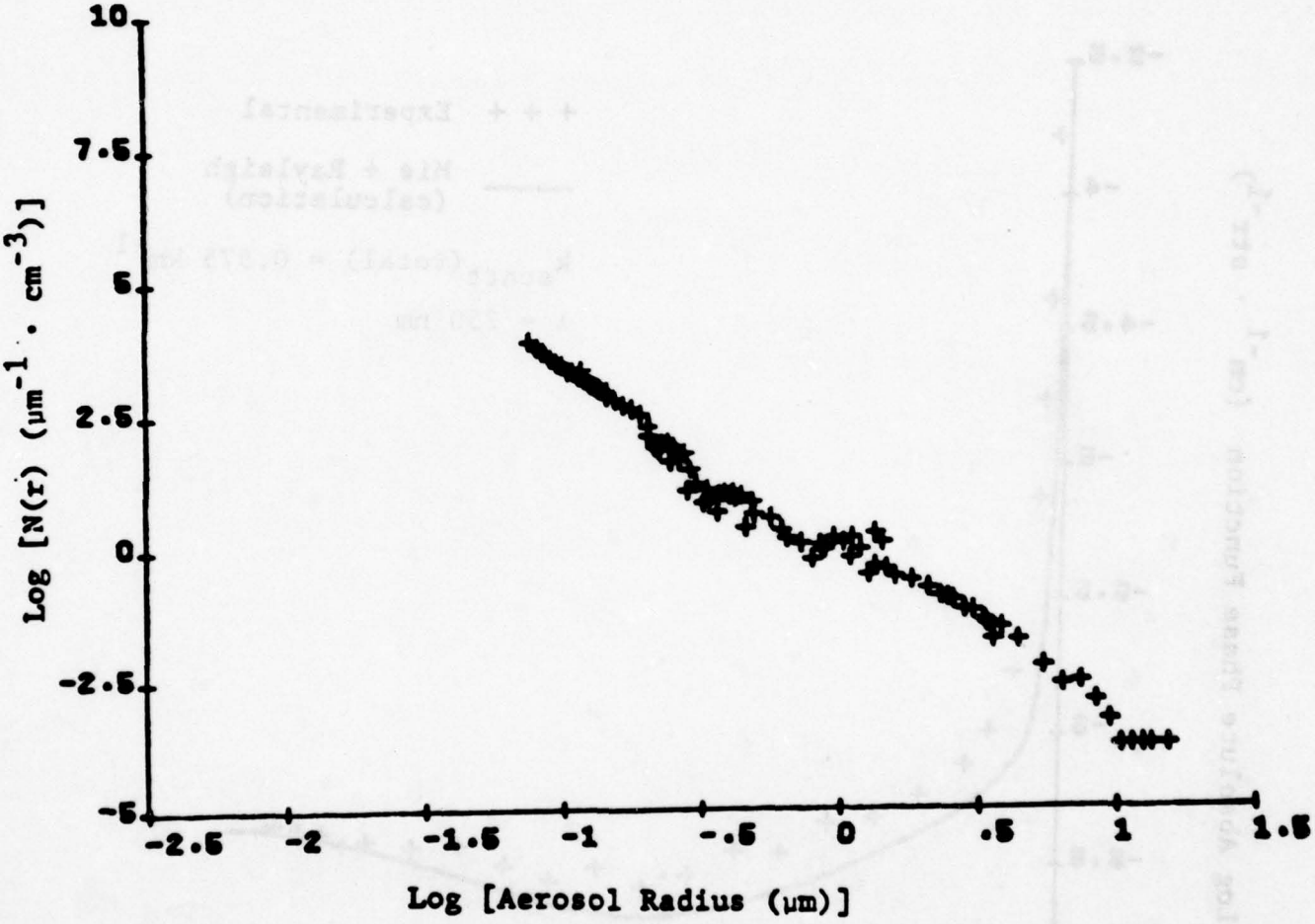

Particle size distribution for phase function measured at 7:45 p.m. on October 18, 1978.

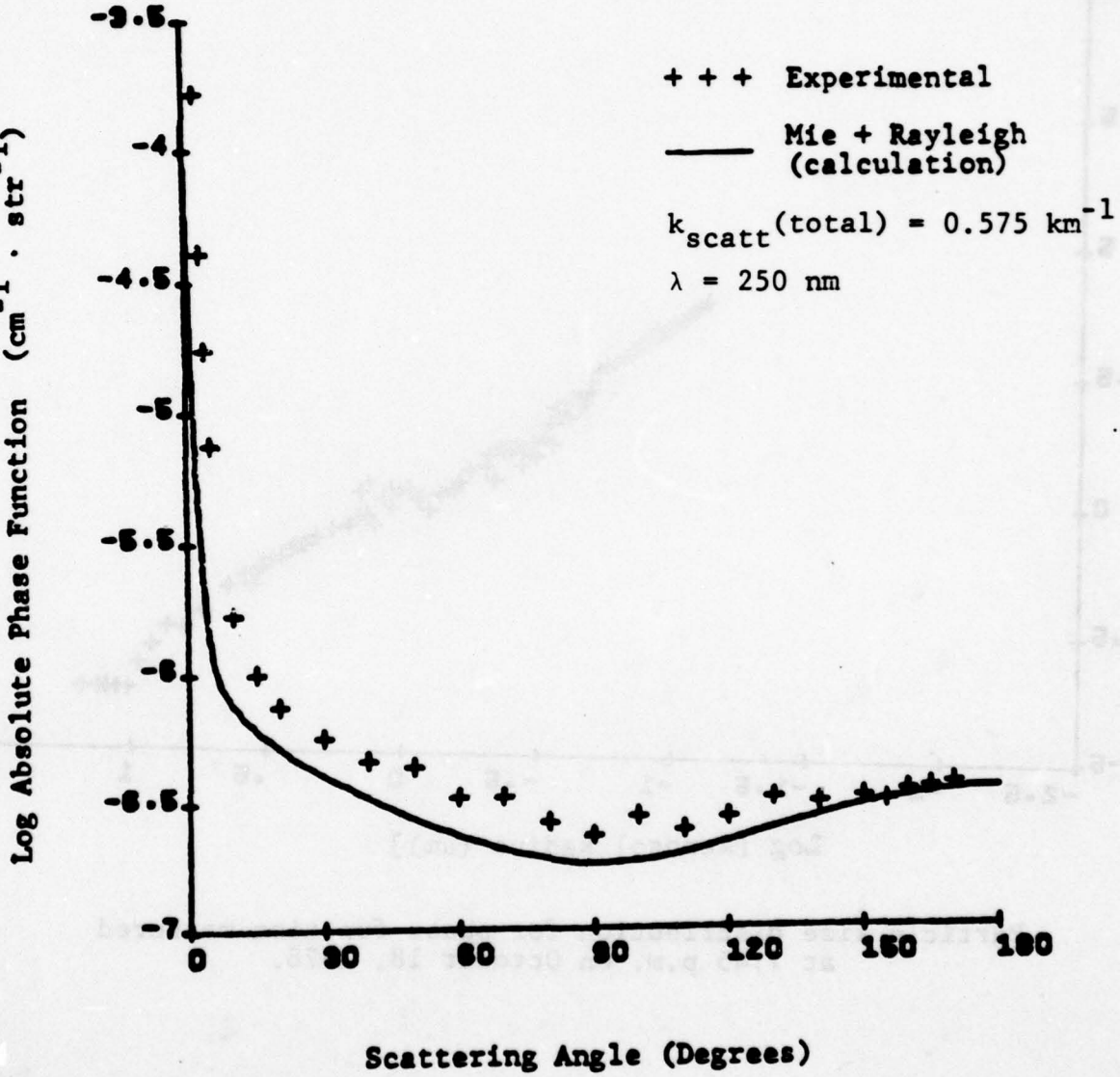

Phase function measured on October 18, 1978 at 7:45 p.m.

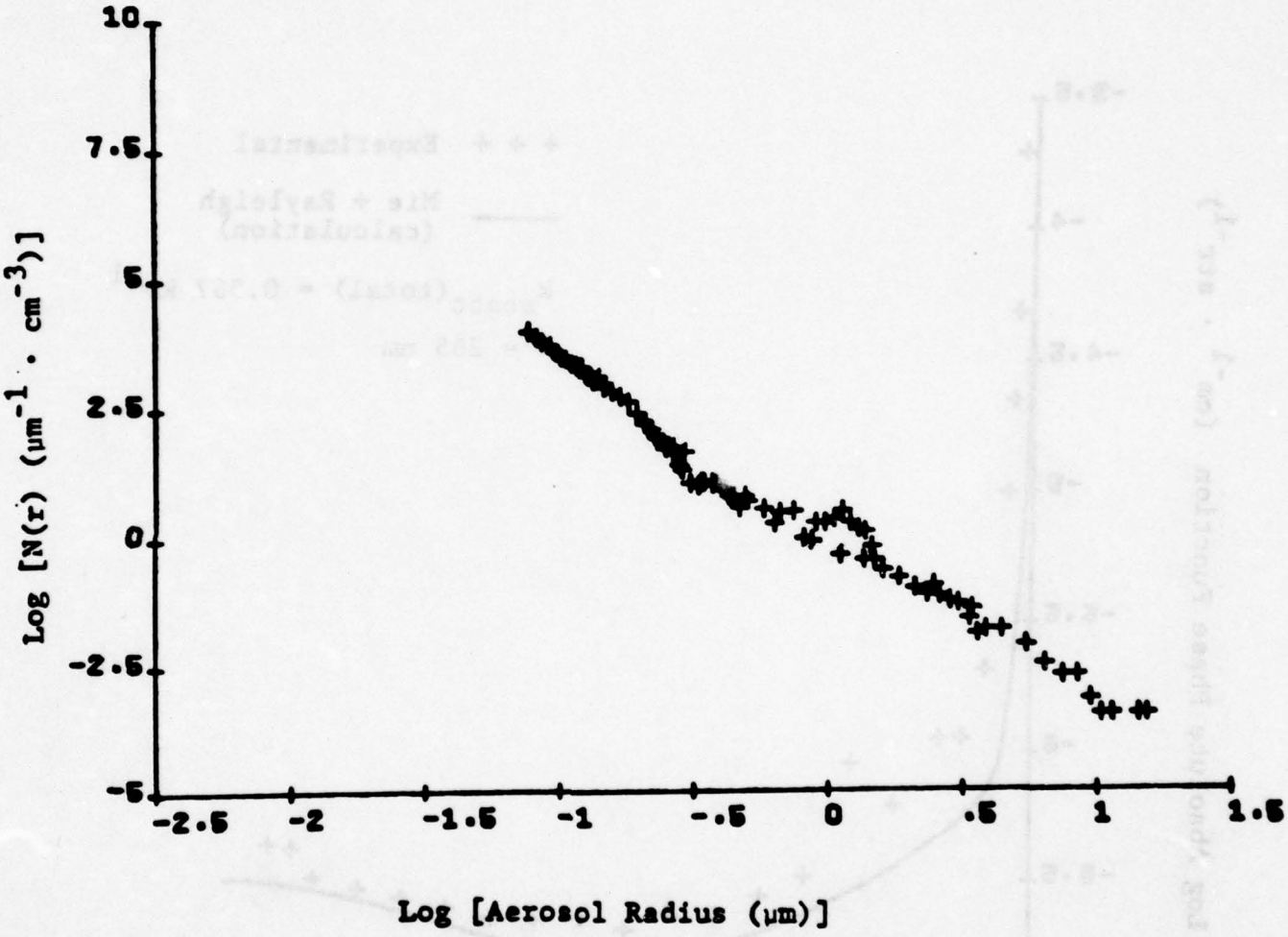

Particle size distribution for phase function measured at 8:25 p.m. on October 18, 1978.

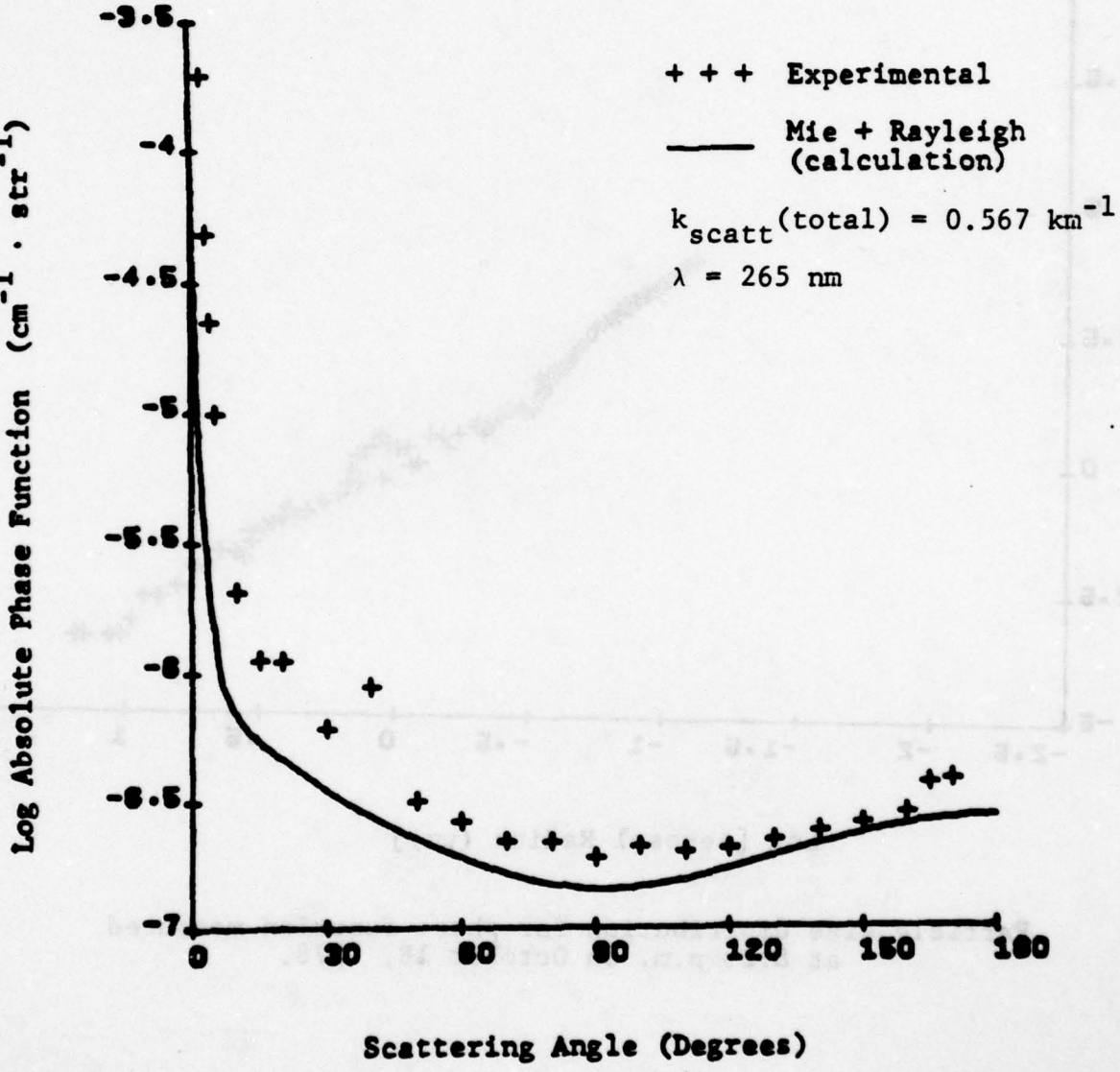

Phase function measured on October 18, 1978 at 8:25 p.m.

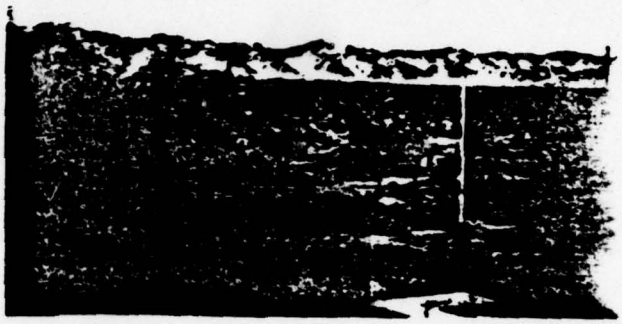

Ground level photograph
October 19, 1978 -- China Lake

Weather.....	sunny, hazy
Visibility.....	25 km
Temperature.....	75°F
Humidity.....	21%
Ozone concentration...	0.06 ppm
$k_{abs}(O_3)$.....	1.51 km^{-1} at 265 nm
k_{scat}(total).....	0.452 km^{-1} at 250 nm
	0.306 km^{-1} at 265 nm

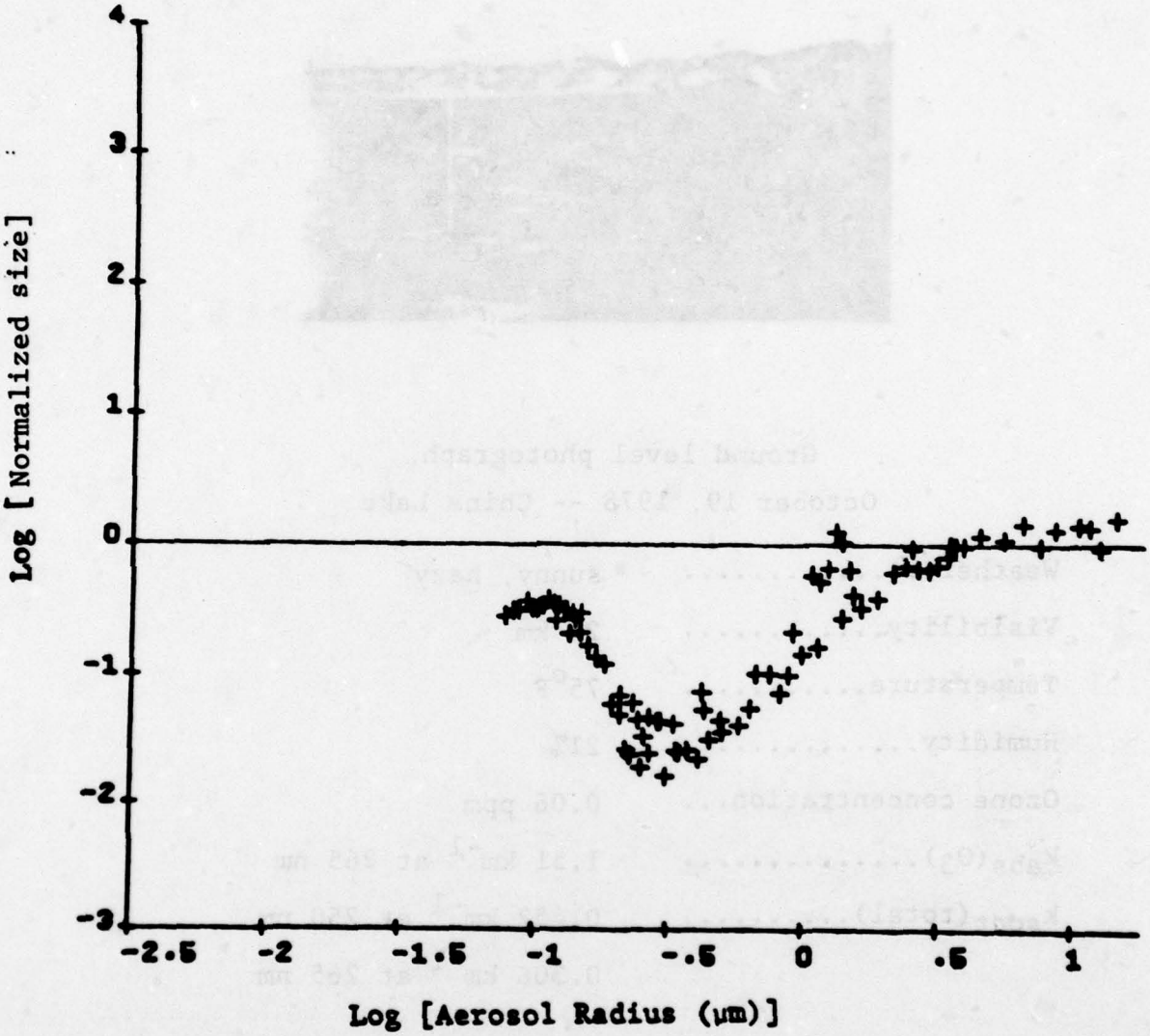

Typical normalized particle size distribution measured on October 19, 1978.

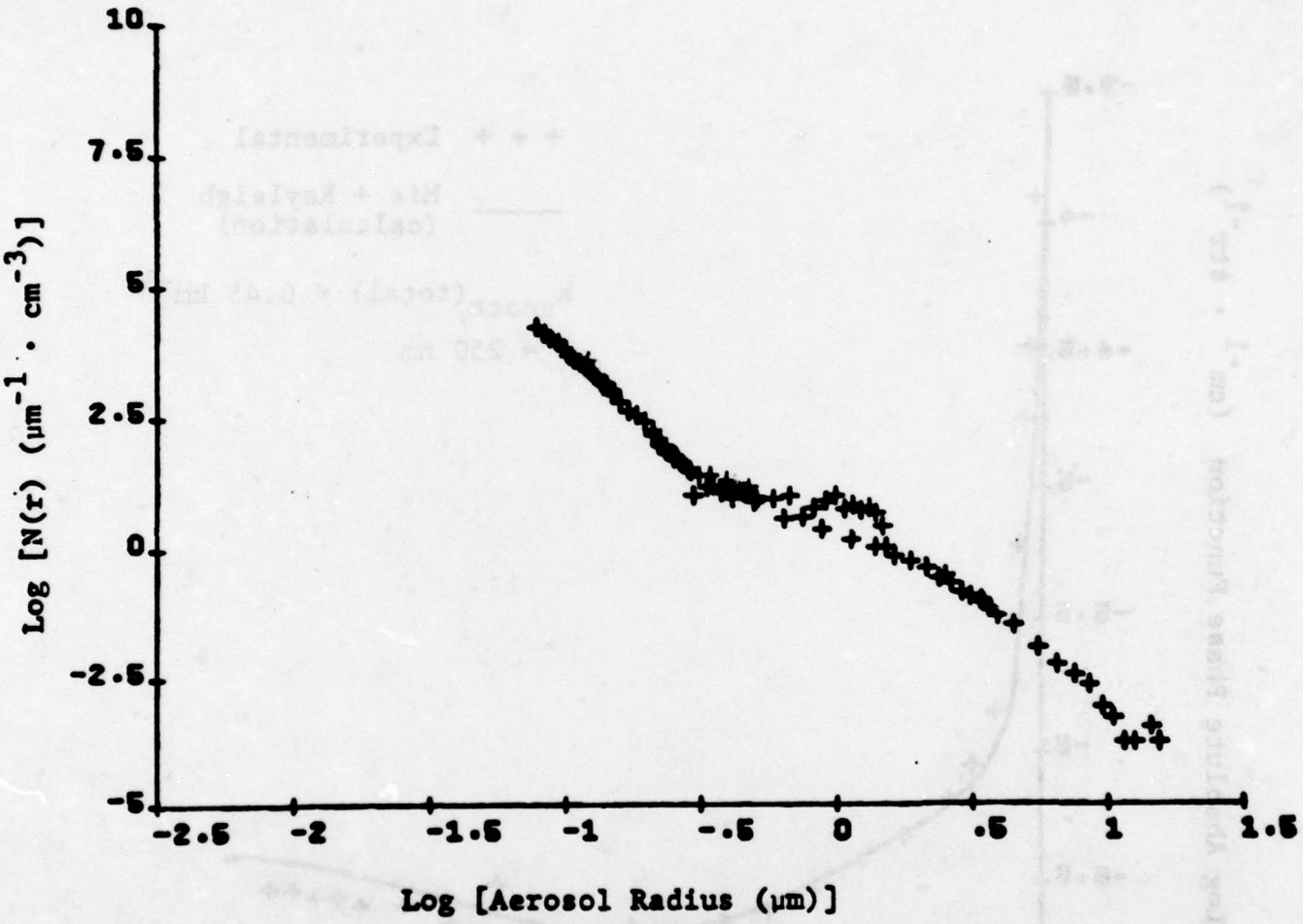

Particle size distribution for phase function measured at 9:20 a.m. on October 19, 1978.

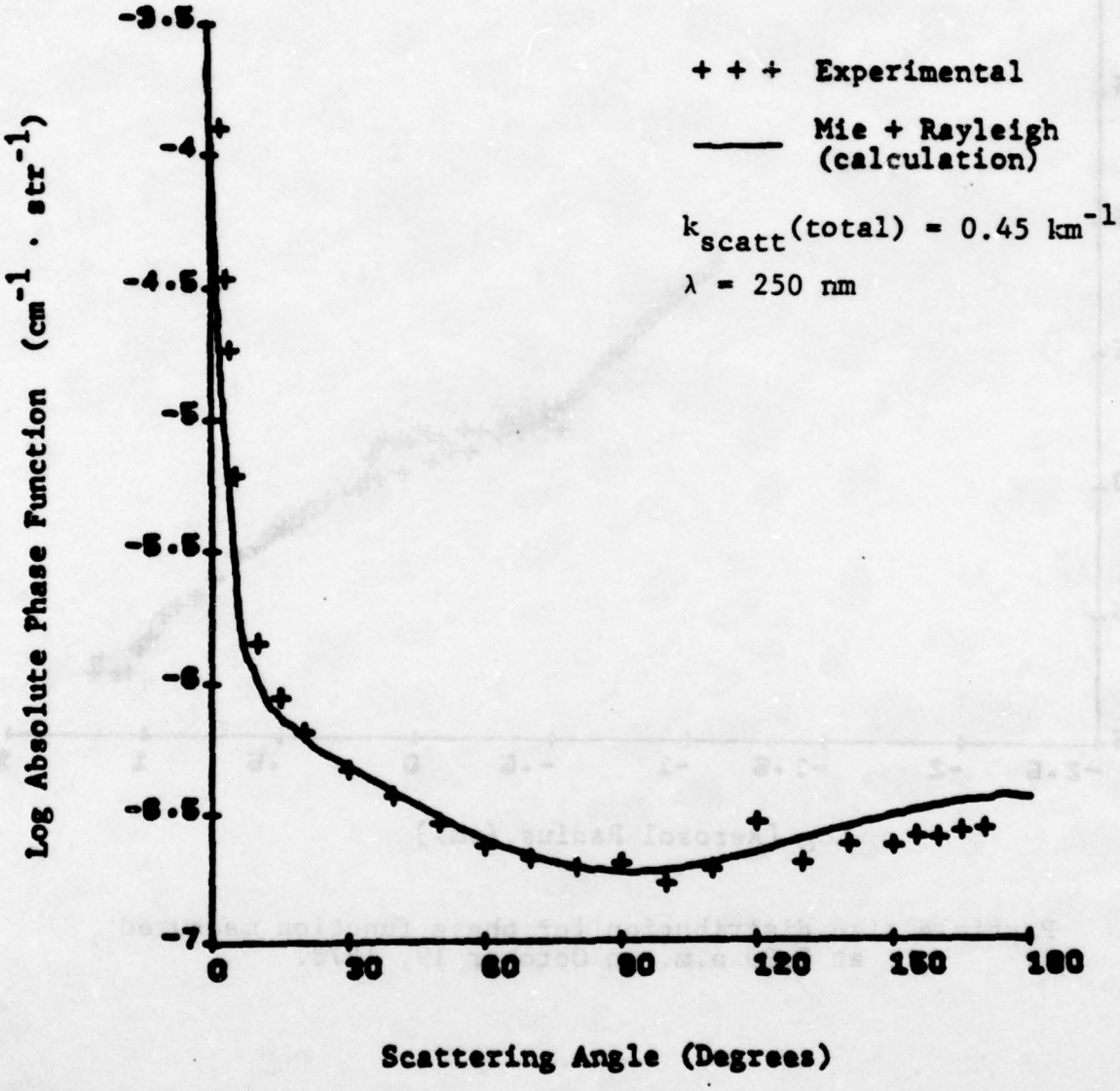

Phase function measured on October 19, 1978 at 9:20 a.m.

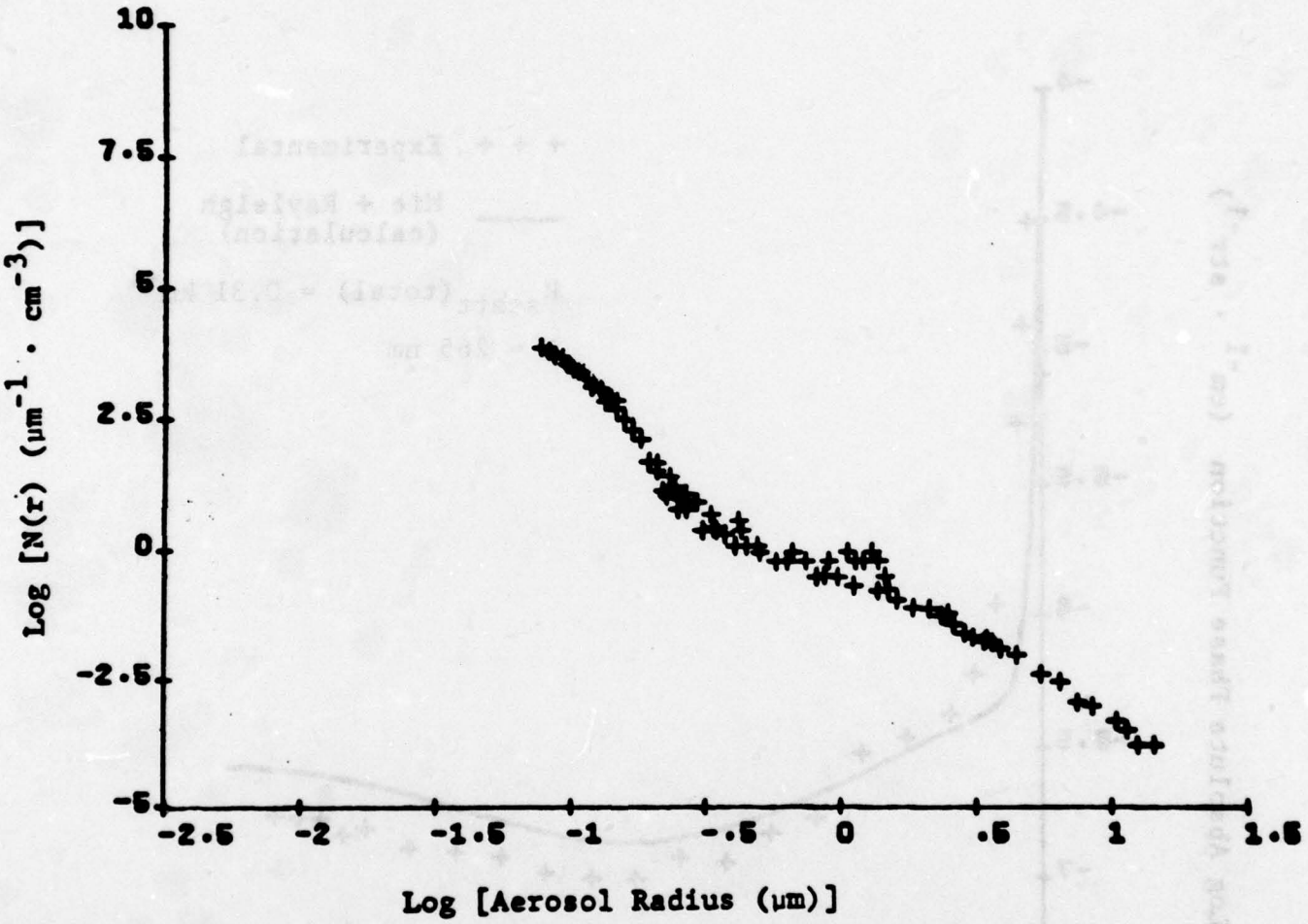

Particle size distribution for phase function measured at 3:25 p.m. on October 19, 1978.

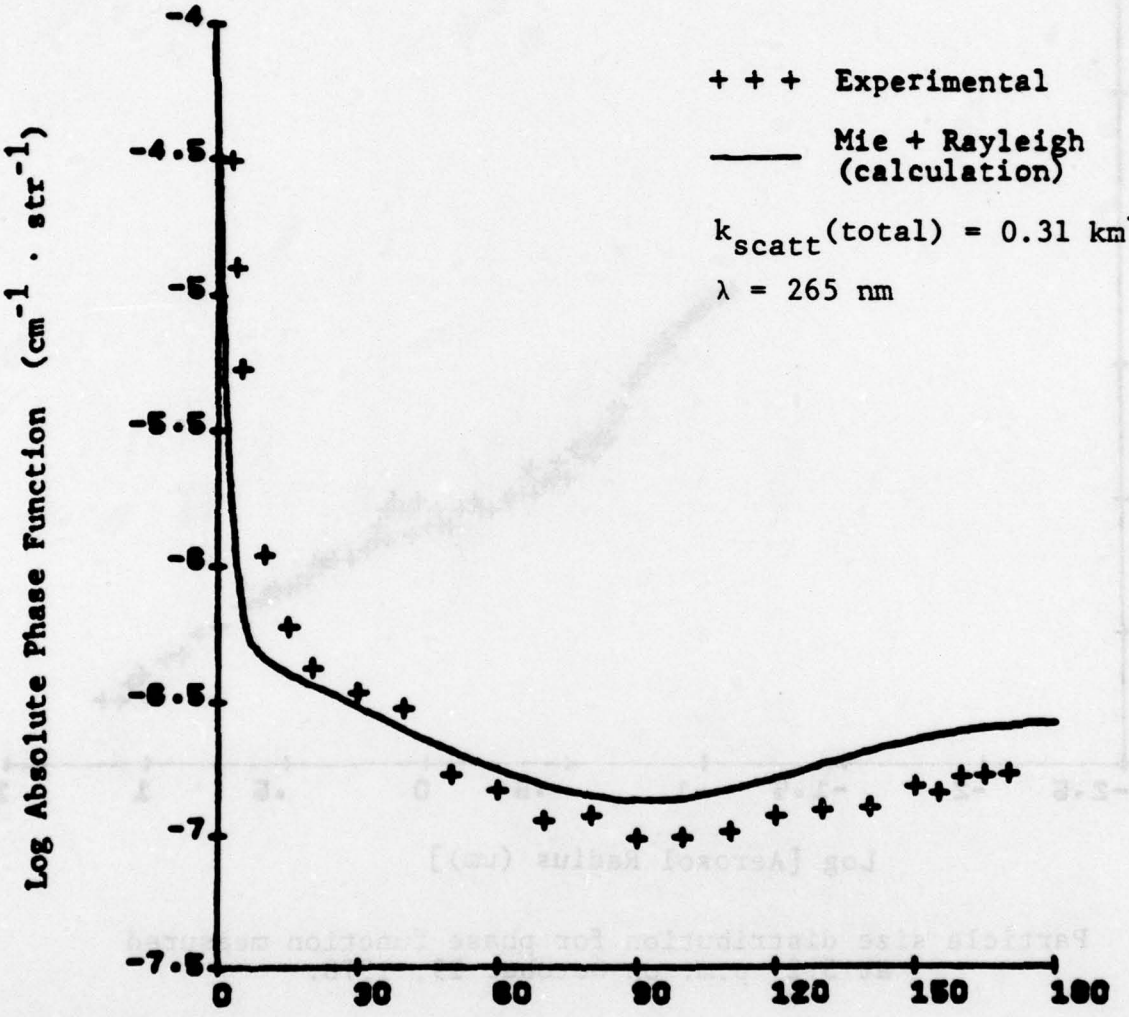

Phase function measured on October 19, 1978 at 3:25 p.m.

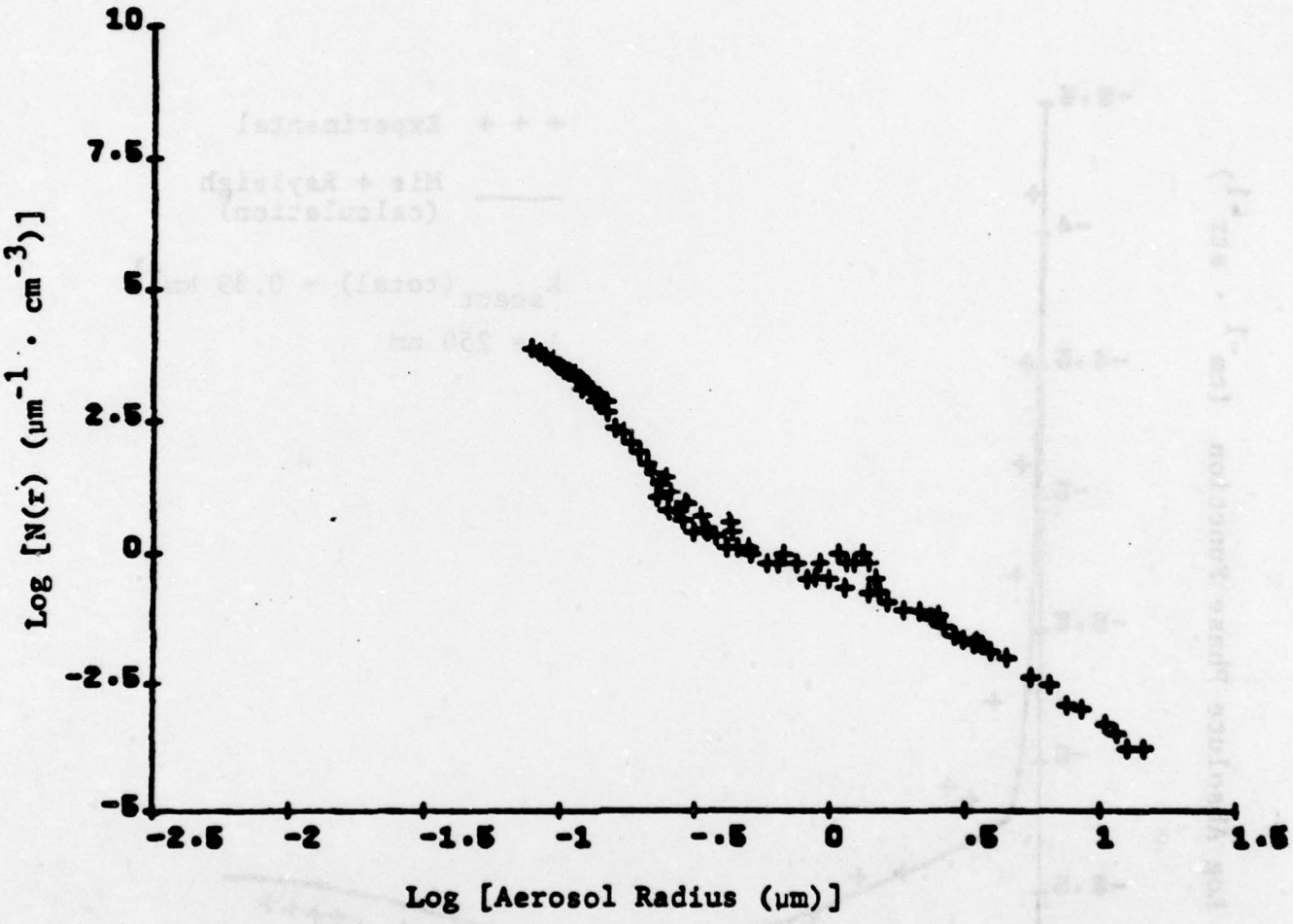

Particle size distribution for phase function measured at 3:45 p.m. on October 19, 1978.

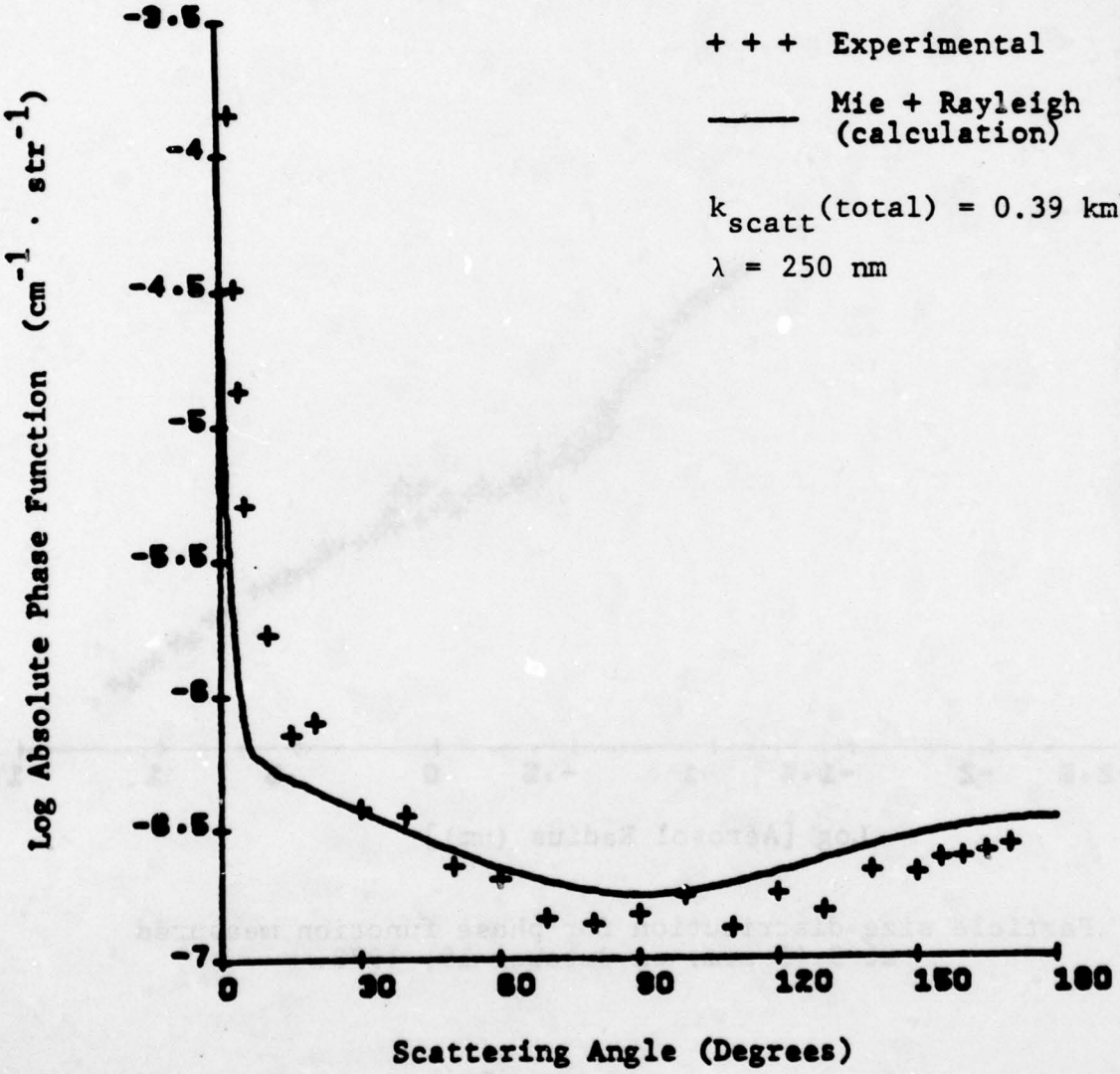

Phase function measured on October 19, 1978 at 3:45 p.m.

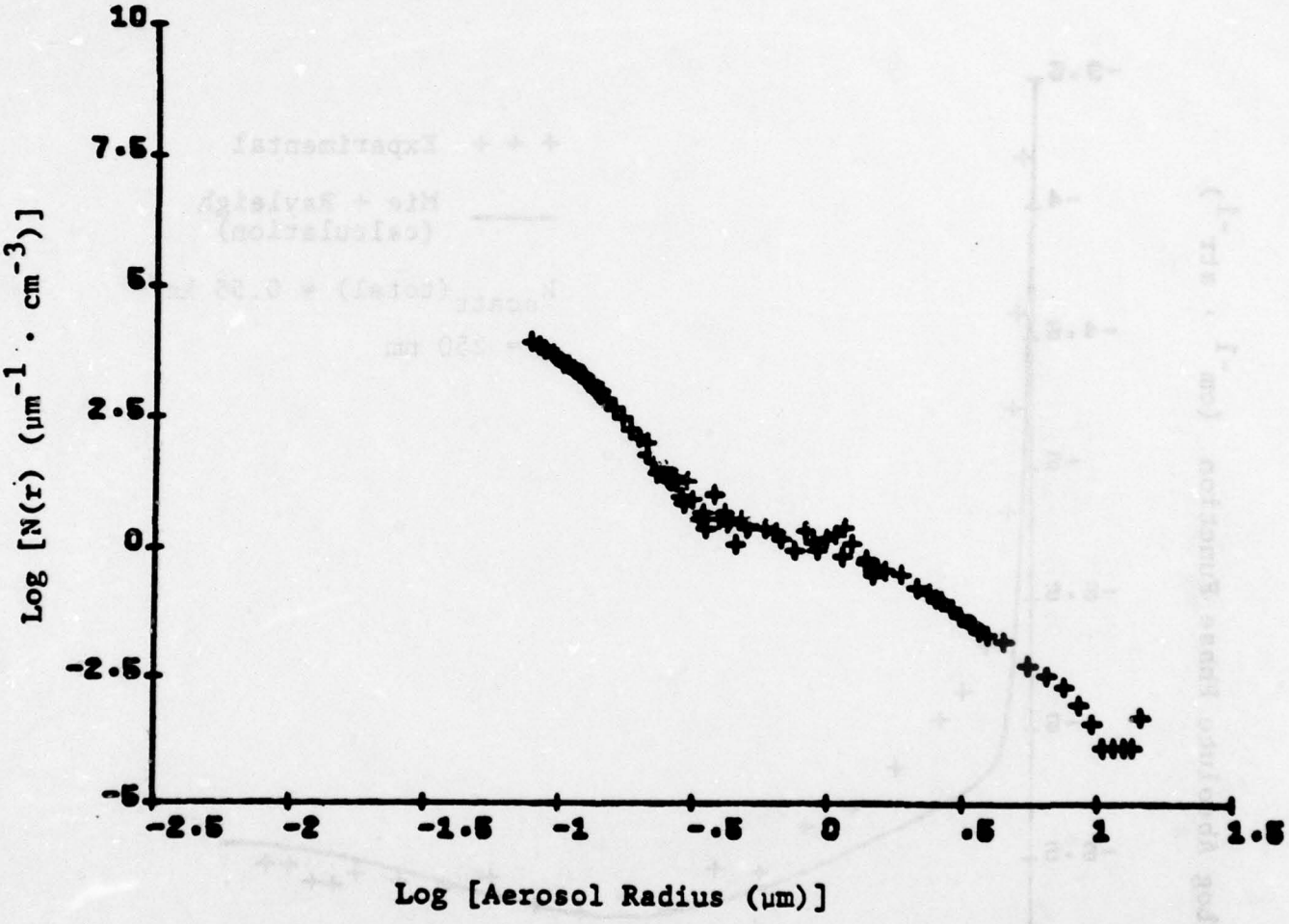

Particle size distribution measured at 11:30 p.m. on October 19, 1978.

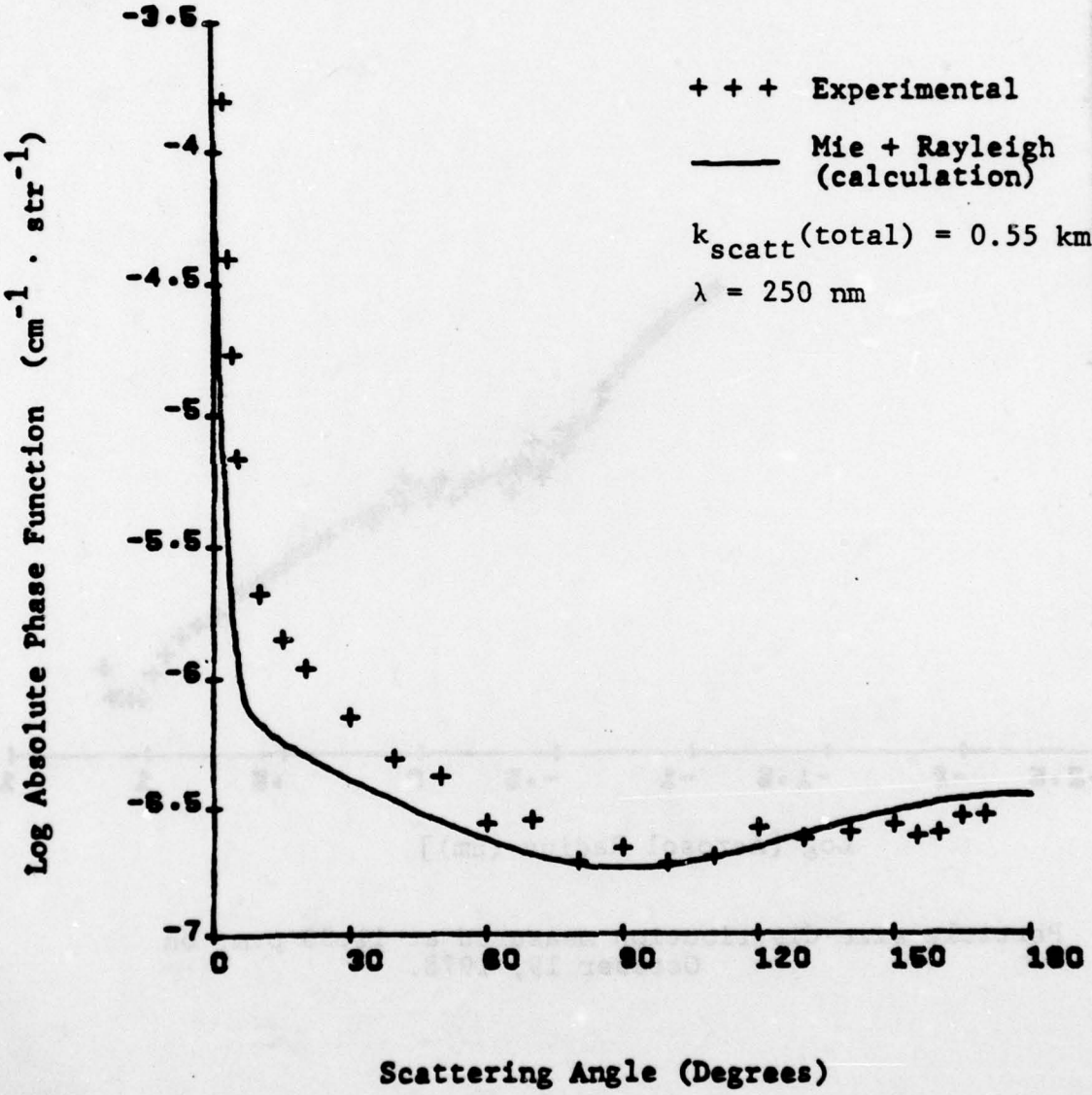

Phase function measured on October 19, 1978 at 11:30 p.m.

Ground level photograph
October 20, 1978 -- China Lake

Weather.....	rain, cloudy
Visibility.....	5 km
Temperature.....	65°F
Humidity.....	65%
Ozone concentration...	0.06 ppm
$k_{abs}(O_3)$.....	1.51 km^{-1} at 265 nm
k_{scat}(total).....	0.81 km^{-1} at 250 nm

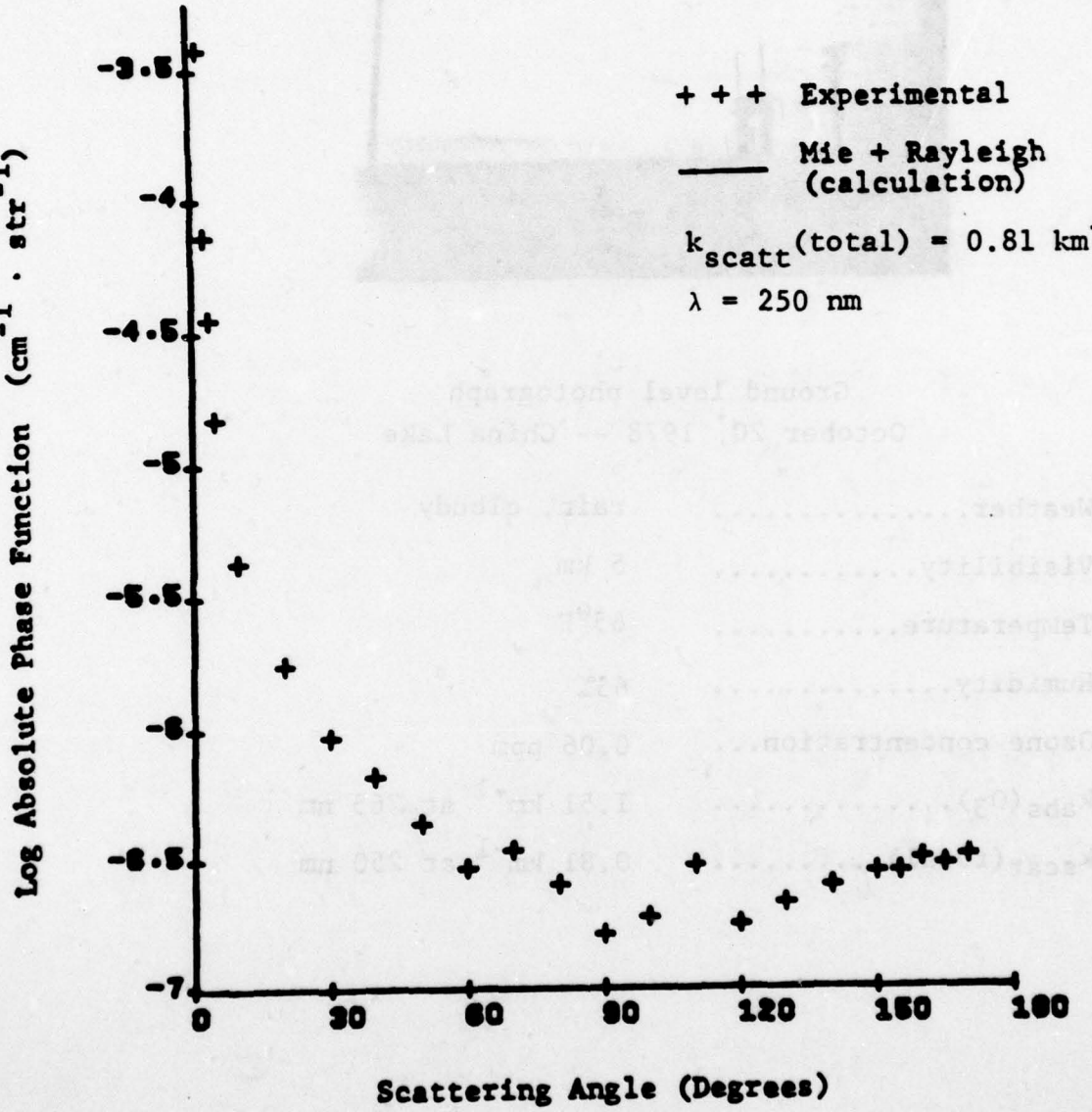

Phase function measured on October 20, 1978 at 11:15 a.m.

No Photograph

January 31, 1978 -- Princeton

Weather.....	overcast, windy
Visibility.....	10 km
Temperature.....	31°F
Humidity.....	50%
Ozone concentration...	-
$k_{abs}(O_3)$.....	-
k_{scat}(total).....	1.09 km^{-1} at 265 nm

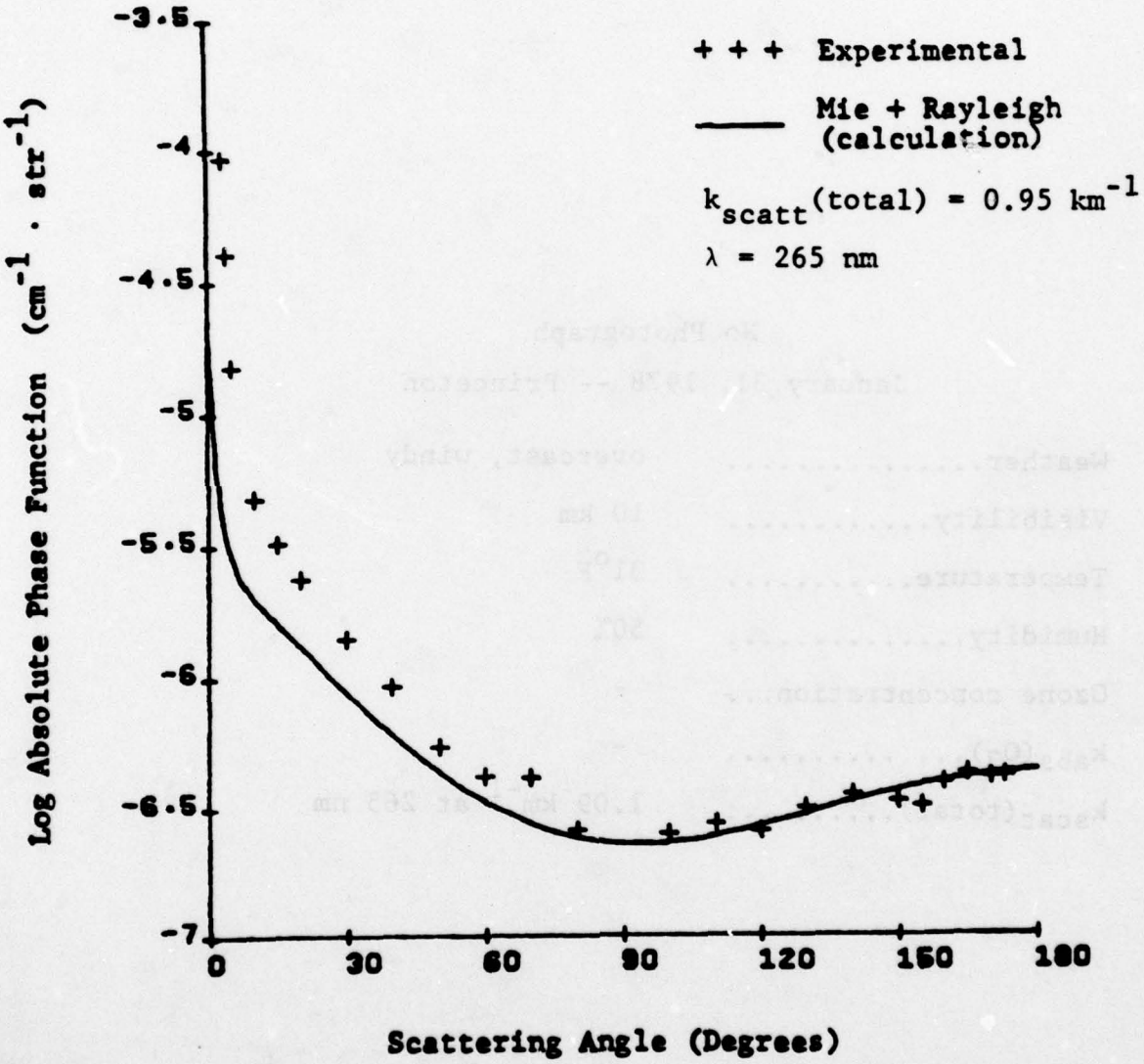

Phase function measured on January 31, 1979.